COMPUTACIONAL STUDIES ON THE MECHANISM OF THE PAUSON-KHAND REACTION

Torstein Fjermestad

ISBN: 978-84-693-9441-0
Dipòsit Legal: T.62-2011

UNIVERSITAT ROVIRA I VIRGILI
COMPUTACIONAL STUDIES ON THE MECHANISM OF THE PAUSON-KHAND REACTION
Torstein Fjermestad
ISBN:978-84-693-9441-0/DL:T.62-2011

UNIVERSITAT ROVIRA I VIRGILI
COMPUTACIONAL STUDIES ON THE MECHANISM OF THE PAUSON-KHAND REACTION
Torstein Fjermestad
ISBN:978-84-693-9441-0/DL:T.62-2011

UNIVERSITAT ROVIRA I VIRGILI
COMPUTACIONAL STUDIES ON THE MECHANISM OF THE PAUSON-KHAND REACTION
Torstein Fjermestad
ISBN:978-84-693-9441-0/DL:T.62-2011

Torstein Fjermestad

Computational Studies on the Mechanism of the Pauson-Khand Reaction

DOCTORAL THESIS

Supervised by Feliu Maseras and Miquel A. Pericàs

Institute of Chemical Research of Catalonia (ICIQ)

UNIVERSITAT ROVIRA I VIRGILI

TARRAGONA

2010

UNIVERSITAT ROVIRA I VIRGILI
COMPUTACIONAL STUDIES ON THE MECHANISM OF THE PAUSON-KHAND REACTION
Torstein Fjermestad
ISBN:978-84-693-9441-0/DL:T.62-2011

UNIVERSITAT ROVIRA I VIRGILI
COMPUTACIONAL STUDIES ON THE MECHANISM OF THE PAUSON-KHAND REACTION
Torstein Fjermestad
ISBN:978-84-693-9441-0/DL:T.62-2011

Institute of Chemical Research of Catalonia (ICIQ)
Avgda. Països Catalans 16
43007 Tarragona (Spain)

WE STATE that the present study, entitled "Computational Studies on the Mechanism of the Pauson-Khand Reaction" presented by Torstein Fjermestad for the award of the degree of Doctor, has been carried out under our supervision at the Institute of Chemical Research of Catalonia (ICIQ), and that it fulfils all the requirements to be eligible for the European Doctorate Award.

Tarragona, November 2010

Feliu Maseras

Miquel A. Pericàs

UNIVERSITAT ROVIRA I VIRGILI
COMPUTACIONAL STUDIES ON THE MECHANISM OF THE PAUSON-KHAND REACTION
Torstein Fjermestad
ISBN:978-84-693-9441-0/DL:T.62-2011

UNIVERSITAT ROVIRA I VIRGILI
COMPUTACIONAL STUDIES ON THE MECHANISM OF THE PAUSON-KHAND REACTION
Torstein Fjermestad
ISBN:978-84-693-9441-0/DL:T.62-2011

Every day you may make progress. Every step may be fruitful. Yet there will stretch out before you an ever-lengthening, ever-ascending, ever-improving path. You know you will never get to the end of the journey. But this, so far from discouraging, only adds to the joy and the glory of the climb.

Winston Churchill

UNIVERSITAT ROVIRA I VIRGILI
COMPUTACIONAL STUDIES ON THE MECHANISM OF THE PAUSON-KHAND REACTION
Torstein Fjermestad
ISBN:978-84-693-9441-0/DL:T.62-2011

UNIVERSITAT ROVIRA I VIRGILI
COMPUTACIONAL STUDIES ON THE MECHANISM OF THE PAUSON-KHAND REACTION
Torstein Fjermestad
ISBN:978-84-693-9441-0/DL:T.62-2011

Acknowledgements

The elaboration of this thesis would not have been possible without the help of many. First and formost I would like to thank my thesis directors Feliu Maseras and Miquel Pericàs. Without your help and support, I would not have been where I am today. Specially I want to thank Feliu for teaching me the importance of being critical to my own work, listening to other peoples view and developing awareness to be able to look for the solution where you might not expect it to be. Thanks to Feliu's help, I have developed skills necessary to continue my career as a researcher.

During these years, I have also received lots of help and support from the past and current members (and visitors) of the three theoretical groups at ICIQ: Prof. Carles Bo, Dr. Núria López, Dr. Ataualpa Braga, Dr. Alfons Nonell, Dr. Peter Carlqvist, Dr. David Balcells, Dr. Marta Feliz, Dr. Eva Santos, Dr. Pere Miró, Dr. Fabienne Bessac, Dr. Josep Maria Campanera Alsina, Dr. Manolo Urbano, Dr. Christophe Gourlaouen, Dr. Erik Zuidema, Abel Locati, Dr. Mónica Garcia, Jaime Gómez, Rene Petz, Dr. Gemma Christian, Dr. Steven Donald, Dr. Martin Perez, Dr. Simon Pierrefixe, Dr. Mickael Gicquel, Jose Javier Plata, Dr. Carina Bäcktorp, Dr. Gerard Novell, Dr. Maria Besora, Cristina Pubill, Dr. Silvia Diez, Charles Goehry, Dr. Elena Herrero, Crisa Vargas, Rocío Recio, Chunhui Liu, Dr. Luca Bellarosa, Dr. David Karhánek, Dr. Alex Hamilton, Dr. Adrià Gil and Leire Baztarrika.

Among these, I would in particular like to highlight Dr. Mónica Garcia. Ever since I got to know her, I have been impressed by her capacity to work hard for long hours. This is a quality I continuously strive to achieve, and in that respect Mónica has been a real source of inspiration.

Also I would like to thank the IT technicians of the group, Martin Gumbau, Joan Iglesias, Oriol Calderó and Hugo Barrera for helping me with technical problems. Also a special thanks to Núria Vendrell for making my unorganised life a bit more organised.

In the first year of my P.h.D. studies, I attended a 4-weeks course on computational chemistry. During that course, I made a lot of new friendships (or should I say future collaborators?). I would like to acknowledge some of them for continued fruitful discussions also after the end of the course: Aurora Jiménez, Elsa Galbis, Juan Manuel Ortiz, Julen Larrucea, Laura Largo Escudero, Nico Otero, Rocío Sánchez, Sílvia Osuna, Violeta Yeguas and Yannick Mercier.

During my P.h.D. studies, I have also visited the research groups of Prof. Stuart MacGregor and Prof. Dr. Walter Thiel. I would like to thank them for their hospitality hosting me in their groups. During these visits I acquired knowledge complementary to what I have learned at ICIQ. These two visits have made me see my reseach field from a different angle, something I believe is very healthy in science.

In Prof. Stuart MacGregor's group, I improved my abilities to relate the computational results to experiments. I would like to thank Prof. MacGregor and his

UNIVERSITAT ROVIRA I VIRGILI
COMPUTACIONAL STUDIES ON THE MECHANISM OF THE PAUSON-KHAND REACTION
Torstein Fjermestad
ISBN:978-84-693-9441-0/DL:T.62-2011

group members: Jenni Goodman, Amalia Poblador-Bahamonde, David McKay, Julian Panetier, Dr. Jonas Häller and Dr. Abu Naser. The visit to Prof. Dr. Walter Thiel's group could probably be summarised in the following sentence: "Man kann doch die Manual lesen". So simple, but o so true! This is the kind of knowledge that seems to have been mostly forgotten in our modern-day society. I would specially like to thank Dr. Stefan Erhardt for all his help during my visit there. Furthermore, I would also like to thank the following group members for fruitful discussions during my visit: Sebastian Metz, Tobias Benighaus, Dr. Elsa Sanchez, Iakov Polyak, Mario Ramos da Silva jun, Dr. Ya-Wen Hsiao, Dr. Mark Waller and Berit Heggen.

I would also like to thank friends and colleagues (current and former) at ICIQ and URV: Alberto Roldán, Ana Escribano, Eloísa Jiménez, Isidoro López, Laia Vilà, Laura Hernández, Mireia Segado, Olivier Diebolt, Ramón Valencia, Rémi Maurice, Sergio Pascual, Sònia Gavaldà, Vanessa Martínez and Verónica López.

I would like to thank Mónica and Eduardo for the flat. Thank you so much! Without you, I would have nowhere to live.

I should also not forget to express my gratitude to Rocío Recio for teaching me how to speak proper Spanish.

Thanks to all people who have helped me in one way or the other. Thank you so much!

Lastly, I would like to thank my family for support.

UNIVERSITAT ROVIRA I VIRGILI
COMPUTACIONAL STUDIES ON THE MECHANISM OF THE PAUSON-KHAND REACTION
Torstein Fjermestad
ISBN:978-84-693-9441-0/DL:T.62-2011

The work of this thesis has been possible thanks to financial support from the "Ministerio de Ciencia e Innovación " and the Institute of Chemical Research of Catalonia (ICIQ). The work has been carried out within the framework of the project "Diseño de Catalizadores para una Química Sostenible: Una Aproximación Integrada" (CONSOLIDER CSD2006-0003) belonging to the program CONSOLIDER-INGENIO 2010 of the " Ministerio de Ciencia e Innovación ".

UNIVERSITAT ROVIRA I VIRGILI
COMPUTACIONAL STUDIES ON THE MECHANISM OF THE PAUSON-KHAND REACTION
Torstein Fjermestad
ISBN:978-84-693-9441-0/DL:T.62-2011

UNIVERSITAT ROVIRA I VIRGILI
COMPUTACIONAL STUDIES ON THE MECHANISM OF THE PAUSON-KHAND REACTION
Torstein Fjermestad
ISBN:978-84-693-9441-0/DL:T.62-2011

Contents

UNIVERSITAT ROVIRA I VIRGILI
COMPUTACIONAL STUDIES ON THE MECHANISM OF THE PAUSON-KHAND REACTION
Torstein Fjermestad
ISBN:978-84-693-9441-0/DL:T.62-2011

CONTENTS

UNIVERSITAT ROVIRA I VIRGILI
COMPUTACIONAL STUDIES ON THE MECHANISM OF THE PAUSON-KHAND REACTION
Torstein Fjermestad
ISBN:978-84-693-9441-0/DL:T.62-2011

UNIVERSITAT ROVIRA I VIRGILI
COMPUTACIONAL STUDIES ON THE MECHANISM OF THE PAUSON-KHAND REACTION
Torstein Fjermestad
ISBN:978-84-693-9441-0/DL:T.62-2011

UNIVERSITAT ROVIRA I VIRGILI
COMPUTACIONAL STUDIES ON THE MECHANISM OF THE PAUSON-KHAND REACTION
Torstein Fjermestad
ISBN:978-84-693-9441-0/DL:T.62-2011

Chapter 1

Introduction

The Pauson-Khand reaction (PKR) is a formal [2+2+1] cycloaddition reaction between an alkene, an alkyne and a carbonyl to form a cyclopentenone in the presence of a metal complex [1–9]. PKR was initially discovered in 1971 in its stoichiometric

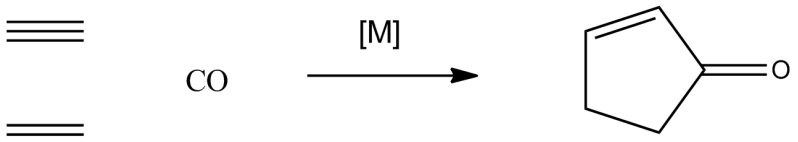

Figure 1.1: Schematic representation of the Pauson-Khand reaction

form after letting an alkyne and norbornadiene react in the presence of a dicobalt complex [1]. Shortly after, PKR was made catalytic [2] albeit requiring harsh conditions of high temperature and CO pressure. Moreover, only strained olefins proved reactive. For about the two first decades after being discovered, the PKR was only known to be catalysed by cobalt. In recent years, however, other metals such as titanium [10, 11], iron [12], rhodium [13–17], ruthenium [18–20], iridium [21, 22], nickel [23], zirconium [24], molybdenum [25, 26], tungsten [27] and palladium [28] are also shown to catalyse/mediate the PKR.

1.1 Synthetic applications

The PKR is capable of significantly upgrading the complexity of the compounds in just a single step. In the case of the intermolecular PKR, a cyclopentenone is made from simple starting materials. In the case of the intramolecular PKR, a bicyclic pentenone derivative is made from a non-cyclic substrate.

In total synthesis, one goal is to be able to make complex molecules from cheap starting material in as few steps as possible. In this respect, the Pauson-Khand reaction becomes a useful tool. We here mention some recent examples of synthesis of interesting molecules making use of the Pauson-Khand reaction. Most of the examples are taken from a recently published review on the topic [9].

UNIVERSITAT ROVIRA I VIRGILI
COMPUTACIONAL STUDIES ON THE MECHANISM OF THE PAUSON-KHAND REACTION
Torstein Fjermestad
ISBN:978-84-693-9441-0/DL:T.62-2011

1.1.1 Estrone E-ring extention

An estrone derived alkene reacted with a dicobalt hexacarbonyl complex to yield E-ring extended estrone derivatives [29] (figure 1.2).

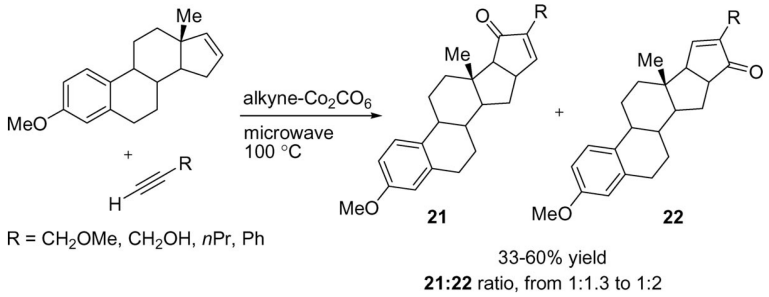

Figure 1.2: E-ring extension of an esterone derived alkene by the Pauson-Khand reaction. Taken from ref. [9]

1.1.2 A Nicolas + Pauson-Khand tandem reaction

Performing a tandem Nicolas + Pauson-Khand reaction results in a construction of a tricyclic compound from an acyclic starting material [30] (Figure 1.3).

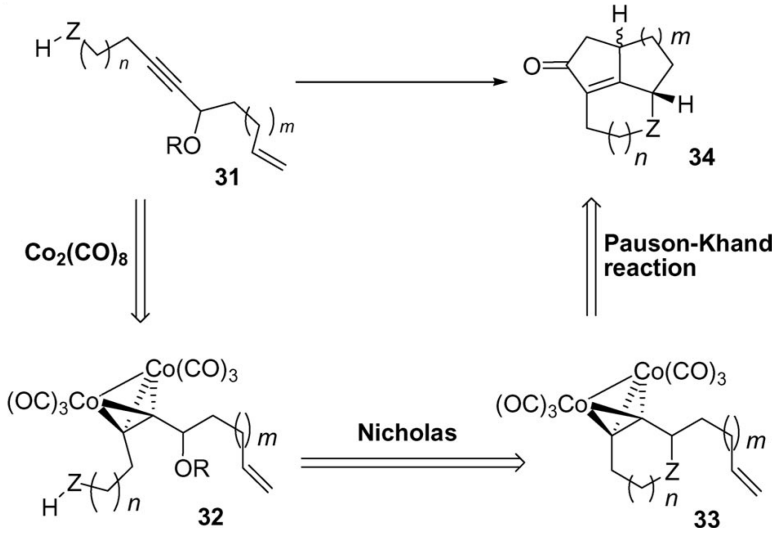

Figure 1.3: A Nicolas + Pauson-Khand tandem reaction. Taken from ref. [9]

1.1.3 Synthesis of carbanucleosides

Verdaguer and Riera have reported the synthesis of the carbanucleosides carbovir and abacavir using the intermolecular PKR as a key step in the synthesis [31] (Figure 1.4).

UNIVERSITAT ROVIRA I VIRGILI
COMPUTACIONAL STUDIES ON THE MECHANISM OF THE PAUSON-KHAND REACTION
Torstein Fjermestad
ISBN:978-84-693-9441-0/DL:T.62-2011

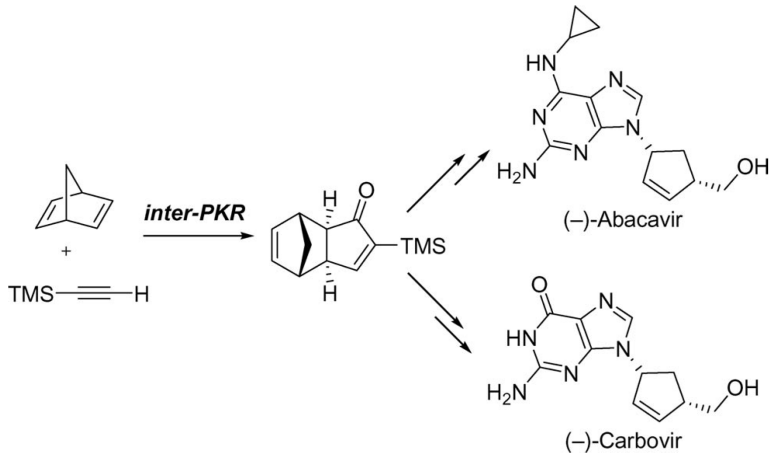

Figure 1.4: Synthesis of carbovir and abacavir with the intermolecular PKR as a key step. Taken from ref. [9]

1.1.4 Synthesis of Prostaglandin and Phytoprostane B_1

Verdaguer and Riera also reported the synthesis of prostaglandin and phytoprostane B_1 [32] (figure 1.5). In the synthesis, the intermolecular Pauson-Khand reaction was a key step.

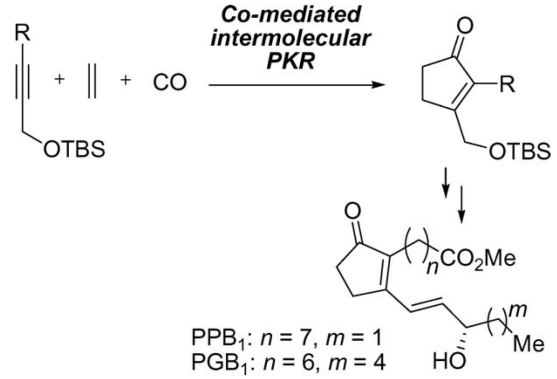

Figure 1.5: Synthesis of prostaglandin and phytoprostane B_1 via an intermolecular PKR

1.1.5 Porphyrin functionalisation

An interesting application of the intermolecular Pauson-Khand reaction was published by Senge *et al.* [33]. They used the intermolecular Pauson-Khand reaction to functionalise a porphyrin substituent (figure 1.6).

Furthermore they dimerized two porphyrins by letting an alkyne substituent of one porphyrin react with an alkene substituent of the other porphyrin in the presence of $Co_2(CO)_8$, i.e. the Pauson-Khand reaction (figure 1.7).

UNIVERSITAT ROVIRA I VIRGILI
COMPUTACIONAL STUDIES ON THE MECHANISM OF THE PAUSON-KHAND REACTION
Torstein Fjermestad
ISBN:978-84-693-9441-0/DL:T.62-2011

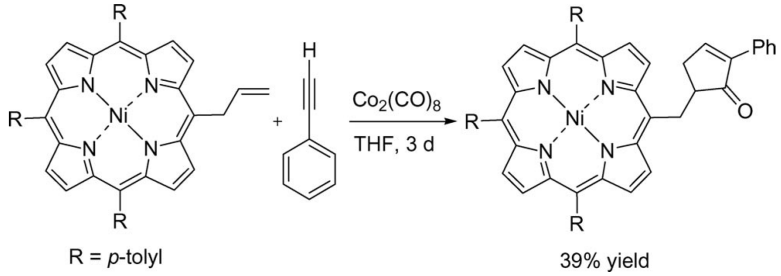

Figure 1.6: Functionalisation of a porphyrin substituent by use of the Pauson-Khand reaction. Taken from ref. [9]

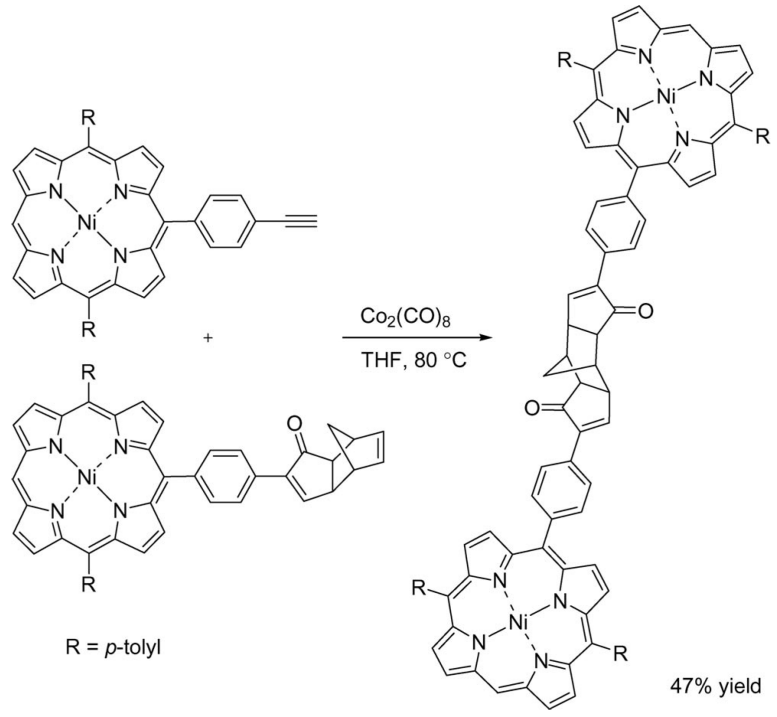

Figure 1.7: Dimerization of two prophyrins by letting their substituent react according to the Pauson-Khand reaction. Taken from ref. [9]

UNIVERSITAT ROVIRA I VIRGILI
COMPUTACIONAL STUDIES ON THE MECHANISM OF THE PAUSON-KHAND REACTION
Torstein Fjermestad
ISBN:978-84-693-9441-0/DL:T.62-2011

1.1.6 Pauson-Khand reaction with fullerene

Martín and co-workers [34] presented a [2+2+1] cycloaddition on a C_{60} fullerene (Figure 1.8).

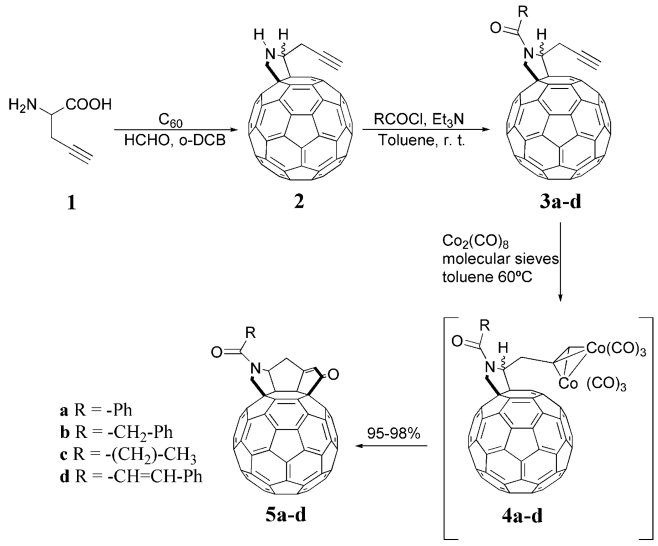

Figure 1.8: A Pauson-Khand reaction on a C_{60} fullerene. Taken from ref. [34]

1.2 Improving the reaction conditions

The PKR was in its original version intermolecular [1, 2]. Later, in 1981, Schore improved the methodology by connecting the alkyne and the alkene moieties by a linker and thus producing the first example of an intramolecular Pauson-Khand reaction [35]. Typical substrates of the intramolecular Pauson-Khand reaction are 1,6- and 1,7-enynes.

Because of the harsh conditions and low substrate scope of the first catalytic Pauson-Khand reaction [2], PKR was mostly carried out in its stoichiometric form. In 1990, however, Rautenstrauch improved the substrate scope by carrying out a catalytic PKR with unstrained olefins [36]. However, high CO pressures were still required. The requirement of high CO pressure was alleviated in 1998 when Livinghouse reported that 1 atm. of CO was sufficient to carry out PKR catalytically [37].

1.3 Mechanism

Detecting intermediates of the Pauson-Khand reaction proved to be difficult. For this reason the mechanism was for a long time unknown. However, in 1985 Magnus [38] and Schore [39] independently proposed the same mechanism consistent with the experimental observations. This proposal (Figure 1.9) has later served as a working hypothesis in experimental and computational studies.

UNIVERSITAT ROVIRA I VIRGILI
COMPUTACIONAL STUDIES ON THE MECHANISM OF THE PAUSON-KHAND REACTION
Torstein Fjermestad
ISBN:978-84-693-9441-0/DL:T.62-2011

At the time of the mechanistic proposal, only the hexacarbonyldicobalt(μ_2-alkyne) complex (**1** in figure 1.9) was known experimentally [40]. Later on, intermediate **2**, with one carbonyl dissociated, has been characterised by NMR spectroscopy for complexes with a substituent on the alkyne moiety that is coordinating to the vacant site of the cobalt atom [41–44]. Recently, also an X-ray structure of a trapped intermediate **3** has been published [45]. Indirect evidence for the metallacycle intermediate **4** has been obtained by interrupting the Pauson-Khand reaction under an atmosphere of O_2 [46].

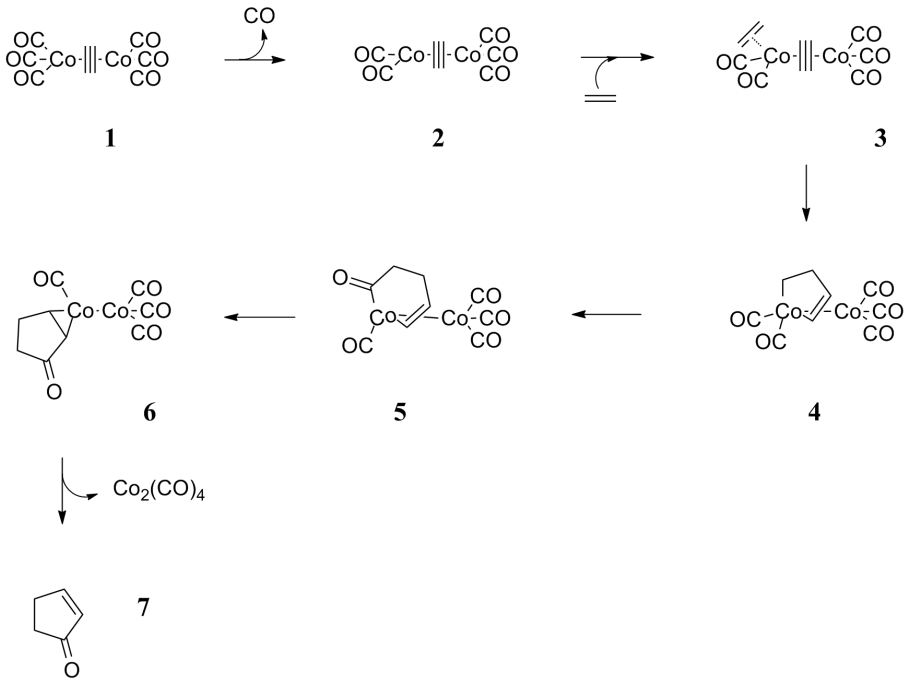

Figure 1.9: Mechanism of the Pauson-Khand reaction as proposed by Magnus [38] and Schore [39]

All these observations provided support for the Magnus-Schore proposal. However, important mechanistic information such as the energetics and the rate- and stereo-determining steps were still missing. The computational studies by Nakamura [47] and Pericàs [48] showed that the Magnus-Schore proposal produced a low-barrier process. Furthermore, these studies shed light on the rate- and stereo-determining events of the reaction. The transition state (TS) of the metallacycle formation, **3** $\longrightarrow$ **4**, is both the rate-determining and stereo-determining TS. Such information is of high value when it comes to the design of efficient catalysts for the Pauson-Khand reaction.

UNIVERSITAT ROVIRA I VIRGILI
COMPUTACIONAL STUDIES ON THE MECHANISM OF THE PAUSON-KHAND REACTION
Torstein Fjermestad
ISBN:978-84-693-9441-0/DL:T.62-2011

1.4 Heterogeneously catalysed Pauson-Khand Reaction

The Pauson-Khand reaction was for a long time only catalysed homogeneously by transition metal complexes. Recently, however, the first versions of PKR catalysed heterogeneously appeared. In 1999, Gibson and co-workers reported on a polymer-supported Pauson-Khand catalyst [49, 50]. The TONs were low, but the reaction could be performed under 1 atm. of CO. Later several heterogeneous Pauson-Khand systems with the catalyst supported on mesoporous silica [51] and charcoal [52] were reported on. Also colloidal Co nanoparticles [53] and Raney cobalt [54] could be used.

1.5 The Asymmetric Pauson-Khand Reaction

Synthesis of enantiopure compounds is of high importance, particularly for pharmaceutical applications. In this respect the asymmetric Pauson-Khand reaction becomes an important tool. Both stoichiometric [55–63] and catalytic [14, 21, 64–67] versions of the asymmetric Pauson-Khand reaction have been reported.

A particular example of a stoichiometric asymmetric Pauson-Khand reaction is the one where a pro-chiral $Co_2(CO)_6(\mu_2$-alkyne) is activated by a chiral N-oxide [68–70] (figure 1.10). In Chapter 6 of this thesis we describe our computational study on the asymmetric Pauson-Khand reaction where the chiral N-oxide is bucine N-oxide.

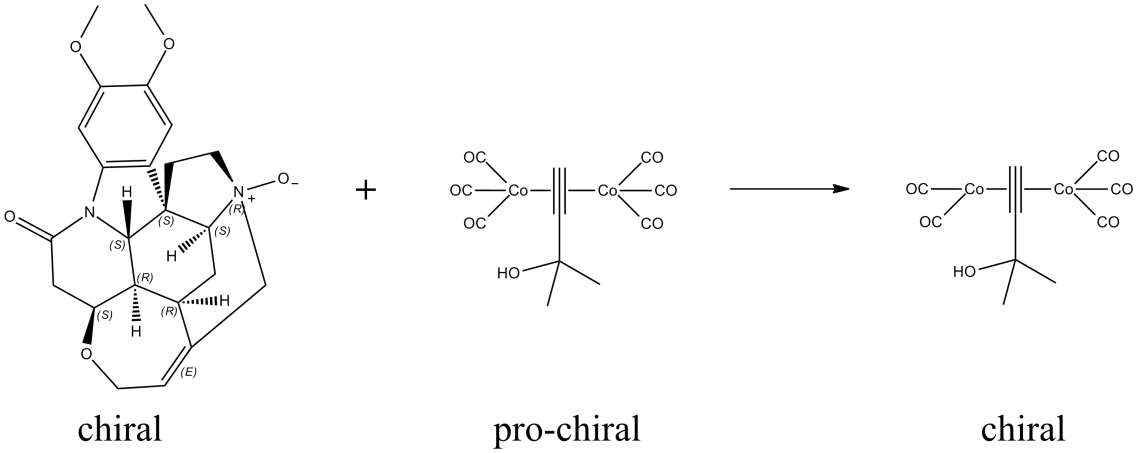

Figure 1.10: The pro-chiral dicobalt complex is activated by brucine. The chirality of the brucine is transferred to the activated dicobalt complex.

Most catalytic asymmetric reactions are being catalysed by a metal complex with a chiral ligand attached. This is also the case for the Pauson-Khand reaction. Two examples of asymmetric catalysts used in the Pauson-Khand reaction are a dicobalt complex with the chiral BINAP ligand attached [65, 71, 72] and a rhodium complex with a BINAP ligand attached [14, 16, 17, 73–75]. In this thesis we describe

UNIVERSITAT ROVIRA I VIRGILI
COMPUTACIONAL STUDIES ON THE MECHANISM OF THE PAUSON-KHAND REACTION
Torstein Fjermestad
ISBN:978-84-693-9441-0/DL:T.62-2011

computational studies on both of these examples. In chapter 4 we describe our computational study on the PKR catalysed by the chiral dicobalt complex, and in chapter 7 we describe our computational study on the PKR catalysed by a chiral rhodium complex.

1.6 Summary

The Pauson-Khand reaction is an important synthetic and catalytic process, specially in terms of complexity generation and atom economy. The catalytic and, specially, the enantioselective versions are, however, still limited in the scope of application. An improved mechanistic understanding would be key in the design of a better and more efficient process. Computational chemistry can be helpful in providing such a mechanistic understanding.

UNIVERSITAT ROVIRA I VIRGILI
COMPUTACIONAL STUDIES ON THE MECHANISM OF THE PAUSON-KHAND REACTION
Torstein Fjermestad
ISBN:978-84-693-9441-0/DL:T.62-2011

Chapter 2

Objectives

Although the Pauson-Khand reaction is a well established method for the synthesis of cyclopentenone rings operating in a variety of conditions, its enantioselective varieties have still a limited range of applications. A better understanding of the mechanistic features involved in enantioselectivity could help the development of more efficient processes.

One of the methods to introduce chirality in the Pauson-Khand reaction is the replacement of some of the carbonyl groups in the dicobalt catalyst by chiral ligands. A particularly relevant example in this concern is the use of $Co_2(CO)_4$(BINAP) as catalyst. A computational study of the mechanism for this process should account for all available experimental data and explain how the chirality is transferred from the ligand to the product.

The other major method for enantioselective Pauson-Khand reactions is the use of chiral activators with the standard catalyst. In this case, a preliminary study is necessary to analyse the reaction of the amine-oxide with metal coordinated carbonyl ligands. This can be accomplished through the study of the activation of metal carbonyl complexes ($M(CO)_{5,6}$) by trimethylamineoxide (TMAO). This understanding can then be applied to a real activator used in experiment, such as the chiral brucine N-oxide. For this case, it is particularly critical to understand the limitations that make the system only applicable at low temperature, and to see if these can be overcome by the use of different activators.

A different approach to enantioselective Pauson-Khand reaction is the use of chiral systems with catalysts not based on the dicobalt carbonyl model. A particularly intriguing example is that of $Rh(CO)(BINAP)^+$. In this case, the first challenge for the computational study is to evaluate if the general mechanism responds to the same Magnus scheme generally accepted for the dicobalt systems.

The mechanism for all these processes will be examined from a computational point of view in this computational thesis.

UNIVERSITAT ROVIRA I VIRGILI
COMPUTACIONAL STUDIES ON THE MECHANISM OF THE PAUSON-KHAND REACTION
Torstein Fjermestad
ISBN:978-84-693-9441-0/DL:T.62-2011

UNIVERSITAT ROVIRA I VIRGILI
COMPUTACIONAL STUDIES ON THE MECHANISM OF THE PAUSON-KHAND REACTION
Torstein Fjermestad
ISBN:978-84-693-9441-0/DL:T.62-2011

Chapter 3

Theory

A basic concept of computational chemistry is the use of results from quantum and classical mechanics to obtain information on the structure and properties of molecules and solids. The structure and properties obtained computationally can be compared with those obtained experimentally to ensure that the theoretical methods give an adequate description. The computational methods can then provide additional information on the system that can not be obtained by experimental techniques. In combination with experimental techniques, computational methods can thus provide important synergy effects in chemistry.

3.1 Methods of energy evaluation

A particularly important property of a molecular system is its energy. Below we briefly describe two methods of energy evaluation, density functional theory (DFT) and molecular mechanics (MM), that are applied in the elaboration of this thesis.

3.1.1 DFT

Density functional theory (DFT) states that the energy, E, of a system can be expressed as a functional of the electron density, $\rho(\mathbf{r})$, of the system:

$$E = F[\rho(\mathbf{r})] \tag{3.1}$$

DFT was developed in the mid 1960 by Hohenberg, Kohn and Sham [76, 77]. The theory further states that the functional is exact and universal, i.e applicable to any molecular system. The functional can be written as a sum of various terms:

$$E = T_S[\rho(\mathbf{r})] + J[\rho(\mathbf{r})] + E_{XC}[\rho(\mathbf{r})] + E_{Ne}[\rho(\mathbf{r})] \tag{3.2}$$

where $T_S[\rho(\mathbf{r})]$ is the kinetic energy of non-interacting electrons, $J[\rho(\mathbf{r})]$ is the classical electron-electron repulsion, $E_{Ne}[\rho(\mathbf{r})]$ is the electron-nucleus interaction and $E_{XC}[\rho(\mathbf{r})]$ is the exchange-correlation energy. $E_{XC}[\rho(\mathbf{r})]$ consists of the quantum-mechanical contributions to the potential energy (self-interaction correction, exchange and correlation) and the part of the kinetic energy that is not included in

UNIVERSITAT ROVIRA I VIRGILI
COMPUTACIONAL STUDIES ON THE MECHANISM OF THE PAUSON-KHAND REACTION
Torstein Fjermestad
ISBN:978-84-693-9441-0/DL:T.62-2011

$T_S[\rho(\mathbf{r})]$ [78, 79]. The exact form of the exchange-correlation functional, $E_{XC}[\rho(\mathbf{r})]$, is unknown and all attempts to calculate the total energy of the system rely on approximations to this term. The density functionals are classified according to the type of approximation that is made to $E_{XC}[\rho(\mathbf{r})]$. The approximation with the lowest level of complexity is the local density approximation (LDA) [78, 79] where the functional form of $E_{XC}[\rho(\mathbf{r})]$ only depends on the electron density, $\rho(\mathbf{r})$, at each point in space. The next level of complexity is the generalised gradient approximation (GGA) [78, 80] where the functional form of $E_{XC}[\rho(\mathbf{r})]$ depends on the electron density, $\rho(\mathbf{r})$, *and* the gradient of the electron density, $\nabla\rho(\mathbf{r})$, at each point in space. Examples of GGA functionals are BP86 [81, 82] and BLYP [81, 83, 84].

The exchange correlation functional, $E_{XC}[\rho(\mathbf{r})]$, includes the exchange energy. The Hartree-Fock theory provides the exact exchange energy and including a part of the Hartree-Fock exchange energy in $E_{XC}[\rho(\mathbf{r})]$ has been done to improve the functionals by reducing or eliminating the artificial self-exchange of the GGA functionals [80]. Functionals that include portions of the Hartree-Fock exchange energy are termed hybrid functionals [78, 80]. B3LYP [85, 86], one of the functionals used in this thesis, is an example of a hybrid-GGA functional.

After the GGA functionals, the next level of complexity is meta-GGA [80] where the spin kinetic energy density or $\nabla^2\rho(\mathbf{r})$ is included in $E_{XC}[\rho(\mathbf{r})]$ in addition to the electron density, $\rho(\mathbf{r})$, and the gradient, $\nabla\rho(\mathbf{r})$. By including the kinetic energy density, the self-correlation can be eliminated [80]. A recently developed meta-GGA functional is M06-L [87].

By adding in a portion of the Hartree-Fock exchange in $E_{XC}[\rho(\mathbf{r})]$, the meta-GGA functionals can be made hybrid thus reducing both the self-exchange and self-correlation present in the GGA functionals [80]. A recently developed hybrid meta-GGA functional is M06 [88] which is used in this thesis.

3.1.2 Molecular mechanics

A different approach to molecular modelling is the use of classical molecular mechanics (MM) instead of the quantum mechanically derived density functional theory. Molecular mechanics use the classical Newton's laws to compute the potential energy of the molecular system. The expression for the potential energy is usually a sum of the terms of different contributions to the potential energy. The potential energy contributions may come from bond stretching, angle bending, torsions and non-bonding interactions. The force field used in this thesis is the UFF force field [89].

The advantage of molecular mechanics methods is that they are computationally much faster than the quantum mechanics (QM) methods. The downside is that they provide no description of the electronic distribution in the system. MM methods are thus not appropriate for describing the bond formation and breaking of chemical reactions where significant changes in the electron distribution take place.

By using a QM/MM partitioning scheme (see below), we can take advantage of the fast MM methods by applying them to regions of the molecular system distant from

UNIVERSITAT ROVIRA I VIRGILI
COMPUTACIONAL STUDIES ON THE MECHANISM OF THE PAUSON-KHAND REACTION
Torstein Fjermestad
ISBN:978-84-693-9441-0/DL:T.62-2011

the region where the bond formation and breaking take place.

3.1.3 QM/MM

QM/MM methods are based on the division of the molecular system into a QM region where higher accuracy is desired and a MM region where some of the accuracy can be compromised. Several QM/MM methods exist [90, 91], differing in the energy expression (subtractive or additive QM/MM schemes), in the way the coupling between the two regions is described (mechanical or electrostatic embedding) and in the and in the treatment of the QM/MM boundary region (link atoms or local orbitals). In this thesis the ONIOM method [92–98], a substractive QM/MM scheme, is employed. Mechanical embedding is used to describe the coupling between the QM and the MM regions and hydrogens are used as link atoms.

3.2 Reaction Mechanism

This thesis concerns the computational study of a chemical reaction, and DFT and ONIOM calculations have been applied to the study of reaction mechanisms. In the rest of this chapter important concepts of reaction mechanisms, kinetics, selectivity and concentration and solvent corrections will be elaborated on.

A reaction mechanism describes how the starting materials of a chemical reaction are transformed into reaction products. This transformation consists in a reorganisation of the connectivity of the molecular system, that is, breaking and formation of chemical bonds. Such a reorganisation of the connectivity is accompanied by a change in the system energy, and along the transformation from reactants to products the system passes through transition states (TS) and minima of the energy surface. The minima of the energy surface are identified as intermediates. The transformation from one intermediate over a TS and further to the next intermediate is called an elementary step. The successive elementary steps connecting the reactants with the products constitute a reaction pathway. Typically for a molecular system there are several reaction pathways that can connect the reactants to the products. That is, there are several ways that the molecular connectivity can reorganise to get from the reactants to the products. Additionally, within each of these pathways, there are several conformational variations. The most likely pathway is the one with the lowest energy barrier when going from reactants to the products. However, a certain portion of the molecules follows the higher energy pathways as well. The distribution among the different pathways is given by the Boltzmann distribution. The Boltzmann distribution gives the probability, P_i, of a molecule to be in state i with an energy of ΔG_i. It is expressed as follows:

$$P_i = \frac{e^{-\Delta G_i/(RT)}}{Q(T)} \tag{3.3}$$

where R is the molar gas constant, T is the temperature and $Q(T)$ is the partition function. Putting in energy and temperature values in equation 3.3, we see that

UNIVERSITAT ROVIRA I VIRGILI
COMPUTACIONAL STUDIES ON THE MECHANISM OF THE PAUSON-KHAND REACTION
Torstein Fjermestad
ISBN:978-84-693-9441-0/DL:T.62-2011

the probability of occupying a state rapidly decreases as the energy increases. At an energy difference of 10 kJ/mol and a temperature of 298 K, the lower-energy state is preferred in 94% of the cases. If we are not concerned with selectivity issues (see below), we can thus only consider the lowest energy reaction pathway when discussing the reaction mechanism.

3.2.1 Kinetics

From the energy profile of the lowest energy reaction pathway, the kinetics of the reaction can be deduced. This can be done by calculating the rate constant of all elementary steps and integrating over time. Such a procedure can be relatively straightforward, but the rate equations and the integration can be tedious to implement. Furthermore, because of the high complexity of the equations, chemical insight to the problem may be difficult to obtain. One would thus prefer to simplify the problem in order to understand what factors determine the overall kinetics of the reaction. Kozuch et al. recently developed the energetic span model [99–102]. According to that model the turnover frequency (TOF) of the specific mechanism is determined from the TOF determining TS (TDTS) and the TOF determining intermediate (TDI). The TDTS and TDI are the pair of states that maximises the energetic span, δE, of the reaction. δE is expressed as follows:

$$\delta E = \begin{cases} T_{TDTS} - I_{TDI} & \text{If TDTS comes after TDI} \\ T_{TDTS} - I_{TDI} + \Delta G_{rx} & \text{If TDTS comes before TDI} \end{cases} \tag{3.4}$$

where T_{TDTS} is the free energy of TDTS, I_{TDI} is the free energy of TDI and ΔG_{rx} is the reaction free energy. To identify the TDTS and TDI, equation (3.4) is applied to all pairs of transition states and intermediates along the reaction profile. The pair that gives the largest δE is identified as TDTS and TDI. From the identified TDTS and TDI, the TOF can be calculated as follows:

$$TOF = \frac{k_B T}{h} \exp^{-\delta E/RT} \tag{3.5}$$

where k_B is Boltzmann's constant, T the temperature, h Planck's constant and R the molar gas constant. From equations (3.4) and (3.5) we see that TOF of the reaction only depends on two states along the free energy profile. The energetic span model thus enables us to better understand how the TOF depends on a key transition state and intermediate of the free energy profile. Furthermore, the energetic span model also makes us able to better understand the limitations of the catalytic system, and how the catalyst can be improved by lowering the TDTS free energy and/or increasing the TDI free energy.

3.2.2 Selectivity

In many cases the reactants can evolve towards several different products and we end up with a distribution of products instead of just one. At a particular intermediate, **I**, during the transformation from reactants to products, the reaction pathway splits

UNIVERSITAT ROVIRA I VIRGILI
COMPUTACIONAL STUDIES ON THE MECHANISM OF THE PAUSON-KHAND REACTION
Torstein Fjermestad
ISBN:978-84-693-9441-0/DL:T.62-2011

and the system has the possibility of evolving further in different directions (see figure 3.1). In the cases where the intermediate **I** is in equilibrium with the final products (figure 3.1, left), the distribution of the products is in accordance with the Boltzmann distribution of the product energies. The selectivity is controlled by the thermodynamics of the system.

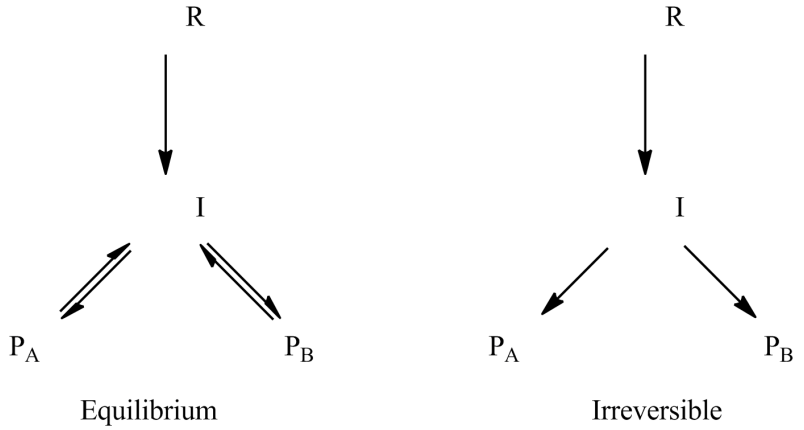

Figure 3.1: Selectivity controlled by thermodynamics (left) and kinetics (right).

In other cases, no equilibrium can be established between the products and intermediate **I**. In this case an irreversible elementary step separates the intermediate **I** from the products. An irreversible elementary step is characterised by having a forward reaction occurring at a much higher rate than the backward reaction. Thus, once the system has passed the TS of an irreversible elementary step, it can not go back again.

We now consider a hypothetical case where two pathways, each of them with an irreversible elementary step, are leading to two different products, A and B (figure 3.1, right). The product distribution would in this case be determined from the Boltzmann distribution of the TS energies of the two irreversible elementary steps leading to product A and B respectively. The two transition states, TS_A and TS_B may then be termed selectivity determining transition states. In this case the energy of the products has no influence on the product distribution. The selectivity is said to be controlled by the kinetics of the system.

We now expand the example of the kinetically controlled selectivity above by considering the possibility that several pathways can lead to the same product, A or B. The pathways leading to product A, we label A1, A2, ..., An and the pathways leading to product B we label B1, B2, ..., Bn. The transition states of the irreversible elementary step corresponding to these pathways, we label TS_{A1}, TS_{A2}, ...,TS_{An} and TS_{B1}, TS_{B2}, ..., TS_{Bn} respectively. From equation 3.3 and trivial probability considerations, we find that the product distribution of A and B, $P_{A/B}$, is given by the ratio of the sum of the Boltzmann weights of the energy of TS_{A1}, TS_{A2}, ...,TS_{An} and the sum of the Boltzmann weights of the energy of TS_{B1}, TS_{B2}, ...,TS_{Bn}:

$$P_{A/B} = \frac{\sum_i e^{-\Delta G_{Ai}/(RT)}}{\sum_i e^{-\Delta G_{Bi}/(RT)}} \tag{3.6}$$

UNIVERSITAT ROVIRA I VIRGILI
COMPUTACIONAL STUDIES ON THE MECHANISM OF THE PAUSON-KHAND REACTION
Torstein Fjermestad
ISBN:978-84-693-9441-0/DL:T.62-2011

where ΔG_{Ai} is the free energy of TS_{Ai} and ΔG_{Bi} is the free energy of TS_{Bi}.

3.2.3 Calculation of Enantiomeric Excess

A particularly important example of selectivity is the enantioselectivity. Two enantiomers are mirror images of one another and must have equal energies. Enantioselectivity can thus only be governed by the kinetics of the system.

On the contrary to enantiomers, diastereomers have different energies. To obtain an enantiomeric excess of a chiral product, the reaction must go through a diastereomeric TS. The origin of the enantioselectivity is that the pathways leading to the minor enantiomer (say the R enantiomer) all go through diastereomeric TSs that are higher in energy compared to the most stable diastereomeric TS leading to the major enantiomer (say the S enantiomer). The enantiomeric ratio, er, is the ratio of the R and the S enantiomers and is given by an equation analogous to equation (3.6):

$$er = \frac{\sum_i e^{-\Delta G_{Ri}/(RT)}}{\sum_i e^{-\Delta G_{Si}/(RT)}} \tag{3.7}$$

where ΔG_{Ri} are energies of TSs leading to the R product and ΔG_{Si} are energies of TSs leading to the S product.

The enantiomeric ratio, er, is related to the enantiomeric excess, ee, through the following equation:

$$\%ee = 100\% * \frac{1 - er}{1 + er} \tag{3.8}$$

Subsequent Racemisation

A particular important concept in the context of enantioselectivity is the possibility of a racemisation occurring after the chirality has been induced (See figure 3.2). In this case, even though the system has passed the enantioselective determining TS, the system can still evolve from the major enantiomer to the minor enantiomer along the racemisation pathway. Chapter 6 shows an example of a subsequent racemisation. There the pathways leading to the R and the S products are interconnected through a racemisation step. The lower the barrier of this racemisation step, the lower the enantiomeric excess of the final product. However good the enantiodiscrimination at a previous step is, the final enantiomeric excess will be largely determined by the barrier of the racemisation step.

3.2.4 Concentration and Standard State corrections of the free energy barriers

When calculating energies of molecular systems using an electronic structure program, concentrations of 1M at standard state are assumed. As long as there is a 1:1 stoichiometry of the reactants, the result is valid at any concentration. In some cases

UNIVERSITAT ROVIRA I VIRGILI
COMPUTACIONAL STUDIES ON THE MECHANISM OF THE PAUSON-KHAND REACTION
Torstein Fjermestad
ISBN:978-84-693-9441-0/DL:T.62-2011

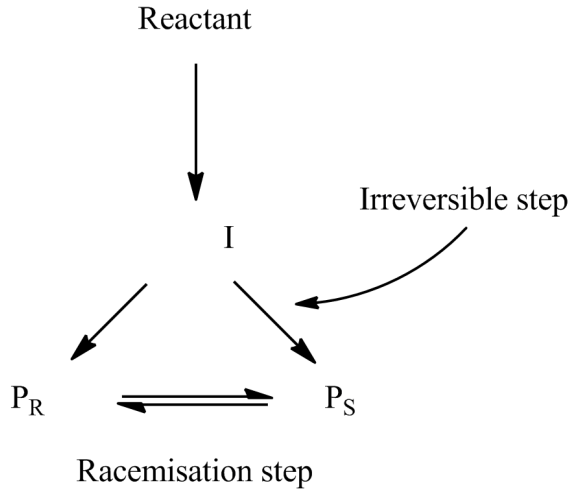

Figure 3.2: The two enantiomers P_R and P_S are connected through a racemisation pathway. The enantiomeric excess will largely be dependent on the height of the racemisation barrier.

however, a 1:1 stoichiometry cannot be assumed. An example is a CO dissociation from a metal complex occurring under an atmosphere of constant CO pressure.

$$M - CO \longrightarrow M + CO(solv) \tag{3.9}$$

In this equilibrium, the total concentration of the metal complexes, $[M - CO]$ and $[M]$ is fixed by the initial concentration of the metal complex put into the reaction mixture. The concentration of [CO(solv)], on the other hand, is fixed by the external CO pressure and the solvation energy of CO. Thus the equilibrium concentrations of the species in equation (3.9) are determined by the external CO pressure. At low CO pressures, the concentration of CO(solv) is low, and the equilibrium will be largely shifted to the right. M has thus a higher concentration than what the ΔG° value of equilibrium (3.9) would suggest. M-CO and M might proceed towards the products along different reaction pathways as shown schematically in figure 3.3.

If we want to compare the reactivity of M-CO and M, we must take into account the higher concentration and thus the higher reactivity of M compared to the standard state conditions. To be able to quantitatively compare transition states with CO coordinated, TS_{MCO}, and transition states with CO dissociated, TS_M, we introduce the quantity *apparent Gibbs free energy*, ΔG_{app}. In the following, we derive an expression relating ΔG_{app} to ΔG°.

We consider the dissociation of one and two carbonyls and derive an expression for ΔG_{app} in each of the cases: ΔG_{app1CO} in the case of one CO dissociation and ΔG_{app2CO} in the case of two CO dissociations.

UNIVERSITAT ROVIRA I VIRGILI
COMPUTACIONAL STUDIES ON THE MECHANISM OF THE PAUSON-KHAND REACTION
Torstein Fjermestad
ISBN:978-84-693-9441-0/DL:T.62-2011

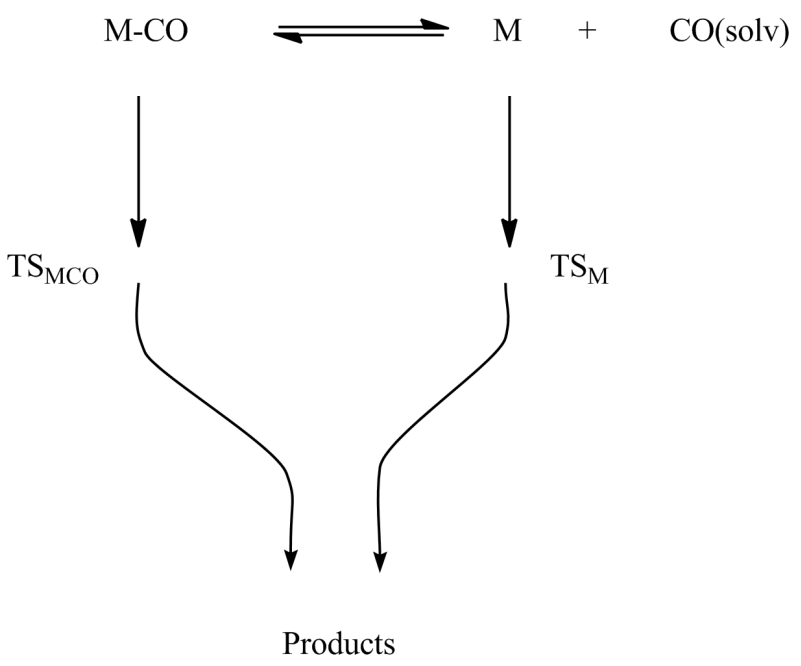

Figure 3.3: Schematic representation of the different reaction pathways of M-CO and M towards the products. The preferred reaction pathway will depend on the relative energies of TS_{MCO} and TS_M *and* the position of the equilibrium.

Dissociation of one carbonyl

The dissociation of one carbonyl is shown in equation (3.9). The corresponding equilibrium constant is

$$K_1 = \frac{[\mathrm{M}][\mathrm{CO(solv)}]}{[\mathrm{M-CO}]} = e^{-\Delta G_1/RT} \tag{3.10}$$

In addition there is an equilibrium between CO in gas phase and CO in solution:

$$\mathrm{CO(g)} \longrightarrow \mathrm{CO(solv)} \tag{3.11}$$

The corresponding equilibrium constant is expressed as:

$$K_{\mathrm{CO},corr} = \frac{[\mathrm{CO(solv)}]}{\mathrm{P_{CO}}} = e^{-\Delta G_{\mathrm{CO},corr}/RT} \tag{3.12}$$

In $\Delta G_{\mathrm{CO},corr}$ the conversion from a standard state of 1 atm. to a standard state of 1M is taken into account (see below).

We proceed by solving equation (3.12) for [CO(solv)] and insert the expression into equation (3.10). We can further define an apparent equilibrium constant, K_{app}, from K_1, $K_{\mathrm{CO},corr}$ and the constant CO pressure, P_{CO}.

$$K_{app} = \frac{K_1}{K_{\mathrm{CO},corr} P_{CO}} = \frac{[\mathrm{M}]}{[\mathrm{M-CO}]} = e^{-(\Delta G_1 - \Delta G_{\mathrm{CO},corr} + RT\ln(P_{CO}))/RT} \tag{3.13}$$

By analogy with equation (3.10), we define $\Delta G_{app1\mathrm{CO}}$ as

$$\Delta G_{app1\mathrm{CO}} = \Delta G_1 - \Delta G_{\mathrm{CO},corr} + RT\ln(P_{CO}) \tag{3.14}$$

We see that $\Delta G_{app1\mathrm{CO}}$ is decreased by increasing $\Delta G_{\mathrm{CO},corr}$ and by lowering the CO pressure.

Dissociation of two carbonyls

Equation (3.15) shows the equilibrium in the case of dissociation of two carbonyls

$$\mathrm{M} - 2\mathrm{CO} \longrightarrow \mathrm{M} + 2\mathrm{CO(solv)} \tag{3.15}$$

The corresponding equilibrium constant is

$$K_2 = \frac{[\mathrm{M}][\mathrm{CO(solv)}]^2}{[\mathrm{M} - 2\mathrm{CO}]} = e^{-\Delta G_2/RT} \tag{3.16}$$

By proceeding in the same manner as for the derivation of $\Delta G_{app1\mathrm{CO}}$, we arrive at the following equation for the apparent equilibrium constant.

$$K_{app} = \frac{K_2}{K^2_{\mathrm{CO},corr}P^2_{CO}} = \frac{[\mathrm{M}]}{[\mathrm{M} - 2\mathrm{CO}]} = e^{-(\Delta G_2 - 2[\Delta G_{\mathrm{CO},corr} + RT\ln(P_{CO})])/RT} \tag{3.17}$$

By analogy with equation (3.17), we define $\Delta G_{app2\mathrm{CO}}$ as

$$\Delta G_{app2\mathrm{CO}} = \Delta G_2 - 2[\Delta G_{\mathrm{CO},corr} + RT\ln(P_{CO})] \tag{3.18}$$

We can generalise equation (3.14) and (3.18) by noting that the coefficient in front of the square bracket in equation (3.18) indicates the number of carbonyls being dissociated. Thus for dissociation of n carbonyls, $\Delta G_{app,n\mathrm{CO}}$ is

$$\Delta G_{app,n\mathrm{CO}} = \Delta G_n - n[\Delta G_{\mathrm{CO},corr} + RT\ln(P_{CO})] \tag{3.19}$$

Standard state conversion

The Gibbs free energy of the CO solvation process, $\Delta G_{\mathrm{CO},corr}$, can be computed as the difference between ΔG for CO in solution and ΔG for CO in gas phase. When using the output from a calculation, we are considering the process of taking 1 M of CO in gas phase to 1 M of CO in solution:

$$CO(g) \quad 1\mathrm{M} \longrightarrow CO(solv) \quad 1\mathrm{M} \tag{3.20}$$

The free energy difference for this process we label $\Delta G^{\circ}_{\mathrm{CO},corr}$. Using the standard free energy change, $\Delta G^{\circ}_{\mathrm{CO},corr}$, can sometimes be impractical however, because gas phase concentrations are normally reported as pressures in atm. A more practical solution would be to compute the free energy change, $\Delta G_{\mathrm{CO},corr}$, of converting 1 atm. of CO in gas phase to 1M of solvated CO [103].

$$\Delta G_{\mathrm{CO},corr} = \Delta G^{\circ}_{\mathrm{CO},corr} + RT\ln\left(\frac{C \quad [1\mathrm{M}]}{P \quad [1\mathrm{atm.}]}\right) \tag{3.21}$$

UNIVERSITAT ROVIRA I VIRGILI
COMPUTACIONAL STUDIES ON THE MECHANISM OF THE PAUSON-KHAND REACTION
Torstein Fjermestad
ISBN:978-84-693-9441-0/DL:T.62-2011

We choose the standard state of the gas phase to be 1 atm. and we calculate how many moles of CO there are in 1 L at 1 atm. and 298 K. Assuming the ideal gas approximation, the concentration of gaseous CO is 1/24.5 mol L^{-1}. $\Delta G_{CO,corr}$ is then calculated as the free energy difference between 1/24.5 M of gaseous CO and 1 M of solvated CO. Putting these two numbers into equation (3.21) we get

$$\Delta G_{CO,corr} = \Delta G^{\circ}_{CO,corr} + RT \ln (24.5) \tag{3.22}$$

Using the values of R = 8.314472 J $mol^{-1}K^{-1}$ and T = 298 K, we see that $RT \ln (24.5)$ is equal to 8 kJ/mol. Thus to compute the correct Gibbs free energy value of the CO solvation process, $\Delta G_{CO,corr}$, we have to add 8 kJ/mol to the value of $\Delta G^{\circ}_{CO,corr}$.

The use of apparent Gibbs free energy, ΔG_{app}, is essential in the study of the cobalt catalysed Pauson-Khand reaction described in Chapter 4 and the rhodium catalysed Pauson-Khand reaction described in Chapter 7. Both of these reactions occur under an atmosphere of constant CO pressure. Furthermore, mechanistic alternatives differing in the number of carbonyls coordinated to the metal centre are available for both systems. Using ΔG_{app}, mechanisms with more carbonyls dissociated are relatively more favoured than what the ΔG° value should suggest.

UNIVERSITAT ROVIRA I VIRGILI
COMPUTACIONAL STUDIES ON THE MECHANISM OF THE PAUSON-KHAND REACTION
Torstein Fjermestad
ISBN:978-84-693-9441-0/DL:T.62-2011

Chapter 4

Co-catalysed Pauson-Khand reaction

Hiroi and co-workers were the first to attach a BINAP ligand to a dicobalt carbonyl complex, and to transform several 1,6-enynes to the corresponding bicyclic pentenones in high enantiomeric excess [65]. Later on, Gibson and co-workers were able to crystallise the (S)-BINAP + dicobalt carbonyl complex. The X-ray structure showed that the BINAP was chelating to one cobalt atom [71, 72]. Figure 4.1 shows the X-ray structure published. The experiments were carried out in

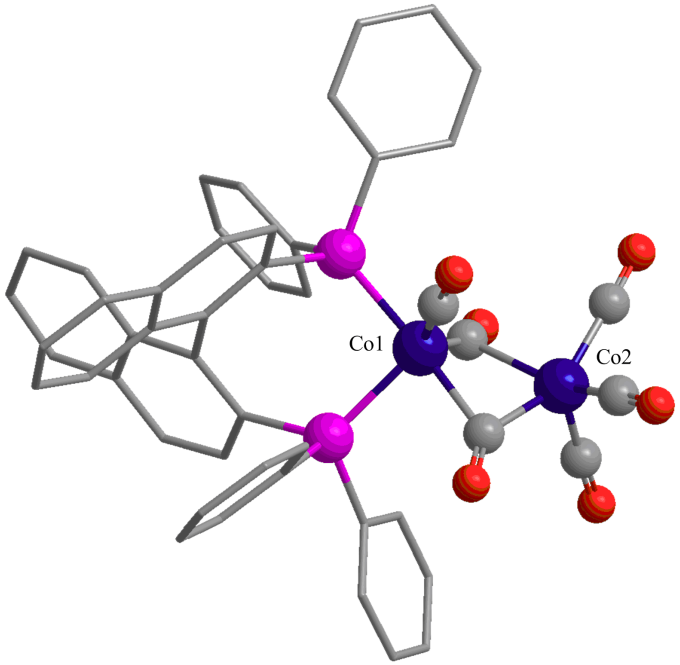

Figure 4.1: X-ray structure of the catalyst precursor published by Gibson [71, 72].

dimethoxyethane (DME) under an atmosphere of CO at a pressure of 1.05 atm. The reaction temperature was 75 °C. In particular the 1,6-enyne *N*-allyl-4-methyl-*N*-(prop-2-yn-1-yl)benzenesulfonamide (see figure 4.2), was converted to the corresponding cyclopentenone in 88% ee (R).

UNIVERSITAT ROVIRA I VIRGILI
COMPUTACIONAL STUDIES ON THE MECHANISM OF THE PAUSON-KHAND REACTION
Torstein Fjermestad
ISBN:978-84-693-9441-0/DL:T.62-2011

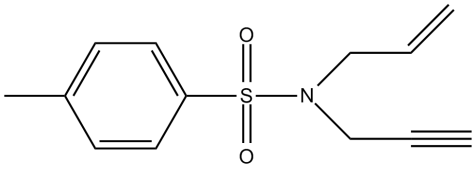

N-allyl-4-methyl-*N*-(prop-2-yn-1-yl)benzenesulfonamide

Figure 4.2: The 1,6-enyne used in the calculations.

The results by Gibson provided important information on the structure of the catalyst, in particular on the binding mode of the chiral ligand BINAP. The overall mechanism was however still unknown. We set out to characterise computationally the mechanism with the goal of identifying the step where enantioselection is determined and the specific role of BINAP directing the selectivity. In our model we used the X-ray structure reported by Gibson (figure 4.1) as catalyst and the 1,6-enyne in figure 4.2 as substrate. The mechanistic alternatives considered are outlined in the following section.

4.1 Mechanistic alternatives

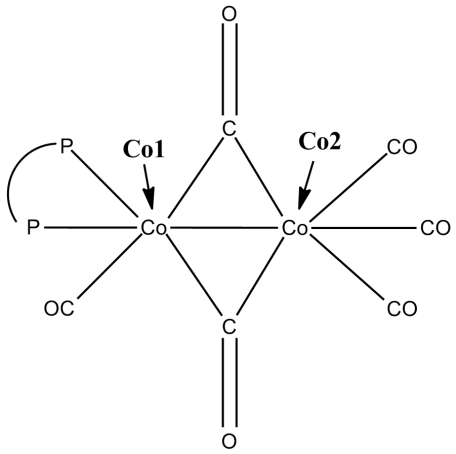

Figure 4.3: Schematic representation of the catalyst precursor reported by Gibson [71, 72].

4.1.1 The Magnus mechanism

The generally accepted mechanism for the Pauson-Khand reaction catalysed by a dicobalt complex is that proposed by Magnus [38] and Schore [39]. According to this proposal, the alkyne moiety of the substrate is exchanged with the two bridging carbonyls of the catalyst precursor and is coordinated in a bridging fashion to the two cobalt atoms. Thereafter one carbonyl of the BINAP-free cobalt (Co2 in figure 4.3) dissociates and leaves a vacant site in the coordination sphere of the cobalt

UNIVERSITAT ROVIRA I VIRGILI
COMPUTACIONAL STUDIES ON THE MECHANISM OF THE PAUSON-KHAND REACTION
Torstein Fjermestad
ISBN:978-84-693-9441-0/DL:T.62-2011

atom for the alkene moiety of the substrate to enter into. The mechanism continues with an oxidative cycloaddition to form a metallacycle intermediate. Further on from the metallacycle intermediate, a carbonyl is inserted into the cobalt-alkene bond forming a carbonylated metallacycle. The cyclopentenone product is released from the complex through a reductive elimination. Figure 4.4 shows a schematic representation of the Magnus mechanism for this system.

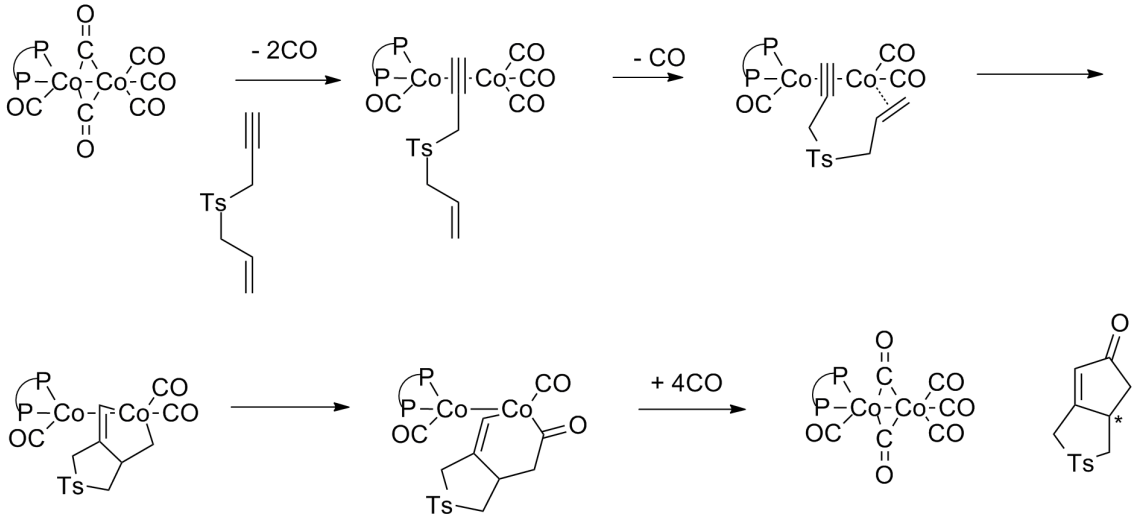

Figure 4.4: Schematic representation of the Magnus mechanism.

4.1.2 A modified Magnus mechanism

Compared to the traditionally employed $Co_2(CO)_8$ complex, the chelating BINAP-complex has two of the terminal carbonyls substituted with phosphorus ligands. A phosphorus ligand is a weaker π acceptor than a carbonyl ligand. The $(BINAP)Co_2(CO)_6$ complex should thus have a higher electron density on the BINAP coordinated cobalt atom (Co1) compared to the cobalt atoms in the $Co_2(CO)_8$ complex. This electronic effect plus the presence of the steric bulk of the BINAP lead Gibson and co-workers to propose a modified Magnus mechanism for this system. The increased electron density on Co1 (see figure 4.3) would disfavour a bridging coordination of the electron rich alkyne. Gibson and co-workers suggested that both the alkyne and alkene of the substrate would coordinate to Co2. Figure 4.5 shows a schematic representation of this modified Magnus mechanism.

4.1.3 CO insertion

A third mechanistic possibility would be an analogue to the mechanism published by Wang and Wu for the Ru catalysed Pauson-Khand mechanism [104]. One of the carbonyls of Co2 could insert into the cobalt-alkyne bond thus creating a four-membered carbonylated metallacycle intermediate. At the same time, the CO insertion would generate a vacant site in the coordination sphere of Co2 for the alkene moiety of the

UNIVERSITAT ROVIRA I VIRGILI
COMPUTACIONAL STUDIES ON THE MECHANISM OF THE PAUSON-KHAND REACTION
Torstein Fjermestad
ISBN:978-84-693-9441-0/DL:T.62-2011

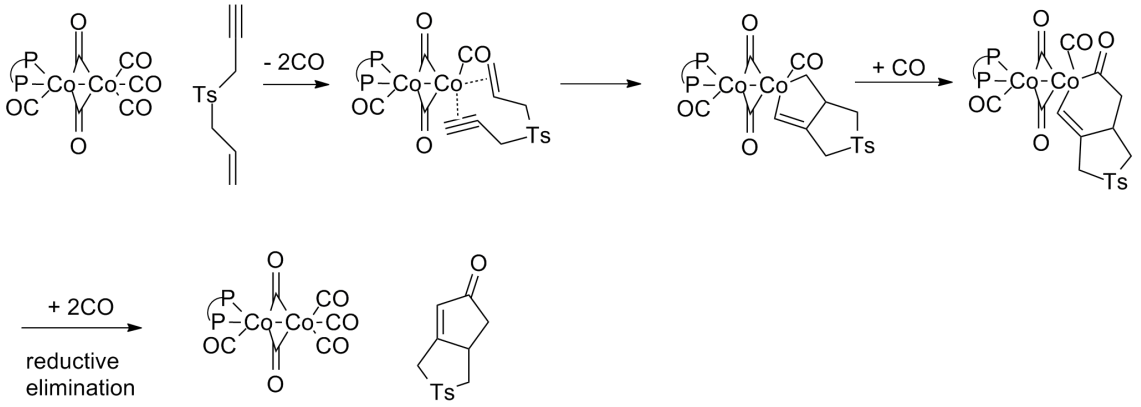

Figure 4.5: Schematic representation of the modified Magnus mechanism.

substrate to enter into. An oxidative coupling between the alkene and alkyne would lead to a 6-membered carbonylated metallacycle intermediate. The cyclopentenone product would then be released through a reductive elimination. Figure 4.6 shows a schematic representation the mechanism.

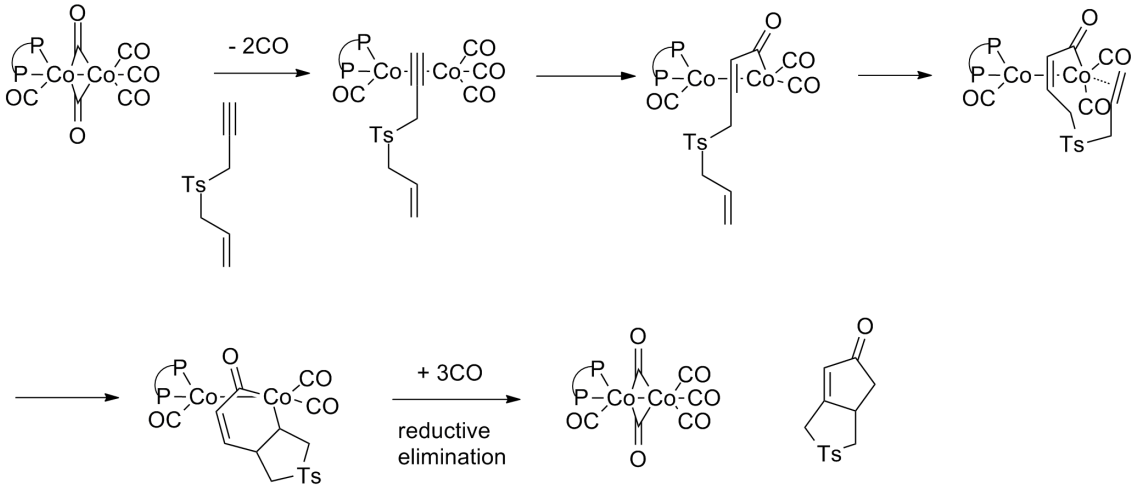

Figure 4.6: Schematic representation of the CO insertion mechanism.

4.2 Computational details

The calculations were carried out using the Gaussian 03 program package [105]. The method used for the energy evaluations was ONIOM(B3LYP:UFF) [85, 86, 89, 92, 95]. The partition between the QM and MM regions used for the mechanistic explorations is that of ONIOM partition 1 shown in figure 4.7. For the calculation of the enantiomeric excess, where more accurate energy differences are required, ONIOM partition 2 and ONIOM partition 3 (see figure 4.7), with extended QM regions were used. The basis set for the non-metal atoms was 6-31G(d) [106]. For the Co atoms, the core electrons were substituted by the Los Alamos effective core

UNIVERSITAT ROVIRA I VIRGILI
COMPUTACIONAL STUDIES ON THE MECHANISM OF THE PAUSON-KHAND REACTION
Torstein Fjermestad
ISBN:978-84-693-9441-0/DL:T.62-2011

potential, LANL2DZ, and the associated double zeta basis set was used for the valence electrons [107]. All minima and transition states were fully optimised without symmetry restrictions. The minima were identified by having only positive eigenvalues in the Hessian matrix whereas the transition states were identified by having a Hessian matrix with exactly one negative eigenvalue. The Gibbs free energy values are reported.

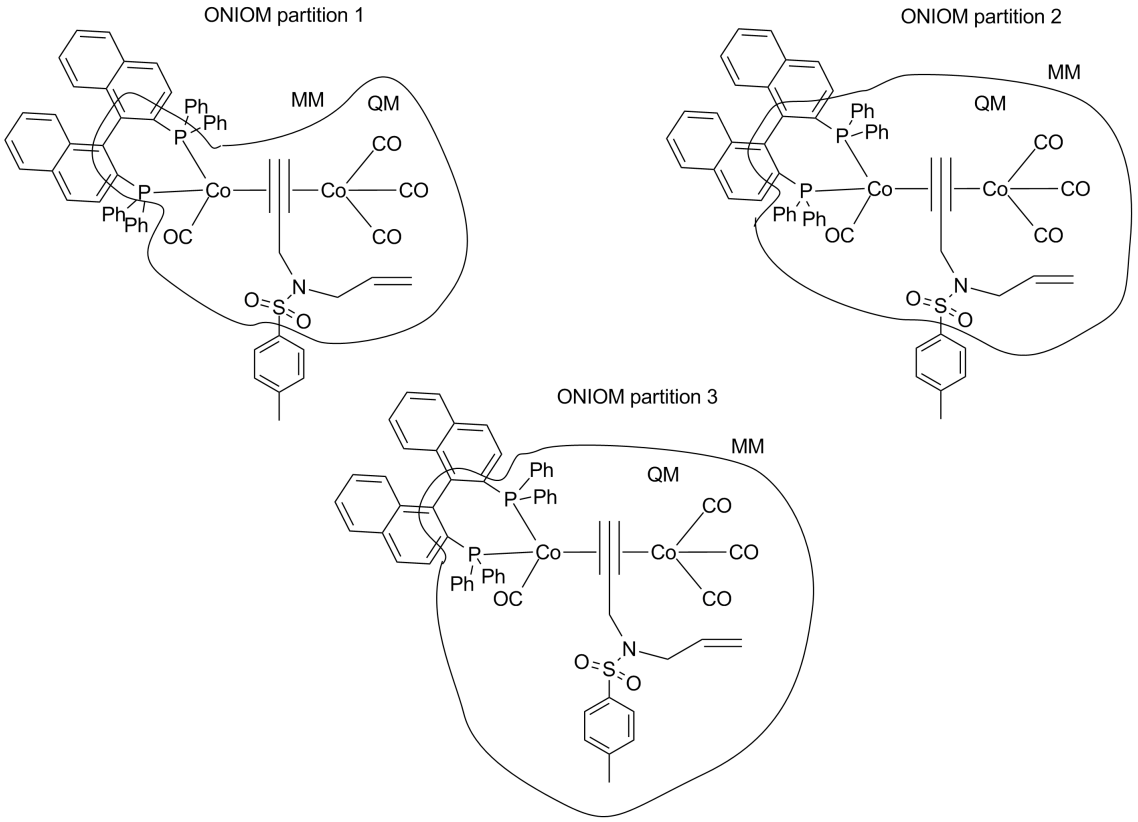

Figure 4.7: The QM and MM regions of ONIOM partition 1, 2 and 3.

An important mechanistic issue is the number of carbonyl ligands coordinated to the dicobalt complex. Enthalpically, the complex will prefer to have all its coordination sites saturated. Entropically however, a dissociation of the carbonyl ligands is preferred. Additionally, the low concentration of CO solvated in DME will further favour CO dissociation. From equation (3.14) we see that at 1 atm. of external CO pressure, the dissociation of CO is favoured by an additional $\Delta G_{\mathrm{CO},corr}$ compared to what would be the case at standard state conditions. To estimate this additional preference for dissociation, we calculated the free energy of the CO solvation process in DME, $\Delta G_{\mathrm{CO},corr}$. The calculation of the free energy of the CO solvation process was done using the SMD solvent model [108] implemented in Gaussian 09. DME is not defined as an option for continuum solvent calculations in Gaussian 09. Because the dielectric constant largely defines the properties of the solvent, we opted for using a different solvent, but with the same dielectric constant as DME. The dielectric constant changes with temperature. The highest temperature value for DME tabulated in the Handbook of Chemistry and Physics [109] is 6.62 at 45°C.

UNIVERSITAT ROVIRA I VIRGILI
COMPUTACIONAL STUDIES ON THE MECHANISM OF THE PAUSON-KHAND REACTION
Torstein Fjermestad
ISBN:978-84-693-9441-0/DL:T.62-2011

In the calculations we thus used as solvent ethanethiol with a dielectric constant of 6.667. Apart from the CO concentration effect, solvent corrections were excluded from the calculations.

4.3 Free energy profiles of the alternative mechanisms

As common zero-level for all the free energy profiles, we use ADD1 (see figure 4.8), the intermediate with the two bridging carbonyl ligands replaced by the alkyne moiety of the enyne. ADD1 contains 4 carbonyl groups. Intermediates and transition states along the different mechanisms with a number of carbonyls different from 4 will have an apparent free energy, ΔG_{app}, different from ΔG° according to equation (3.19). In particular structures containing 3 carbonyl groups (one CO dissociated), have a ΔG_{app} being $\Delta G_{\mathrm{CO},corr} + RT\ln(P_{CO})$ lower than ΔG°. For structures containing 5 carbonyl groups, ΔG_{app} is $\Delta G_{\mathrm{CO},corr} + RT\ln(P_{CO})$ higher than ΔG°. $\Delta G_{\mathrm{CO},corr}$ of CO in DME is 19 kJ/mol. At 1.05 atm. of external pressure, structures with three carbonyl groups will be lowered by 19 kJ/mol whereas structures with five carbonyl groups will have their energy risen by 19 kJ/mol. In the free energy profiles below, the free energy at standard state conditions, ΔG°, is indicated with a black line. The apparent free energy, ΔG_{app}, is indicated with a magenta line.

4.3.1 Magnus mechanism

The Magnus mechanism catalysed by the $Co_2(CO)_8$ complex has been previously investigated computationally [47, 48] as mentioned in the introduction. However, substituting two of the carbonyls by a BINAP could lead to qualitative changes in the free energy reaction profile. Furthermore, the lower barrier of ΔG_{app} as a consequence of the CO dissociation has not been taken into account in the context of the Pauson-Khand reaction. Previous computational works assumed that the metallacycle and the carbonylated metallacycle intermediates were most stable when the coordination sphere of Co2 was saturated with an additional CO ligand. Considering the relative preference for CO dissociation at low CO concentration, the mechanism may as well be without this saturation. In the following we consider mechanistic alternatives where the metallacycle and the carbonylated metallacycle intermediates have 3 or 4 carbonyls incorporated in the complex. Another mechanistic variation concerns the carbonylated metallacycle formation. The CO could insert into the cobalt-alkenyl bond as well as into the cobalt-alkyl bond of the metallacyle. This makes in total four mechanistic variations of the Magnus mechanism:

- **Magnus1**: Three carbonyls incorporated in the metallacycle and the carbonylated metallacycle intermediates, and CO insertion into the cobalt-alkyl bond.
- **Magnus2**: Three carbonyls incorporated in the metallacycle and the carbonylated metallacycle intermediates, and CO insertion into the cobalt-alkenyl bond.

UNIVERSITAT ROVIRA I VIRGILI
COMPUTACIONAL STUDIES ON THE MECHANISM OF THE PAUSON-KHAND REACTION
Torstein Fjermestad
ISBN:978-84-693-9441-0/DL:T.62-2011

- **Magnus3**: Four carbonyls incorporated in the metallacycle and the carbonylated metallacycle intermediates, and CO insertion into the cobalt-alkyl bond. This was the mechanism considered in previous computational studies [47, 48].

- **Magnus4**: Four carbonyls incorporated in the metallacycle and the carbonylated metallacycle intermediates, and CO insertion into the cobalt-alkenyl bond.

We have tested all possibilities and the free energy profiles, ΔG° and ΔG_{app}, are shown below.

Magnus1. Four carbonyls incorporated and carbon monoxide insertion into the cobalt-alkyl bond

Figure 4.8 shows the free energy profiles, ΔG° and ΔG_{app}, of the **Magnus1** mechanism. In the following, when we discuss the profiles of the individual mechanisms,

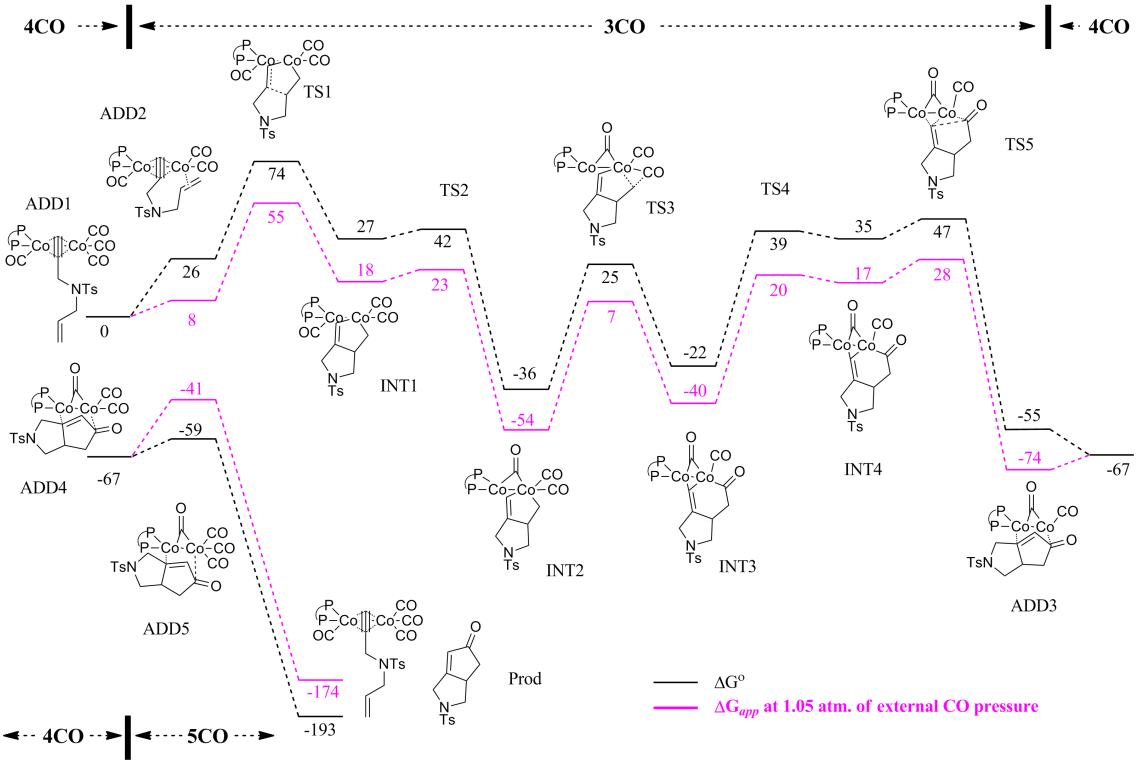

Figure 4.8: Free energy profiles, ΔG° and ΔG_{app}, of the **Magnus1** mechanism. Energies in kJ/mol. The ranges of the mechanistic pathway with three, four and five carbonyls incorporated in the complex are indicated.

we use the values of the ΔG°. Afterwards, when comparing the mechanisms, we will be using ΔG_{app} values.

The reaction starts from ADD1 and passes on to ADD2 (26 kJ/mol) through a ligand exchange between a carbonyl on Co2 and the alkene moiety of the enyne.

UNIVERSITAT ROVIRA I VIRGILI
COMPUTACIONAL STUDIES ON THE MECHANISM OF THE PAUSON-KHAND REACTION
Torstein Fjermestad
ISBN:978-84-693-9441-0/DL:T.62-2011

From ADD2 an oxidative metallacycle formation leads to a metallacycle intermediate (INT1, 37 kJ/mol) through transition state TS1 (74 kJ/mol). The three carbonyls of INT1 are all terminal. A significant stabilisation is obtained when the terminal carbonyl of Co1 becomes bridging between the two cobalt atoms. Intermediate INT2 with this structural motif, has a free energy of -36 kJ/mol, a stabilisation of 72 kJ/mol relative to INT1. Further on from INT2, a carbonyl insertion into the cobalt-alkyl bond of the metallacycle leads to the carbonylated metallacycle INT3 (-22 kJ/mol) through transition state TS3 (25 kJ/mol). The carbonylated metallacycle then goes through a conformational change mainly consisting of a shortening of the distance between the carbon atoms that are forming a bond in the reductive elimination. This conformational change is accompanied by an energy increase of 57 kJ/mol. From the new carbonylated metallacycle intermediate, INT4 (35 kJ/mol), the system goes through a reductive elimination to ADD3 (-55 kJ/mol). ADD3 contains three carbonyl groups. Two subsequent CO additions take the system through ADD4 (-67 kJ/mol) and ADD5 (-59 kJ/mol) before the cyclopentenone product is exchanged with the substrate thus closing the catalytic cycle. The reaction Gibbs free energy of -193 kJ/mol confirms the exergonicity of the reaction.

Magnus2. Three carbonyls incorporated and carbon monoxide insertion into the cobalt-alkenyl bond

At intermediate INT2, the **Magnus2** mechanism separates from the **Magnus1** mechanism in that the carbonyl is inserted into the cobalt-alkenyl bond instead of the cobalt-alkyl bond. From INT2, the complex goes through a reorganisation mainly consisting of a shortening of the C-C distance between the carbonyl and the alkenyl that are forming a bond in the CO insertion. This reorganisation of the complex increases its free energy to 48 kJ/mol (INT10). From INT10, the reaction continues over TS12 (66 kJ/mol) to the carbonylated metallacycle intermediate, INT11 (53 kJ/mol). From INT11, the reaction continues through a high-barrier reductive elimination (TS13, 129 kJ/mol) to product adduct ADD8 (-56 kJ/mol).

Magnus3. Four carbonyls incorporated and carbon monoxide insertion into the cobalt-alkyl bond

The **Magnus3** mechanism coincides with the **Magnus1** mechanism up to intermediate INT1. At that stage, an extra carbonyl is added and INT5 (23 kJ/mol) is formed. From INT5 the reaction continues with a carbonyl insertion into the cobalt-alkyl bond. This takes the system to the carbonylated metallacycle intermediate INT6 (4 kJ/mol) over transition state TS6 (65 kJ/mol). Further on from INT6, a reductive elimination takes the system to ADD4 over transition state TS7 (33 kJ/mol). ADD4 also forms part of the free energy profile of the **Magnus1** mechanism. At ADD4, the **Magnus3** mechanism merges with the **Magnus1** mechanism and follows the same reaction path until the formation of the products. Figure 4.10 shows the free energy profiles, ΔG° and ΔG_{app}, for the **Magnus3** mechanism up to ADD4.

UNIVERSITAT ROVIRA I VIRGILI
COMPUTACIONAL STUDIES ON THE MECHANISM OF THE PAUSON-KHAND REACTION
Torstein Fjermestad
ISBN:978-84-693-9441-0/DL:T.62-2011

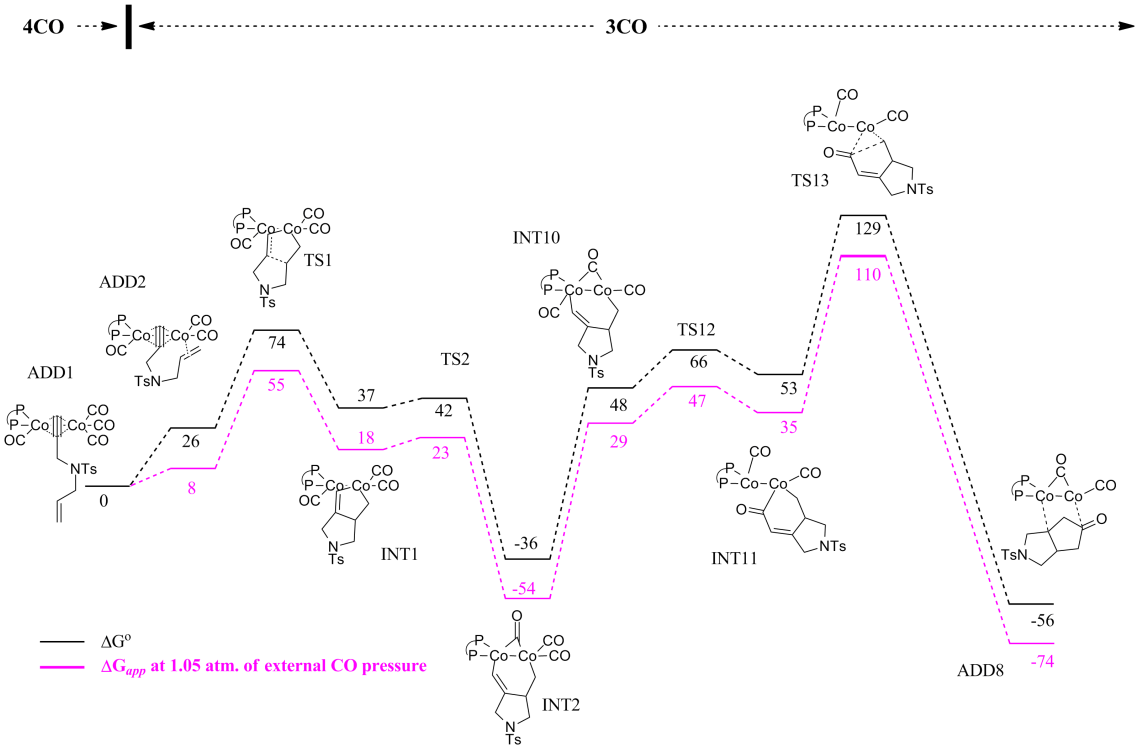

Figure 4.9: Free energy profiles, ΔG° and ΔG_{app}, of the **Magnus2** mechanism. Energies in kJ/mol. The ranges of the mechanistic pathway with three and four carbonyls incorporated in the complex are indicated.

Magnus4. Four carbonyls incorporated and carbon monoxide insertion into the cobalt-alkenyl bond

Up to intermediate INT5, the **Magnus4** mechanism, coincides with mechanism **Magnus3** presented in figure 4.10. From metallacycle intermediate INT5, the system evolves further through a carbonyl insertion into the cobalt-alkenyl bond. This insertion takes the system to the carbonylated metallacycle INT7 (45 kJ/mol) over transition state TS8 of 70 kJ/mol. From INT7 the reaction continues through a reductive elimination to product adduct ADD4 (-67 kJ/mol) over transition state TS9 (87 kJ/mol). From the product adduct ADD4, the **Magnus4** mechanism coincides with the mechanisms **Magnus1** - **Magnus3**. Figure 4.11 shows the Gibbs free energy profiles of the **Magnus4** mechanism up to ADD4.

4.3.2 Modified Magnus mechanism

The modified Magnus mechanism proposed by Gibson [71] does not involve any carbonyl dissociations and /or coordinations relative to ADD1, the common reference level of the mechanisms discussed for this system. Thus the free energies ΔG° and ΔG_{app} do not differ. The modified Magnus mechanism goes through ADD6 where both the alkene and the alkyne of the enyne are coordinated to Co2. ADD6 has a free energy of 57 kJ/mol above the reference structure ADD1. From ADD6 the

UNIVERSITAT ROVIRA I VIRGILI
COMPUTACIONAL STUDIES ON THE MECHANISM OF THE PAUSON-KHAND REACTION
Torstein Fjermestad
ISBN:978-84-693-9441-0/DL:T.62-2011

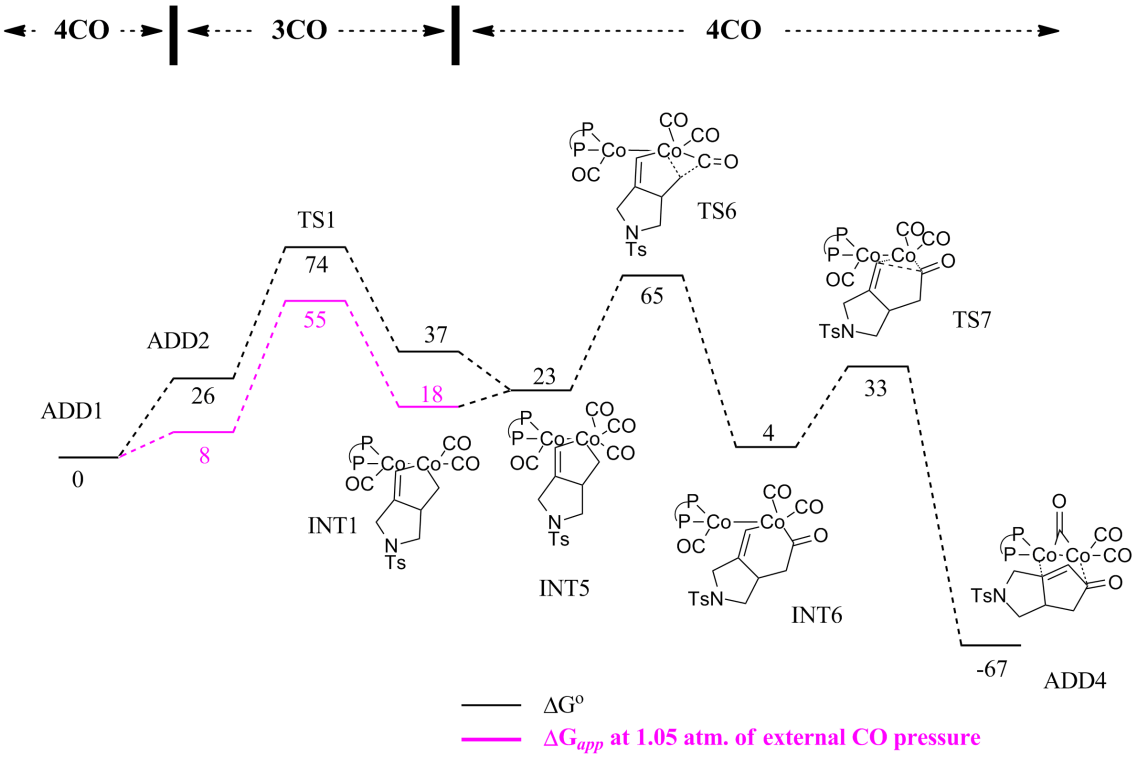

Figure 4.10: Free energy profiles, ΔG° and ΔG_{app}, of the **Magnus3** mechanism. Energies in kJ/mol. The ranges of the mechanistic pathway with three and four carbonyls incorporated in the complex are indicated.

UNIVERSITAT ROVIRA I VIRGILI
COMPUTACIONAL STUDIES ON THE MECHANISM OF THE PAUSON-KHAND REACTION
Torstein Fjermestad
ISBN:978-84-693-9441-0/DL:T.62-2011

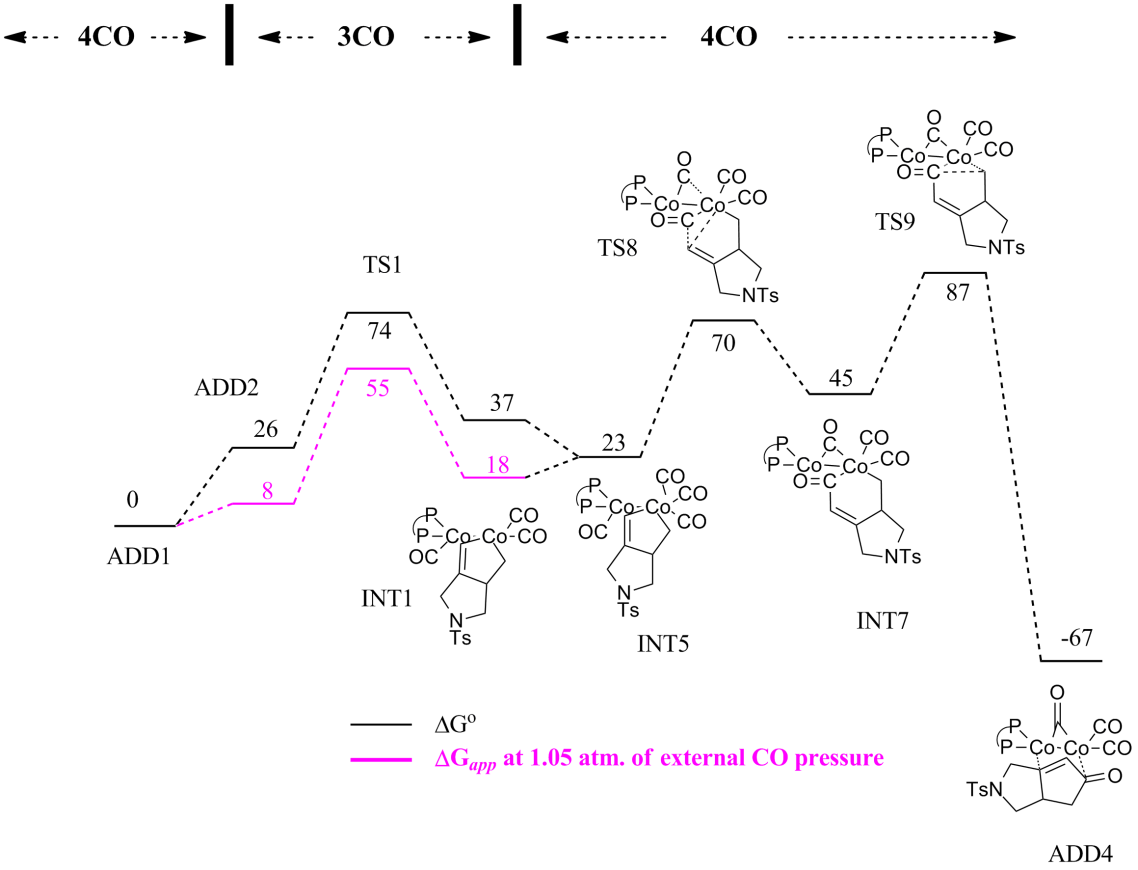

Figure 4.11: Free energy profiles, ΔG° and ΔG_{app}, of mechanism **Magnus4**. Energies in kJ/mol. The ranges of the mechanistic pathway with three and four carbonyls incorporated in the complex are indicated.

UNIVERSITAT ROVIRA I VIRGILI
COMPUTACIONAL STUDIES ON THE MECHANISM OF THE PAUSON-KHAND REACTION
Torstein Fjermestad
ISBN:978-84-693-9441-0/DL:T.62-2011

reaction continues through a oxidative cycloaddition over transition state TS10 (93 kJ/mol) onto the metallacycle intermediate INT8 (11 kJ/mol). Figure 4.12 shows the free energy profile of the oxidative cycloaddition of the modified Magnus mechanism. Because of the high free energy of TS10 compared to the Magnus mechanisms reported in the previous subsection, we decided not to study this mechanism further on.

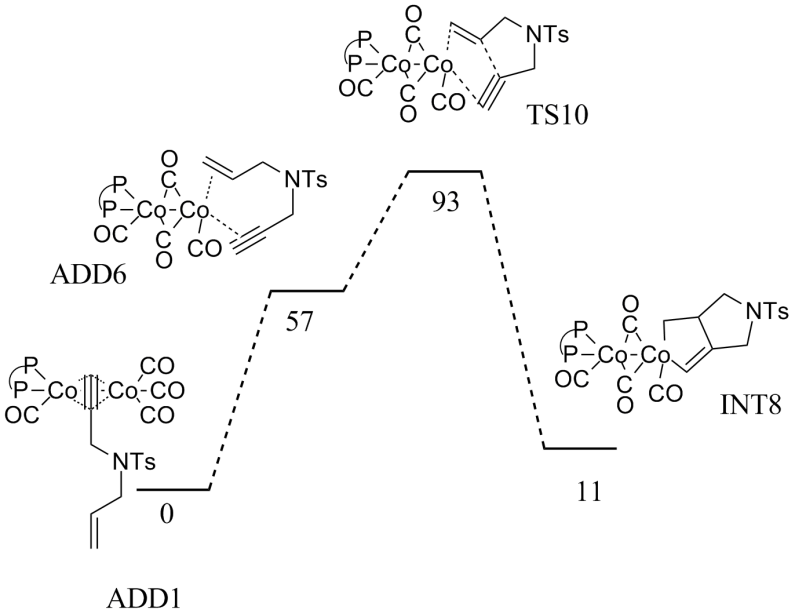

Figure 4.12: Free energy profile, ΔG°, of the first step of the modified Magnus mechanism. Energies in kJ/mol.

4.3.3 CO insertion

The CO insertion mechanism shown by Wang and Wu to be operative in the Ru catalysed Pauson-Khand reaction [104] does not involve any CO dissociations or associations relative to the starting adduct, ADD7. The ΔG° and ΔG_{app} thus coincide. The profile of the first step of this mechanism is shown in figure 4.13. The CO insertion mechanism goes through ADD7. ADD7 differs from ADD1 by the orientation of the substrate relative to the equatorial phosphorus of the BINAP ligand. In ADD7, the substituent of the alkyne is located on the same side as the equatorial phosphorus. From ADD7, the reaction proceeds over TS11 (98 kJ/mol) to the CO inserted intermediate, INT9 (50 kJ/mol). Because of the high free energy of TS11, we decided not to study this mechanism in more detail.

4.3.4 Discussion

When comparing the different mechanisms, we use the apparent Gibbs free energy, ΔG_{app}, in order to take into account the relative preference for pathways with a CO

UNIVERSITAT ROVIRA I VIRGILI
COMPUTACIONAL STUDIES ON THE MECHANISM OF THE PAUSON-KHAND REACTION
Torstein Fjermestad
ISBN:978-84-693-9441-0/DL:T.62-2011

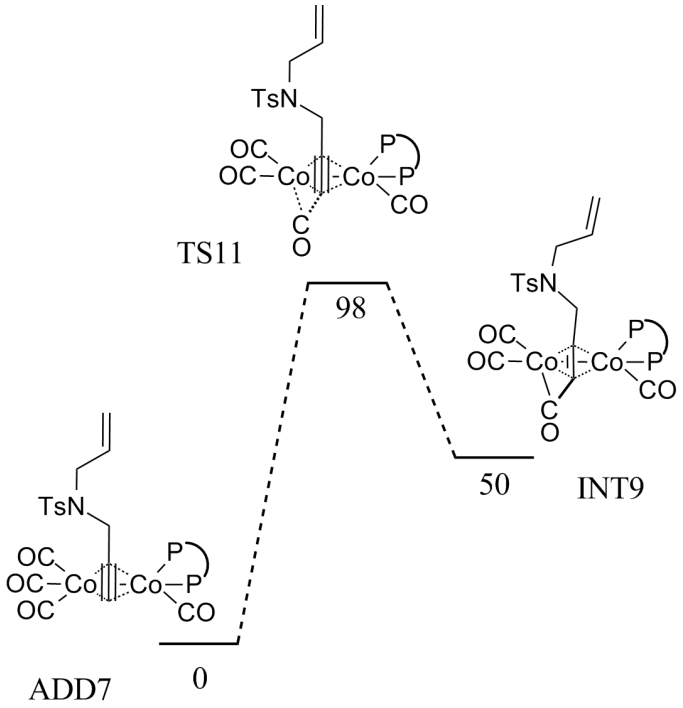

Figure 4.13: Free energy profile, ΔG°, of the first step of the CO insertion into the Co-alkyne bond. Energies in kJ/mol.

dissociated. Table 4.1 shows the transition states of the highest apparent Gibbs free energy, ΔG_{app}, for each of the mechanisms studied. These TSs are termed selectivity-determining TSs in that their relative energies determine the operative mechanism of the system. From the comparison in table 4.1, we see that the **Magnus1** mechanism

Table 4.1: The highest apparent Gibbs free energy, ΔG_{app}, for the mechanisms studied.

	ΔG_{app} / (kJ/mol)
Magnus1 (TS1)	55
Magnus2 (TS13)	110
Magnus3 (TS6)	65
Magnus4 (TS9)	87
Modified Magnus (TS10)	93
CO insertion (TS11)	98

is the preferred one. Remarkably, this is different from what had been proposed in previous computational studies for the $Co_2(CO)_8$ catalyst [47, 48], that had assumed the **Magnus3** mechanism. However, the enantioselectivity-determining transition state will still be the same as previously proposed.

In the energy span model [99–101], the turnover frequency will be decided by the energy of an intermediate and a transition state along the catalytic cycle. In the case of the **Magnus1** mechanism (Figure 4.8), these will be INT2 and TS5. Thus, the key to the efficiency of the catalytic cycle is in the reductive elimination step

UNIVERSITAT ROVIRA I VIRGILI
COMPUTACIONAL STUDIES ON THE MECHANISM OF THE PAUSON-KHAND REACTION
Torstein Fjermestad
ISBN:978-84-693-9441-0/DL:T.62-2011

(TS5). However, this is not where enantioselection takes place. From INT2 to TS5 the stereogenic centre is not modified. The enantioselectivity is determined by comparing the energies of the transition states of first irreversible step of the reaction profile after the new chiral centre has been created, see chapter 3. From figure 4.8 we see that the first irreversible step after the formation of the chiral centre is the oxidative metallacycle formation. Once the reaction has passed TS1, the transition state of this step, any forward reaction is faster than any backward reaction and the sense of chirality in the product is determined. Because of this, the analysis that follows will concentrate on the energy of the different variations of TS1 that lead to the different enantiomers.

4.4 Conformational search on the enantiodetermining transition state

X-ray structures reported by Gibson [72] indicate that for ADD1 there is an equilibrium between structures having the substituent of the alkyne moiety on the same or the opposite side of the phosphorus ligand in the equatorial position (see figure 4.14). Furthermore, NMR evidence indicates that the two phosphorus centres have equivalent signals thus suggesting an equilibrium between structures having a phosphorus ligand coordinated to one or the other equatorial position of Co1. Each of these four structures of ADD1 would lead to four different configurations of transition state TS1. These are labelled configuration A, B, C and D as shown in figure 4.14

Each of the four configurations of TS1 corresponds to a mechanistic manifold of the **Magnus1** mechanism. The manifolds to which the TS1 configurations belong are labelled manifold A, B, C, and D in the same manner. When computing the enantiomeric excess of the reaction, we have to consider the R/S selectivity within each of the four manifolds.

We label the diastereomeric transition states corresponding to TS1 according to the manifolds they belong to (A, B, C or D) and the chiral centre being created in TS1 (R or S). This makes in total eight TS1 configurations to consider. To distinguish the different conformers within each TS1 configuration, we add a number to the label. The labels used are thus the following: N_Tn, where N = A, B, C or D; T=R or S and n = 1,2,$\cdots$.

4.4.1 Conformational search

In our search for the different conformations of TS1, we used two methodologies. Method 1 consisted of a systematic change of geometrical parameters, followed by subsequent transition state optimisations with ONIOM partitions 1, 2 and 3.

Method 2 consisted of a Monte Carlo conformational search [110, 111] followed by a clustering analysis [112] of the structures found. One representative structure in each cluster was submitted to a reoptimisation with ONIOM partition 1.

UNIVERSITAT ROVIRA I VIRGILI
COMPUTACIONAL STUDIES ON THE MECHANISM OF THE PAUSON-KHAND REACTION
Torstein Fjermestad
ISBN:978-84-693-9441-0/DL:T.62-2011

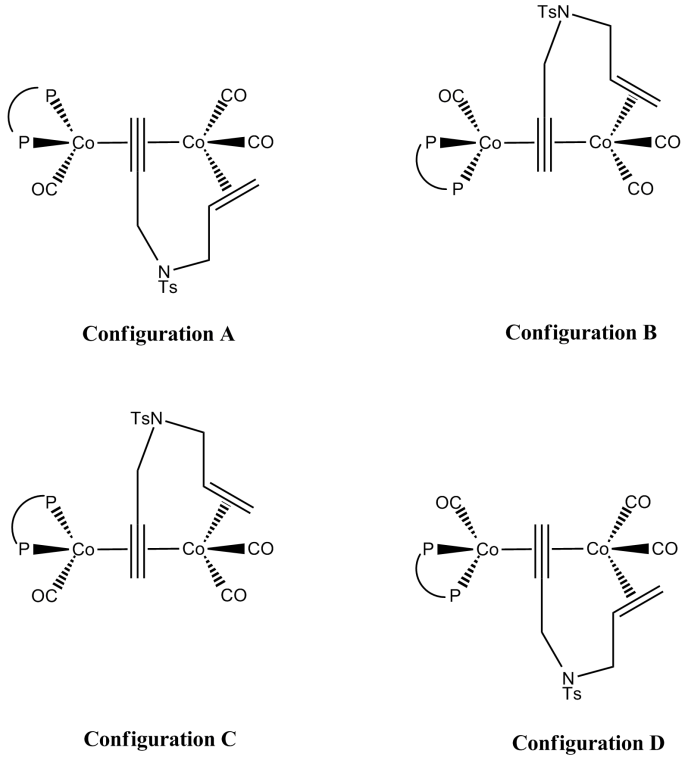

Figure 4.14: The four configurations of TS1.

On the ONIOM1 optimised structures, a second clustering analysis was performed. From each cluster of structures, the lowest energy structure was submitted to an optimisation with ONIOM partition 2. On the ONIOM2 optimised structures, a third clustering analysis was done. From each cluster, the lowest energy structure was submitted to an optimisation with ONIOM partition 3. Finally, the ONIOM3 optimised structures were used in the computation of the enantiomeric excess.

The two methods produced comparable sets of structures. Through the use of two different methods for conformational search, we expect to have properly identified the most stable structures.

Conformational search for manifold A

Our search for transition state conformers belonging to manifold A started off with method 1. The geometrical parameters varied were the following ones: (i) The absolute configuration of the chiral centre created, (ii) the absolute configuration of the chiral centre on the nitrogen atom and (iii) the torsion around the N-S bond of the substrate (three possible staggered arrangements). Varying these parameters resulted in 12 hypothetical transition states to look for. Six of them, A_R1, A_R2, ... ,A_R6, would belong to the A_R TS1 configuration, and the other six, A_S1, A_S2, ... ,A_S6, would belong to the A_S TS1 configuration. Upon ONIOM1 optimisation of these 12 transition states, 6 became redundant by collapsing into other transition states of the set. The non-redundant transition states were the following: A_R1, A_R2, A_R3, A_R6, A_S2 and A_S3. Their relative energies are

UNIVERSITAT ROVIRA I VIRGILI
COMPUTACIONAL STUDIES ON THE MECHANISM OF THE PAUSON-KHAND REACTION
Torstein Fjermestad
ISBN:978-84-693-9441-0/DL:T.62-2011

shown in table 4.2. Among these transition states, A_R3 is of lowest energy, and will hereafter be used as the origin of the energy scale. The ONIOM1 optimised structures were then refined by a reoptimisation with ONIOM partition 2 and thereafter with ONIOM partition 3 (see table 4.2).

Table 4.2: Relative Gibbs free energies (kJ/mol) of transition states A_R1, A_R2, A_R3, A_R6, A_S2 and A_S3 for the ONIOM partitions 1, 2 and 3

Conformer	ΔG (ONIOM1)	ΔG (ONIOM2)	ΔG (ONIOM3)
A_R1	5	-3	-1
A_R2	7	6	-2
A_R3	0	0	0
A_R6	6	4	-3
A_S2	9	22	12
A_S3	11	9	17

The conformational space sampled with method 1 is limited because there are dihedral angles in the substrate and in the BINAP ligand that are not systematically changed. To make the sampling more complete, we performed a Monte Carlo (MC) conformational search (Method 2), allowing the rotation of all important bonds. The bonds rotated were the following: The C-N bond of the substrate (to allow the chirality of the nitrogen atom to change), the N-S bond of the substrate, S-toluene bond of the substrate and the six phosphorus-phenyl/naphtyl bonds of the BINAP (see figure 4.15). The force field used in MC conformational search was the 2001 version of OPLS-AA [113]. The search method was Monte Carlo multiple minimum (MCMM) [114] and only the structures in the lower 50 kJ/mol range were accepted. General-purpose force fields like OPLS-AA usually give a poor description of transition metal complexes as well as transition state structures. Because of this, the cobalt atoms, the first coordination sphere, and the atoms involved in the breaking and formation of bonds, were kept frozen during the Monte Carlo conformational search. This meant that the atoms involved in the formation of the chiral centre were frozen as well. A separate conformational search were thus performed for the A_R TS1 configuration and the A_S TS1 configuration.

The conformational searches resulted in a large number of structures (approximately 500 for each search), many of them redundant. To remove the redundant structures, we performed a cluster analysis [112] with all heavy atoms as comparison atoms. The structures from each conformational search (A_R and A_S) were grouped into 15 clusters.[1] A representative structure from each cluster was submitted to a reoptimisation with ONIOM partition 1. The ONIOM1 optimised A_R structures from the MC conformational search (A_R7 - A_R21) were submitted to a cluster analysis. The lowest energy structure from each cluster is presented in table 4.3.

Likewise, the ONIOM1 optimised A_S structures from the MC conformational search

[1]The choice of 15 clusters is somehow arbitrary. The real number of conformers may be higher or lower. However, the fact that several of the structures collapsed into others after the ONIOM optimisations (see below) suggests that the choice of 15 clusters does not leave out any important conformers.

UNIVERSITAT ROVIRA I VIRGILI
COMPUTACIONAL STUDIES ON THE MECHANISM OF THE PAUSON-KHAND REACTION
Torstein Fjermestad
ISBN:978-84-693-9441-0/DL:T.62-2011

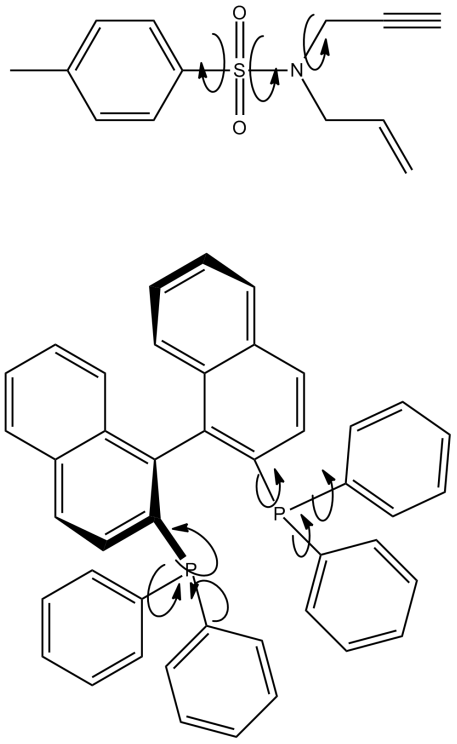

Figure 4.15: Bonds rotated in the conformational Monte Carlo search.

(labelled A_S7 - A_S21) were submitted to a cluster analysis and the lowest energy structure from each cluster is shown in table 4.3.

From table 4.3 we see that six A_R structures and nine A_S structures became redundant during the ONIOM1 optimisation.

The nine A_R structures in table 4.3 were submitted to a reoptimisation with ONIOM partition 2. After the ONIOM2 optimisation, a clustering analysis was performed. The lowest energy structure of each cluster is presented in table 4.4 Likewise, the six A_S structures in table 4.3 were submitted to a reoptimisation with ONIOM partition 2. After the ONIOM2 optimisation a cluster analysis was performed. The lowest energy structure of each cluster is presented in table 4.4 From table 4.4 we see that one A_R structure and three A_S structures got redundant during the ONIOM2 optimisation.

The eight A_R structures in table 4.4 were submitted to a reoptimisation with ONIOM partition 3. A clustering analysis was done on the ONIOM3 optimised structures. The lowest energy structure within each cluster is shown in table 4.5 Likewise, the three A_S structures in table 4.4 were submitted to a reoptimisation with ONIOM partition 3. A cluster analysis was done on the ONIOM3 optimised structures, but the three A_S structures did not form clusters with more than one member. The ONIOM3 optimised A_S structures are shown in table 4.5.

In table 4.5, we also included the ONIOM3 optimised A_R and A_S structures obtained from method 1 (see table 4.2) . A cluster analysis put A_R6 and A_R19 in the same cluster, and only the lowest one (A_R19) is given in table 4.5. The

UNIVERSITAT ROVIRA I VIRGILI
COMPUTACIONAL STUDIES ON THE MECHANISM OF THE PAUSON-KHAND REACTION
Torstein Fjermestad
ISBN:978-84-693-9441-0/DL:T.62-2011

Table 4.3: ONIOM1 optimised structures of TS1 configuration A_R and A_S

conform.	ΔG (ONIOM1) / (kJ/mol)
A_R	
A_R7	4
A_R9	0
A_R10	7
A_R11	23
A_R14	5
A_R17	29
A_R18	-3
A_R19	12
A_R21	8
A_S	
A_S9	9
A_S12	12
A_S13	12
A_S14	24
A_S18	10
A_S21	14

Table 4.4: Gibbs free energies (kJ/mol) of the A_R and A_S structures optimised with ONIOM partition 2

conform.	ΔG (ONIOM2)/ (kJ/mol)
A_R	
A_R7	0
A_R9	4
A_R10	7
A_R11	5
A_R14	4
A_R17	31
A_R19	1
A_R21	-5
A_S	
A_S11	8
A_S14	14
A_S18	20

UNIVERSITAT ROVIRA I VIRGILI
COMPUTACIONAL STUDIES ON THE MECHANISM OF THE PAUSON-KHAND REACTION
Torstein Fjermestad
ISBN:978-84-693-9441-0/DL:T.62-2011

structures given in table 4.5 are used in the computation of the enantiomeric excess (see section 4.5).

Table 4.5: ONIOM3 optimised structures of manifold A used in the computation of the enantiomeric excess.

conformer	ΔG (ONIOM3)/(kJ/mol)
A_R	
A_R9	-9
A_R11	4
A_R10	-4
A_R21	0
A_R19	-6
A_R1	-1
A_R2	-2
A_R3	0
A_S	
A_S11	18
A_S14	16
A_S18	9
A_S2	12
A_S3	17

Conformational search for manifold B

For TS1 transition state structures of manifold B, we first optimised structures with geometrical parameters corresponding to the transition states A_R1, A_R2, A_R3, A_R6, A_S2, and A_S3 of manifold A. These manifold B structures we label B_S1, B_S2, B_S3, B_S6, B_R2 and B_R3 in an analogue way. Because of the different orientation of the substrate relative to the catalyst, transition states with corresponding geometrical parameters in the two manifolds will lead to different enantiomers. As indicated by the labels, structures B_S1, B_S2, B_S3 and B_S6 lead to the S enantiomer whereas structures B_R2 and B_R3 lead to the R enantiomer. In table 4.6 the Gibbs free energies of these B_S and B_R transition states are given.

Also for manifold B we supplemented the structures found by method 1 with structures found by a Monte Carlo conformational search (Method 2). The force field (OPLS2001) and the search algorithm (MCMM) were the same as described for manifold A. The Monte Carlo search for B_S TS1 configuration resulted in a high number of structures, many of them redundant. To remove the redundant structures, we performed a cluster analysis, putting the structures into 15 groups.[2] A representative structure from each group was submitted to an optimisation with ONIOM partition 1. After the ONIOM1 optimisation, structures were grouped into clusters and the lowest energy structure from each cluster is shown in table 4.7.

[2]See footnote on page 50

UNIVERSITAT ROVIRA I VIRGILI
COMPUTACIONAL STUDIES ON THE MECHANISM OF THE PAUSON-KHAND REACTION
Torstein Fjermestad
ISBN:978-84-693-9441-0/DL:T.62-2011

Table 4.6: Relative Gibbs free energies (kJ/mol) of transition states B_S1, B_S2, B_S3, B_S6, B_R2 and B_R3 for the ONIOM partitions 1, 2 and 3

Conformer	ΔG (ONIOM1)	ΔG (ONIOM2)	ΔG (ONIOM3)
B_S1	12	16	9
B_S2	16	15	11
B_S3	24	62	-[a]
B_S6	13	14	7
B_R2	19	28	15
B_R3	15	24	28

[a] The ONIOM3 optimisation of B_S3 is not done because of the high Gibbs free energy of the ONIOM2 optimisation.

Likewise for the B_R TS1 configuration, the Monte Carlo search resulted in a high number of structures, many of them redundant. The redundant structures were removed by clustering them into 15 groups.[3] A representative structure from each of the 15 groups were submitted to an optimisation with ONIOM partition 1.

Table 4.7: ONIOM1 B_S TS1 structures. Free energies in kJ/mol.

conformer	ΔG (ONIOM1)/(kJ/mol)
B_S8	3
B_S9	10
B_S11	17
B_S14	9
B_S15	12
B_S16	10
B_S17	13
B_S18	12
B_S20	5
B_S21	17

For the B_S TS1 configuration, the Monte Carlo conformational search was able to find low-energy structures (e.g B_S8, 3 kJ/mol) that had not previously been located by method 1. On the other hand, for the B_R structures, method 2 was not able to find structures lower in energy than those already found by method 1. Thus of the B_R TS1 structures, only B_R2 and B_R3 (table 4.6) will be used in the final computation of the enantiomeric excess.

The B_S TS1 structures in table 4.7 were then submitted to an optimisation with ONIOM partition 2. On the ONIOM2 optimised structures, a cluster analysis was applied, and the lowest energy structure of each cluster is presented in table 4.8.

The ONIOM2 optimised structures in table 4.8 were submitted to a reoptimisation with ONIOM partition 3. On the ONIOM3 optimised structures, a cluster analysis

[3]See footnote on page 50

UNIVERSITAT ROVIRA I VIRGILI
COMPUTACIONAL STUDIES ON THE MECHANISM OF THE PAUSON-KHAND REACTION
Torstein Fjermestad
ISBN:978-84-693-9441-0/DL:T.62-2011

Table 4.8: ONIOM2 optimised B_S TS1 structures. Gibbs free energies in kJ/mol.

conform	ΔG (ONIOM2) /(kJ/mol)
B_S8	7
B_S9	15
B_S15	14
B_S16	14
B_S17	14
B_S20	8

was applied, and the lowest energy structure from each cluster is presented in table 4.9.

In table 4.9, we also included the ONIOM3 optimised B_R and B_S structures obtained from method 1 (see table 4.6). A cluster analysis put B_S1, B_S15 and B_S16 in the same cluster, and only the lowest one (B_S15) is given in table 4.9. The structures in table 4.9 are used in the computation of the enantiomeric excess.

Table 4.9: Gibbs free energy (kJ/mol) of ONIOM3 optimised B_S TS1 structures.

Conform	ΔG (ONIOM3)/(kJ/mol)
B_S2	11
B_S6	7
B_S8	10
B_S9	1
B_S15	8
B_S17	15
B_S20	17
B_R2	15
B_R3	28

Exclusion of manifolds C and D

A priori we saw that manifolds C and D with the alkyne substituent on the same side as the equatorial phosphorus ligand, were likely to give rise to high-energetic structures due to steric repulsion between the phenyls of the BINAP and the substituent of the alkyne moiety. We optimised, with ONIOM1, a representative structure for each of the manifolds C and D to test this hypothesis. The transition state of manifold C had a free energy of 29 kJ/mol above A_R3. The transition state of manifold D had a free energy of 49 kJ/mol above A_R3. Manifold C and D were thus excluded as viable pathways for this system.

4.5 Computed enantiomeric excess

From the Gibbs free energies of the ONIOM 3 optimised structures, we compute the enantiomeric excess as indicated in equations (3.7) and (3.8). This resulted in an

UNIVERSITAT ROVIRA I VIRGILI
COMPUTACIONAL STUDIES ON THE MECHANISM OF THE PAUSON-KHAND REACTION
Torstein Fjermestad
ISBN:978-84-693-9441-0/DL:T.62-2011

enantiomeric excess of 95% (R), in good agreement with the experimental result of 88% (R).

4.6 Discussion

The good agreement with the experimental result suggests that the **Magnus1** mechanism assumed in the calculation of the enantiomeric excess is the correct one. The results above show that within manifold A the transition states leading to the R enantiomer are favoured over the transition states leading to the S enantiomer. Conversely, within manifold B the transition states leading to the S enantiomer are favoured over the transition states leading to the R enantiomer. The TSs of manifold B are less stable than the TSs of manifold A, and therefore the R enantiomer is favoured over the S enantiomer. In the rest of this section, we will analyse the origin of the selectivity of the R and the S enantiomer within each of the manifolds A and B.

4.6.1 Selectivity within manifold A

Table 4.5 shows that all R TSs are favoured over the S TSs for manifold A. To understand this energy order, we proceed to analyse the structures of the most stable R TS and the most stable S TS. The most stable R TS is A_R9 of -9 kJ/mol. The most stable S TS is A_S18 of 9 kJ/mol. The preference of 18 kJ/mol for A_R9 over A_S18 seems to be due to a smaller steric constraint in the 5-membered ring being formed in this step. Figure 4.16 shows the structures of A_R9 (left) and A_S18 (right) with the stereogenic centre being formed indicated with a *. In A_R9, the R configuration of the stereogenic centre is indicated by having its hydrogen pointing downwards. This stereoconfiguration causes the 5-membered ring to be relatively unstrained and close to planarity. The RMS deviation from a plane fitted to the five atoms of the ring is 0.180 Å. In A_S18, the S configuration of the stereogenic centre is indicated by having its hydrogen pointing upwards. This stereoconfiguration introduces more strain in the 5-membered ring being formed. The RMS deviation from a plane fitted to the five atoms is 0.279 Å. The higher stability of A_R9 compared to A_S18 is thus due to the less strained 5-membered ring being formed in the R transition state. When reacting along the A manifold, strain in the enantiodetermining transition state is avoided by adopting the R configuration. Manifold A thus favours the R enantiomer.

4.6.2 Selectivity within manifold B

Table 4.9 shows that for manifold B, the transition states leading to the S enantiomer are generally more stable than the transition states leading to the R enantiomer. The most stable R TS B_R2 has a free energy of 15 kJ/mol while the most stable S TS, B_S9, has a free energy of 1 kJ/mol. Figure 4.17 shows the structures of B_R2 (left) and B_S9 (right) with the stereogenic centre being formed indicated with a *. By the

UNIVERSITAT ROVIRA I VIRGILI
COMPUTACIONAL STUDIES ON THE MECHANISM OF THE PAUSON-KHAND REACTION
Torstein Fjermestad
ISBN:978-84-693-9441-0/DL:T.62-2011

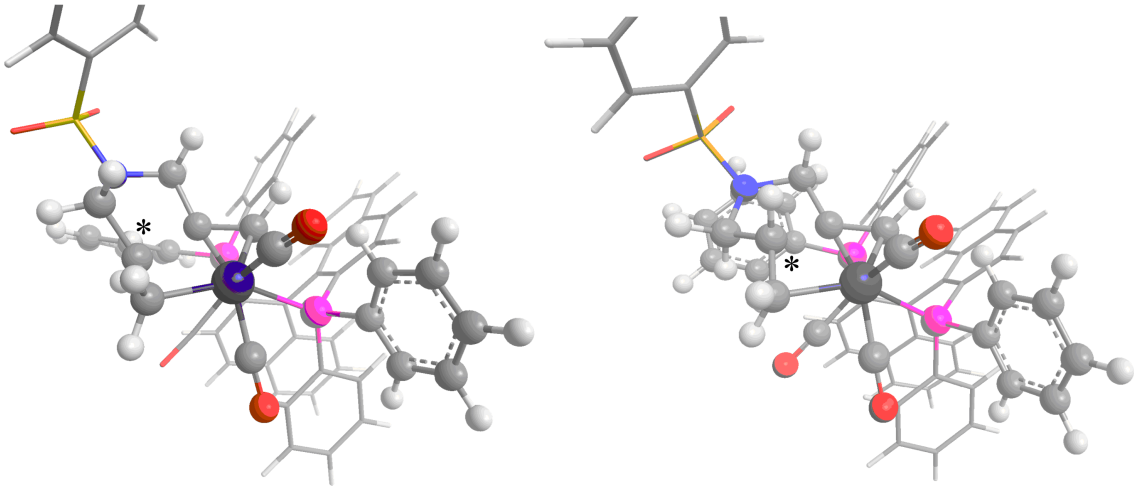

Figure 4.16: Structures of the transition states A_R9 (-9 kJ/mol, left) and A_S18 (9 kJ/mol, right) of manifold A viewed along the Co-Co axis. The carbon atom where the stereogenic centre is being formed is indicated with a *.

same reasoning as for manifold A, B_S9 is more stable than B_R2. The 5-membered ring of B_S9 is closer to planarity with a RMS deviation of 0.173 Å. The RMS deviation from planarity of the 5-membered ring in B_R2 is 0.285 Å. Thus when reacting along the B manifold, strain in the enantiodetermining transition state is avoided by adopting the S configuration. Manifold B thus favours the S enantiomer.

4.6.3 Comparison between manifold A and B

Manifold A favours the R enantiomer and manifold B favours the S enantiomer. However, the most stable TS of manifold A (A_R9) is 10 kJ/mol lower than the most stable TS of manifold B (B_S9). Overall the system thus favour the formation of the R enantiomer.

The reason why A_R9 of manifold A is lower than B_S9 of manifold B lies in the stereogenic features of the BINAP ligand. The binaphtyl backbone puts a stronger steric constrain on one of the phenyls of each of phosphorus centre. These phenyls are highlighted in ball-and-stick representation in figure 4.18. The phenyl of the axial phosphorus is labelled “axial” and the phenyl of the equatorial phosphorus is labelled “equatorial”. The steric role of the axial phenyl seems quite similar in both manifold A and B. The equatorial phenyl, however, exerts a different steric influence on the rest of the structure in the two manifolds. In particular the steric interactions between the equatorial phenyls and the two carbonyls on Co2 are markedly different in the two manifolds. In conformer A_R9 (Manifold A), the equatorial phenyl points towards the area between the two carbonyls of Co2 and steric repulsion is minimised. The closest contact between the phenyl carbons and the oxygen of the axial carbonyl is 3.594 Å. In conformer B_S9 (Manifold B) on the other hand, the equatorial phenyl is eclipsed to the equatorial carbonyl (when viewed along the Co-P axis). The closest contact between the phenyl carbons and the oxygen of the equatorial carbonyl is

UNIVERSITAT ROVIRA I VIRGILI
COMPUTACIONAL STUDIES ON THE MECHANISM OF THE PAUSON-KHAND REACTION
Torstein Fjermestad
ISBN:978-84-693-9441-0/DL:T.62-2011

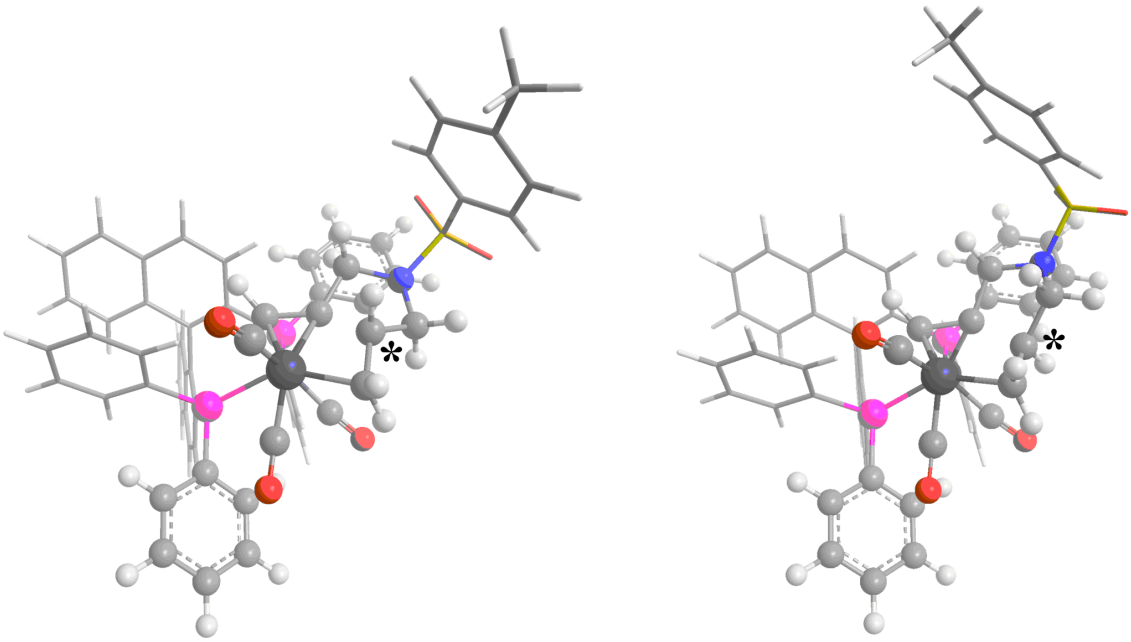

Figure 4.17: Structures of the transition states B_R2 (15 kJ/mol, left) and B_S9 (1 kJ/mol, right) of manifold B viewed along the Co-Co axis. The stereogenic centre being created is indicated with a *.

3.216 Å. The closer contact in the case of B_S9 (Manifold B) is the cause of its higher energy relative to A_R9 (Manifold A). Figure 4.18 shows these two transition states with the closest contact distances indicated.

From the above discussion, it is clear that the mechanism of enantiodiscrimination is not a direct steric interaction between the substrate and the chiral ligand. The chiral BINAP forces the alkene moiety of the substrate to coordinate at the side opposite to the equatorial phosphorus. That is, manifolds A and B are highly favoured over manifolds C and D. Because of the linker connecting the alkyne and alkene moieties of the substrate, the TSs with the hydrogen of the stereogenic centre pointing down (as oriented in figures 4.16 to 4.18) are favoured. This is true both for manifold A and manifold B. The stereocentres with hydrogen pointing down have the R configuration in manifolds A and the S configuration in manifold B. Seemingly, the preference for the opposite enantiomer in the two manifolds would lead to a low enantiomeric excess. However, structures of manifold B are destabilised with respect to structures of manifold A because of the enhanced steric repulsion between the equatorial phenyl and the equatorial carbonyl at Co2.

The enantiomeric discrimination is thus not caused by any difference in the substrate-catalyst interactions, but rather by a difference in the stability of two isomeric forms, A and B, of the catalyst.

UNIVERSITAT ROVIRA I VIRGILI
COMPUTACIONAL STUDIES ON THE MECHANISM OF THE PAUSON-KHAND REACTION
Torstein Fjermestad
ISBN:978-84-693-9441-0/DL:T.62-2011

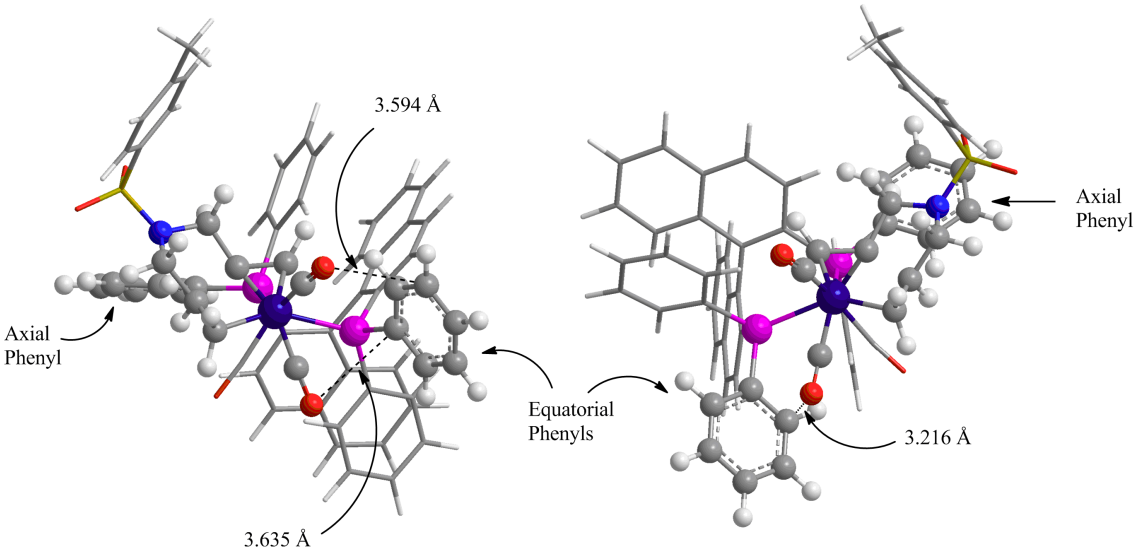

Figure 4.18: The lowest energy conformers of TS1 leading to the R (A_R9, -9 kJ/mol, left) and the S (B_S9, 1 kJ/mol, right) enantiomers. Viewed along the Co-Co axis

4.7 Conclusions

We have performed a DFT/MM study on the asymmetric Pauson-Khand reaction. The mechanism of the reaction is the one proposed by Magnus [38], Schore [39], Nakamura [47] and Pericàs [48] (although with a slight modification concerning the number of carbonyls coordinated in the metallacycle intermediate and the carbonylated metallacycle intermediate). The enantiodetermining transition state is the transition state of the oxidative metallacycle formation. The reaction favours the formation of the R enantiomer over the S enantiomer. The calculations predict an enantiomeric excess of 95% (R) in good agreement with the experimental value of 88% (R). The enantiodiscrimination is caused by a difference in the steric interaction between a carbonyl and a phenyl located on the side of the catalyst opposite to where the chiral centre is created.

UNIVERSITAT ROVIRA I VIRGILI
COMPUTACIONAL STUDIES ON THE MECHANISM OF THE PAUSON-KHAND REACTION
Torstein Fjermestad
ISBN:978-84-693-9441-0/DL:T.62-2011

UNIVERSITAT ROVIRA I VIRGILI
COMPUTACIONAL STUDIES ON THE MECHANISM OF THE PAUSON-KHAND REACTION
Torstein Fjermestad
ISBN:978-84-693-9441-0/DL:T.62-2011

Chapter 5

Activation of metal carbonyl complexes

Reactions mediated by transition metal complexes often start with an activation step that consists of an exchange between a ligand of the metal complex and the substrate that are to be transformed. Metal carbonyl complexes are commonly used as catalysts or mediators of various reactions. In particular, the stoichiometric Pauson-Khand reaction is mediated by a dicobalt carbonyl complex. The first step is assumed to be a ligand exchange between one of the carbonyls and the Pauson-Khand substrate. In the conventional Pauson-Khand protocol the system is subject to vigorous heating for an extended amount of time. However, in the early 1990s Schreiber [115] and Jeong [116] showed that the stoichiometric Pauson-Khand reaction was accelerated dramatically in the presence of N-oxides.

About a decade later Kerr and co-workers expanded the methodology and used a chiral N-oxide, brucine N-oxide, to induce chirality in the final Pauson-Khand product [70, 117]. This methodology had, however, some limitations: A reaction temperature of -60°C was required and the highest enantioselectivity obtained was 78% ee. The corresponding reaction time and yield were 120h and 63% respectively [70]. Our motivation to study this system is to understand the origin of these limitations and, if possible, suggest methods to eliminate them in order to make the methodology more practical. To achieve this goal, a general understanding of the mechanism is necessary.

5.1 Trimethylamineoxide as an activator

No previous computational nor kinetic studies exist on the mechanism of enantioinduction in this system. In order to obtain preliminary mechanistic knowledge, we decided to carry out a computational study on chemically related, but simpler, systems for which extensive kinetic data were available. The systems in question are the family of metal carbonyl complexes, $M(CO)_5$ (M = Fe, Ru, Os) and $M(CO)_6$ (M = Cr, Mo, W), which react with PPh_3 in the presence of the N-oxide trimethy-

UNIVERSITAT ROVIRA I VIRGILI
COMPUTACIONAL STUDIES ON THE MECHANISM OF THE PAUSON-KHAND REACTION
Torstein Fjermestad
ISBN:978-84-693-9441-0/DL:T.62-2011

lamineoxide (TMAO) [118, 119].

$$M(CO)_y + PPh_3 + TMAO \longrightarrow M(CO)_{y-1}PPh_3 + TMA + CO_2 \qquad (5.1)$$

The kinetic studies show that the reaction is first order in the concentration of TMAO, first order in the concentration of the metal carbonyl complex, but zero order in the concentration of PPh_3. Based on these data, the authors proposed the mechanism depicted in figure 5.1.

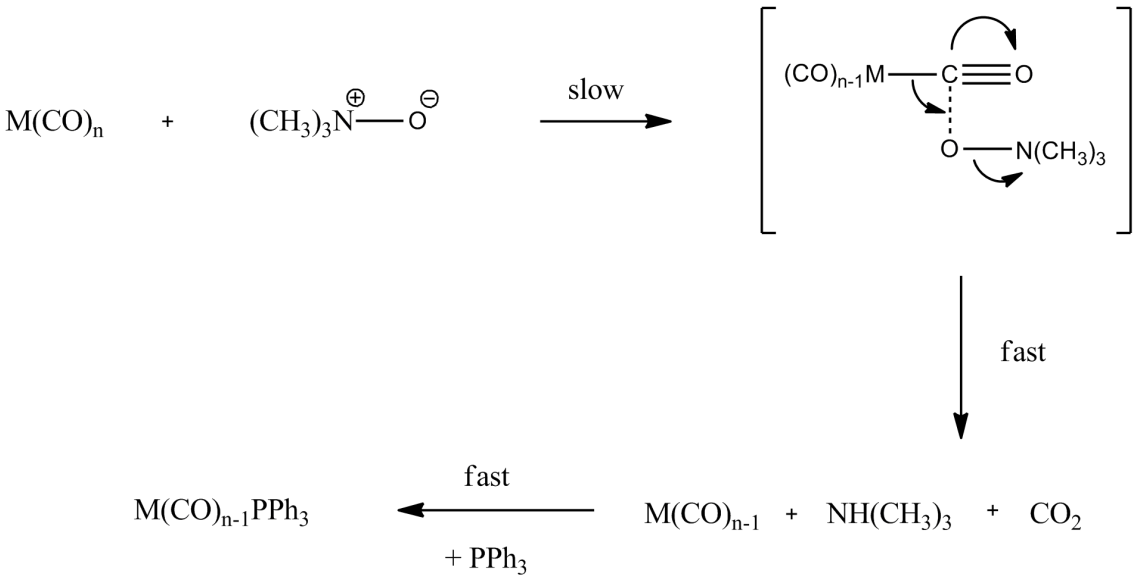

Figure 5.1: Proposed mechanism of the TMAO accelerated ligand exchange in metal carbonyl complexes [118, 119].

According to the proposal, the rate-determining step is the attack of the the metal carbonyl complex by TMAO. The PPh_3 enters rapidly into the vacant site created in the first step. The proposed mechanism is thus a two-step mechanism, consisting first of an abstraction of the carbonyl from the coordination sphere of the metal, followed by an insertion of the new ligand.

Because of the chemical similarity between the metalcarbonyl system and the Pauson-Khand system, it is likely that the same mechanism is operating in the two systems. In this respect, the computational results on the metal carbonyl system provide an important link between the kinetic experiment and the brucine assisted reaction we are interrested in.

In order to provide additional support for the assumption that the same mechanism is operating in both systems, the mechanism of the metal carbonyls will be tested on a simplified model of the Pauson-Khand system. Additionally, orbital analysis will be done to identify similarities and/or differences between the two systems at the electronic level.

In the following we present our computational results for the decarbonylation of metal carbonyl complexes, $M(CO)_6$ and $M(CO)_5$, as well as the decarbonylation of the Pauson-Khand precursor. Afterwards, the orbital analysis is presented.

UNIVERSITAT ROVIRA I VIRGILI
COMPUTACIONAL STUDIES ON THE MECHANISM OF THE PAUSON-KHAND REACTION
Torstein Fjermestad
ISBN:978-84-693-9441-0/DL:T.62-2011

5.2 Computational details

The calculations were carried out using the Gaussian 03 program package [105]. The energy evaluations were done with the B3LYP functional. The basis set for the non-metal atoms was 6-31G(d) [106]. For the metal atoms the core electrons were substituted by the Los Alamos LANL2DZ effective core potential and the associated double zeta basis set was used for the valence electrons [107]. For the calculations of the reaction profiles, all minima and transition states were fully optimised without symmetry restrictions. The minima were identified by having only positive eigenvalues in the Hessian matrix. The transition states were identified by having exactly one negative eigenvalue in the Hessian matrix. Unless otherwise stated, all energies reported are free energies including zero-points and entropy corrections. For the orbital analysis, the metal carbonyl complexes, $M(CO)_5$ and $M(CO)_6$, and the Pauson-Khand precursor, $Co_2(CO)_6$(1-propyne), were optimised with symmetry restrictions in order to make the orbital interpretations easier. The pentacarbonyl complexes, $M(CO)_5$, were restricted to the D_{3h} point group during the optimisation. The hexacarbonyl complexes, $M(CO)_6$, were restricted to the O_h point group during the optimisation. The Pauson-Khand precursor, $Co_2(CO)_6$(1-propyne), was restricted to the C_s point group during the optimisation. Solvent effects were not included in the calculations because we assumed that the effect would be the same for all complexes whose energy we wanted to compare.

5.3 Activation of hexacarbonyl complexes $M(CO)_6$

The reaction of TMAO with the metal hexacarbonyl complexes ($M(CO)_6$, M=Cr, Mo, W) was first considered. The metal hexacarbonyl complexes belong to the O_h point group and all of their carbonyl ligands are chemically equal. There is therefore no preference for the attack to occur at any particular carbonyl group. We were able to locate a transition state (TS) corresponding to this mechanism for each of the systems considered, **TS1_Cr** for the activation of $Cr(CO)_6$, **TS1_Mo** for the activation of $Mo(CO)_6$ and **TS1_W** for the activation of $W(CO)_6$. From these TS geometries, we performed an IRC calculation, which produced the reactant-side intermediates, **ADD1_Cr**, **ADD1_Mo** and **ADD1_W**, as well as the product-side intermediates, **ADD2_Cr**, **ADD2_Mo** and **ADD2_W**. The geometries shared the same qualitative features for the three systems (see the discussion of the TS geometries further down), and only those corresponding to the Cr system are shown in Figure 5.2.

The relative free energies for the computed stationary points are collected in Table 5.1. As expected, the reaction is in all cases very exergonic. This is both because of the release of the very stable CO_2 molecule and TMAO being a very strong oxidating agent. We define the computed barrier for the activation of the metal hexacarbonyl complexes to be the difference between the free energies of the TS and the reactant-side adduct ($\Delta G^{\ddagger}$= G(TS1) - G(ADD1)). We first of all see that the height of the barrier varies very little within the three metal hexacarbonyl activations, being 57

UNIVERSITAT ROVIRA I VIRGILI
COMPUTACIONAL STUDIES ON THE MECHANISM OF THE PAUSON-KHAND REACTION
Torstein Fjermestad
ISBN:978-84-693-9441-0/DL:T.62-2011

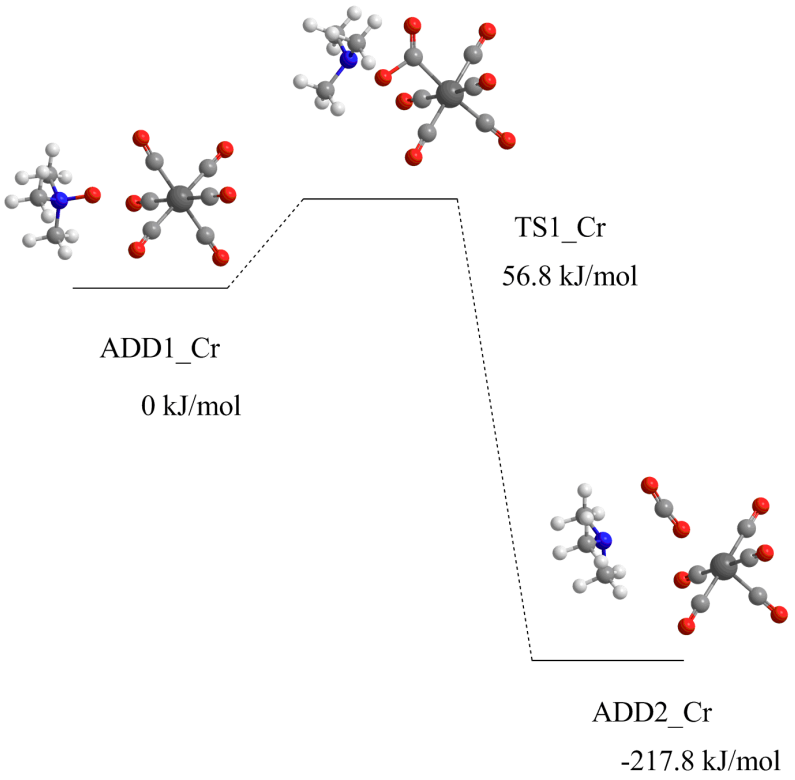

Figure 5.2: B3LYP optimised structures for the three species involved in the reaction of $Cr(CO)_6$ with TMAO: reactant-side adduct **ADD1_Cr**, transition state **TS_Cr** and product-side adduct **ADD2_Cr**.

UNIVERSITAT ROVIRA I VIRGILI
COMPUTACIONAL STUDIES ON THE MECHANISM OF THE PAUSON-KHAND REACTION
Torstein Fjermestad
ISBN:978-84-693-9441-0/DL:T.62-2011

$kJ{\cdot}mol^{-1}$ for the activation of $Cr(CO)_6$, 56 $kJ{\cdot}mol^{-1}$ for the activation of $Mo(CO)_6$ and 55 $kJ{\cdot}mol^{-1}$ for the activation of $W(CO)_6$. Albeit showing a small variation in the activation barrier of the metal hexacarbonyl complexes, we see a trend towards lower barriers when going down the column. The barrier is 1 $kJ{\cdot}mol^{-1}$ lower for $Mo(CO)_6$ than for $Cr(CO)_6$, and 2 $kJ{\cdot}mol^{-1}$ lower for $W(CO)_6$ than for $Cr(CO)_6$. These differences are certainly small, in fact in the limit of the expected accuracy of our computational methods. However, it is worth noting that they reproduce the expected trend from the experimental data. In their study on the reaction between $M(CO)_6$, PPh_3 and TMAO, Shi, Basolo and co-workers [118] found the following ratios between the rate constants, $k_{Mo}/k_{Cr} = 1.3$ and $k_W/k_{Cr} = 2.5$. The trivial conversion from quotient between rate constants to difference in activation energies using simple transition state theory, results in the $\Delta\Delta G^{\ddagger}_{exper}$ values shown in Table 5.1. The agreement with computed values is perfect! Of course, the precision of both the experimental and computational techniques does not allow to appreciate tenths of $kJ{\cdot}mol^{-1}$, which limits the merit of the achievement. However, the agreement between both sets of results is encouraging, and strongly hints that the simple mechanistic proposal is the correct one for this case. The reaction proceeds thus through a single step of oxygen transfer from amine oxide to a metal-bound carbonyl group. The phosphine reactant is necessary to capture the coordinatively unsaturated complex resulting from carbonyl loss, but plays no role in the rate determining step.

Table 5.1: Computed relative free energies (kJ/mol) of species involved in the reaction between $M(CO)_6$ and TMAO.

M	ADD1	TS	ADD2	$\Delta\Delta G^{\ddagger}_{comp}$ [a]	$\Delta\Delta G^{\ddagger}_{exper}$ [ab]
Cr	0	57	-218	0	0
Mo	0	56	-221	-1	-1
W	0	55	-190	-2	-2

[a] $\Delta\Delta G^{\ddagger} = \Delta\Delta G^{\ddagger}_{\mathrm{M}} - \Delta\Delta G^{\ddagger}_{\mathrm{Cr}}$

[b] Experimental value estimated from reported rate constants ratio [118]

5.3.1 Transition state geometries

We proceed to discuss the transition state geometries, **TS1_Cr**, **TS1_Mo** and **TS1_W**, of the three activations.

Activation of $Cr(CO)_6$

In **TS1_Cr** (see figure 5.3) the leaving CO_2 is still within the coordination sphere of the chromium atom (Cr1) with a Cr1-C1 distance of 2.115 Å. The TMAO oxygen (O1) is partly transferred to the carbonyl carbon (C1) with the N1-O1 distance

UNIVERSITAT ROVIRA I VIRGILI
COMPUTACIONAL STUDIES ON THE MECHANISM OF THE PAUSON-KHAND REACTION
Torstein Fjermestad
ISBN:978-84-693-9441-0/DL:T.62-2011

being 1.593 Å and the O1-C1 distance being 1.437 Å. By comparison with the corresponding distances in the reactant side intermediate, **ADD1_Cr** (Cr1-C1: 1.923 Å and O1-N1: 1.367 Å), and the product side intermediate, **ADD2_Cr** (O1-C1: 1.173 Å), we see that transition state **TS1_Cr** lies approximately midway along the reaction coordinate.

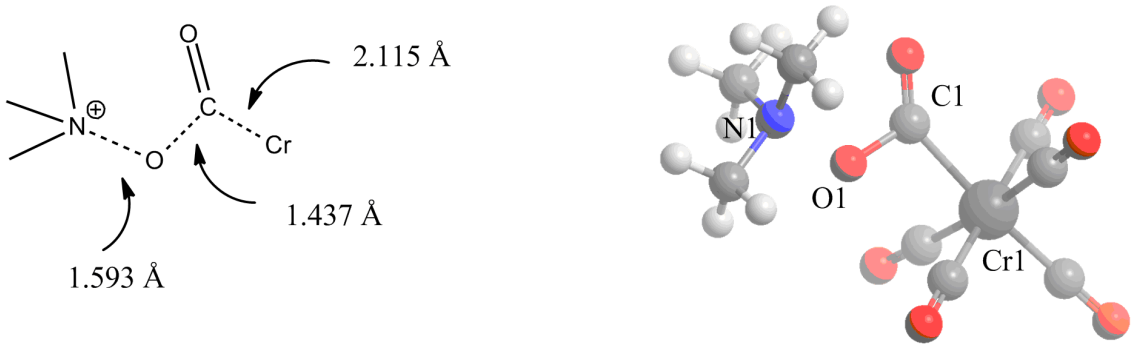

Figure 5.3: Transition state of the TMAO attack of $Cr(CO)_6$. Schematic representation of the bonds being broken and formed (left, dashed lines) and a 3D representation of the TS geometry (right).

Activation of $Mo(CO)_6$

TS1_Mo represented in figure 5.4 is qualitatively similar to **TS1_Cr**. The Mo1-C1 distance is 2.266 Å, the N1-O1 distance is 1.588 Å and the O1-C1 distance is 1.446 Å. Comparing these distances with the corresponding distances in the reactant side intermediate, **ADD1_Mo** (Mo1-C1: 2.090 Å and O1-N1: 1.370 Å), and the product side intermediate, **ADD2_Mo** (O1-C1: 1.176 Å), we see that **TS1_Mo** lies approximately midway along the reaction coordinate.

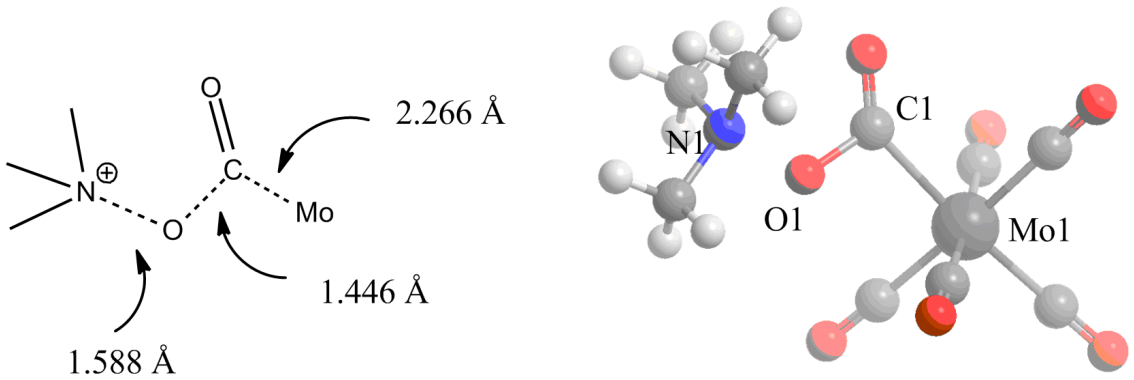

Figure 5.4: Transition state of the TMAO attack of $Mo(CO)_6$. Schematic representation of the bonds being broken and formed (left, dashed lines) and a 3D representation of the TS geometry (right).

UNIVERSITAT ROVIRA I VIRGILI
COMPUTACIONAL STUDIES ON THE MECHANISM OF THE PAUSON-KHAND REACTION
Torstein Fjermestad
ISBN:978-84-693-9441-0/DL:T.62-2011

Activation of $W(CO)_6$

TS1_W represented in figure 5.5 is qualitatively similar to **TS1_Cr** and **TS1_Mo**. The W1-C1 distance is 2.250 Å, the N1-O1 distance is 1.610 Å and the O1-C1 distance is 1.432 Å. Comparing these distances with the corresponding distances in the reactant side intermediate, **ADD1_W** (W1-C1: 2.076 Å and O1-N1: 1.370 Å), and the product side intermediate, **ADD2_W** (O1-C1: 1.233 Å), we see that **TS1_W** lies approximately midway along the reaction coordinate.

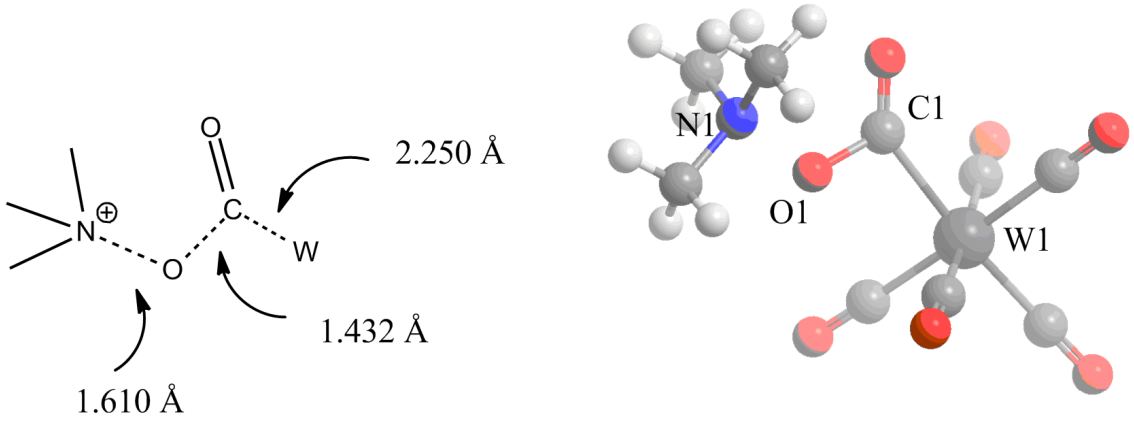

Figure 5.5: Transition state of the TMAO attack of $W(CO)_6$. Schematic representation of the bonds being broken and formed (left, dashed lines) and a 3D representation of the TS geometry (right).

Comparison of the three TS geometries

Table 5.2 shows the bond distances described above in the reactant side intermediate and the transition states of the three activations. The bond distances in the reactant side intermediate, **ADD1**, and the transition state, **TS1**, are very similar in the $Mo(CO)_6$ and $W(CO)_6$ activations. Both in **ADD1_Cr** and **TS1_Cr**, the metal - carbonyl distance is about 0.2 Å shorter than in the second and third row activations. When looking at the change in the bond distance when going from **ADD1** to **TS1** there are practically no change between the three activations. The metal - carbonyl bonds are in all cases stretched by about 0.2 Å and the N-O bonds by about 0.2 Å.

This high similarity between the transition states and the reactant side intermediates for the different activations ($Cr(CO)_6$, $Mo(CO)_6$ and $W(CO)_6$) is likely to be the cause of the small variation in the activation barriers.

5.4 Activation of pentacarbonyl complexes $M(CO)_5$

Next we went on to study the activation of the metal pentacarbonyl complexes ($M(CO)_5$, M=Fe, Ru, Os) by TMAO. The trigonalbipyramidal (TBP) structure of metal pentacarbonyl complexes represents a selectivity issue in that the TMAO can

UNIVERSITAT ROVIRA I VIRGILI
COMPUTACIONAL STUDIES ON THE MECHANISM OF THE PAUSON-KHAND REACTION
Torstein Fjermestad
ISBN:978-84-693-9441-0/DL:T.62-2011

Table 5.2: Distances (Å) of the bonds being broken and formed during the TMAO activation. The values in the reactant side intermediate, **ADD1**, the transition state, **TS1**, and the change, $\Delta_{TS-ADD1}$, are given.

	ADD1	**TS**	$\Delta_{TS-ADD1}$
Cr			
Cr1-C1	1.923	2.115	0.192
N1-O1	1.367	1.593	0.226
O1-C1	2.838	1.437	-1.401
Mo			
Mo1-C1	2.090	2.266	0.176
N1-O1	1.370	1.588	0.218
O1-C1	2.794	1.446	-1.348
W			
W-C1	2.076	2.250	0.174
N1-O1	1.370	1.610	0.240
O1-C1	2.801	1.432	-1.369

attack an axial carbonyl ligand as well as an equatorial carbonyl ligand. Attempts to optimise TSs for the equatorial attack collapsed into TSs for the axial attack. In order to make an approximate assessment of the preference for the axial attack over the equatorial attack, we carried out constrained TS optimisations forcing the attack to occur at the equatorial site. The equatorial carbonyls were constrained to be in a plane perpendicular to the two axial carbonyl groups. The angle between each of the equatorial carbonyls was constrained to 120°. The energies of these constrained equatorial TSs were compared to the energies of the axial TSs optimised with the same constraints. The potential energy differences between the constrained equatorial TSs and axial TSs were the following: 18 kJ/mol for $Fe(CO)_5$, 19 kJ/mol for $Ru(CO)_5$ and 18 kJ/mol for $Os(CO)_5$. Due to this large potential energy difference, we excluded the possibility of an equatorial attack. We have thus established that TMAO attacks an axial carbonyl ligand. From the TS geometries located for the attack of an axial carbonyl ligand, we performed an IRC calculation in order to determine the intermediates these TSs connect. In the following, we discuss each of the cases, $Fe(CO)_5$, $Ru(CO)_5$ and $Os(CO)_5$, separately.

In the case of $Fe(CO)_5$, the reactant side intermediate, **ADD1_Fe**, corresponded to the adduct of the reactants, TMAO + $Fe(CO)_5$. The product side intermediate, **ADD2_Fe**, corresponded to an adduct of TMA, CO_2 and $Fe(CO)_4$.

The structures in figure 5.6 are calculated for the singlet state. However, it is known that the most stable spin state of $Fe(CO)_4$ is the triplet state [120]. On the other hand the spin state of the reactant $Fe(CO)_5$ is a singlet, and a surface crossing must thus occur at some point during the reaction. Optimising the triplet state of $Fe(CO)_5$ resulted in a dissociation of one of the carbonyl ligands. A surface crossing to the triplet state seems thus to occur after a complete detachment of the leaving carbonyl from the iron complex has taken place. The singlet TS in figure 5.6, **TS1_Fe**, has still the leaving carbonyl group within the inner coordination sphere. A single point

UNIVERSITAT ROVIRA I VIRGILI
COMPUTACIONAL STUDIES ON THE MECHANISM OF THE PAUSON-KHAND REACTION
Torstein Fjermestad
ISBN:978-84-693-9441-0/DL:T.62-2011

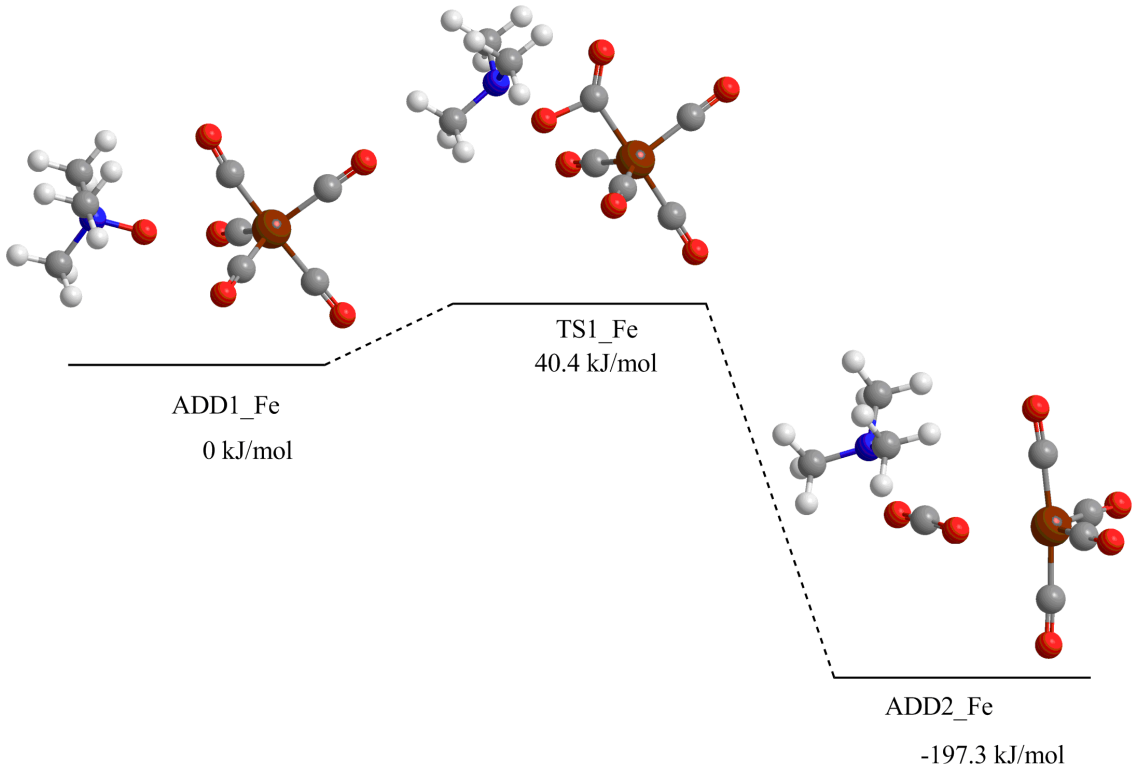

Figure 5.6: B3LYP optimised structures for the three species involved in the reaction of $Fe(CO)_5$ with TMAO: reactant-side adduct **ADD1_Fe**, transition state **TS1_Fe** and product-side adduct **ADD2_Fe**.

UNIVERSITAT ROVIRA I VIRGILI
COMPUTACIONAL STUDIES ON THE MECHANISM OF THE PAUSON-KHAND REACTION
Torstein Fjermestad
ISBN:978-84-693-9441-0/DL:T.62-2011

calculation of the triplet state of **TS1_Fe** gave a potential energy of 209.4 kJ/mol above the singlet state. This indicates that the surface crossing takes place after the singlet TS, **TS1_Fe**, and that the triplet state of $Fe(CO)_4$ does not affect the kinetics of the reaction.

In the case of $Ru(CO)_5$ we performed an IRC calculation towards the reactant side intermediate and the product side intermediate. The reactant side intermediate, **ADD1_Ru**, corresponded to an adduct of the reactants TMAO and $Ru(CO)_5$. The product side intermediate, **ADD2_Ru**, corresponded to an adduct of TMA, CO_2 and $Ru(CO)_4$. The free energy profile together with the structures of the stationary points is shown in figure 5.7.

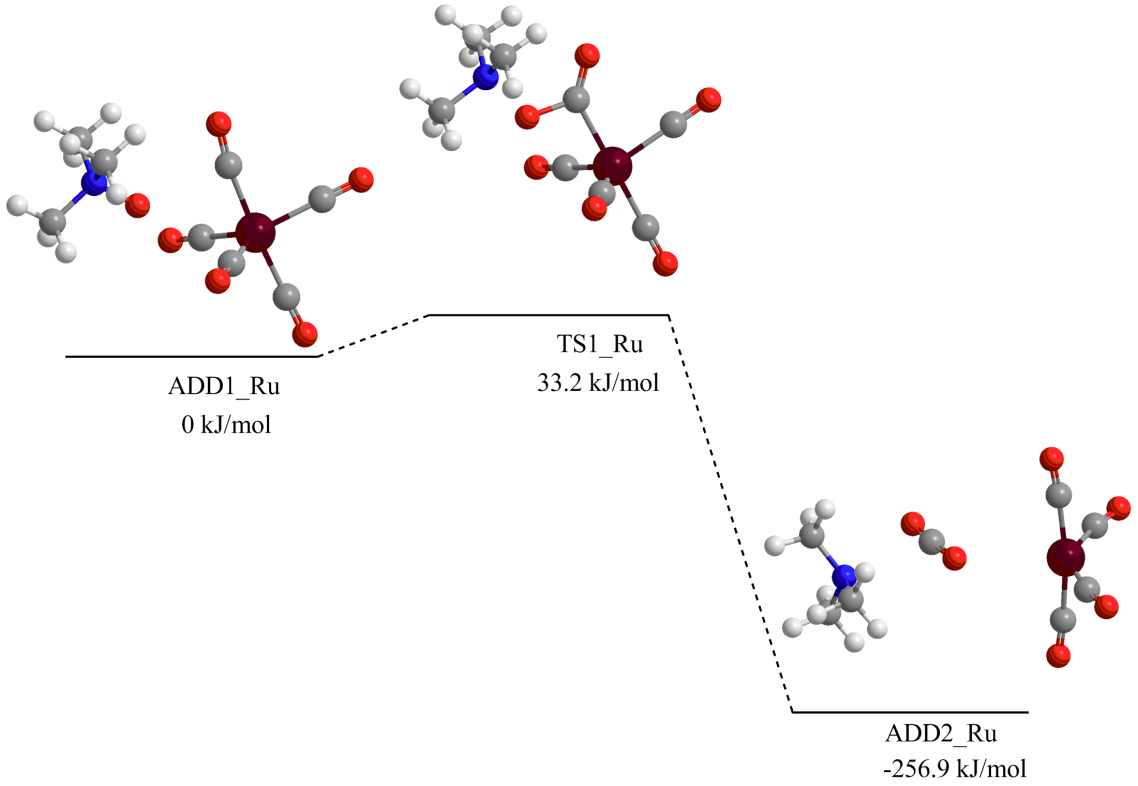

Figure 5.7: B3LYP optimised structures for the three species involved in the reaction of $Ru(CO)_5$ with TMAO: reactant-side adduct **ADD1_Ru**, transition state **TS1_Ru** and product-side adduct **ADD2_Ru**.

On the contrary to $Fe(CO)_4$, the triplet state of $Ru(CO)_4$ is less stable than the singlet and no surface crossing takes place.

In the case of $Os(CO)_5$, the IRC calculation from the TS, **TS2_Os**, ended up in intermediates that were rather different from those located in the case of $Fe(CO)_5$ and $Ru(CO)_5$. The reactant side intermediate ended up in a very shallow intermediate, **INT1_Os**. **INT1_Os** is connected to the adduct of the reactants, TMAO and $Os(CO)_5$, **ADD1_Os**, through a very flat TS, **TS1_Os**, with an eigenvalue of 36.2i of the vibrational mode. The product side intermediate of **TS2_Os** ended up in an intermediate, **INT2_Os**, with the CO_2 partially formed, but still coordinated to the

UNIVERSITAT ROVIRA I VIRGILI
COMPUTACIONAL STUDIES ON THE MECHANISM OF THE PAUSON-KHAND REACTION
Torstein Fjermestad
ISBN:978-84-693-9441-0/DL:T.62-2011

osmium complex (the angle of O-C-O is 140.9 °). This intermediate is connected to the product adduct (TMA + CO_2 + $Os(CO)_4$) , **ADD2_Os**, through **TS3_Os**. Concerning the product adduct, the triplet state of $Os(CO)_4$ is less stable than the singlet state and no surface crossing takes place. Figure 5.8 shows the free energy profile of the activation of $Os(CO)_5$ with the structures of the stationary points inserted.

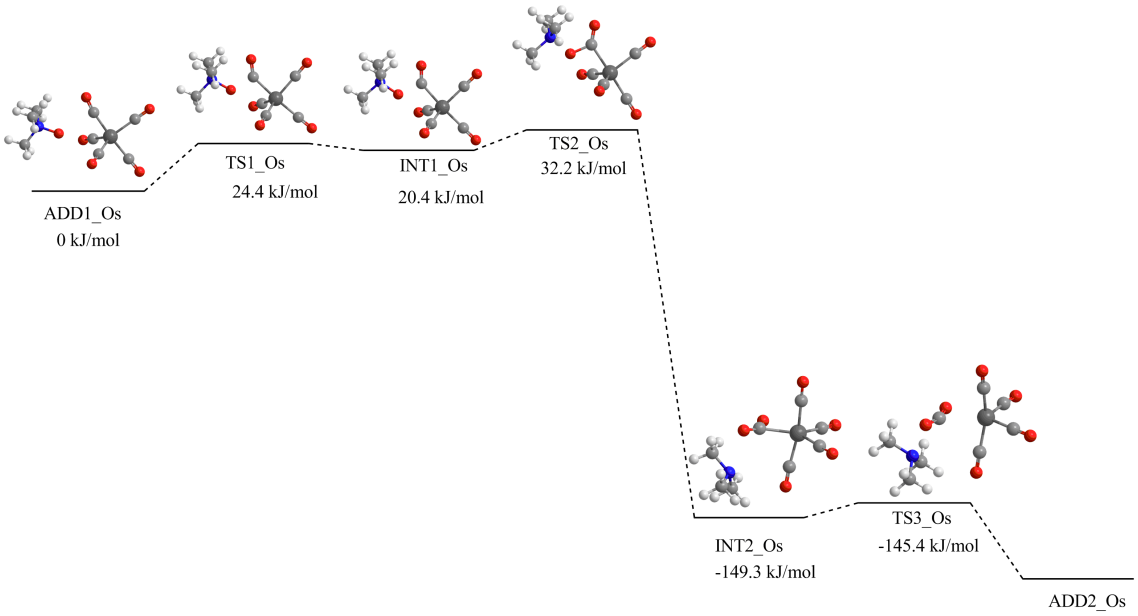

Figure 5.8: B3LYP optimised structures for the species involved in the reaction of $Os(CO)_5$ with TMAO.

In the activation of the metal pentacarbonyl complexes, we define the computed reaction barrier as the free energy difference between the rate-determining TS and the reactant adduct, $\Delta G^{\ddagger}_{TS1\_Fe-ADD1\_Fe}$, $\Delta G^{\ddagger}_{TS1\_Ru-ADD1\_Ru}$ and $\Delta G^{\ddagger}_{TS2\_Os-ADD1\_Os}$. The height of the reaction barrier is decreasing as we go down the triad. For the activation of $Fe(CO)_5$, the computed barrier is 40.4 kJ/mol, for the activation of $Ru(CO)_5$, the computed barrier is 33.2 kJ/mol and for the activation of $Os(CO)_5$, the computed barrier is 32.2 kJ/mol. This trend is similar to the trend of computed barrier heights for the metal hexacarbonyl activation. However, in the case of the metal pentacarbonyl activation, we see a more pronounced decrease between the first-row complex, $Fe(CO)_5$, and the second-row complex $Ru(CO)_5$. The activation barriers for $Ru(CO)_5$ and $Os(CO)_5$ are respectively 7.2 kJ/mol and 8.2 kJ/mol lower than the activation barrier for $Fe(CO)_5$. This trend agrees well with the increase in the experimentally determined rate constants observed when going down the triad. At 20.6°C, the rate constant for the activation of $Fe(CO)_5$, k_{Fe}, is $2.37{\cdot}10^{-2}$ $M^{-1}s^{-1}$, the rate constant for the activation of $Ru(CO)_5$, k_{Ru}, is $7.41{\cdot}10^{-2}$ $M^{-1}s^{-1}$ and the rate constant for the activation of $Os(CO)_5$, k_{Os}, is $9.70{\cdot}10^{-2}$ $M^{-1}s^{-1}$. To get a direct comparison between the experimentally determined rate constants and the computationally determined activation barriers, we convert the ratio of the rate constants k_{Ru}/k_{Fe} and k_{Os}/k_{Fe} to the corresponding difference in the free energy of

UNIVERSITAT ROVIRA I VIRGILI
COMPUTACIONAL STUDIES ON THE MECHANISM OF THE PAUSON-KHAND REACTION
Torstein Fjermestad
ISBN:978-84-693-9441-0/DL:T.62-2011

activation, $\Delta\Delta G^{\ddagger}_{exper}$. The comparison is shown in table 5.3, and the agreement is good.

Table 5.3: Computed relative free energies (kJ/mol) of species involved in the reaction between $M(CO)_5$ and TMAO.

M	ADD1	TS	ADD2	$\Delta\Delta G^{\ddagger}_{\text{comp}}$ [a]	$\Delta\Delta G^{\ddagger}_{\text{exper}}$ [ab]
Fe	0	40	-197	0	0
Ru	0	33	-257	-7	-3
Os	0	32	-209	-8	-4

[a] $\Delta\Delta G^{\ddagger} = \Delta\Delta G^{\ddagger}_{\text{M}} - \Delta\Delta G^{\ddagger}_{\text{Fe}}$

[b] Experimental value estimated from reported rate constants ratio [119]

The good agreement of the computationally determined reaction barriers and the experimentally determined rate constants, gives us an indication that the mechanism found is the correct one. For the activation of $Fe(CO)_5$ and $Ru(CO)_5$, the mechanism is a one-step mechanism whereas for the activation of $Os(CO)_5$, the mechanism is a three-step mechanism.

Comparing the computed barriers of activations for the metal hexacarbonyl complexes with the computed barriers for the metal pentacarbonyl complexes, we see that barriers for the activation of the metal hexacarbonyl complexes are higher than the barriers of activation of the metal pentacarbonyl complexes. This is in agreement with the experimental observation of a more difficult activation of metal hexacarbonyl complexes [119].

5.4.1 Transition state geometries

The geometries of the rate-determining transition state of the activation of $Fe(CO)_5$ (**TS1_Fe**), $Ru(CO)_5$ (**TS1_Ru**) and $Os(CO)_5$ (**TS2_Os**) all share the same qualitative features. These indicate an oxygen transfer from the amine nitrogen to the carbonyl carbon and a concerted expulsion of CO_2 from the coordination sphere of the metal.

Activation of $Fe(CO)_5$

In **TS1_Fe** (See figure 5.9), the Fe1-C1 distance is 1.985 Å, the N1-O1 distance is 1.633 Å and the O1-C1 distance is 1.412 Å. Comparison with the corresponding distances in the reactant side intermediate, **ADD1_Fe** (Fe1-C1: 1.824 Å) and N1-O1: 1.371 Å), and the product side intermediate, **ADD2_Fe** (O1-C1: 1.179 Å), shows that the transition state is located approximately midway along the reaction coordinate.

UNIVERSITAT ROVIRA I VIRGILI
COMPUTACIONAL STUDIES ON THE MECHANISM OF THE PAUSON-KHAND REACTION
Torstein Fjermestad
ISBN:978-84-693-9441-0/DL:T.62-2011

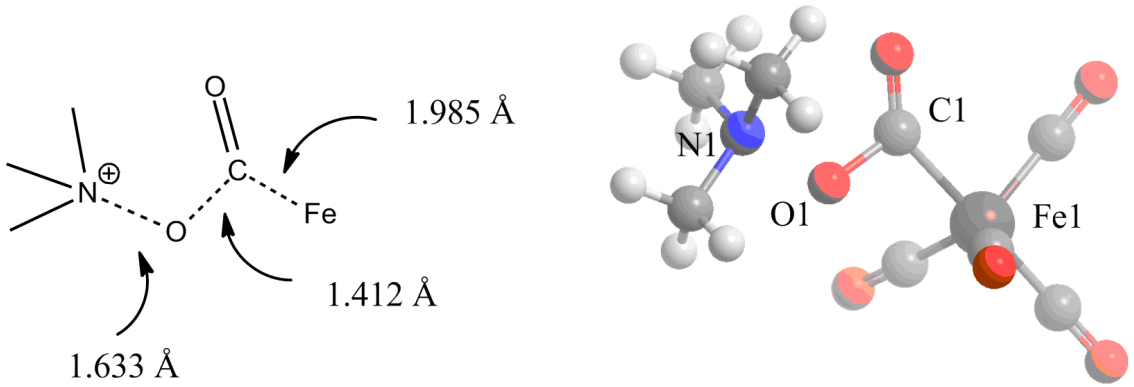

Figure 5.9: Transition state of the TMAO attack of $Fe(CO)_5$. Schematic representation of the bonds being broken and formed (left, dashed lines) and a 3D representation of the TS geometry (right).

Activation of $Ru(CO)_5$

In **TS1_Ru** (See figure 5.10), the Ru1-C1 distance is 2.128 Å, the N1-O1 distance is 1.623 Å and the O1-C1 distance is 1.414 Å. Comparison with the corresponding distances in the reactant side intermediate, **ADD1_Ru** (Ru1-C1: 1.985 Å) and N1-O1: 1.373 Å), and the product side intermediate, **ADD2_Ru** (O1-C1: 1.174 Å), shows that the transition state is located approximately midway along the reaction coordinate.

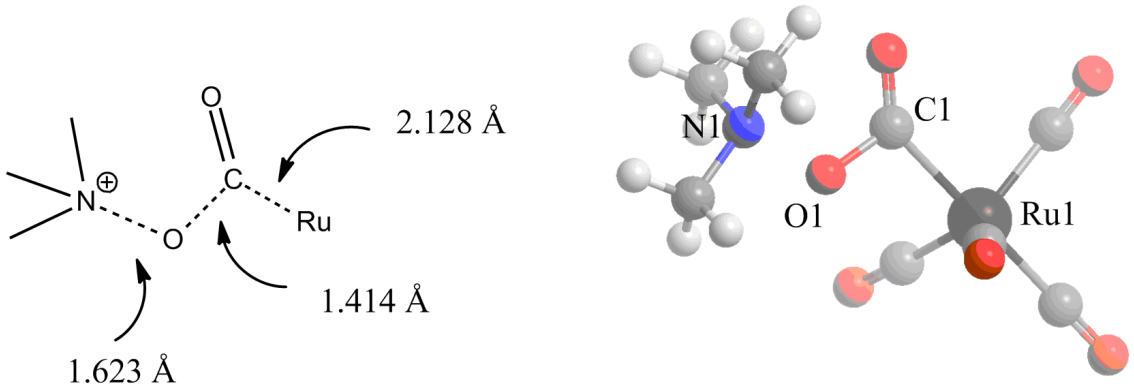

Figure 5.10: Transition state of the TMAO attack of $Ru(CO)_5$. Schematic representation of the bonds being broken and formed (left, dashed lines) and a 3D representation of the TS geometry (right).

Activation of $Os(CO)_5$

In **TS2_Os** (See figure 5.11), the Os1-C1 distance is 2.140 Å, the N1-O1 distance is 1.645 Å and the O1-C1 distance is 1.410 Å. Comparison with the corresponding distances in the reactant side intermediate, **ADD1_Os** (Os1-C1: 1.986 Å) and N1-O1: 1.372 Å), and the product side intermediate, **ADD2_Os** (O1-C1: 1.172 Å),

UNIVERSITAT ROVIRA I VIRGILI
COMPUTACIONAL STUDIES ON THE MECHANISM OF THE PAUSON-KHAND REACTION
Torstein Fjermestad
ISBN:978-84-693-9441-0/DL:T.62-2011

shows that the transition state is located approximately midway along the reaction coordinate.

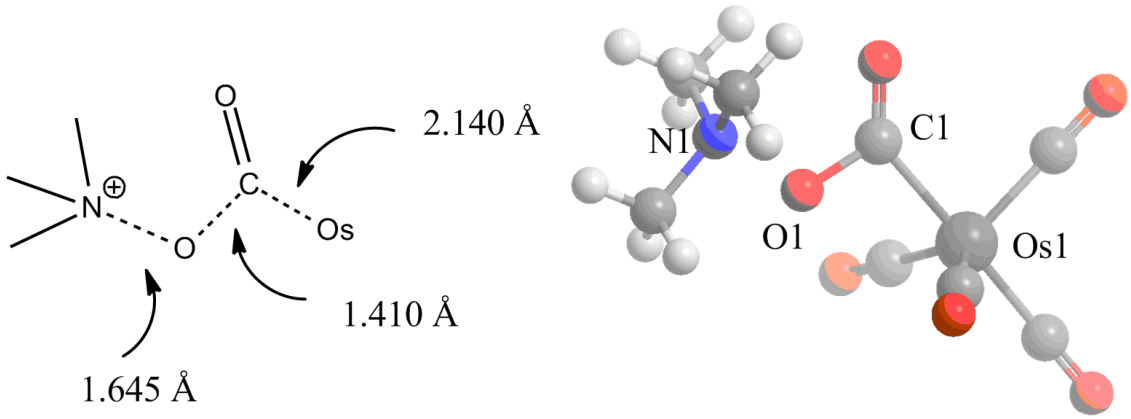

Figure 5.11: Transition state of the TMAO attack of $Os(CO)_5$. Schematic representation of the bonds being broken and formed (left, dashed lines) and a 3D representation of the TS geometry (right).

Comparison of the three TS geometries

Table 5.4 shows the distances of the bonds being broken or formed in the TMAO activation of the metal pentacarbonyl complexes.

Table 5.4: Distances (Å) of the bonds being broken and formed during the TMAO activation of metal pentacarbonyl complexes. The values of the reactant side intermediate, **ADD1**, the transition state, **TS**, and the change, $\Delta_{TS-ADD1}$, are given.

	ADD1	**TS**	$\Delta_{TS-ADD1}$
Fe			
Fe1-C1	1.824	1.985	0.161
N1-O1	1.371	1.633	0.262
O1-C1	2.684	1.412	-1.272
Ru			
Ru1-C1	1.985	2.128	0.143
N1-O1	1.373	1.623	0.250
O1-C1	2.637	1.414	-1.223
Os			
Os1-C1	1.986	2.140	0.154
N1-O1	1.372	1.645	0.273
O1-C1	2.647	1.410	-1.237

Overall the geometries of the rate-determining transition states are similar for the three activations. However, the TS geometry of the activation of the first-row complex $Fe(CO)_5$ shows a discrepancy from the TS geometries of the second and third

UNIVERSITAT ROVIRA I VIRGILI
COMPUTACIONAL STUDIES ON THE MECHANISM OF THE PAUSON-KHAND REACTION
Torstein Fjermestad
ISBN:978-84-693-9441-0/DL:T.62-2011

row complexes. In both **ADD1_Fe** and **TS1_Fe** the metal-carbonyl distance is 0.1 Å shorter than in the corresponding geometries of the $Ru(CO)_5$ and $Os(CO)_5$ activations. It is interesting to see that also the barrier of the $Fe(CO)_5$ activation is markedly higher than for the other two activations.

5.5 Activation of the PKR precursor

Having explored the mechanism of the TMAO assisted activation of metal hexacarbonyl complexes, $M(CO)_6$, and metal pentacarbonyl complexes, $M(CO)_5$, we wanted to test the viability of this mechanism in relation to the Pauson-Khand reaction. The stoichiometric Pauson-Khand reaction is mediated by a dicobalt carbonyl complex. N-oxides are commonly used as promoters in this reaction [115, 116]. An example of the stoichiometric Pauson-Khand reaction is shown in figure 5.13. Presumably, the first step consists of an activation of the dicobalt complex similar to the TMAO assisted activation of the metal carbonyl complexes $M(CO)_6$ and $M(CO)_5$.

In our computational model of this activation step, we represented the N-oxide as TMAO. Representing the N-oxide as TMAO allows us to make better comparisons between the metal carbonyl activation and the activation of the Pauson-Khand precursor (see the orbital analysis in section 5.6). The Pauson-Khand precursor itself we modelled as $Co_2(CO)_6(\mu_2$-1-propyne). This complex can be considered as a pseudo TBP complex with two of the carbonyls, **Eq1** and **Eq2**, and the propyne in the equatorial position, and the other cobalt atom and the third carbonyl, **Ax**, in the axial position (see figure 5.12).

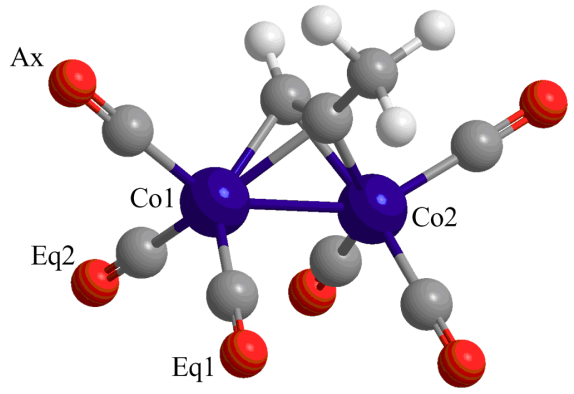

Figure 5.12: $Co_2(CO)_6(\mu_2$-1-propyne) with the labelling of the carbonyl ligands indicated.

We computed the free energy profiles for the attack of TMAO on the axial carbonyl, **Ax**, as well as the two equatorial carbonyls, **Eq1** and **Eq2**. From the transition state of each attack, we optimised reactant and product adducts. The reactant adduct optimised from the transition state of the axial attack, **R_ADD_Ax**, turned out to be the most stable reactant adduct, and this was used as the common zero level.

UNIVERSITAT ROVIRA I VIRGILI
COMPUTACIONAL STUDIES ON THE MECHANISM OF THE PAUSON-KHAND REACTION
Torstein Fjermestad
ISBN:978-84-693-9441-0/DL:T.62-2011

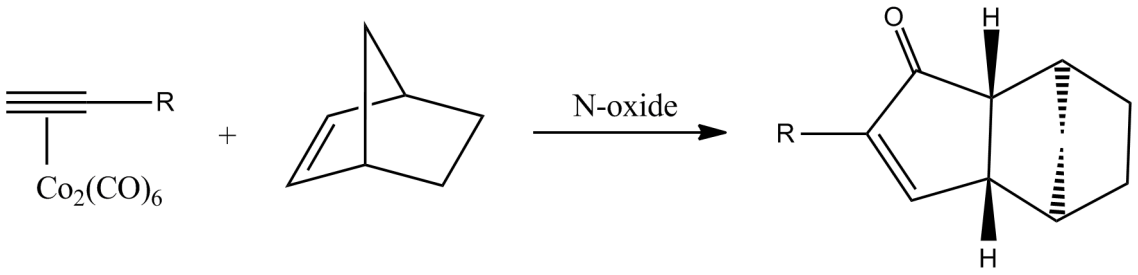

Figure 5.13: A stoichiometric Pauson-Khand reaction between norbornene and an alkyne activated by an N-oxide.

5.5.1 TMAO attack on the axial carbonyl ligand

The free energy profile of the TMAO attack on the axial carbonyl ligand is shown in figure 5.14. From the reactant adduct, **R_ADD_Ax**, the reaction goes over transi-

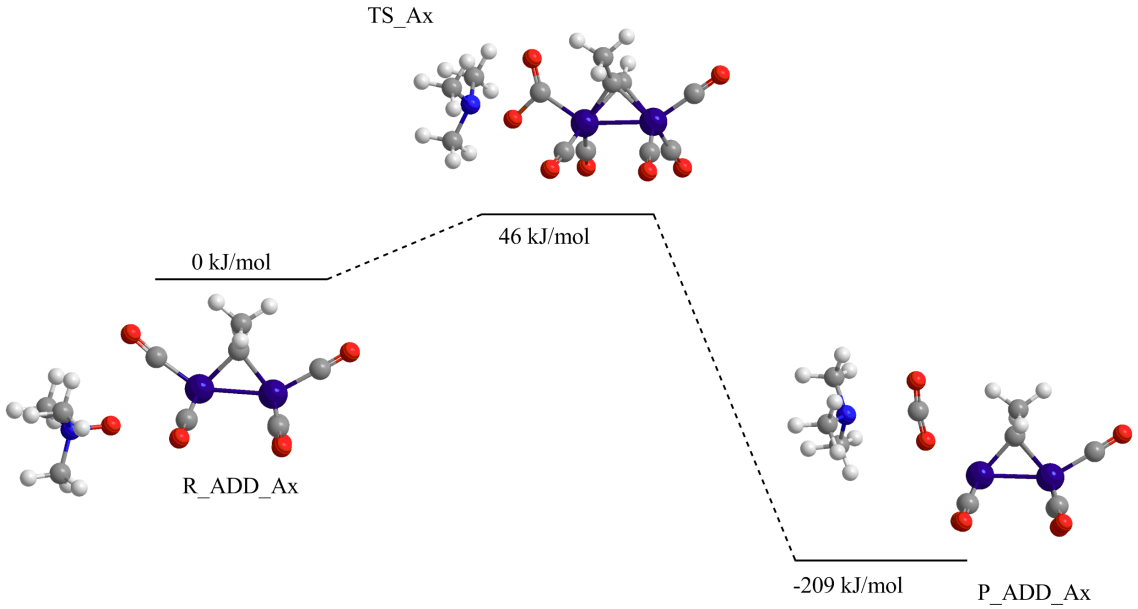

Figure 5.14: Free energy profile (kJ/mol) of the attack of TMAO on the axial carbonyl ligand.

tion state **TS_Ax** (46 kJ/mol) and further on to the product adduct, **P_ADD_Ax** (-209 kJ/mol). The reaction is very exergonic because of the strong oxidising agent TMAO and the release of the stable CO_2 molecule.

In the transition state, **TS_Ax**, the leaving CO_2 is still within the coordination sphere of the cobalt atom, with the Co1-C1 distance being 1.917 Å. The TMAO oxygen is partly transferred to the carbonyl with the N1-O1 distance being 1.616 Å and the C1-O1 distance being 1.416 Å (see figure 5.15). By comparison with the corresponding distances in the reactant adduct (N1-O1: 1.370 Å and Co1-C1: 1.783 Å) and the product adduct (C1-O1: 1.180 Å), we see that the transition state geometry is located approximately midway along the reaction coordinate.

UNIVERSITAT ROVIRA I VIRGILI
COMPUTACIONAL STUDIES ON THE MECHANISM OF THE PAUSON-KHAND REACTION
Torstein Fjermestad
ISBN:978-84-693-9441-0/DL:T.62-2011

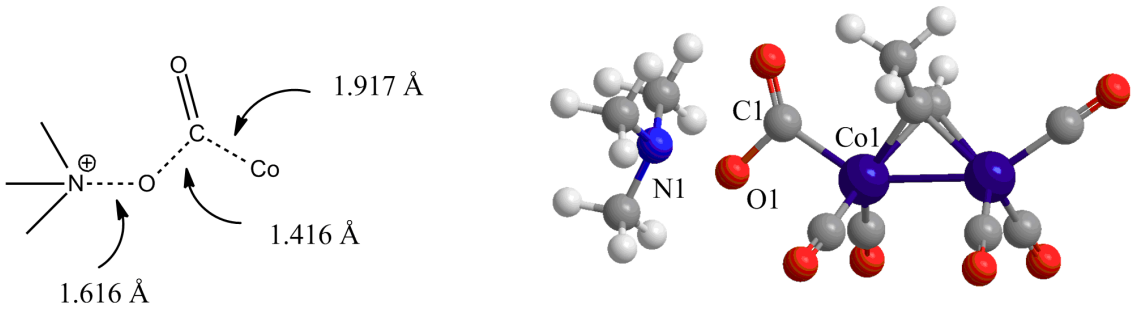

Figure 5.15: Transition state of the TMAO attack on the axial carbonyl ligand. Schematic representation of the bonds being broken and formed (left, dashed lines) and a 3D representation of the TS geometry (right).

5.5.2 TMAO attack on the equatorial carbonyl ligand Eq1

The free energy profile of the TMAO attack on the equatorial carbonyl ligand **Eq1** is presented in figure 5.16. From the reactant adduct **R_ADD_Eq1** (6 kJ/mol),

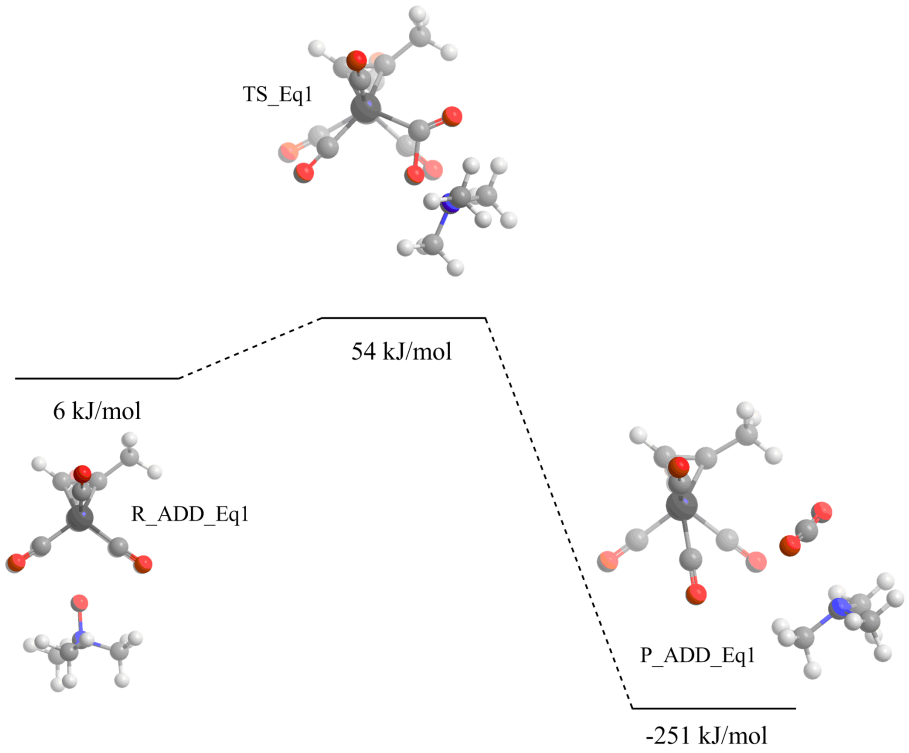

Figure 5.16: Free energy profile of the TMAO attack on the equatorial carbonyl ligand **Eq1** *cis* to the methyl group of the alkyne.

the reaction goes over **TS_Eq1** (54 kJ/mol) to product adduct **P_ADD_Eq1** (-251 kJ/mol).

In the transition state, **TS_Eq1**, the leaving CO_2 is still within the coordination sphere of the cobalt atom, with the Co1-C1 distance being 1.978 Å. The TMAO oxygen is partly transferred to the carbonyl with the N1-O1 distance being 1.545

UNIVERSITAT ROVIRA I VIRGILI
COMPUTACIONAL STUDIES ON THE MECHANISM OF THE PAUSON-KHAND REACTION
Torstein Fjermestad
ISBN:978-84-693-9441-0/DL:T.62-2011

Å and the C1-O1 distance being 1.466 Å (see figure 5.17). By comparison with the corresponding distances in the reactant adduct **R_ADD_Eq1** (N1-O1: 1.373 Å and Co1-C1: 1.821 Å) and the product adduct **P_ADD_Eq1** (C1-O1: 1.171 Å), we see that the transition state geometry is located approximately midway along the reaction coordinate.

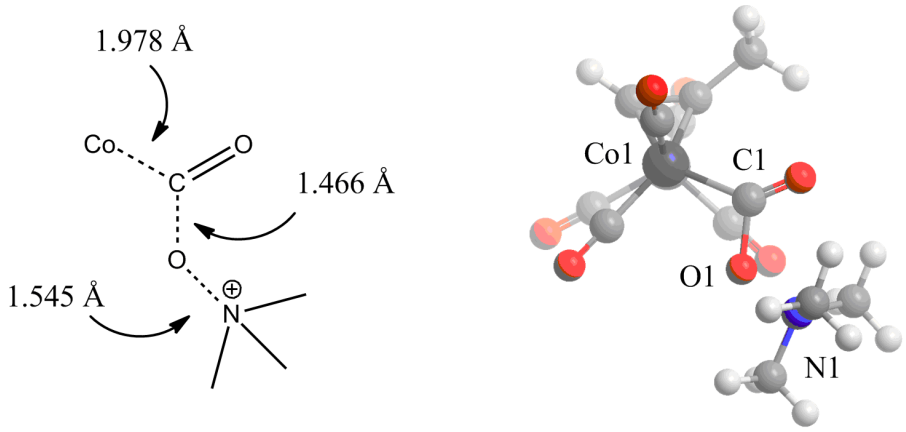

Figure 5.17: Transition state of the TMAO attack on the equatorial carbonyl ligand **Eq1**. Schematic representation of the bonds being broken and formed (left, dashed lines) and a 3D representation of the TS geometry (right).

5.5.3 TMAO attack on the equatorial carbonyl ligand Eq2

The free energy profile of the TMAO attack on the equatorial carbonyl ligand **Eq2** is presented in figure 5.18. From the reactant adduct **R_ADD_Eq2** (5 kJ/mol), the reaction goes over **TS_Eq2** (49 kJ/mol) to product adduct **P_ADD_Eq2** (-254 kJ/mol).

In the transition state, **TS_Eq2**, the leaving CO_2 is still within the coordination sphere of the cobalt atom, with the Co1-C1 distance being 1.985 Å. The TMAO oxygen is partly transferred to the carbonyl with the N1-O1 distance being 1.548 Å and the C1-O1 distance being 1.462 Å (see figure 5.19). By comparison with the corresponding distances in the reactant adduct **R_ADD_Eq2** (N1-O1: 1.373 Å and Co1-C1: 1.828 Å) and the product adduct **P_ADD_Eq2** (C1-O1: 1.171 Å), we see that the transition state geometry is located approximately midway along the reaction coordinate.

5.5.4 Trends in the activation barriers

Table 5.5 shows the Gibbs free energy and important bond distances of the transition states for the attack of the different carbonyl ligands.

The TMAO attack of the axial carbonyl ligand (TS_{Ax} = 46 kJ/mol) is favoured over the attack of the equatorial carbonyl ligands (TS_{Eq1} = 54 kJ/mol and TS_{Eq2} = 49

UNIVERSITAT ROVIRA I VIRGILI
COMPUTACIONAL STUDIES ON THE MECHANISM OF THE PAUSON-KHAND REACTION
Torstein Fjermestad
ISBN:978-84-693-9441-0/DL:T.62-2011

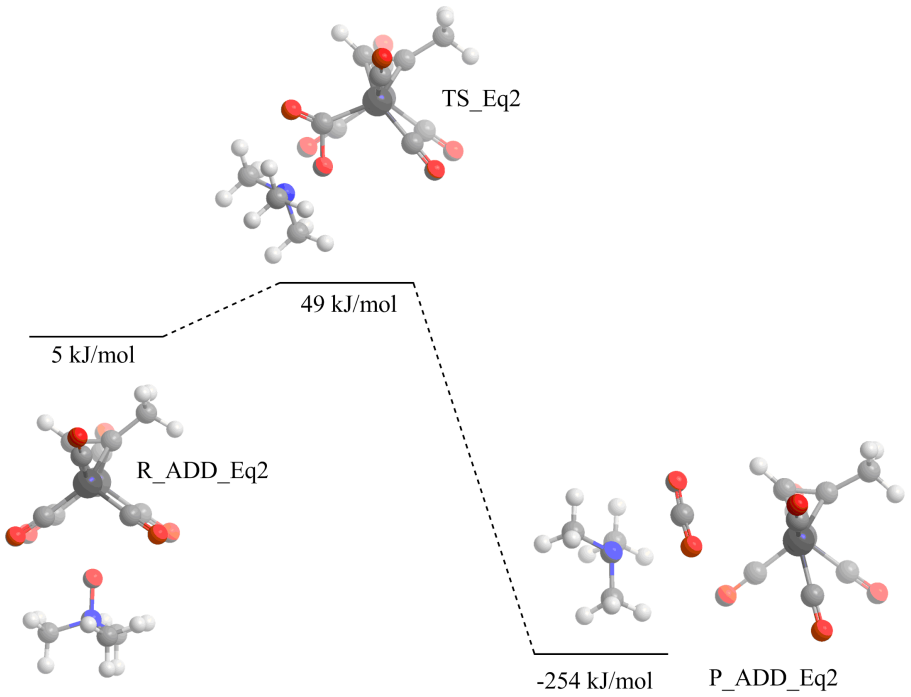

Figure 5.18: Free energy profile of the TMAO attack on the equatorial carbonyl ligand **Eq2** *trans* to the methyl group of the alkyne.

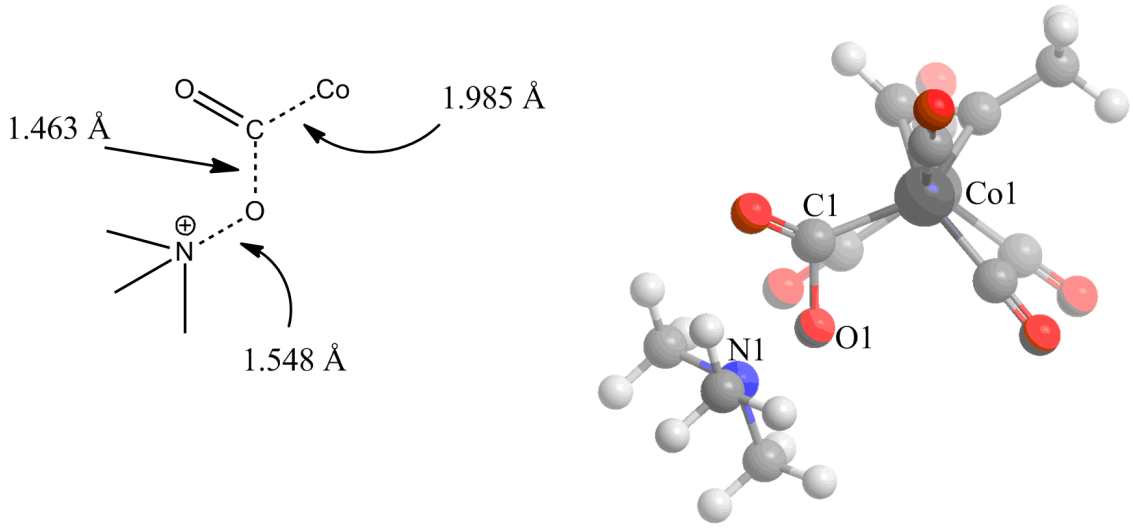

Figure 5.19: Transition state of the TMAO attack on the equatorial carbonyl ligand **Eq2** *trans* to the methyl group. Schematic representation of the bonds being broken and formed (left, dashed lines) and a 3D representation of the TS geometry (right).

UNIVERSITAT ROVIRA I VIRGILI
COMPUTACIONAL STUDIES ON THE MECHANISM OF THE PAUSON-KHAND REACTION
Torstein Fjermestad
ISBN:978-84-693-9441-0/DL:T.62-2011

Table 5.5: Gibbs free energy and important bond distances of the TSs of the TMAO activation of the Pauson-Khand precursor.

	ΔG/(kJ/mol)	Co1-C1 / Å	N1-O1 / Å	O1-C1 / Å
TS_{Ax}	46	1.917	1.616	1.416
TS_{Eq_1}	54	1.978	1.545	1.466
TS_{Eq_2}	49	1.985	1.548	1.463

kJ/mol). The distances of the bonds involved in the reaction are very similar in the TSs of the equatorial attacks (differing by at most 0.01 Å). The corresponding bond distances of the axial attack differ markedly. The cobalt-carbonyl distance and the oxygen - carbon distance are shorter (-0.06 Å and -0.04 Å respectively) and the nitrogen - oxygen distance is longer (+0.07 Å). Overall, however, the discrimination between the different carbonyl ligands is rather small and in the case of studying real systems with larger N-oxides and alkynes, we can not exclude the possibility of an attack at any of the three carbonyl ligands.

5.6 Orbital analysis

To better understand the differences and similarities between the activation of the metal carbonyl complexes $M(CO)_n$ ($n = 5,6$) and the activation of the Pauson-Khand precursor, an orbital analysis was undertaken. In our models, TMAO is activating both the metal carbonyl complexes $M(CO)_n$ ($n = 5,6$) as well as the Pauson-Khand precursor. Any orbital difference leading to the observed differences in the reaction barriers must thus be on the metal carbonyl complex itself. The attack of the TMAO on the carbonyl carbon is of nucleophilic nature. There is thus a net electron flow from the oxygen of TMAO to the carbon of the carbonyl. That is, there is a flow of electrons from the HOMO of the TMAO to an unoccupied molecular orbital (UMO) of right symmetry on the metal carbonyl complex. The energy and shape of the UMO should thus be important descriptors for the reaction barriers of the TMAO assisted activation of metal carbonyl complexes.

The oxygen of the TMAO is transferred to the carbonyl carbon along a vector perpendicular to the M-C bond. The UMO of appropriate symmetry should thus have a large component along a p AO centred on the carbonyl carbon and oriented perpendicular to the M-C bond.

5.6.1 Metal hexacarbonyl complexes

Qualitative orbital scheme

Figure 5.20 (left) shows a schematic drawing of a metal hexacarbonyl complex, with the atom labelling and the orientation that will be used in the following discussion. Figure 5.21 shows the direction of the attack of TMAO. If we assume the reaction takes place on the carbonyl ligand on the $+z$ axis (carbon 2), the attack occurs

UNIVERSITAT ROVIRA I VIRGILI
COMPUTACIONAL STUDIES ON THE MECHANISM OF THE PAUSON-KHAND REACTION
Torstein Fjermestad
ISBN:978-84-693-9441-0/DL:T.62-2011

approximately in the plane bisecting the xz and yz planes. The empty molecular orbital in the metal complex responsible for the interaction with TMAO must therefore have large coefficients on the p_x and p_y atomic orbitals of carbon 2.

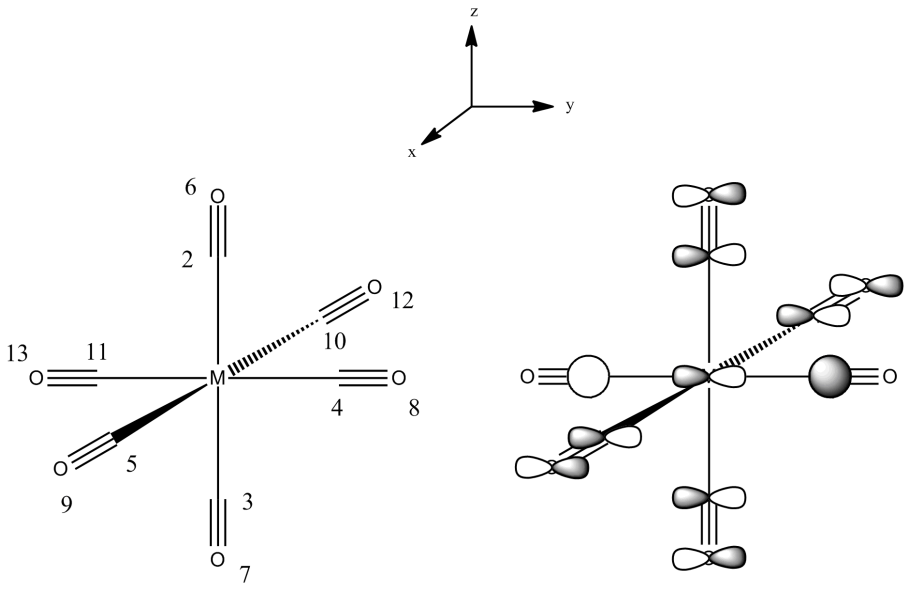

Figure 5.20: Orientation of the metal hexacarbonyl complex in a Cartesian coordinate system (left) and schematic representation of a t_{1u} orbital (right).

The O_h symmetry of the complex adds a complication to the identification of the most appropriate molecular orbital, because it corresponds to a degenerate orbital within the $t1u$ set. We can label these three degenerate orbitals (which indeed include the LUMO of the system) as t_{1u}_x, t_{1u}_y and t_{1u}_z according to the p orbitals they include. Figure 5.20 (right) shows a schematic drawing of the t_{1u}_y orbital. The fragment orbital most appropriate for interaction with TMAO would correspond to a linear combination of t_{1u}_x and t_{1u}_y.

Quantitative analysis for the $M(CO)_6$ complexes

Two of the three degenerated LUMOs have large components along p AO on a given carbon atom (see figure 5.20 (right)). If we again choose this atom to be carbon atom 2, the two LUMOs with large coefficients for the p AOs perpendicular to the M-C bond will be t_{1u}_x and t_{1u}_y.

Tables 5.6, 5.7 and 5.8 present respectively the results corresponding to the complexes with Cr, Mo and W. The decomposition of the molecular orbital in atomic orbitals is further complicated by the fact that the base applied in the calculation is valence double zeta for the metal and the carbon, thus requiring the consideration of coefficients of multiple atomic orbitals for each molecular orbital.

Considering the coefficients of the carbon atom of the three complexes, we see that they vary very little between the three cases. The 2P atomic orbital has its maximum value of 0.27 at $Cr(CO)_6$ and its minimum value of 0.25 at $W(CO)_6$. Likewise the

UNIVERSITAT ROVIRA I VIRGILI
COMPUTACIONAL STUDIES ON THE MECHANISM OF THE PAUSON-KHAND REACTION
Torstein Fjermestad
ISBN:978-84-693-9441-0/DL:T.62-2011

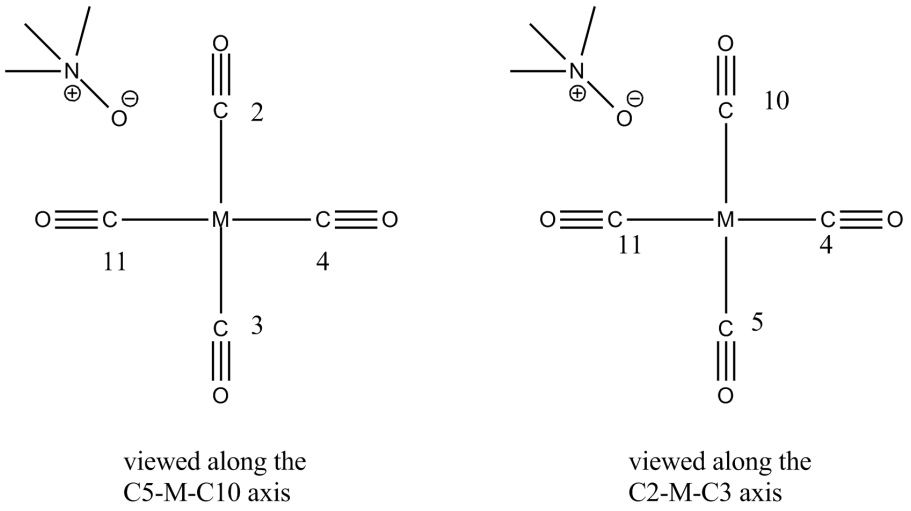

Figure 5.21: The direction of attack of TMAO on the hexacarbonyl complexes. Viewed along the x-axis (left) and the z-axis (right).

Table 5.6: Data for the t_{1u}_x and t_{1u}_y LUMOs of $Cr(CO)_6$. The coefficients are shown for the p AOs of the Cr atom and for the p AOs of carbon atom 2 located on the positive z-axis.

Cr(CO)6		
MO:	LUMO	LUMO
symmetry:	T_{1u}	T_{1u}
energy:	-0.05320	-0.05320
label;:	t_{1u}_x	t_{1u}_y
	coefficients:	coefficients:
Atom:	**Cr**	
5PX	0.39	0
5PY	0	0.39
6PX	-0.03	0
6PY	0	-0.03
Atom:	**2C**	
2PX	0.27	0
2PY	0	0.27
3PX	0.21	0
3PY	0	0.21

UNIVERSITAT ROVIRA I VIRGILI
COMPUTACIONAL STUDIES ON THE MECHANISM OF THE PAUSON-KHAND REACTION
Torstein Fjermestad
ISBN:978-84-693-9441-0/DL:T.62-2011

Table 5.7: Data for the t_{1u}–x and t_{1u}–y LUMOs of $Mo(CO)_6$. The coefficients are shown for the p AOs of the Mo atom and for the p AOs of carbon atom 2 located on the positive z-axis.

Mo(CO)6		
MO:	LUMO	LUMO
symmetry:	T_{1u}	T_{1u}
energy/Hartrees:	-0.06813	-0.06813
label:	t_{1u}–x	t_{1u}–y
	coefficients:	coefficients:
Atom:	**Mo**	
5PX	0.56	0
5PY	0	0.56
6PX	0.02	0
6PY	0	0.02
Atom:	**2C**	
2PX	0.26	0
2PY	0	0.26
3PX	0.18	0
3PY	0	0.18

Table 5.8: Data for the t_{1u}–x and t_{1u}–y LUMOs of $W(CO)_6$. The coefficients are shown for the p AOs of the W atom and for the p AOs of carbon atom 2 located on the positive z-axis.

W(CO)6		
MO:	LUMO	LUMO
symmetry:	T_{1u}	T_{1u}
energy/Hartrees:	-0.07412	-0.07412
label:	t_{1u}–x	t_{1u}–y
	coefficients:	coefficients:
Atom:	**W**	
5PX	0.59	0
5PY	0	0.59
6PX	0.05	0
6PY	0	0.05
Atom:	**2C**	
2PX	0.25	0
2PY	0	0.25
3PX	0.18	0
3PY	0	0.18

UNIVERSITAT ROVIRA I VIRGILI
COMPUTACIONAL STUDIES ON THE MECHANISM OF THE PAUSON-KHAND REACTION
Torstein Fjermestad
ISBN:978-84-693-9441-0/DL:T.62-2011

coefficient of the 3P atomic orbital varies from 0.21 at $Cr(CO)_6$ to 0.18 at $W(CO)_6$. On the other hand, the energies of the LUMO vary significantly between the three complexes. For the $Cr(CO)_6$ complex it is -0.05320 Hartrees, for $Mo(CO)_6$ it is -0.06813 Hartrees and for $W(CO)_6$ it is -0.07412 Hartrees. We thus observe a lowering of the LUMO energy as we go down the group. The free energy reaction barrier for the nucleophilic attack by TMAO also decreases down the group as shown in the following:

- $Cr(CO)_6$: 57 kJ/mol
- $Mo(CO)_6$: 56 kJ/mol
- $W(CO)_6$: 55 kJ/mol

There is a good correlation between the two quantities. As the LUMO energy lowers, so does the reaction barrier.

5.6.2 Pentacarbonyl complexes, axial

For the metal pentacarbonyl complexes, the equatorial and axial carbonyl ligands will be treated separately.

Qualitative orbital scheme

Figure 5.22 (left) shows a schematic drawing of a metal pentacarbonyl complex and figure 5.23 shows the direction of attack of the TMAO. We assume the reaction takes place on the carbonyl ligand on the $+z$ axis (carbon 3). The empty molecular orbital interacting with TMAO must therefore have large coefficients on the p_x and p_y AOs on carbon 3.

The MOs of E' symmetry of the D_{3h} complex do have large coefficients on the p_x and p_y AOs on carbon 3 (see figure 5.22, right), and we therefore chose empty e' orbitals as the appropriate UMOs interacting with the TMAO. The e' MOs are doubly generated and we label them e'_x and e'_y according to on which p AO on carbon 3 they have large coefficients.

Quantitative orbital analysis

For $Fe(CO)_5$, the lowest UMO of the E' symmetry is LUMO +1 (see table 5.9 for data).

For $Ru(CO)_5$ the lowest UMO of the E' symmetry is LUMO (see table 5.10 for data).

For $Os(CO)_5$ the lowest UMO of the E' symmetry is LUMO (see table 5.11 for data).

UNIVERSITAT ROVIRA I VIRGILI
COMPUTACIONAL STUDIES ON THE MECHANISM OF THE PAUSON-KHAND REACTION
Torstein Fjermestad
ISBN:978-84-693-9441-0/DL:T.62-2011

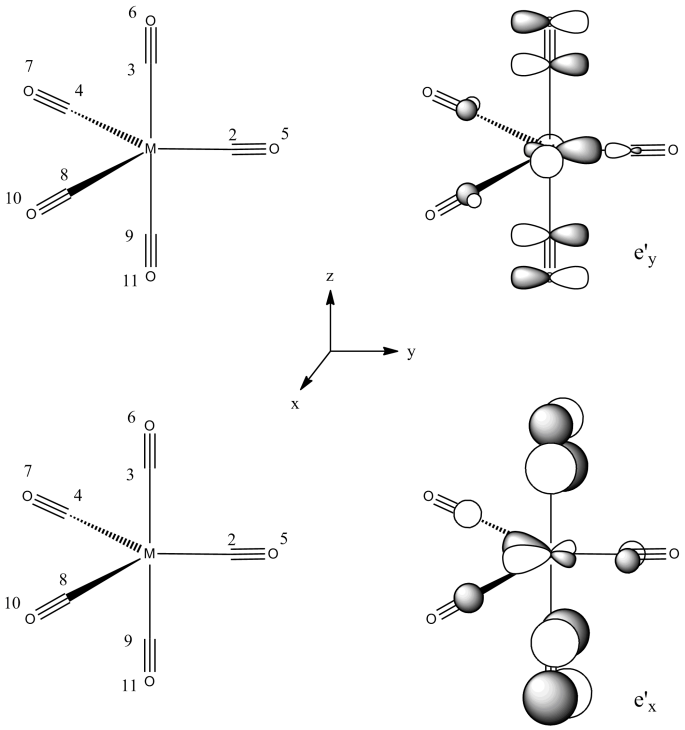

Figure 5.22: The doubly degenerated e' orbital for the metal pentacarbonyl complexes.

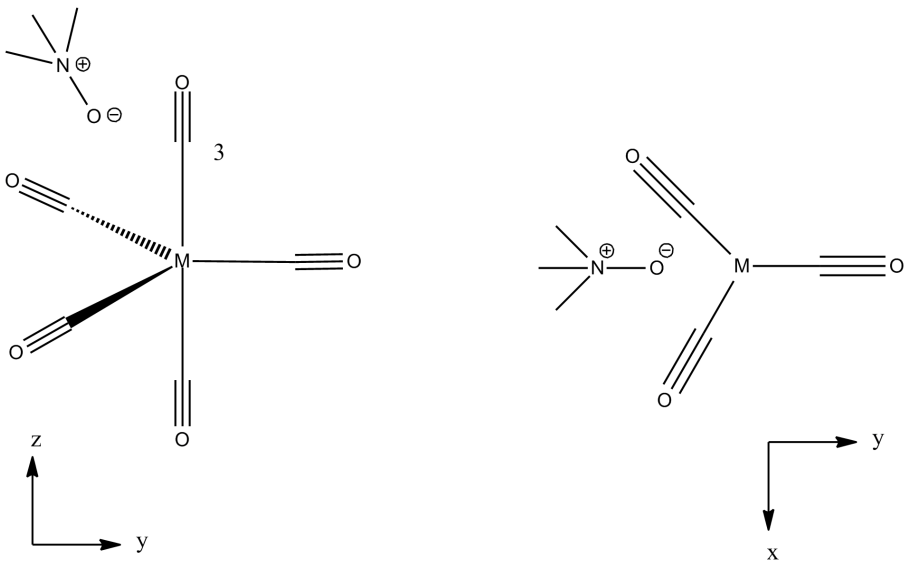

Figure 5.23: Direction of attack of TMAO on the axial carbonyl of the metal pentacarbonyl complex. Viewed along the x-axis (left) and the z-axis (right).

UNIVERSITAT ROVIRA I VIRGILI
COMPUTACIONAL STUDIES ON THE MECHANISM OF THE PAUSON-KHAND REACTION
Torstein Fjermestad
ISBN:978-84-693-9441-0/DL:T.62-2011

Table 5.9: The LUMO +1 orbital of $Fe(CO)_5$. Its coefficients along Fe centred AOs in the xy plane and along carbon atom 3 centred AOs in the x and y direction are shown.

Fe(CO)5		
MOs:	LUMO +1	LUMO +1
symmetry	E'	E'
energy/Hartrees	-0.03947	-0.03947
label:	e'_x	e'_y
	coefficients	coefficients
Atom:	**Fe**	
5PX	0.12	0
5PY	0	0.12
6PX	-0.03	0
6PY	0	-0.03
7D+2 ($d_{x^2-y^2}$)	0	-0.24
7D-2 (d_{xy})	-0.24	0
8D+2 ($d_{x^2-y^2}$)	0	-0.10
8D-2 (d_{xy})	-0.10	0
Atom: 3C		
2PX	0.41	0
2PY	0	0.41
3PX	0.36	0
3PY	0	0.36

UNIVERSITAT ROVIRA I VIRGILI
COMPUTACIONAL STUDIES ON THE MECHANISM OF THE PAUSON-KHAND REACTION
Torstein Fjermestad
ISBN:978-84-693-9441-0/DL:T.62-2011

Table 5.10: The LUMO orbital of $Ru(CO)_5$. Its coefficients along Ru centred AOs in the xy plane and along carbon atom 3 centred AOs in the x and y direction are shown.

Ru(CO)5		
MOs:	LUMO	LUMO
symmetry:	E'	E'
energy/Hartrees:	-0.05668	-0.05668
label:	e'_x	e'_y
	coefficients	coefficients
Atom:	**Ru**	
5PX	0.24	0
5PY	0	0.24
6PX	-0.03	0
6PY	0	-0.03
7D+2 ($d_{x^2-y^2}$)	0	-0.16
7D-2 (d_{xy})	-0.16	0
8D+2 ($d_{x^2-y^2}$)	0	-0.15
8D-2 (d_{xy})	-0.15	0
Atom:	**3C ax**	
2PX	0.4	0
2PY	0	0.4
3PX	0.35	0
3PY	0	0.35

UNIVERSITAT ROVIRA I VIRGILI
COMPUTACIONAL STUDIES ON THE MECHANISM OF THE PAUSON-KHAND REACTION
Torstein Fjermestad
ISBN:978-84-693-9441-0/DL:T.62-2011

Table 5.11: The LUMO orbital of $Os(CO)_5$. Its coefficients along Os centred AOs in the xy plane and along carbon atom 3 centred AOs in the x and y direction are shown

Os(CO)5		
MOs:	LUMO	LUMO
symmetry:	E'	E'
energy/Hartrees:	-0.06414	-0.06414
label:	e'_x	e'_y
	coefficients	coefficients
Atom:	**Os**	
5PX	0.34	0
5PY	0	-0.34
6PX	-0.04	0
6PY	0	0.04
7D+2 ($d_{x^2-y^2}$)	0	0.11
7D-2 (d_{xy})	-0.11	0
8D+2 ($d_{x^2-y^2}$)	0	0.22
8D-2 (d_{xy})	-0.22	0
Atom:	**3C ax**	
2PX	0.39	0
2PY	0	-0.39
3PX	0.34	0
3PY	0	-0.34

UNIVERSITAT ROVIRA I VIRGILI
COMPUTACIONAL STUDIES ON THE MECHANISM OF THE PAUSON-KHAND REACTION
Torstein Fjermestad
ISBN:978-84-693-9441-0/DL:T.62-2011

Tables 5.9, 5.10 and 5.11 show that the coefficients of the p AO on carbon atom 3 do not vary very much between the three complexes. Looking at the orbital energies on the other hand, we see a decrease in the orbital energies as we go down the group. The energy of LUMO +1 for $Fe(CO)_5$ is -0.03947 Hartrees, the energy of LUMO for $Ru(CO)_5$ is -0.05668 Hartrees and the energy of LUMO for $Os(CO)_5$ is -0.06414 Hartrees. For the nucleophilic attack of the pentacarbonyl complexes by TMAO, the computed reaction free energy barriers for the three complexes are as follows:

- $Fe(CO)_5$, axial: 40 kJ/mol
- $Ru(CO)_5$, axial: 33 kJ/mol
- $Os(CO)_5$, axial: 32 kJ/mol

The trend in the orbital energy and the trend in the reaction free energy barrier agree very well with each other. This good correlation explain the observed variation in the reactivity within the group: the lower the orbital energy, the faster the reaction.

5.6.3 Pentacarbonyl complexes, equatorial

Qualitative orbital scheme

Figure 5.24 (left) shows a schematic drawing of a metal pentacarbonyl complex and figure 5.25 shows the direction of attack of the TMAO. We assume the reaction takes place on the equatorial carbonyl ligand on the $+y$ axis (carbon 2). The empty molecular orbital interacting with TMAO must therefore have large coefficients on the p_z AO on carbon 2.

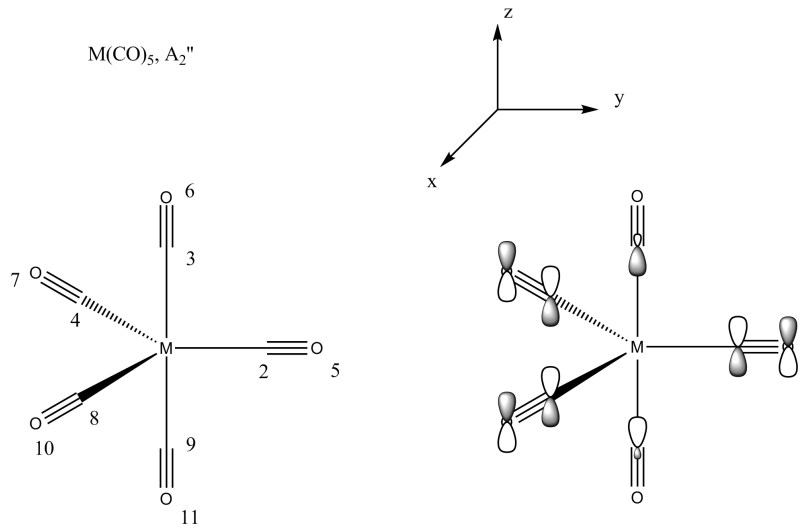

Figure 5.24: Schematic representation of the a_2'' orbital of the metal pentacarbonyl complexes.

UNIVERSITAT ROVIRA I VIRGILI
COMPUTACIONAL STUDIES ON THE MECHANISM OF THE PAUSON-KHAND REACTION
Torstein Fjermestad
ISBN:978-84-693-9441-0/DL:T.62-2011

The MOs of A_2'' symmetry of the D_{3h} complex (see figure 5.24, right) do have large coefficients on the p_z AO on carbon 2, and we therefore choose an empty a_2'' orbital as an appropriate UMO interacting with TMAO.

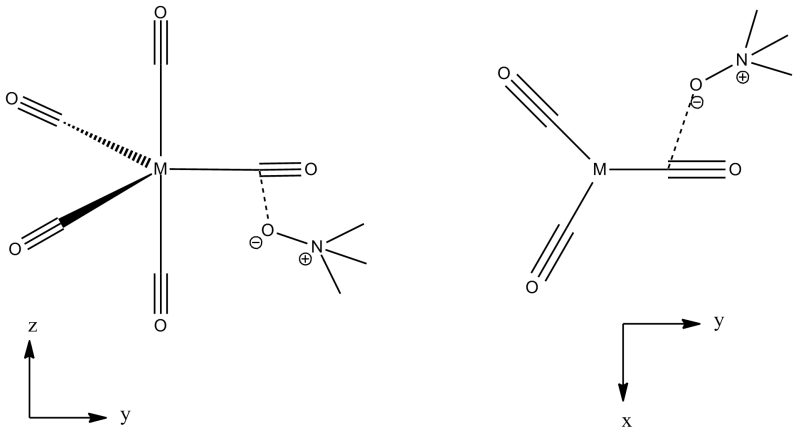

Figure 5.25: Direction of attack of the TMAO on the equatorial carbonyl ligand. Viewed along the x-axis (left) and along the z-axis (right).

Quantitative orbital analysis

For $Fe(CO)_5$ the lowest UMO of the A_2'' symmetry is LUMO +2. The nucleophilic attack takes place on the equatorial carbonyl carbons, and the LUMO +2 coefficients of p_z AOs centred on these carbons will be used in the analysis. Because of the D_{3h} symmetry of the $Fe(CO)_5$ complex, the AO coefficients on all equatorial carbonyl carbons will be the same. Thus only the p_z AOs centred on carbon atom 2 (see figure 5.24) will be tabulated (Table 5.12).

Table 5.12: The energy of the LUMO +2 orbital of $Fe(CO)_5$ and its coefficients of the AOs centred on the Fe atom and on carbon atom 2 (figure 5.24).

Fe(CO)5	
MOs:	LUMO +2
symmetry:	A_2''
energy/Hartrees:	-0.03222
label:	a_2''
	coefficients
Atom:	**Fe**
5PZ	0.40
6PZ	0.01
	2C
2PZ	0.33
3PZ	0.25

For $Ru(CO)_5$ the lowest UMO of the A_2'' symmetry is LUMO +1. Because the nucleophilic attack occurs at the equatorial carbonyl carbon, the LUMO +1 coefficients

UNIVERSITAT ROVIRA I VIRGILI
COMPUTACIONAL STUDIES ON THE MECHANISM OF THE PAUSON-KHAND REACTION
Torstein Fjermestad
ISBN:978-84-693-9441-0/DL:T.62-2011

of the p_z AOs centred on these atoms are tabulated (table 5.13)

Table 5.13: The energy of the LUMO +1 orbital of $Ru(CO)_5$ and its coefficients of the AOs centred on the Ru atom and on carbon atom 2 (figure 5.24).

Ru(CO)5	
MOs:	LUMO +1
symmetry:	A_2''
energy/ Hartrees:	-0.05124
label:	a_2''
	coefficients
Atom:	**Ru**
5PZ	0.48
6PZ	0.06
Atom:	**2C**
2PZ	0.31
3PZ	0.23

For $Os(CO)_5$ the lowest UMO of the A_2'' symmetry is LUMO +1. The nucleophilic attack occurs at the equatorial carbonyl carbon and the LUMO +1 coefficients of the p_z AOs centred on these atoms are tabulated (Table 5.14).

Table 5.14: The energy of the LUMO +1 orbital of $Os(CO)_5$ and its coefficients of the AOs centred on the Os atom and on carbon atom 2 (figure 5.24).

Os(CO)5	
MOs:	LUMO +1
symmetry:	A_2''
energy /Hartrees:	-0.06096
label:	a_2''
	coefficients
Atom:	**Os**
5PZ	0.52
6PZ	0.07
Atom:	**2C**
2PZ	0.31
3PZ	0.23

UNIVERSITAT ROVIRA I VIRGILI
COMPUTACIONAL STUDIES ON THE MECHANISM OF THE PAUSON-KHAND REACTION
Torstein Fjermestad
ISBN:978-84-693-9441-0/DL:T.62-2011

From the tables 5.12, 5.13 and 5.14, we see that the contribution to the UMOs from the p_z AO located on the equatorial carbon atom is fairly constant for the three complexes. However, considering the orbital energies, we see a decrease as we go down the group. The computed free energy reaction barriers of the nucleophilic attack of the three complexes by TMAO are as follows:

- $Fe(CO)_5$, equatorial: 60 kJ/mol
- $Ru(CO)_5$, equatorial: 59 kJ/mol
- $Os(CO)_5$, equatorial: 52 kJ/mol

We observe a good correlation between the two quantities. As the orbital energy lowers, the reaction barrier lowers as well.

5.6.4 Discussion of the overall pattern

Within each group (hexacarbonyls, pentacarbonyls with a nucleophilic attack of the axial carbonyl and pentacarbonyls with a nucleophilic attack of the equatorial carbonyl) the reaction barrier decreases with decreasing orbital energy. However, between the three groups, the orbital energies show a poor correlation with the reaction barriers. When explaining the variation in the reaction barriers between the different groups, the coefficients of the p AO located at the carbonyl carbon become a better measure. To quantitatively compare the values between the different groups, we calculated the sum of squares (SOS) of the coefficients at each carbon. The values are given in table 5.15. We see that there is a good correlation between the sum

Table 5.15: Sum of squares (SOS) of the coefficients on the carbon atoms of the different complexes

complex	carbonyl being attacked	SOS
$Fe(CO)_5$	axial	0.60
$Ru(CO)_5$	axial	0.56
$Os(CO)_5$	axial	0.54
$Fe(CO)_5$	equatorial	0.17
$Ru(CO)_5$	equatorial	0.15
$Os(CO)_5$	equatorial	0.15
$Cr(CO)_6$		0.23
$Mo(CO)_6$		0.20
$W(CO)_6$		0.19

of squares of the coefficients and the reaction barriers. The metal pentacarbonyl complexes (attack on axial carbonyl carbon) react the fastest, and they have the highest sum of squares of the coefficients. Furthermore the high barriers for the hexacarbonyl complexes and the equatorial attack of the pentacarbonyl complexes are reflected in the lower sum of squares of the coefficients.

UNIVERSITAT ROVIRA I VIRGILI
COMPUTACIONAL STUDIES ON THE MECHANISM OF THE PAUSON-KHAND REACTION
Torstein Fjermestad
ISBN:978-84-693-9441-0/DL:T.62-2011

The dependence of the activation barrier on the UMO energy and the SOS of the AO coefficients is presented in figure 5.26. Again we see how the UMO energy determines the activation energy within the different groups, whereas the SOS of the AO coefficients is the important parameter when discussing the variation of the activation barrier between the different groups. From figure 5.26 it also becomes clear that reactions with similar activation barriers have their corresponding data points in the same area of the parameter space. In particular we see that the pentacarbonyl complexes being attacked at an equatorial carbonyl and the hexacarbonyl complexes (activation barriers in the range 52-60 kJ/mol) form one group whereas the pentacarbonyl complexes being attacked at an axial carbonyl (activation barriers in the range 32-40 kJ/mol) form another group.

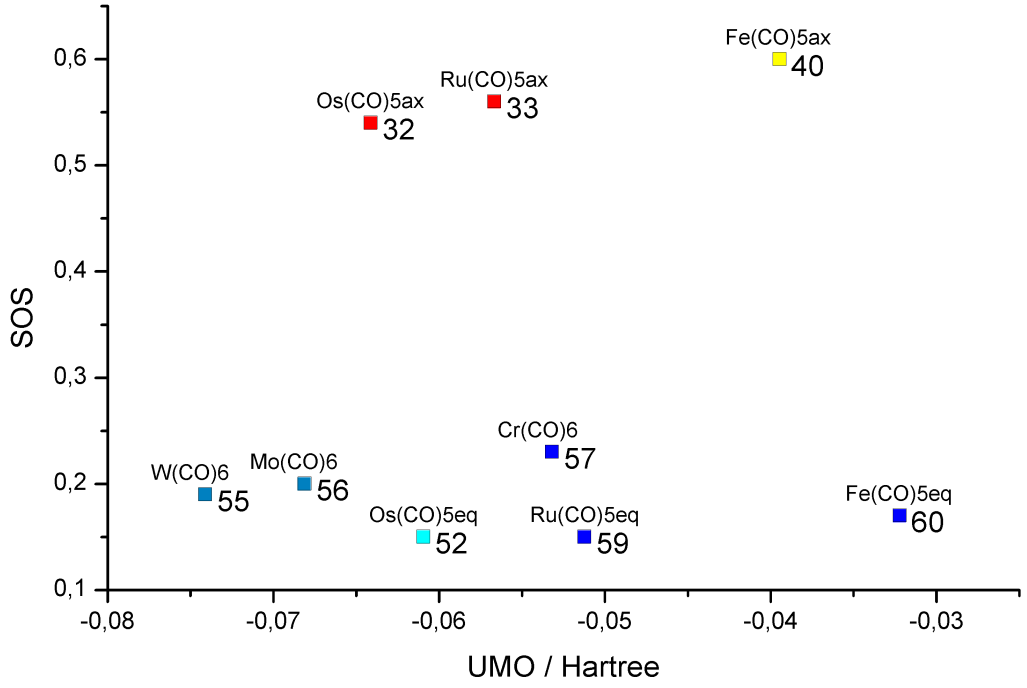

Figure 5.26: Scatter plot of the UMO energy (Hartree) and sum of squares (SOS) of the AO coefficients. The values of the activation free energy barriers are shown next to the corresponding data points.

5.6.5 The dicobalt hexacarbonyl complex

In light of the good correlation between the reaction barriers and the shape and energy of the appropriate UMO shown above, we wanted to see if a similar correlation could be established for the activation of the Pauson-Khand precursor, dicobalthexacarbonyl(μ_2-prop-1-yne). Looking at the different UMOs, we found LUMO +1 and LUMO+2 to be of appropriate symmetry. LUMO+1 and LUMO+2 are of very similar energies, -0.04347 Hartrees and -0.04289 Hartrees respectively.

UNIVERSITAT ROVIRA I VIRGILI
COMPUTACIONAL STUDIES ON THE MECHANISM OF THE PAUSON-KHAND REACTION
Torstein Fjermestad
ISBN:978-84-693-9441-0/DL:T.62-2011

Table 5.16: The LUMO+1 and LUMO+2 coefficients of the p AOs centred on the carbonyl carbons.

MOs:	LUMO +1	LUMO +2
Energy / Hartrees	-0.04347	-0.04289
Atom:	C_eq_trans	
2PX	0.01	0
2PY	-0.03	0.07
2PZ	-0.24	0.05
3PX	0.06	0
3PY	-0.04	0.05
3PZ	-0.21	0.07
Atom:	C_eq_cis	
2PX	-0.06	0.02
2PY	0.02	-0.02
2PZ	0.02	-0.25
3PX	-0.05	0.01
3PY	0.01	-0.07
3PZ	0.05	-0.23
Atom:	C_ax	
2PX	-0.17	0.05
2PY	0.04	0.17
2PZ	-0.12	-0.11
3PX	-0.17	0.06
3PY	0.04	0.17
3PZ	-0.09	-0.08

UNIVERSITAT ROVIRA I VIRGILI
COMPUTACIONAL STUDIES ON THE MECHANISM OF THE PAUSON-KHAND REACTION
Torstein Fjermestad
ISBN:978-84-693-9441-0/DL:T.62-2011

Table 5.16 shows the LUMO+1 and LUMO+2 coefficients of the p AOs centred on the carbonyl carbons. For the equatorial carbonyl carbons, C_eq_trans and C_eq_cis, LUMO+1 and LUMO+2 have a large components along the p_z AOs respectively (see figure 5.27 for the orientation of the coordinate system). For the axial carbonyl

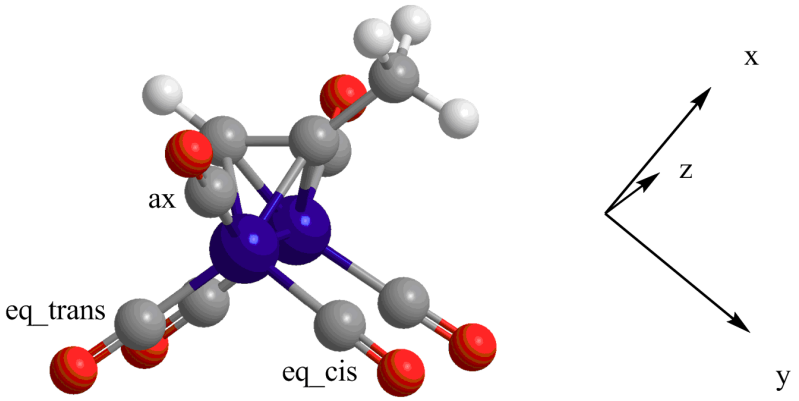

Figure 5.27: The Co2CO6(μ-pent-1-yne) complex with the Cartesian coordinate axes indicated

carbon, C_ax, LUMO+1 and LUMO+2 have large components along the p_x AO and p_y AO respectively.

For the equatorial carbonyl ligands, the attack of TMAO takes place in the xy plane (as defined in figure 5.27). The large component along the p_z AO is thus not available. For the axial carbonyl ligand, the TMAO attacks in a plane perpendicular to the xy plane about 40 degrees out of the xz plane. The large 2PY and 3PY components on C_ax of LUMO +2 (see table 5.16) become available for the electrons of the attacking TMAO, and the attack on the axial carbonyl ligand should be favoured over the attack on the equatorial ligand. This agrees well with the relative Gibbs free energies of the TSs: the axial attack is preferred by 7 kJ/mol over the equatorial attack of the carbonyl *cis* to the methyl group and by 3 kJ/mol over the attack of the equatorial carbonyl *trans* to the methyl group.

5.7 Conclusions

In summary we have explained the reactivity of metal carbonyl complexes. Within the same type of complexes, the nucleophilic attack is favoured by a lower UMO energy. Between the different types of complexes, i.e. hexacarbonyl complexes, pentacarbonyl complexes with the nucleophilic attack on the axial carbonyl and pentacarbonyl complexes with the nucleophilic attack on the equatorial carbonyl, the nucleophilic attack is favoured by a larger UMO coefficient along the p AO of the carbonyl being attacked.

For the activation of the Pauson-Khand precursor, $Co_2(CO)_6$(μ_2-prop-1-yne), the orbital analysis shows that both LUMO+1 and LUMO+2 have a larger component along the p_z AO of the equatorial carbonyls than along any of the AO of the axial

UNIVERSITAT ROVIRA I VIRGILI
COMPUTACIONAL STUDIES ON THE MECHANISM OF THE PAUSON-KHAND REACTION
Torstein Fjermestad
ISBN:978-84-693-9441-0/DL:T.62-2011

carbonyl. However, because of steric hindrance, the p_z AO of the equatorial carbonyls is not available for nucleophilic attack, and therefore the nucleophilic attack of the axial carbonyl is preferred over the attack of the equatorial carbonyl.

In this chapter we have described the reactivity of metal carbonyl complexes and the PKR-precursor upon activation by TMAO. In the next chapter we will continue to study the same type of activation, but now with a chiral N-oxide, brucine N-oxide, that can induce chirality in a pro-chiral PKR-precursor.

UNIVERSITAT ROVIRA I VIRGILI
COMPUTACIONAL STUDIES ON THE MECHANISM OF THE PAUSON-KHAND REACTION
Torstein Fjermestad
ISBN:978-84-693-9441-0/DL:T.62-2011

Chapter 6

Activation of the PKR precursor by brucine N-oxide

The final goal in the study of the TMAO activation of metal carbonyl complexes and the Pauson-Khand precursor was to understand the mechanism of enantioselection in the brucine N-oxide assisted stoichiometric Pauson-Khand reaction. This reaction was studied experimentally by Kerr [70] and Laschat [121]. Figure 6.1 shows a schematic representation of the reaction. Kerr performed a systematic study vary-

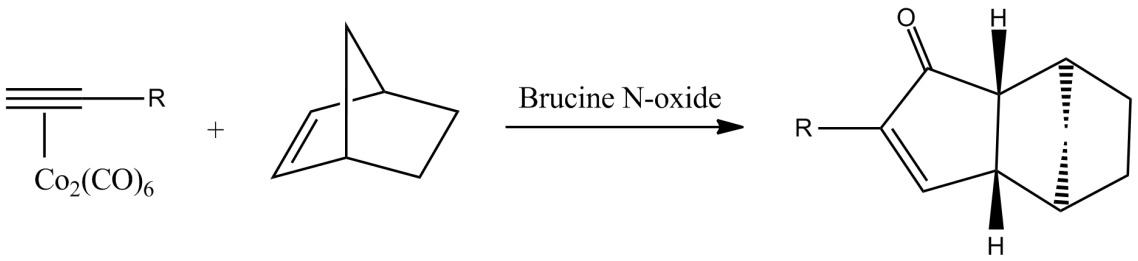

Figure 6.1: Schematic representation of the brucine N-oxide assisted stoichiometric Pauson-Khand reaction.

ing the substituent, R, of the alkyne moiety of the dicobalt complex [70]. The study showed that the enantiomeric excess of the Pauson-Khand product varied enormously with very small structural changes in the substituent, R. In particular the alkyne 2-methylbut-3-yn-2-ol gave an enantiomeric excess of 56% in acetone. Removing the two methyl groups of this alkyne dramatically decreased the enantioselectivity to 4%. Likewise, substituting the hydroxyl group with a methyl group resulted in an enantioselectivity of 16%. Furthermore, the solvent also proved to have an important effect on the enantioselectivity. When carried out in dimethoxyethane (DME), the enantiomeric excess of the system with 2-methylbut-3-yn-2-ol increased from 56% to 78%

Lanschat extended the study by exploring the possibility of other N-oxides to induce high enantiomeric excess. All other N-oxides resulted in enantiomeric excess inferior to that of brucine N-oxide (BNO) [121]. Lanschat also measured the optical rotations of the products and found that the major enantiomer showed negative optical

UNIVERSITAT ROVIRA I VIRGILI
COMPUTACIONAL STUDIES ON THE MECHANISM OF THE PAUSON-KHAND REACTION
Torstein Fjermestad
ISBN:978-84-693-9441-0/DL:T.62-2011

rotation. By comparison to previous work [56], the negative optical rotation could be related to an R absolute configuration.

When BNO is used as a chiral activator, the presence of steric bulk as well as an OH group in the substituent R seems to be a prerequisite for high enantiomeric excess. According to the mechanistic proposal by Kerr [70], the OH group forms a hydrogen bond to some polar group of the BNO. This hydrogen bond forces the BNO closer to the bulky methyl groups of the R substituent. This closer contact between bulky groups may be the cause of the enantiodiscrimination between the attack of carbonyls attached to Co1 and carbonyls attached to Co2.

Our objective of this computational study has been to confirm (or refute) the mechanistic proposal to better understand how to improve the system to make it more practical for synthetic applications.

6.1 Concepts of chirality transfer

Chirality transfer refers to how the chirality of an enantiopure compound is transferred to a pro-chiral compound when the two are reacting with each other. In the TS of the reaction, the pro-chiral compound can interact with the chiral compound through its pro-R face or its pro-S face. These two ways of interaction form a diastereomeric pair with different energies. The larger this energy difference is, the more effective the chirality transfer. To prevent the chiral product of the reaction equilibrating back to its pro-chiral form, the reaction must be irreversible.

In the case of the BNO activated Pauson-Khand reaction, the chirality is transferred from the enantiopure BNO to the Pauson-Khand product. The chirality transfer occurs in two steps: first from BNO to the dicobalt complex, thereafter from the dicobalt complex to the norbornene. The chirality transferred to the norbornene is also the chirality of the product.

6.1.1 Chirality transfer from the brucine N-oxide to the dicobalt complex

The dicobalt complex, $Co_2(CO)_6(\mu_2$-alkyne), used as reactant in the Pauson-Khand reaction is pro-chiral. When viewed along an axis perpendicular to both the alkyne triple bond and the Co-Co bond (pointing away from the reader in figure 6.2), we observe that a removal of one carbonyl from either Co1 or Co2 would make the complex chiral. From the rules of assigning absolute configuration to chiral structures, we see that a carbonyl detachment from Co1 would lead to the R configuration whereas a carbonyl detachment from Co2 would lead to the S configuration (see figure 6.2).

As we have seen in chapter 5, a carbonyl can be detached from a metal complex through activation by N-oxide. When the N-oxide is made chiral, that chirality can potentially be transferred to the pro-chiral $Co_2(CO)_6(\mu_2$-alkyne) complex.

UNIVERSITAT ROVIRA I VIRGILI
COMPUTACIONAL STUDIES ON THE MECHANISM OF THE PAUSON-KHAND REACTION
Torstein Fjermestad
ISBN:978-84-693-9441-0/DL:T.62-2011

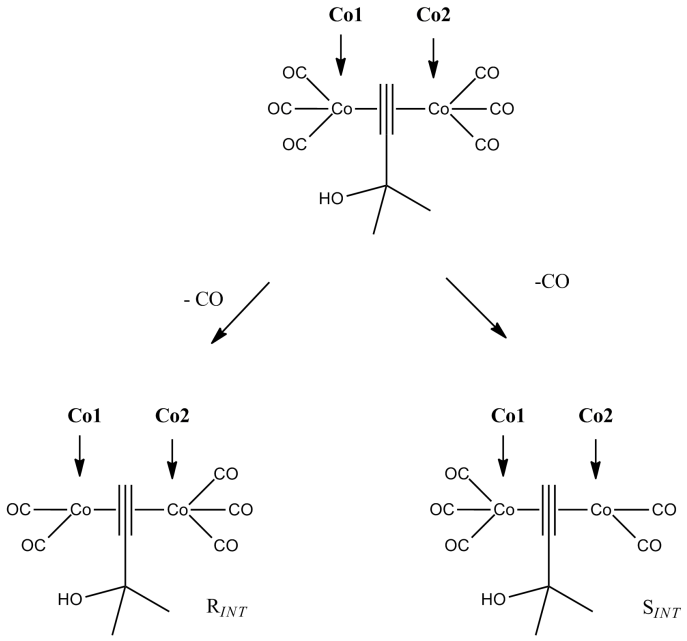

Figure 6.2: Carbonyl detachment giving rise to the R and S enantiomers of the activated dicobalt complex.

The differences in the diastereomeric interactions between the chiral N-oxide and the dicobalt complex in the TSs leading to the R intermediate, R_{INT}, and the TSs leading to the S intermediate, S_{INT}, determines whether CO removal from Co1 or Co2 will be favoured.

From the activation of metal carbonyls (see chapter 5) we know that the extrusion of CO through a formation of CO_2 is highly exergonic and irreversible. The sense of chirality of the activated dicobalt complex, R or S, is thus determined once the reaction has passed the transition state of the CO removal (see also chapter 3).

When using BNO as chiral N-oxide, the diastereomeric transition states have the (R(N),R) configuration for CO removal from Co1, and the (R(N),S) configuration for CO removal from Co2. R(N) refers to the absolute configuration on the positively charged nitrogen of BNO (see figure 6.3) and R and S refer to the absolute configuration of the activated dicobalt complexes, R_{INT} and S_{INT}. These enantiomeric labels do not have a direct correlation with the chirality of the product. As will be seen below, both R and S products can be obtained from any of the dicobalt complexes.

6.1.2 Epimerisation of the activated complex

Because of the diastereomeric interaction between the BNO and the dicobalt complex, one of the enantiomers of the activated complex, R_{INT} or S_{INT}, will be formed in excess of the other. This excess can, however, be reduced through a subsequent epimerisation (an inversion of a chiral element) of the chiral complex that will lead to a partial racemisation of the intermediate. A carbonyl of the saturated cobalt

UNIVERSITAT ROVIRA I VIRGILI
COMPUTACIONAL STUDIES ON THE MECHANISM OF THE PAUSON-KHAND REACTION
Torstein Fjermestad
ISBN:978-84-693-9441-0/DL:T.62-2011

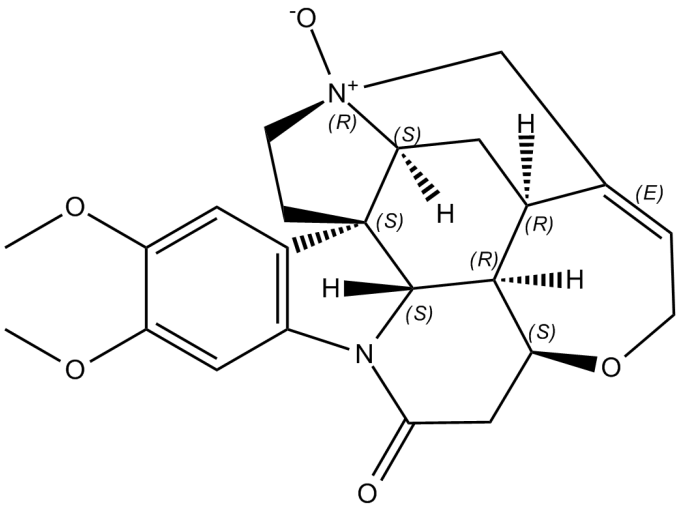

Strychnidin-10-one, 2,3-dimethoxy-, 19-oxide
(brucine N-oxide)

Figure 6.3: Schematic drawing of the brucine N-oxide with the absolute configuration of the stereocentres indicated.

atom can migrate to the unsaturated cobalt atom, thus producing the opposite enantiomer, see figure 6.4.

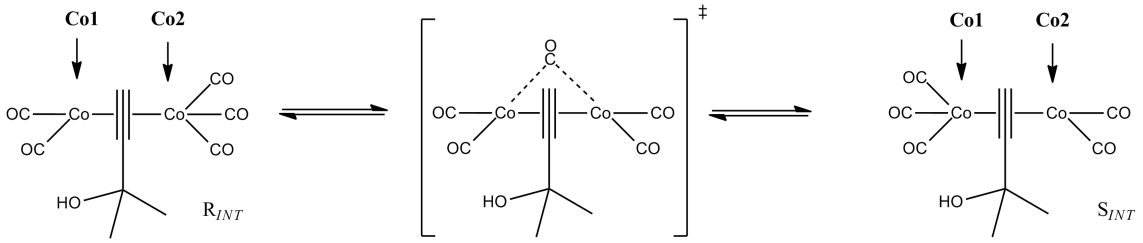

Figure 6.4: Epimerisation of the activated dicobalt complex through a carbonyl migration.

6.1.3 Chirality transfer to the norbornene

The norbornene coordinates to the vacant site of the chiral dicobalt complex and the Pauson-Khand reaction is initiated. Norbornene is pro-chiral and can coordinate to the chiral dicobalt complex, R_{INT} or S_{INT}, with its pro-R face or its pro-S face. Following coordination, the metallacycle formation takes place. Previous computational studies [47, 48] have shown that this step is irreversible. The energy difference between TSs of this step corresponding to the pro-R coordination and the pro-S coordination thus determines whether the R or the S product is formed. In the case where the chiral dicobalt complex R_{INT} or S_{INT} is present in enantiopure form, this energy difference is directly related to the enantiomeric excess of the reaction through equation (3.7) and (3.8). The chiral dicobalt complex is, however, not in

UNIVERSITAT ROVIRA I VIRGILI
COMPUTACIONAL STUDIES ON THE MECHANISM OF THE PAUSON-KHAND REACTION
Torstein Fjermestad
ISBN:978-84-693-9441-0/DL:T.62-2011

enantiopure form. Thus in the calculation of the enantioselectivity, four modes of coordination must be taken into consideration: (pro-R, R), (pro-S, R), (pro-R, S) and (pro-S, S). pro-S /pro-R refers to the pro-chiral face of the norbornene that coordinates to the vacant site, R / S refers to the chirality of the activated dicobalt complex to which norbornene coordinates (see figure 6.5).

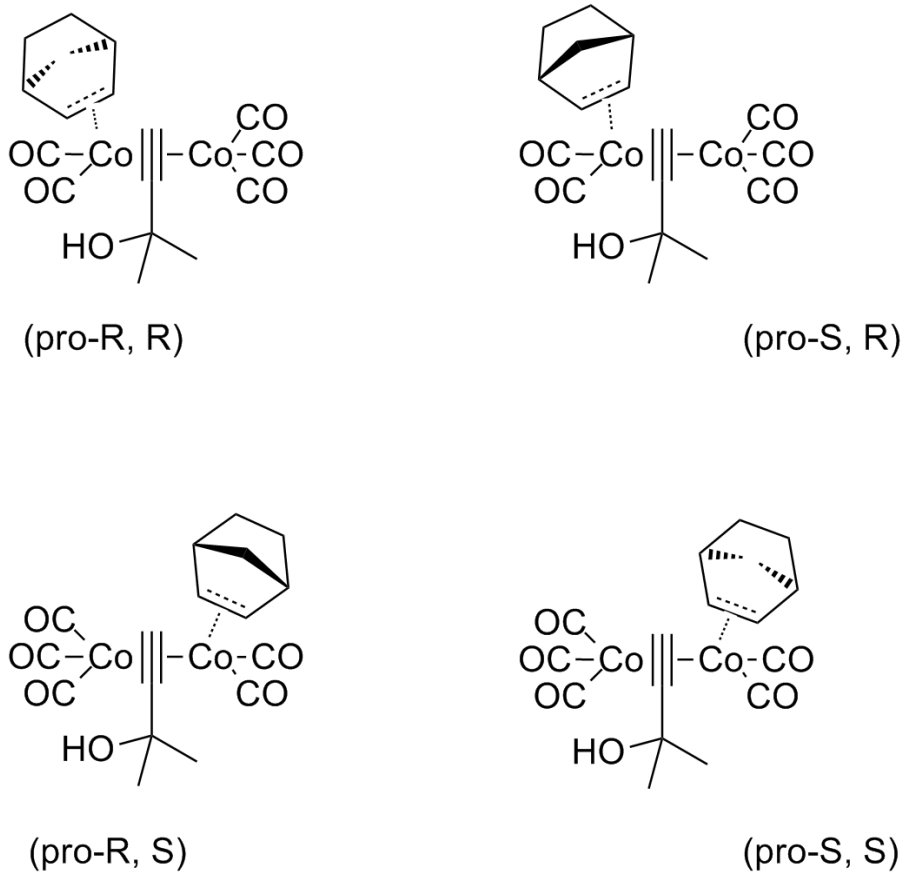

Figure 6.5: The four modes of norbornene coordination to the chiral dicobalt complex.

The four coordination modes can be divided in two enantiomeric pairs. Thus, for the reaction between norbornene and the dicobalt complex, we only have to compute two modes of coordination corresponding to one diastereomeric pair. The diastereomeric pair we compute will be (pro-R, R) and (pro-S, R).

Because (pro-S, S) and (pro-R, S) are enantiomers of (pro-R, R) and (pro-S, R) respectively, it follows that the enantioselectivity of the S_{INT} intermediate will be exactly the opposite to that of the R_{INT} intermediate.

6.2 Computational details

The calculations were carried out using the Gaussian 03 and Gaussian 09 program packages [105]. Depending on the accuracy we wanted to obtain, several meth-

UNIVERSITAT ROVIRA I VIRGILI
COMPUTACIONAL STUDIES ON THE MECHANISM OF THE PAUSON-KHAND REACTION
Torstein Fjermestad
ISBN:978-84-693-9441-0/DL:T.62-2011

ods of energy evaluation were used. These methods were ONIOM(B3LYP:UFF) [85, 86, 89, 92, 95], B3LYP [85, 86] and M06[88]. For the ONIOM calculations, the partition between the QM and MM regions is shown in figure 6.6. The ba-

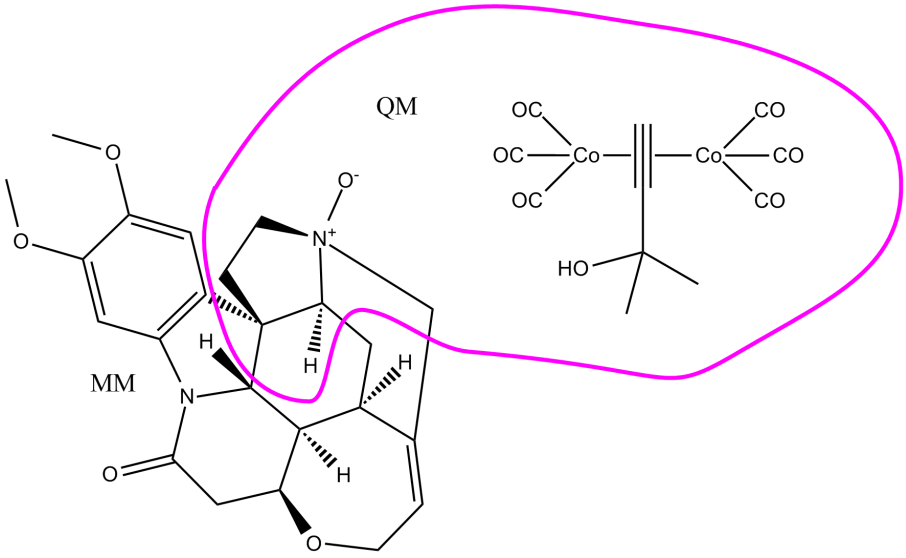

Figure 6.6: Partitioning scheme in the ONIOM calculations of the real system

sis set for the non-metal atoms was 6-31G(d) [106] in all of the calculations. For the Co atoms the core electrons were substituted by the Los Alamos LANL2DZ effective core potential, for the valence electrons the associated double zeta basis set [107] was used. All minima and transition states were fully optimised without symmetry restrictions. The minima were identified by having only positive eigenvalues in the Hessian matrix whereas the transition states were identified by having a Hessian matrix with exactly one negative eigenvalue. Unless otherwise stated, all energies reported are free energies including zero-point and entropy corrections. The M06 optimised structures were reoptimised in acetone and dimethoxyethane to check the influence of these solvents. SMD [108] was used as method of solvation. Dimethoxyethane is not defined as an option for continuum solvent calculations in Gaussian 09. Because the dielectric constant largely defines the properties of the solvent, we opted for using a different solvent, but with the same dielectric constant as DME. The dielectric constant changes with temperature. The lowest temperature value for DME tabulated in the Handbook of Chemistry and Physics [109] is 9.39 at -17°C. In the calculations we thus used as solvent 2,4-dimethylpyridine with a dielectric constant of 9.4176.

6.3 Computation of the enantiomeric excess

The presence of three enantioselective processes complicates the calculation of the enantiomeric excess. First there is an enantioselective process leading to the formation of the intermediates R_{INT} and S_{INT} (steps A and E in figure 6.7). Each of these intermediates can finally lead to the R or the S product (steps B, F, D, G in

UNIVERSITAT ROVIRA I VIRGILI
COMPUTACIONAL STUDIES ON THE MECHANISM OF THE PAUSON-KHAND REACTION
Torstein Fjermestad
ISBN:978-84-693-9441-0/DL:T.62-2011

figure 6.7). To compute the enantiomeric excess, we need to know the probability of

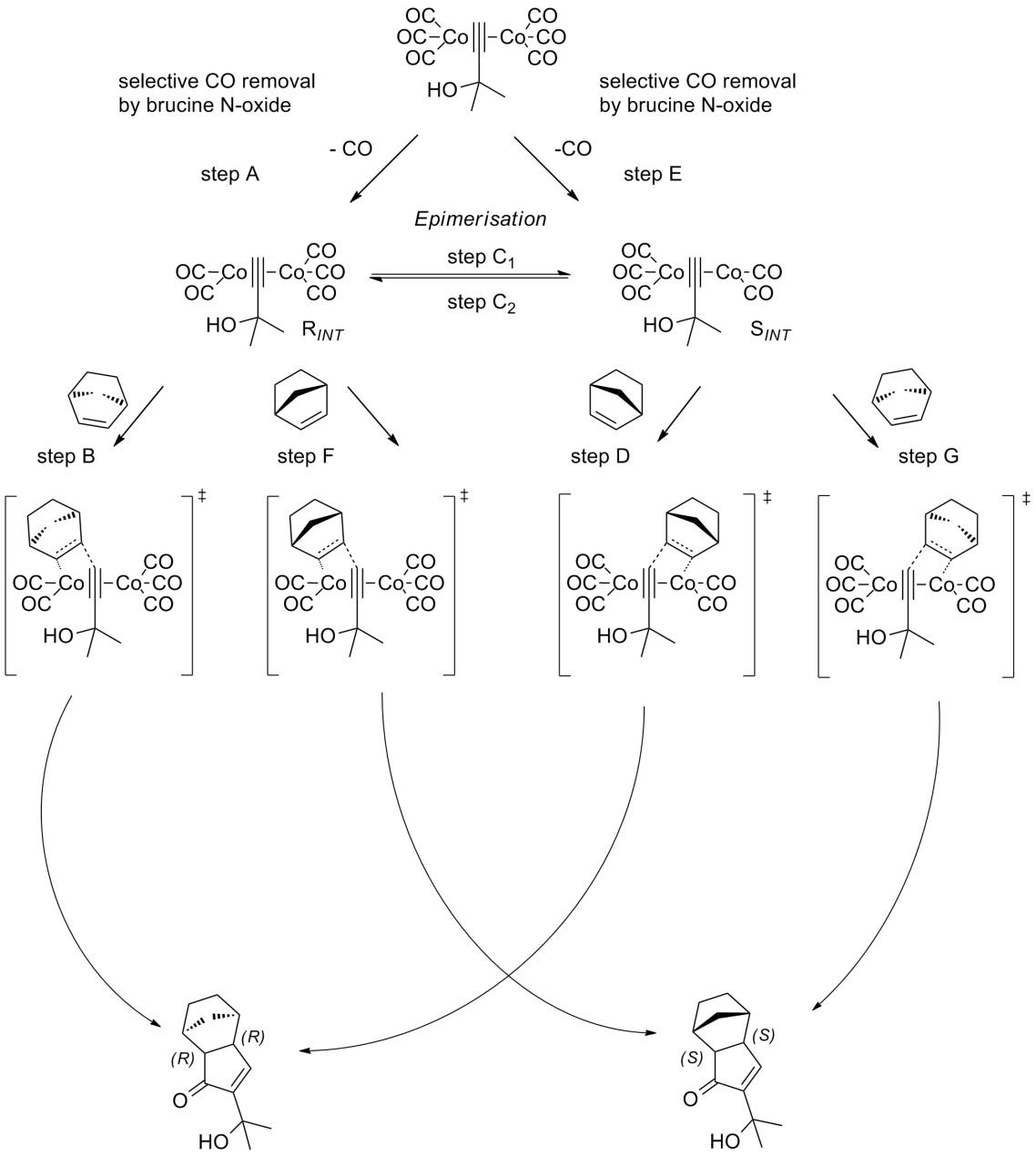

Figure 6.7: Mechanism of enantioselection in the brucine N-oxide activated Pauson-Khand reaction.

producing the R and the S product respectively. This can be done by computing the probability of getting to the R or the S product along each of the reaction pathways leading to the respective products.

The probability of getting to one of the final products along a particular hypothetical reaction pathway of two steps, $P_{path,n}$, is the probability that the second step occurs, $P(\text{2nd step})$, multiplied by the probability that the first step occurs, $P(\text{1st step})$:

$$P_{path,n} = P(\text{2nd step})P(\text{1st step}) \tag{6.1}$$

UNIVERSITAT ROVIRA I VIRGILI
COMPUTACIONAL STUDIES ON THE MECHANISM OF THE PAUSON-KHAND REACTION
Torstein Fjermestad
ISBN:978-84-693-9441-0/DL:T.62-2011

We now turn to the real case of the BNO activated Pauson-Khand reaction. Let us consider the pathway consisting of step A and step B leading to the R product (see figure 6.7). This pathway we label pathway 1. The probability of reaching the R product along pathway 1 is

$$P_{path,1} = P(\text{stepB})P(\text{stepA}) \tag{6.2}$$

There are other pathways by which the system can reach product R. Three of them are:

Pathway 2: CO removal to intermediate R_{INT} (step A), followed by epimerisation to intermediate S_{INT} (step C_1) and thereafter to the final product through coordination of the pro-R face of norbornene to the dicobalt complex (step D)

Pathway 3: CO removal to intermediate S_{INT} (step E) followed by coordination of the pro-R face of norbornene to the dicobalt complex (step D).

Pathway 4: CO removal to intermediate S_{INT} (step E), followed by epimerisation to intermediate R_{INT} (step C_2) and thereafter to the final product through coordination of the pro-R face of the norbornene to the dicobalt complex (step B).

The probabilities that the system follows each of these pathways are

$$\begin{aligned} P_{path,2} &= P(\text{stepD})P(\text{step}C_1)P(\text{stepA}) && (6.3)\\ P_{path,3} &= P(\text{stepD})P(\text{stepE}) && (6.4)\\ P_{path,4} &= P(\text{stepB})P(\text{step}C_2)P(\text{stepE}) && (6.5) \end{aligned}$$

Additionally from intermediates R_{INT} and S_{INT} the system can epimerise to the opposite enantiomer and back again along step C_1 and step C_2. We can thus define four new pathways. They will be largely the same as those above, but with the difference that once the system reaches intermediates R_{INT} or S_{INT}, it will epimerise to the opposite enantiomer before going back again and continue towards the final product. We label these pathways as pathways 1*b* to 4*b* and compute their probabilities as

$$\begin{aligned} P_{path,1b} &= P(\text{step}C_1)P(\text{step}C_2) * P_{path,1} && (6.6)\\ P_{path,2b} &= P(\text{step}C_1)P(\text{step}C_2) * P_{path,2} && (6.7)\\ P_{path,3b} &= P(\text{step}C_1)P(\text{step}C_2) * P_{path,3} && (6.8)\\ P_{path,4b} &= P(\text{step}C_1)P(\text{step}C_2) * P_{path,4} && (6.9) \end{aligned}$$

The system can epimerise back and forth between R_{INT} and S_{INT} many more times, in principle an infinite amount of times. The event of following one reaction pathway is mutually exclusive to the event of following another reaction pathway. We can thus calculate the probability of producing the R product as the sum of the probabilities of following reaction pathways that lead to product R. We define the sum of the probabilities of following pathways 1 to 4, $P_{R,1-4}$, as

$$P_{R,1-4} = P_{path,1} + P_{path,2} + P_{path,3} + P_{path,4} \tag{6.10}$$

UNIVERSITAT ROVIRA I VIRGILI
COMPUTACIONAL STUDIES ON THE MECHANISM OF THE PAUSON-KHAND REACTION
Torstein Fjermestad
ISBN:978-84-693-9441-0/DL:T.62-2011

The total probability of producing product R can then be expressed as

$$\begin{aligned} P_{R,tot} &= P_{R,1-4} + P(\text{stepC}_1)P(\text{stepC}_2) * P_{R,1-4} \\ &+ \left[P(\text{stepC}_1)P(\text{stepC}_2)\right]^2 * P_{R,1-4} + \cdots \\ &+ \left[P(\text{stepC}_1)P(\text{stepC}_2)\right]^k * P_{R,1-4} \end{aligned} \tag{6.11}$$

This sum can be simplified as

$$P_{R,tot} = \sum_{k=0}^{\infty} P_{R,1-4} * \left[P(\text{stepC}_1)P(\text{stepC}_2)\right]^k \tag{6.12}$$

We note that because $P(\text{stepC}_1)P(\text{stepC}_2)$ is < 1, the sum above is a convergent geometric series. Its sum is

$$P_{R,tot} = \frac{P_{R,1-4}}{1 - P(\text{stepC}_1)P(\text{stepC}_2)} \tag{6.13}$$

Because R_{INT} and S_{INT} are enantiomers of each other, it follows that $P(\text{stepC}_1) = P(\text{stepC}_2) = P(\text{stepC})$ and equation (6.13) can be simplified to

$$P_{R,tot} = \frac{P_{R,1-4}}{1 - P(\text{stepC})^2} \tag{6.14}$$

The probability of producing the S product, $P_{S,tot}$, can be derived analogously as follows: As for the R product, the system can reach the S product along four different pathways that do not involve any additional epimerisation back and forth along step C_1 and step C_2. These pathways are (see figure 6.7)

Pathway 5: Step A followed by step F

Pathway 6: Step A followed by step C_1 and step G

Pathway 7: Step E followed by step G

Pathway 8: Step E followed by step C_2 and step F

The total probability of reaching the S product along any of the pathways 5 to 8, $P_{S,5-8}$, is

$$P_{S,5-8} = P_{path,5} + P_{path,6} + P_{path,7} + P_{path,8} \tag{6.15}$$

The total probability of producing the S product taking into account pathways involving additional epimerisation is

$$P_{S,tot} = \frac{P_{S,5-8}}{1 - P(\text{stepC})^2} \tag{6.16}$$

The enantiomeric ratio, er, can now be calculated as

$$er = \frac{P_{S,tot}}{P_{R,tot}} \tag{6.17}$$

UNIVERSITAT ROVIRA I VIRGILI
COMPUTACIONAL STUDIES ON THE MECHANISM OF THE PAUSON-KHAND REACTION
Torstein Fjermestad
ISBN:978-84-693-9441-0/DL:T.62-2011

and the enantiomeric excess, ee, as

$$\%ee = 100\% * \frac{1-er}{1+er} \tag{6.18}$$

We now consider the computation of the probability that the system passes an individual elementary reaction step. The reaction steps that constitute pathways leading to the R product are: step A, step B, step C_1, step C_2, step D and step E. Their probabilities are P(stepA), P(stepB), P(stepC), P(stepC), P(stepD) and P(stepE). The probability of the system to go from an intermediate through a particular transition state, TS_{1N}, can be found by taking the ratio between its Boltzmann weight and the sum of the Boltzmann weights of all TSs available from that particular intermediate:

$$P_{TS_{1N}} = \frac{e^{-\Delta G_{TS_{1N}}/(RT)}}{\sum_i e^{-\Delta G_{TS_i}/(RT)}} \tag{6.19}$$

TS_{1N} belongs to the elementary step N. The probability of going through step N, P_{stepN}, is the sum of the probabilities of going through transition states of this elementary step:

$$P_{stepN} = P_{TS_1N} + P_{TS_2N} + \cdots + P_{TS_nN} \tag{6.20}$$

By substituting the expression for P_{TS_1N} to P_{TS_nN} into equation (6.20), P_{stepN} can be expressed in terms of TSs of step N as well as other available TSs:

$$P_{stepN} = \frac{\sum_i e^{-\Delta G_{TS_{iN}}/(RT)}}{\sum_i e^{-\Delta G_{TS_i}/(RT)}} \tag{6.21}$$

Applying equation (6.21) to the reaction steps in figure 6.7, we see that P_{stepA} can be expressed as

$$P_{stepA} = \frac{\sum_i e^{-\Delta G_{TS_{iA}}/(RT)}}{\sum_i e^{-\Delta G_{TS_{iA}}/(RT)} + \sum_i e^{-\Delta G_{TS_{iE}}/(RT)}} \tag{6.22}$$

P_{stepE} can be expressed as

$$P_{stepE} = \frac{\sum_i e^{-\Delta G_{TS_{iE}}/(RT)}}{\sum_i e^{-\Delta G_{TS_{iA}}/(RT)} + \sum_i e^{-\Delta G_{TS_{iE}}/(RT)}} \tag{6.23}$$

and P_{stepB} as

$$P_{stepB} = \frac{\sum_i e^{-\Delta G_{TS_{iB}}/(RT)}}{\sum_i e^{-\Delta G_{TS_{iB}}/(RT)} + \sum_i e^{-\Delta G_{TS_{iF}}/(RT)} + \sum_i e^{-\Delta G_{TS_{iC}}/(RT)}} \tag{6.24}$$

Because steps B, F and C only have one TS each, equation (6.24) can be simplified to

$$P_{stepB} = \frac{e^{-\Delta G_{TS_B}/(RT)}}{e^{-\Delta G_{TS_B}/(RT)} + e^{-\Delta G_{TS_F}/(RT)} + e^{-\Delta G_{TS_C}/(RT)}} \tag{6.25}$$

The probability for the rest of the elementary steps can be derived analogously.

In the next sections we will compute the numerical values for P_{stepA} to P_{stepG} The analyses of the different reaction steps are presented according to the order of occurrence in the reaction. The selective CO removal by BNO, steps A and E, is presented first, secondly, the analysis of the epimerisation (step C) is presented and lastly the oxidative metallacycle formation (step B, D, F and G) is presented.

UNIVERSITAT ROVIRA I VIRGILI
COMPUTACIONAL STUDIES ON THE MECHANISM OF THE PAUSON-KHAND REACTION
Torstein Fjermestad
ISBN:978-84-693-9441-0/DL:T.62-2011

6.4 The selective CO removal by brucine N-oxide, step A and E

The selective CO removal by BNO involves a high number of conformers. Thus, to quickly discard any high energy transition states, we started off by performing a conformational search on a small model system. Afterwards we kept the lower energy TS geometries from this search and expanded the model to the real system by adding the appropriate groups.

6.4.1 Conformational search on model system I

Two model systems were used in the conformational search. In model system I, the brucine N-oxide is modelled as TMAO and the methyl groups of the alkyne are substituted by hydrogens. Transition states corresponding to attack of the axial as well as the equatorial carbonyls were calculated. For the attack of the axial carbonyl group, the following dihedral angles (shown in figure 6.8 on a representative transition state geometry) were varied:

- Dihedral 1: Rotation around the Co-C(ax) bond
- Dihedral 2: Rotation around the C-C bond of the alkyne
- Dihedral 3: Rotation around the C-O bond of the alkyne

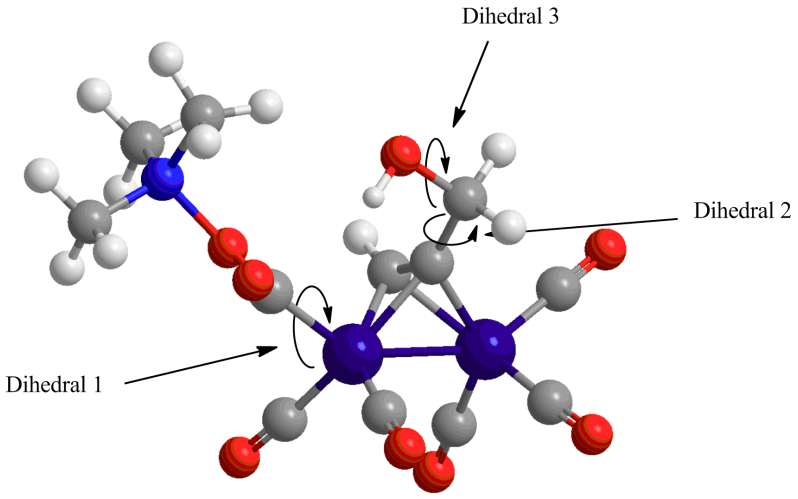

Figure 6.8: Transition state geometry (model system I) with the dihedral angles used in the conformational search indicated.

For the attack of an equatorial carbonyl group, the conformational flexibility is more restricted. The analysis in section 5.5 and subsection 5.6.5 showed that the attack of the carbonyl by TMAO takes place in the *xy*-plane (as defined in figure 5.27), that is in a plane perpendicular to the Co-Co bond. In the case of the attack of the carbonyl group *cis* to the R-substituent of the alkyne, several transition states

UNIVERSITAT ROVIRA I VIRGILI
COMPUTACIONAL STUDIES ON THE MECHANISM OF THE PAUSON-KHAND REACTION
Torstein Fjermestad
ISBN:978-84-693-9441-0/DL:T.62-2011

were located systematically varying dihedral 2 and 3 defined above. Only those geometries with the hydrogen of the OH group pointing towards one of the oxygens involved in the reaction (see figure 6.9) resulted in low-energy structures.

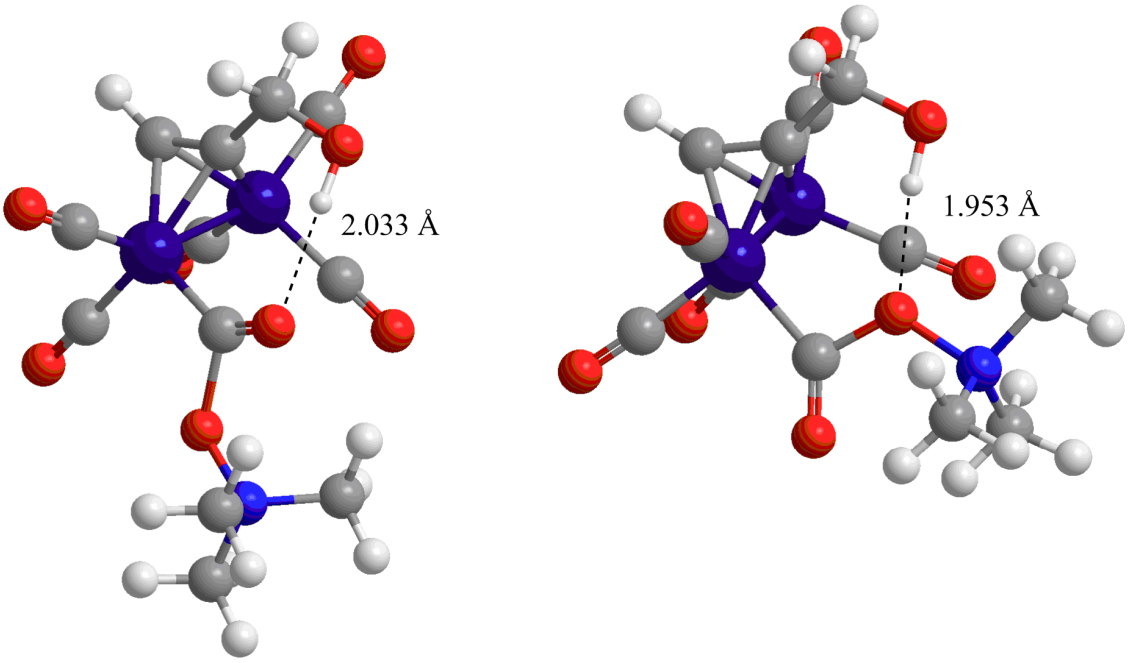

Figure 6.9: Transition state geometries (model system I) for the attack of the equatorial *cis* carbonyl.

In the case of the attack of the carbonyl group *trans* to the R-substituent of the alkyne, only two representative transition state structures were located. This was assumed to be sufficient because the OH group that potentially could stabilise the transition state is out of reach for the *trans* attack.

The structures within the lower 10 kJ/mol range in terms of potential energy were submitted to reoptimisation with model system II.

6.4.2 Reoptimisation on model system II

The expansion from model system I to model system II consists of the substitution of the hydrogens of the R substituent by methyl groups. Figure 6.10 shows a transition state optimised with model system II.

Reoptimisation of the conformers selected from model system I, resulted in the conformers given in table 6.1

In chapter 5 we analysed the TMAO assisted CO removal from a Pauson-Khand precursor with a methyl as the R substituent. Compared to that analysis, we see that also with the R substituent of the real system, the removal of the axial carbonyl is favoured. Relative to the most stable transition state of the axial attack, the removal of an equatorial carbonyl *cis* to the R substituent is disfavoured by 8 kJ/mol.

UNIVERSITAT ROVIRA I VIRGILI
COMPUTACIONAL STUDIES ON THE MECHANISM OF THE PAUSON-KHAND REACTION
Torstein Fjermestad
ISBN:978-84-693-9441-0/DL:T.62-2011

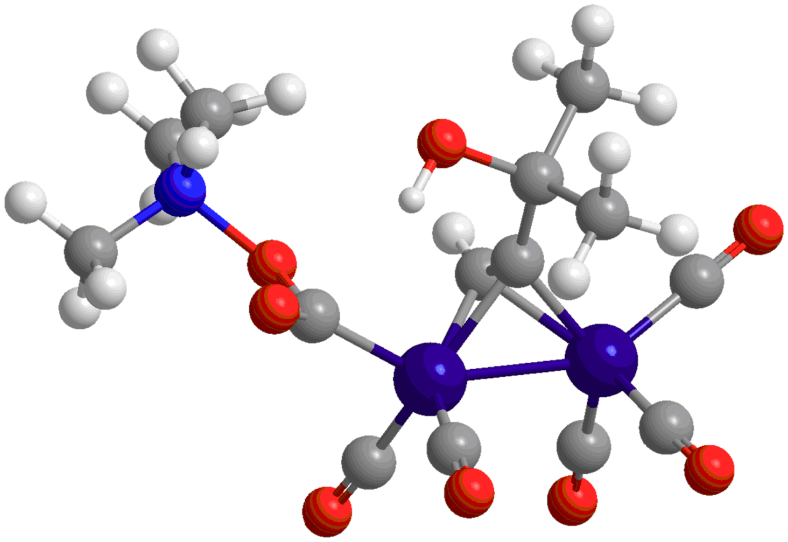

Figure 6.10: A transition state geometry of model system II.

Table 6.1: Gibbs free energies in kJ/mol of the conformers reoptimised with model system II.

	ΔG /(kJ/mol)
axial conformers	
conformer 1	6
conformer 2	7
conformer 3	8
conformer 4	2
conformer 5	3
conformer 6	1
conformer 7	0
conformer 8	7
conformer 9	8
equatorial *cis* conformers	
conformer 10	8
conformer 11	8
equatorial *trans* conformers	
conformer 12	12
conformer 13	14

UNIVERSITAT ROVIRA I VIRGILI
COMPUTACIONAL STUDIES ON THE MECHANISM OF THE PAUSON-KHAND REACTION
Torstein Fjermestad
ISBN:978-84-693-9441-0/DL:T.62-2011

The removal of an equatorial carbonyl *trans* to the R substituent is disfavoured by 12 kJ/mol. The attack of the two equatorial carbonyls show an opposite trend compared to the equatorial attacks analysed in chapter 5. With the R substituent being methyl, the attack of the equatorial carbonyl *trans* to the R substituent is disfavoured by 2 kJ/mol relative to the attack of the axial carbonyl. The attack of the equatorial carbonyl *cis* to the R substituent is disfavoured by 7 kJ/mol relative to the attack of the axial carbonyl. Apparently the OH group is stabilising the attack of the *cis* equatorial carbonyl.

6.4.3 Conformational search on the real system

The energy range of the model system II optimised structures is 14 kJ/mol. Upon expansion to the real system (substitution of TMAO by brucine N-oxide), transition state geometries corresponding to high energy structures in model system II may be considerably stabilised in the real system. Likewise, transition state geometries corresponding to the low energy structures in model system II, may be considerably destabilised in the real system. Thus, all of the model system II optimised transition state geometries were submitted to a conformational search on the real system.

When replacing the TMAO with brucine N-oxide, the system becomes diastereomeric and the two cobalt atoms are no longer equivalent. Furthermore, the steric bulk of the brucine N-oxide makes structures related by a 120° rotation around the O-N bond inequivalent. Thus for each of the 13 structures of the model system, there are 6 structures of the real system. This makes in total 78 hypothetical TS structures to explore: 9 * 6 = 54 axial TS structures, 2 * 6 = 12 equatorial *cis* TS structures and 2 * 6 = 12 equatorial *trans* TS structures.

We initially envisioned that the ONIOM(B3LYP:UFF) calculation would give us a satisfactory description of the energies and geometries of the transition states.

Because of the relatively high number of TS conformers of the axial attack, the optimisations of these were followed by cluster analyses [112, 114] to exclude possible redundant conformers. Due to the rather constrained TS structures of the *cis* and *trans* equatorial attacks, we deemed the possibility of structures collapsing into one another as low. Cluster analyses were thus not done for the equatorial TS conformers.

For the axial TS conformers, two independent cluster analyses were carried out. One for the transition state structures of the (R(N),R) configuration and one for the transition state structures of the (R(N),S) configuration.

27 TS structures of the (R(N),R) configuration were optimised and 27 TS structures of the (R(N),S) configuration were optimised. The cluster analyses showed that five conformers of the (R(N),R) configuration and three structures of the (R(N),S) configuration became redundant.

Table 6.2 shows the non-redundant ONIOM optimised TS structures. From a given conformer of model system II, a group of six conformers of the real system can be defined. Of these six conformers, three have stereoconfiguration R of the dicobalt

UNIVERSITAT ROVIRA I VIRGILI
COMPUTACIONAL STUDIES ON THE MECHANISM OF THE PAUSON-KHAND REACTION
Torstein Fjermestad
ISBN:978-84-693-9441-0/DL:T.62-2011

complex; the other three have stereoconfiguration S. We label conformers belonging to a particular group with a particular stereoconfiguration with the conformer number of model system II and the stereoconfiguration as follows: conf*n*_II_T, where *n*_II is the conformer of model system II and T is the stereoconfiguration of the dicobalt complex (R or S). In the following discussion we also refer to the group of conformer *n* as group *n*. To distinguish the conformers of the same group with the same stereoconfiguration, we add *a*, *b* and *c* to the label.

Table 6.2: Non-redundant ONIOM optimised TS structures.

conformer	ΔG /(kJ/mol)	conformer	ΔG /(kJ/mol)
conf1		conf5	
conf1_II_R_a	16	conf5_II_R_a	Redundant
conf1_II_R_b	Redundant	conf5_II_R_b	11
conf1_II_R_c	13	conf5_II_R_c	7
conf1_II_S_a	Redundant	conf5_II_S_a	18
conf1_II_S_b	11	conf5_II_S_b	Redundant
conf1_II_S_c	12	conf5_II_S_c	Redundant
conf2		conf6	
conf2_II_R_a	Redundant	conf6_II_R_a	7
conf2_II_R_b	12	conf6_II_R_b	Redundant
conf2_II_R_c	Redundant	conf6_II_R_c	8
conf2_II_S_a	19	conf6_II_S_a	17
conf2_II_S_b	10	conf6_II_S_b	10
conf2_II_S_c	12	conf6_II_S_c	4
conf3		conf7	
conf3_II_R_a	13	conf7_II_R_a	15
conf3_II_R_b	18	conf7_II_R_b	0
conf3_II_R_c	17	conf7_II_R_c	3
conf3_II_S_a	19	conf7_II_S_a	6
conf3_II_S_b	14	conf7_II_S_b	4
conf3_II_S_c	16	conf7_II_S_c	3
conf9		conf10 (equat. *cis*)	
conf9_II_R_a	14	conf10_II_R_a	TS opt. failed
conf9_II_R_b	20	conf10_II_R_b	16
conf9_II_R_c	15	conf10_II_R_c	TS opt. failed
conf9_II_S_a	18	conf10_II_S_a	TS opt. failed

continued on next page

UNIVERSITAT ROVIRA I VIRGILI
COMPUTACIONAL STUDIES ON THE MECHANISM OF THE PAUSON-KHAND REACTION
Torstein Fjermestad
ISBN:978-84-693-9441-0/DL:T.62-2011

Table 6.2 –continued from previous page

conformer	ΔG /(kJ/mol)	conformer	ΔG /(kJ/mol)
conf9_II_S_b	17	conf10_II_S_b	TS opt. failed
conf9_II_S_c	21	conf10_II_S_c	TS opt. failed
conf8		conf11 (equat. *cis*)	
conf8_II_R_a	20	conf11_II_R_a	6
conf8_II_R_b	10	conf11_II_R_b	11
conf8_II_R_c	9	conf11_II_R_c	19
conf8_II_S_a	18	conf11_II_S_a	12
conf8_II_S_b	14	conf11_II_S_b	9
conf8_II_S_c	8	conf11_II_S_c	14
conf4		conf12 (equat. *trans*)	
conf4_II_R_a	6	conf12_II_R_a	25
conf4_II_R_b	6	conf12_II_R_b	21
conf4_II_R_c	3	conf12_II_R_c	20
conf4_II_S_a	1	conf12_II_S_a	18
conf4_II_S_b	3	conf12_II_S_b	22
conf4_II_S_c	16	conf12_II_S_c	21
conf13 (equat. *trans*)			
conf13_II_R_a	21		
conf13_II_R_b	27		
conf13_II_R_c	TS opt. failed		
conf13_II_S_a	20		
conf13_II_S_b	27		
conf13_II_S_c	21		

6.5 Analysis of results for selective CO removal

6.5.1 ONIOM results

Apart from the eight axial transition states that collapsed into other axial transition states, we failed to optimise five of the hypothetical transition states belonging to group 10 (equatorial *cis*) and one hypothetical TS structure of group 13 (equatorial *trans*). We attribute the failure in these optimisations to excessive steric constraint and we do not expect the corresponding pathways to be competitive. We were thus left with 64 TS structures for further analysis.

We applied to the Gibbs free energy of these optimised non-redundant structures equations (3.7) and (3.8) to obtain the enantiomeric excess. The ONIOM calculations gave an enantiomeric excess of 12% (R).

The ONIOM calculations predict the formation of the R enantiomer in preference of the S enantiomer in agreement with experiment. However, the calculated enantiomeric excess (12% R) is far off the experimentally determined enantiomeric excess of 78% (R) (in DME). As discussed in section 6.3, this step alone will not directly give the observed ee in the product, but further steps will only diminish it. Therefore

UNIVERSITAT ROVIRA I VIRGILI
COMPUTACIONAL STUDIES ON THE MECHANISM OF THE PAUSON-KHAND REACTION
Torstein Fjermestad
ISBN:978-84-693-9441-0/DL:T.62-2011

this result is too far from experiment to be acceptable.

6.5.2 Validation of the ONIOM results

The ONIOM optimised geometries were submitted to a full QM reoptimisation to see whether this would alter the relative energies of the transition states. The full QM calculations were done with the B3LYP functional [85, 86] as well as with the M06 functional [88]. B3LYP was chosen because this would correspond to an expansion to the full system of the QM region of the ONIOM calculation. M06 was chosen because it is shown to generally produce more accurate results for non-bonding interactions [80, 88]. Table 6.3 shows the Gibbs free energy of the selected structures calculated with the three different methods: ONIOM(B3LYP:UFF), B3LYP and M06.

Table 6.3: Gibbs free energy (kJ/mol) of selected structures optimised with ONIOM(B3LYP:UFF), B3LYP and M06.

Conformer	ONIOM(B3LYP:UFF)	B3LYP	M06
(R(N),R_a)			
conf7_II_R_*b*	0	0	0
conf6_II_R_*a*	7	1	-4
conf11_II_R_*a*	6	5	1
conf4_II_R_*a*	6	-2	-13
conf4_II_R_*b*	6	6	7
conf4_II_R_*c*	3	1	7
(R(N),S_a)			
conf7_II_S_*a*	6	1	-4
conf6_II_S_*c*	4	4	3
conf11_II_S_*b*	9	5	5
conf11_II_S_*a*	12	7	-3
conf4_II_S_*a*	1	2	-4
conf4_II_S_*b*	3	4	4

For many of the structures in table 6.3, the relative free energies vary significantly between the different methods. It is clear that ONIOM(B3LYP:UFF) does not give a satisfactory description of the system, and a full QM calculation is necessary. Because the two functionals tested (B3LYP and M06) give rise to significantly different results, we opted for M06 because it is supposed to bring better quality [80, 88].

6.5.3 Full QM results. M06, gas phase

The ONIOM optimised structures in the lower 20 kJ/mol range were submitted to a full QM reoptimisation with the M06 functional. The optimisations were done in gas phase and the Gibbs free energy values are shown in table 6.4.

UNIVERSITAT ROVIRA I VIRGILI
COMPUTACIONAL STUDIES ON THE MECHANISM OF THE PAUSON-KHAND REACTION
Torstein Fjermestad
ISBN:978-84-693-9441-0/DL:T.62-2011

Table 6.4: M06 optimised TS structures in gas phase. Relative Gibbs free energy in kJ/mol.

conformer	ΔG /(kJ/mol)	conformer	ΔG /(kJ/mol)
conf1		conf5	
conf1_II_R_a	12	conf5_II_R_b	9
conf1_II_R_c	12	conf5_II_R_c	11
conf1_II_S_b	2	conf5_II_S_a	6
conf1_II_S_c	14		
conf2		conf6	
conf2_II_R_b	9	conf6_II_R_a	-4
conf2_II_S_a	5	conf6_II_R_c	4
conf2_II_S_b	14	conf6_II_S_a	10
conf2_II_S_c	14	conf6_II_S_b	13
		conf6_II_S_c	3
conf3		conf7	
conf3_II_R_a	20	conf7_II_R_a	9
conf3_II_R_b	15	conf7_II_R_b	0
conf3_II_R_c	21	conf7_II_R_c	10
conf3_II_S_a	16	conf7_II_S_a	-4
conf3_II_S_b	25	conf7_II_S_b	3
conf3_II_S_c	18	conf7_II_S_c	6
conf9		conf10 (equat. *cis*)	
conf9_II_R_a	21	conf10_II_R_b	-3
conf9_II_R_b	9		
conf9_II_R_c	14		
conf9_II_S_a	17		
conf9_II_S_b	16		
conf8		conf11 (equat. *cis*)	
conf8_II_R_a	11	conf11_II_R_a	1
conf8_II_R_b	10	conf11_II_R_b	4
conf8_II_R_c	8	conf11_II_R_c	11
conf8_II_S_a	0	conf11_II_S_a	-3
conf8_II_S_b	12	conf11_II_S_b	5

continued on next page

UNIVERSITAT ROVIRA I VIRGILI
COMPUTACIONAL STUDIES ON THE MECHANISM OF THE PAUSON-KHAND REACTION
Torstein Fjermestad
ISBN:978-84-693-9441-0/DL:T.62-2011

Table 6.4 –continued from previous page

conformer	ΔG /(kJ/mol)	conformer	ΔG /(kJ/mol)
conf8_II_S_c	9	conf11_II_S_c	15
conf4		conf12 (equat. *trans*)	
conf4_II_R_a	-13		
conf4_II_R_b	7		
conf4_II_R_c	7	conf12_II_R_c	15
conf4_II_S_a	-4	conf12_II_S_a	11
conf4_II_S_b	4	conf12_II_S_b	11
conf4_II_S_c	9		
conf13 (equat. *trans*)			
conf13_II_S_a	23		

From the Gibbs free energies in table 6.4, we find that the probability for the reaction to go through step A, P_{stepA}, is 0.98. Because we are only considering step A and E as possible pathways from the initial complex $Co_2(CO)_6$(alkyne), the probability of taking step E, P_{stepE}, is 0.02.

6.5.4 M06, acetone

The experiments by Kerr [70] show that the enantiomeric excess depends on the solvent. When carried out in acetone, the enantiomeric excess is 56% whereas in dimethoxyethane (DME) the enantiomeric excess is 78%. To better understand the role of the solvent in determining the enantiomeric excess, we reoptimised the gas phase TS structures in acetone as well as DME (see computational details, section 6.2). Table 6.5 shows the free energies of the TS structures optimised in acetone.

Table 6.5: M06 optimised TS structures in acetone. Relative Gibbs free energy in kJ/mol.

conformer	ΔG /(kJ/mol)	conformer	ΔG /(kJ/mol)
conf1		conf5	
conf1_II_R_a	7	conf5_II_R_b	5
conf1_II_R_c	12	conf5_II_R_c	5
conf1_II_S_b	3	conf5_II_S_a	2
conf1_II_S_c	7		
conf2		conf6	
conf2_II_R_b	10		
conf2_II_S_a	5	conf6_II_R_a	-5
conf2_II_S_b	7	conf6_II_R_c	8

continued on next page

UNIVERSITAT ROVIRA I VIRGILI
COMPUTACIONAL STUDIES ON THE MECHANISM OF THE PAUSON-KHAND REACTION
Torstein Fjermestad
ISBN:978-84-693-9441-0/DL:T.62-2011

Table 6.5 –continued from previous page

conformer	ΔG /(kJ/mol)	conformer	ΔG /(kJ/mol)
conf2_II_S_c	10	conf6_II_S_a	9
		conf6_II_S_b	12
		conf6_II_S_c	-1
conf3		conf7	
conf3_II_R_a	1	conf7_II_R_a	2
conf3_II_R_b	9	conf7_II_R_b	0
conf3_II_R_c	6	conf7_II_R_c	3
conf3_II_S_a	9	conf7_II_S_a	2
conf3_II_S_b	11	conf7_II_S_b	5
conf3_II_S_c	9	conf7_II_S_c	6
conf9		conf10 (equat. *cis*)	
conf9_II_R_a	13	conf10_II_R_b	-8
conf9_II_R_b	15		
conf9_II_R_c	4		
conf9_II_S_a	7		
conf9_II_S_b	3		
conf8		conf11 (equat. *cis*)	
conf8_II_R_a	13	conf11_II_R_a	11
conf8_II_R_b	4	conf11_II_R_b	11
conf8_II_R_c	10	conf11_II_R_c	18
conf8_II_S_a	0	conf11_II_S_a	6
conf8_II_S_b	5	conf11_II_S_b	15
conf8_II_S_c	9	conf11_II_S_c	16
conf4		conf12 (equat. *trans*)	
conf4_II_R_a	-3		
conf4_II_R_b	8		
conf4_II_R_c	7	conf12_II_R_c	19
conf4_II_S_a	0	conf12_II_S_a	20
conf4_II_S_b	5	conf12_II_S_b	11
conf4_II_S_c	11		
conf13 (equat. *trans*)			
conf13_II_S_a	16		

From the free energy values tabulated in table 6.5 we find that the probability of going though step A in acetone, $P_{\text{stepA,acetone}}$ is 0.95. The probability of taking step E in acetone, $P_{\text{stepE,acetone}}$ is 0.05.

6.5.5 M06, dimethoxyethane

The gas phase TS geometries were reoptimised in DME as described in the computational details. The Gibbs free energy values of these solvent optimised TS structures are shown in table 6.6.

UNIVERSITAT ROVIRA I VIRGILI
COMPUTACIONAL STUDIES ON THE MECHANISM OF THE PAUSON-KHAND REACTION
Torstein Fjermestad
ISBN:978-84-693-9441-0/DL:T.62-2011

Table 6.6: M06 optimised TS structures in DME. Relative Gibbs free energy in kJ/mol.

conformer	ΔG /(kJ/mol)	conformer	ΔG /(kJ/mol)
conf1		conf5	
conf1_II_R_a	9	conf5_II_R_b	7
conf1_II_R_c	14	conf5_II_R_c	3
conf1_II_S_b	1	conf5_II_S_a	2
conf1_II_S_c	9		
conf2		conf6	
conf2_II_R_b	9	conf6_II_R_a	-4
conf2_II_S_a	4	conf6_II_R_c	8
conf2_II_S_b	8	conf6_II_S_a	10
conf2_II_S_c	13	conf6_II_S_b	10
		conf6_II_S_c	2
conf3		conf7	
conf3_II_R_a	6	conf7_II_R_a	5
conf3_II_R_b	9	conf7_II_R_b	0
conf3_II_R_c	7	conf7_II_R_c	4
conf3_II_S_a	5	conf7_II_S_a	0
conf3_II_S_b	11	conf7_II_S_b	5
conf3_II_S_c	11	conf7_II_S_c	6
conf9		conf10 (equat. *cis*)	
conf9_II_R_a	10	conf10_II_R_b	-5
conf9_II_R_b	13		
conf9_II_R_c	2		
conf9_II_S_a	7		
conf9_II_S_b	5		
conf8		conf11 (equat. *cis*)	
conf8_II_R_a	14	conf11_II_R_a	11
conf8_II_R_b	6	conf11_II_R_b	12
conf8_II_R_c	10	conf11_II_R_c	19
conf8_II_S_a	1	conf11_II_S_a	6
conf8_II_S_b	4	conf11_II_S_b	9

continued on next page

UNIVERSITAT ROVIRA I VIRGILI
COMPUTACIONAL STUDIES ON THE MECHANISM OF THE PAUSON-KHAND REACTION
Torstein Fjermestad
ISBN:978-84-693-9441-0/DL:T.62-2011

Table 6.6 –continued from previous page

conformer	ΔG /(kJ/mol)	conformer	ΔG /(kJ/mol)
conf8_II_S_c	13	conf11_II_S_c	17
conf4		conf12 (equat. *trans*)	
conf4_II_R_a	-3		
conf4_II_R_b	3		
conf4_II_R_c	-1	conf12_II_R_c	15
conf4_II_S_a	7	conf12_II_S_a	15
conf4_II_S_b	6	conf12_II_S_b	10
conf4_II_S_c	9		
conf13			
conf13_II_S_a	20		

Based on the Gibbs free energy values in table 6.6, the probability of taking step A in DME, $P_{\text{stepA,DME}}$, is 0.92. Likewise the probability of taking step E in DME, $P_{\text{stepE,DME}}$, is 0.08.

6.6 Epimerisation, step C

The epimerisation (step C) competes with the oxidative metallacycle formation (step B, F, D, and G). To compare their relative heights, we must choose a common zero level. The chosen zero level will be intermediate R_{INT} with the norbornene coordinated. The epimerisation consists of two processes: first the dissociation of norbornene, thereafter the CO migration between the two cobalt atoms. We located a transition state of the CO migration occurring at the side of the complex *trans* to the R substituent of the alkyne. Also, we located the intermediate R_{INT} with and without the norbornene coordinated.

The gas phase Gibbs free energy of the transition state of step C is 41 kJ/mol. 6 kJ/mol comes from the norbornene dissociation and 35 kJ/mol comes from the CO migration between the two cobalt atoms.

Upon reoptimisation in acetone, the dissociation energy of norbornene showed a small change from 6 kJ/mol to 5 kJ/mol. The barrier of CO migration increased to 41 kJ/mol thus giving an epimerisation barrier of 46 kJ/mol relative to the zero level (see figure 6.11).

Upon reoptimisation in DME, the dissociation energy of norbornene increased from 5 kJ/mol to 10 kJ/mol. The barrier of CO migration showed no change at 41 kJ/mol. The total barrier for the epimerisation in DME is thus 51 kJ/mol.

UNIVERSITAT ROVIRA I VIRGILI
COMPUTACIONAL STUDIES ON THE MECHANISM OF THE PAUSON-KHAND REACTION
Torstein Fjermestad
ISBN:978-84-693-9441-0/DL:T.62-2011

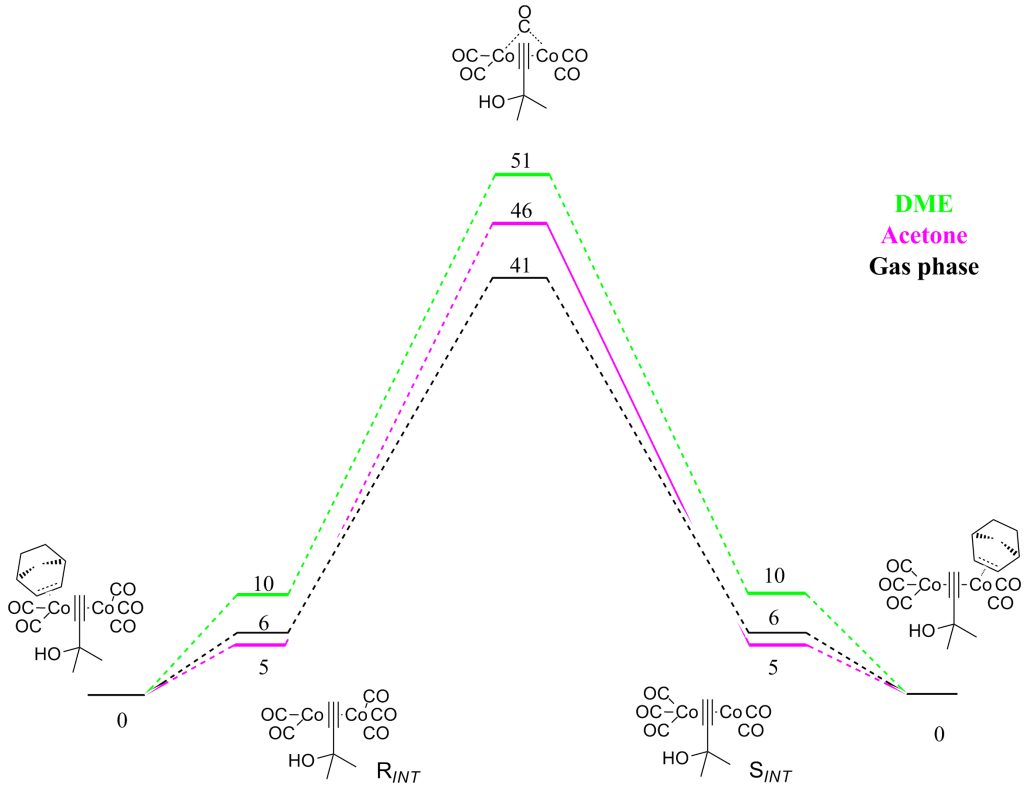

Figure 6.11: Free energy profiles (kJ/mol) for the epimerisation in gas phase, acetone and DME.

6.7 Oxidative metallacycle formation, step B, F, D and G

We located two transition states of the oxidative metallacycle formation corresponding to the pro-R (step B) and pro-S (step F) attacks of the norbornene to the R_{INT} intermediate. Relative to the R_{INT} intermediate with the norbornene coordinated, the gas phase free energy of the pro-R transition state is 46 kJ/mol and the gas phase free energy of the pro-S transition state is 43 kJ/mol.

The oxidative metallacycle formation competes with the epimerisation process. From intermediate R_{INT}, the reaction can proceed through step B, step F and step C_1. From intermediate S_{INT}, the reaction can proceed through step D, step G and step C_2. Because the R_{INT} and S_{INT} intermediates are enantiomers of each other, the TS of step B, TS_B, and the TS of step G, TS_G form an enantiomeric pair. Likewise, the TS of step F, TS_F and the TS of step D, TS_D are enantiomers of each other. Thus, when calculating the probability for the reaction to go through any of the steps B, C, D, F and G, we do not need to calculate the energy of TS_D and TS_G because their energies will be exactly the same as TS_F and TS_B respectively.

When calculating the probability for the reaction to go through step B and step D, it thus suffice to consider the TSs of step B, step F and step C. From the derivation in section 6.3, we obtain that, in gas phase, the probability of going through step B,

UNIVERSITAT ROVIRA I VIRGILI
COMPUTACIONAL STUDIES ON THE MECHANISM OF THE PAUSON-KHAND REACTION
Torstein Fjermestad
ISBN:978-84-693-9441-0/DL:T.62-2011

P_{stepB}, is 0.07 and the probability of going through step D, P_{stepD}, is 0.26.

Upon reoptimisation in acetone, the transition states of the oxidative metallacycle formation, TS_B and TS_F, change to 41 kJ/mol and 46 kJ/mol respectively. From the derivation in section 6.3, we obtain that the probability of going through step B, $P_{\text{stepB,acetone}}$, is 0.87 and the probability of going through step D, $P_{\text{stepD,acetone}}$, is 0.04.

In DME the transition states of the metallacycle formation, TS_B and TS_F, changes to 39 kJ/mol and 45 kJ/mol respectively. The probability of going through step B, $P_{\text{stepB,DME}}$, is then 0.95 and the probability of going through step D, $P_{\text{stepD,DME}}$, is 0.05

From the transition state energies of the epimerisation and the oxidative metallacycle formation, we can now calculate the probability for the system to epimerise in the three cases. In gas phase the probability of epimerisation, P_{stepC} is 0.67. In acetone the probability of epimerisation $P_{\text{stepC,acetone}}$ is 0.09 and in DME the probability of epimerisation, $P_{\text{stepD,DME}}$, is 0.001.

6.8 Enantiomeric excess

From equations (6.13) to (6.18), we compute the enantioselectivities of the three cases considered: the reaction in gas phase, in acetone and in DME.

In gas phase, the epimerisation pathway (41 kJ/mol) is favoured over the pathways for oxidative metallacycle formation, 46 kJ/mol for step B and step G and 43 kJ/mol for step F and step D. This leads to a low enantiomeric excess of 11% (S).

In acetone, the TS of the epimerisation pathway is 45 kJ/mol. The transition states of step B and step G of the oxidative metallacycle formation are 41 kJ/mol. The transition states of step F and step D are 46 kJ/mol. This leads to an enantiomeric excess of 68% (R). This is in good agreement with the experimental result of 56% ee (R).

In DME, the TS of the epimerisation pathway is 51 kJ/mol. The transition states of step B and G of the oxidative metallacycle formation are 39 kJ/mol. The transition states of step F and step D are 45 kJ/mol. This leads to an enantiomeric excess of 76% (R). This is in good agreement with the experimentally determined enantiomeric excess of 78% (R).

6.9 Discussion

The calculated enantiomeric excess in acetone is 12% above the experimentally determined value. At -60°C, the difference between 68% ee (R) and 56% ee (R) corresponds to an energy difference of 0.70 kJ/mol. The calculated enantiomeric excess in DME is 2% below the experimentally determined value. At -60°C, the difference between 76% ee (R) and 78% ee (R) corresponds to an energy difference of 0.17 kJ/mol. Taking into account that the enantioselectivity in this system depends on

UNIVERSITAT ROVIRA I VIRGILI
COMPUTACIONAL STUDIES ON THE MECHANISM OF THE PAUSON-KHAND REACTION
Torstein Fjermestad
ISBN:978-84-693-9441-0/DL:T.62-2011

three enantioselctive processes (The selective CO removal, the pro-R / pro-S attack of the norbonene on the R_{INT} intermediate and the pro-R / pro-S attack of the norbonene on the S_{INT} intermediate) as well as the epimerisation, the result for both solvents must be said to be in good agreement with the experimental results. This good agreement gives us confidence that the mechanism of enantioselection in this system is the correct one.

The reaction in gas phase is an interesting case. Compared to the reaction in solvent, the gas phase reaction is characterised by an epimerisation barrier being lower than the barrier of the oxidative metallacycle formation. The relatively easy epimerisation towards the opposite enantiomer reduces the enantiomeric excess significantly with respect to the two solvent cases. Another interesting feature of the gas phase reaction is the reversal of the enantioselectivity of the oxidative metallacycle formation. The enantiomeric excess is thus small and slightly in favour of the S product (11% ee).

6.9.1 The contribution of the individual steps to the overall enantioselectivity

Because there are several steps that contribute to the determination of the enantiomeric excess, an analysis of the contribution of the individual steps would be appropriate. We first analyse the enantiomeric excess obtained in the step of the selective CO removal. Afterwards we analyse the contribution from the oxidative metallacycle formation.

The selective CO removal

From the probabilities P_{stepA} and P_{stepE}, the enantiomeric excess of the intermediates R_{INT} and S_{INT} resulting from the selective CO removal can be calculated. In gas phase this is 96%, in acetone it is 89% and in DME it is 84%. These ee values are all in favour of the the R_{INT} intermediate.

The oxidative metallacycle formation

The contribution of the oxidative metallacycle formation to the overall enantiomeric excess is coupled with the epimerisation. The lower the epimerisation barrier, the more will be produced of the minor enantiomer, S_{INT}, which shows an enantioselectivity exactly opposite to that of R_{INT}. Thus, the lower the epimerisation barrier, the lower the enantiomeric excess. The epimerisation is clearly complicating the analysis of the oxidative metallacycle formation. To avoid this complication, we will consider the limiting case where the epimerisation barrier is high enough to prevent any equilibration between intermediates R_{INT} and S_{INT}. This limiting case would also represent the enantioselectivity of the system in the hypothetical case of a 100% selective CO removal *and* a negligible epimerisation process. Studying this limiting case provides us with information on how much the enantioselectivity can be improved by increasing the epimerisation barrier and making the CO removal more

UNIVERSITAT ROVIRA I VIRGILI
COMPUTACIONAL STUDIES ON THE MECHANISM OF THE PAUSON-KHAND REACTION
Torstein Fjermestad
ISBN:978-84-693-9441-0/DL:T.62-2011

selective.

The enantioselectivity in this limiting case will be calculated from a comparison of the transition states TS_B and TS_F of step B and step F respectively. This enantioselectivity is a result of a difference in steric repulsions between the R substituent of the dicobalt complex and pro-R and pro-S faces of the norbornene. For this reason we term it the intrinsic enantioselectivity.

In gas phase the intrinsic enantioselectivity is 55% (S).

In acetone, the intrinsic enantioselectivity is 90% (R). The experimental ee value in acetone is 56% (R). By improving the selectivity of the CO removal (e.g by using a more selective chiral N-oxide.) and completely preventing epimerisation, the ee value can be raised to at most 90%. An increase in the enantioselectivity beyond 90% would require a modification of the substrate (norbonene) and/or a modification of the chiral pocket on the catalyst (e.g. using a different substituent on the alkyne moiety).

In DME, the intrinsic enantioselectivity is 90% (R). The experimental ee value in DME is 78%. Our calculations show that by increasing the selectivity of the CO removal as well as the barrier of the epimerisation, the enantiomeric excess can not be increased beyond 90% ee.

Summary

For the reaction in gas phase, we see that the first step shows nearly complete enantioselectivity with 96% ee in favour of the R_{INT} intermediate. This high level of enantioselectivity is reduced to 11% (S) in the subsequent steps due to the low barrier of epimerisation (41 kJ/mol) as well as the small energy difference between the pro-R TSs and the pro-S TSs of the oxidative metallacycle formation (3 kJ/mol).

For the reaction in acetone, the first step shows an enantioseletivity of 89% ee in favour of the R_{INT} intermediate. This level of enantioselectivity is reduced to 68% ee in the subsequent steps.

For the reaction in DME, the first step shows an enantioselectivity of 85% ee in favour of the R_{INT} intermediate. This level of enantioselectivity is reduced to 76% ee in the subsequent steps.

When comparing the two solvents, we see that they reach quite similar enantiomeric excess in the first step, 89% ee in the case of acetone and 85% ee in the case of DME. In the subsequent steps, however, the enantiomeric excess of acetone is reduced much more (68%) than what is the case of DME (76%). Both solvents also show the same intrinsic enantioselectivity (90% ee). It is thus clear that the more pronounced reduction of ee in the case of acetone is due to the lower barrier of epimerisation.

UNIVERSITAT ROVIRA I VIRGILI
COMPUTACIONAL STUDIES ON THE MECHANISM OF THE PAUSON-KHAND REACTION
Torstein Fjermestad
ISBN:978-84-693-9441-0/DL:T.62-2011

6.9.2 Mechanism of enantiodiscrimination in the brucine N-oxide assisted CO removal

The cause of the enantiodiscrimination in the oxidative metallacycle formation seems to be due to steric repulsions between the R substituent of the dicobalt complex and the two faces of the norbonene. The repulsions are more pronounced in TS_F and TS_D which leads to a preference of step B and step G over step F and step D.

For the selective CO removal, step A and step E, the enantiodiscrimination is more complex. The brucine N-oxide can attack both equatorial and axial carbonyl ligands and both attacks give rise to low-energy TSs. In the following we will analyse the contributions to the enantiomeric excess both from the attack on equatorial carbonyl ligands as well as attack on axial carbonyl ligands.

The experimental results by Kerr and co-workers [70] show that the OH group as well as the methyl groups of the R substituent are important for achieving high enantiomeric excess. The mechanistic proposal of the authors suggests a tethering mechanism where the OH group forms weak interactions to some group of the brucine N-oxide thus pulling it closer to the bulky methyl groups of the R substituent. The closer contact between bulky groups of BNO and the methyl groups of the R substituent increases the steric repulsion between these groups. However, the steric repulsions differ depending on whether BNO attacks a carbonyl at Co1 or a carbonyl at Co2, and this leads to an enantiodiscrimination between the respective TSs.

In what follows, we will analyse the role of the OH group and the methyl groups in the TSs of the equatorial and the axial attacks.

6.9.3 Selective CO removal, equatorial attack

Both in acetone and DME conformer conf10_II_R_b, leading to the formation of the R_{INT} intermediate, is the most stable TS of the equatorial attack (-8 kJ/mol in acetone and -5 kJ/mol in DME). Its structure is characterised by having the bulky groups of BNO lying between the equatorial carbonyl ligands of the dicobalt complex (see figure 6.12 (left)). The structure is further characterised by having a hydrogen bond between the OH group of the R substituent and the oxygen of the carbonyl ligand being attacked. These two structural motifs seem to be associated with a low energy. Interestingly, the same two structural motifs are not possible in any TS structure leading to the S_{INT} intermediate. This can be understood by looking at the structure and energy of conf12_II_S_b (figure 6.12 (right), 11 kJ/mol in acetone and 10 kJ/mol in DME). Also in conf12_II_S_b the bulky groups of BNO are located in between the equatorial carbonyl ligands. However, to obtain that structural motif, BNO must attack a carbonyl ligand *trans* to the R substituent. The OH group can then not form a stabilising hydrogen bond to the carbonyl being attacked. Because of this lack of a stabilising H-bond in the S transition state, the R_{INT} intermediate is favoured for the BNO attack of the equatorial carbonyl ligand. The role of the OH group in relation to enantioselectivity is thus to stabilise the conf10_II_R_b TS leading to the formation of the R_{INT} intermediate. This is in

UNIVERSITAT ROVIRA I VIRGILI
COMPUTACIONAL STUDIES ON THE MECHANISM OF THE PAUSON-KHAND REACTION
Torstein Fjermestad
ISBN:978-84-693-9441-0/DL:T.62-2011

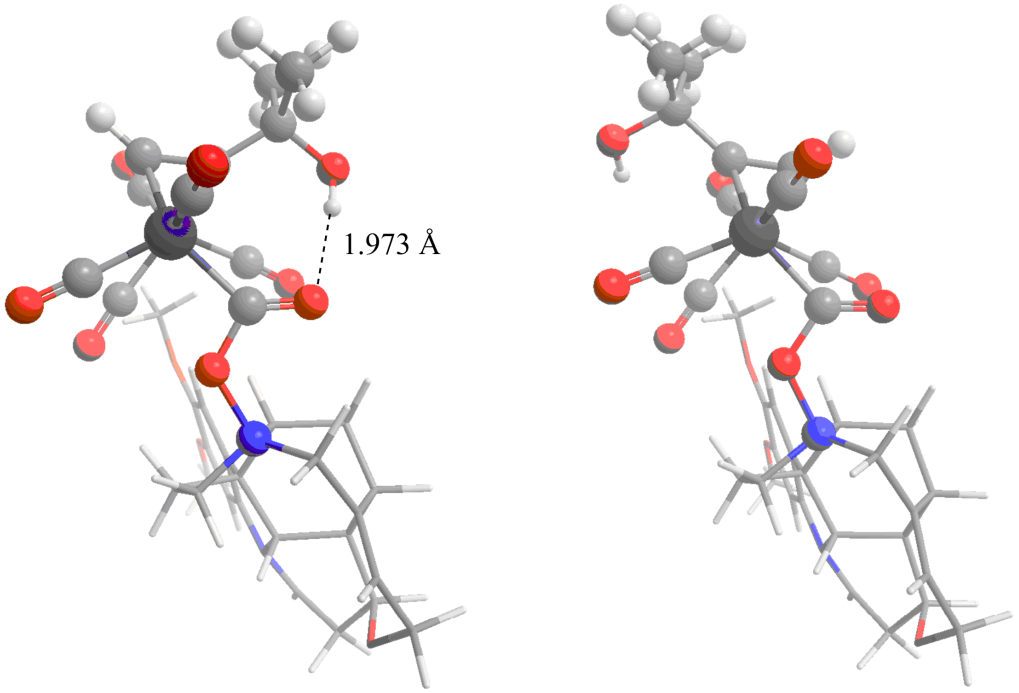

Figure 6.12: Gas phase optimised structures of conf10_II_R_b (left) and conf12_II_S_b (right).

contradiction to the tethering proposal by Kerr and co-workers [70].

Both in conf10_II_R_b and conf12_II_S_b, the methyl groups of the R substituent are located in a region far from the bulky groups of the BNO. Thus for the equatorial attack, there is no obvious influence of the methyl groups on the enantiomeric excess.

6.9.4 Selective CO removal, axial attack

The role of the OH group and the methyl groups for the axial attack seems less obvious and a more elaborate analysis was necessary. In the following we will analyse the role of the OH group and the methyl groups separately.

The role of the OH group

For TSs of the axial attack, BNO is in closer proximity to the R substituent of the dicobalt complex and the tethering mechanism proposed by Kerr and co-workers may be possible. To test the proposed tethering mechanism, we performed a computational study, investigating the effect of the OH group. This study consisted of comparing the TS geometries containing the OH group with geometries where the OH group had been substituted by a hydrogen atom. The change in energy upon this substitution may give us an indication of the mechanistic role of the OH group.

We first did a single point gas phase calculations on a selection of DME optimised TS geometries. The choice of DME geometries was made in order to have a better

UNIVERSITAT ROVIRA I VIRGILI
COMPUTACIONAL STUDIES ON THE MECHANISM OF THE PAUSON-KHAND REACTION
Torstein Fjermestad
ISBN:978-84-693-9441-0/DL:T.62-2011

relation to the geometries of the real system. The OH group was then substituted by a hydrogen and the C-H bond length was optimised. The rest of the structure was kept frozen. By keeping all atoms but the hydrogen frozen, we make sure that the only change between the two structures is due to the OH group. We opted for gas phase calculations because substituting a polar group with a non-polar group may change the solute - solvent interaction thus causing an additional change in the system that could make the analysis more difficult. As the energy origin of this analysis, we chose a structure where the OH group of the alkyne substituent is rotated away from the BNO. The OH group in that structure cannot form any interaction with the BNO and no change is likely to occur upon substitution with a hydrogen atom.

Table 6.7 shows the relative potential energies of the structures with the OH group ($E_{p,\mathrm{OH}}$), the relative potential energies of the structures with the OH group substituted with a hydrogen ($E_{p,\mathrm{H}}$) and the difference between these two ($\Delta_{E_{p,\mathrm{H}}-E_{p,\mathrm{OH}}}$). Upon substitution of the OH group with the hydrogen atom, all structures show a destabilisation. It is clear that the role of the OH group is to stabilise the axial transition states of the BNO activated CO removal. However, the degree of destabilisation is significantly different between the different structures. Based on the criteria of a C-H-O donor angle between 130° and 180° and a H-O non-bonding distance between 2.2Å and 3.2Å[1], several structures possessed C-H$\cdots$O interactions between the hydroxy oxygen and two hydrogen atoms of the BNO (see figure 6.13). The structures with these C-H$\cdots$O interactions are also those with the lowest energies ($E_{p,\mathrm{OH}}$ in the range -41 kJ/mol to -22 kJ/mol) and the largest destabilisation ($\Delta_{E_{p,\mathrm{H}}-E_{p,\mathrm{OH}}}$ in the range 19 kJ/mol to 31 kJ/mol) upon substitution with a hydrogen atom.

The two C-H$\cdots$O interactions indicated in figure 6.13 do indeed pull the methoxy groups of BNO closer to the methyl groups of the R substituent of the alkyne. This closer contact between bulky groups increases the steric repulsion. However, the C-H$\cdots$O interactions stabilise the structure more and the total energy is low (e.g conf4_II_R_a = -41 kJ/mol) in spite of the increased steric repulsions.

Influence of OH on the enantiomeric excess

Table 6.7 shows that the range of energy values is larger for the structures with the OH group (33 kJ/mol) than for the structures with OH substituted by H (19 kJ/mol). Upon substitution of OH by H, more structures compete with the most stable R TS and the most stable S TS.

For the structures with the OH group, the energy difference between the most stable R TS (conf4_II_R_a: -41 kJ/mol) and the most stable S TS (conf7_II_S_a: -34 kJ/mol) is 7 kJ/mol. Both of these structures possess the C-H$\cdots$O interactions indicated in figure 6.13. Upon substitution of OH by H, conf4_II_R_a (-11 kJ/mol) is still the most stable R TS. However, conf4_II_S_b (-7 kJ/mol) with no apparent motif of C-H$\cdots$O interactions, is now the most stable S transition state. The difference between these two is now 4 kJ/mol. This change in the order of relative

[1]These criteria are based on what may be classified as an intermediate or weak C-H$\cdots$O interaction [122, 123]

UNIVERSITAT ROVIRA I VIRGILI
COMPUTACIONAL STUDIES ON THE MECHANISM OF THE PAUSON-KHAND REACTION
Torstein Fjermestad
ISBN:978-84-693-9441-0/DL:T.62-2011

Table 6.7: Relative potential energies (kJ/mol), C-H-O angles (deg) and H-O distances (Å). The most stable R and S transition states of the two groups are shown in boldface.

	$E_{p,\mathrm{OH}}$	$E_{p,\mathrm{H}}$	$\Delta_{E_{p,\mathrm{H}}-E_{p,\mathrm{OH}}}$		C-H$\cdots$O?[a]
ref. structure	0	0	0		N
conf7_II_R_b	-31	0	31		Y
conf7_II_S_a	**-34**	-3	31		Y
conf7_II_S_b	-18	3	20		N
conf7_II_S_c	-19	2	21		N
conf6_II_R_a	-29	1	29		Y
conf6_II_S_a	-12	2	14		N
conf6_II_S_b	-11	8	19		N
conf4_II_R_a	**-41**	**-11**	30		Y
conf4_II_S_a	-28	1	29		Y
conf4_II_S_b	-24	**-7**	17		N
conf1_II_S_b	-28	-1	26		Y
conf5_II_R_b	-13	5	19		N
conf5_II_R_c	-16	8	25		N
conf8_II_R_a	-8	-3	5		N
conf8_II_R_b	-22	-3	19		Y
conf8_II_S_a	-30	-6	24		Y
conf8_II_S_b	-11	2	13		N
conf8_II_S_c	-9	3	12		N
	C(sp2)H-O	C(sp2)H-O	C(sp3)H-O	C(sp3)H-O	C-H$\cdots$O?[a]
ref. structure	5.37	145.5	5.39	155.4	N
conf7_II_R_b	2.3	159.4	2.39	178.2	Y
conf7_II_S_a	2.4	167.3	2.53	172.1	Y
conf7_II_S_b	5.40	118.3	4.92	93.3	N
conf7_II_S_c	7.23	121.5	5.04	79.5	N
conf6_II_R_a	2.36	166.3	2.56	152.4	Y
conf6_II_S_a	7.18	119.5	5.25	74.7	N
conf6_II_S_b	3.51	134.8	2.42	135.8	N
conf4_II_R_a	2.34	164.1	2.35	174.1	Y
conf4_II_S_a	2.24	167.2	2.37	177.7	Y
conf4_II_S_b	4.57	121.1	4.26	99.6	N
conf1_II_S_b	2.44	153.2	2.31	172.6	Y
conf5_II_R_b	6.66	118.3	5.13	76.7	N
conf5_II_R_c	5.69	125.7	3.73	96.4	N
conf8_II_R_a	7.50	124.4	5.47	80.2	N
conf8_II_R_b	2.51	142.9	2.38	159.3	Y
conf8_II_S_a	2.19	166.7	2.43	159.1	Y
conf8_II_S_b	6.47	120	5.27	82.2	N
conf8_II_S_c	6.39	123.5	4.29	88.2	N

[a] Based on the criteria of a C-H-O donor angle between 130° and 180° and a H-O non-bonding distance between 2.2Å and 3.2Å

UNIVERSITAT ROVIRA I VIRGILI
COMPUTACIONAL STUDIES ON THE MECHANISM OF THE PAUSON-KHAND REACTION
Torstein Fjermestad
ISBN:978-84-693-9441-0/DL:T.62-2011

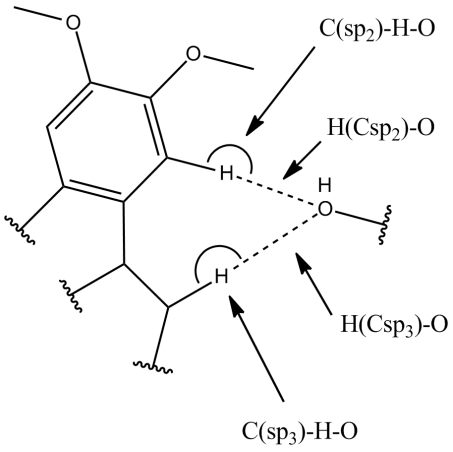

Figure 6.13: Schematic representation of the C-H-O angles and H-O distances in table 6.7.

energies is represented in figure 6.14. The substitution of OH by H decreases the

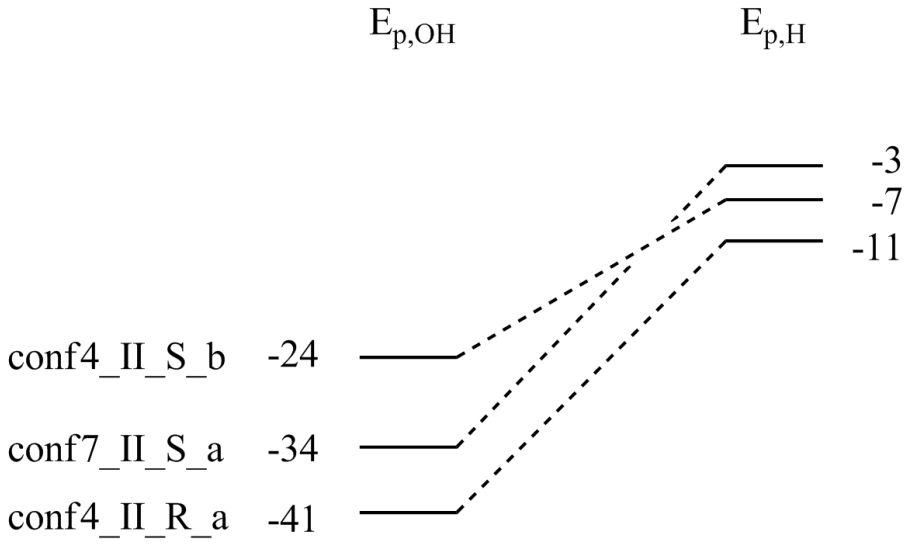

Figure 6.14: Change in the relative potential energy of conf4_II_R_a, conf4_II_S_b and conf7_II_S_a upon the substitution of OH by H. Energies in kJ/mol.

energy difference between the most stable R TS and the most stable S TS, thus reducing the enantiomeric excess. Thus for the BNO attack of the axial carbonyl ligands, the presence of the OH group stabilises transition states possessing C-H$\cdots$O interactions. Because of a difference in steric repulsions (see below), the TSs leading to the R_{INT} intermediate are stabilised more than the TSs leading to the S_{INT} intermediate. The stabilisation of the TSs possessing C-H$\cdots$O interactions confirms the tethering mechanism of Kerr and co-workers [70].

UNIVERSITAT ROVIRA I VIRGILI
COMPUTACIONAL STUDIES ON THE MECHANISM OF THE PAUSON-KHAND REACTION
Torstein Fjermestad
ISBN:978-84-693-9441-0/DL:T.62-2011

The role of the methyl groups

The presence of the methyl groups in the R substituent is also shown to dramatically affect the enantiomeric excess. We here analyse their role in the two most stable R and S TSs of the axial BNO attack.

The gas phase optimised structures of conf4_II_R_a (-13 kJ/mol) and conf7_II_S_a (-4 kJ/mol), show features of C-H$\cdots$O interactions (see figure 6.15) that indicate a tethering mechanism. Moreover, in these TSs, a methoxy group of the BNO is in close proximity to the methyl groups of the R substituent. In the conf4_II_R_a structure, the closest contact distance between the methoxy carbon and the methyl carbons is 3.720 Å. In the conf7_II_S_a structure, the closest contact distance is 3.528 Å. In the conf7_II_S_a structure, the distances of the weak C-H$\cdots$O interactions

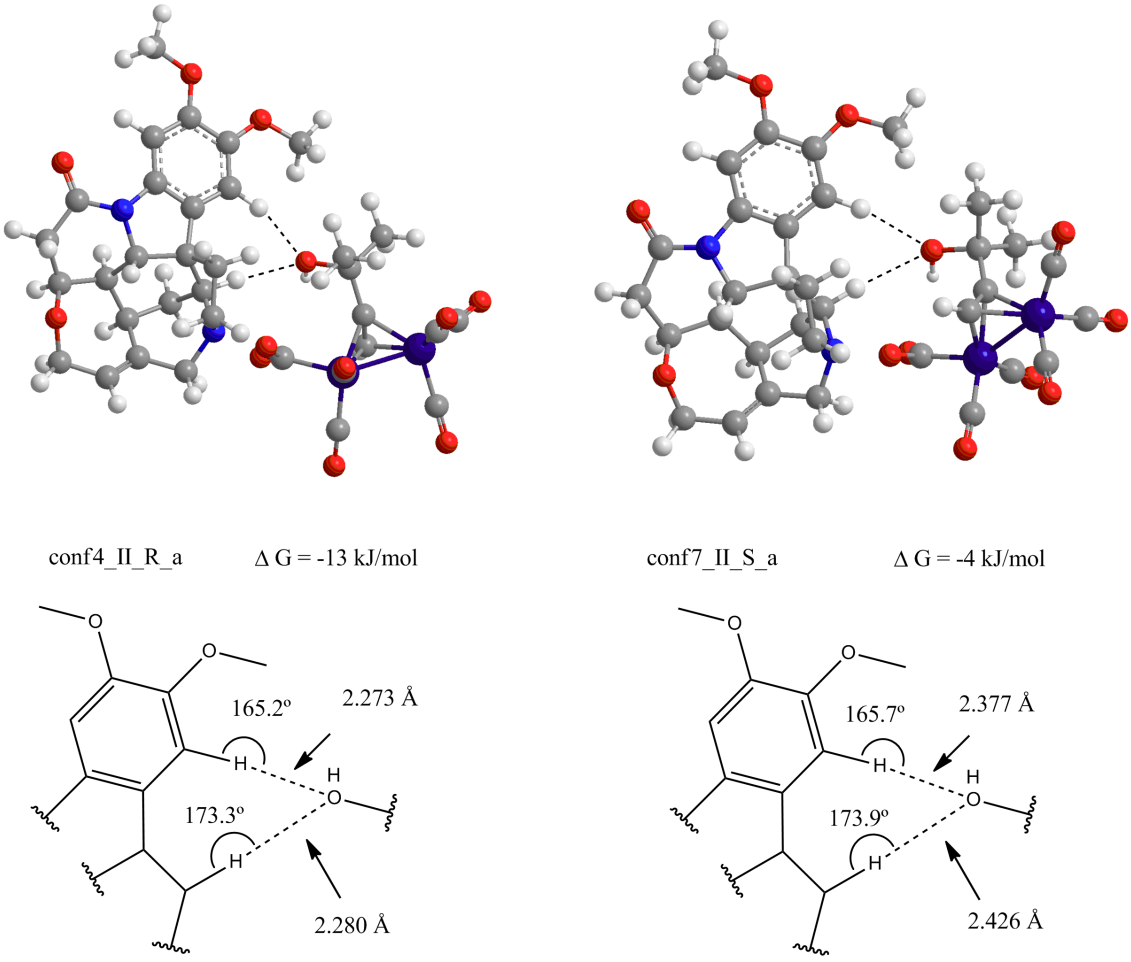

Figure 6.15: 3D structures and schematic drawings indicating H-bond features of the conf4_II_R_a structure (left) and the conf7_II_S_a structure (right).

are about 0.1 Å longer than in the conf4_II_R_a structure. Thus, the role of the methyl groups seems to be the following: In the conf7_II_S_a structure, the shorter closest contact distance raises the energy because of the increased steric repulsion. Additionally, the steric repulsion prevents the BNO from approaching the OH group closer. The structure will therefore not obtain the additional stabilisation a shorter

UNIVERSITAT ROVIRA I VIRGILI
COMPUTACIONAL STUDIES ON THE MECHANISM OF THE PAUSON-KHAND REACTION
Torstein Fjermestad
ISBN:978-84-693-9441-0/DL:T.62-2011

intramolecular O-H interaction would give. The conf4_II_R_a TS structure leading to the R_{INT} intermediate is thus preferred.

6.9.5 Summary of the enantioselectivity of the BNO assisted CO removal

The enantioselectivity of the BNO assisted CO removal is caused by a discrimination between R and S transition states of both equatorial and axial attacks.

For the equatorial attack, the OH group stabilises transition states leading to the R_{INT} intermediate. This stabilisation, however, is not caused by a tethering mechanism as proposed by Kerr [70], but rather by a hydrogen bond between the OH group and the oxygen of the carbonyl group being attacked. Importantly, the methyl groups play no role in the discrimination between the R TS and the S TS for the equatorial attack.

For the axial attack, on the other hand, the OH and methyl groups play a different role. The attractive C-H$\cdots$O interactions stabilise TS structures where a methoxy group of the BNO is in close proximity of the methyl groups of the R substituent of the alkyne moiety. Because of the different relative orientation of the BNO and the R substituent in R TS and the S TS, the steric repulsions between the methoxy and methyl groups are different in the two TS structures. This difference in the steric repulsion causes the enantiodiscrimination between the two structures. Thus, for the axial attack, the tethering mechanism of Kerr [70] is indeed operative.

The experimental results [70] show that the presence of both the methyl groups as well as the OH group is necessary to achieve a high enantioselctivity. Our computational results are in agreement. For the equatorial attack the OH group stabilises the R transition state. For the axial attack the OH group stabilises both R and S TSs. The methyl groups destabilise the axial S TSs and the axial R TSs are favoured.

6.10 Conclusions

Our calculations explain the mechanism of enantioselection in the BNO activated stoichiometric Pauson-Khand reaction. The interactions between the chiral BNO and the pro-chiral dicobalt complex are responsible for the moderately high ee of this system. The enantiomeric excess of the R_{INT} intermediate in the first step is reduced in the subsequent steps of epimerisation and oxidative metallacycle formation.

The reaction in DME gives the highest enantiomeric excess of the product. This is caused both by a high enantiodiscrimination in the BNO activation step and a negligible epimerisation process.

Our analysis of the enantioselectivity of the system shows that by only improving the enantioselectivity of the BNO activation step, the enantiomeric excess can at most be increased to 90%. An increase in the enantiomeric excess beyond 90% would additionally require an improvement of the enantioselectivity of the oxidative

UNIVERSITAT ROVIRA I VIRGILI
COMPUTACIONAL STUDIES ON THE MECHANISM OF THE PAUSON-KHAND REACTION
Torstein Fjermestad
ISBN:978-84-693-9441-0/DL:T.62-2011

metallacycle formation.

UNIVERSITAT ROVIRA I VIRGILI
COMPUTACIONAL STUDIES ON THE MECHANISM OF THE PAUSON-KHAND REACTION
Torstein Fjermestad
ISBN:978-84-693-9441-0/DL:T.62-2011

Chapter 7

Rh-catalysed Pauson-Khand reaction

In the 1990s, the first publications concerning Pauson-Khand reactions catalysed by metals other than cobalt appeared [124]. The rhodium catalysed Pauson-Khand reaction was first published in 1998 [13], and later, in 2001, the first example of an asymmetric Rh-catalysed Pauson-Khand reaction appeared [14]. In that system, the catalyst $[Rh(CO)_2(S\text{-}BINAP)]^+$ was able to convert an 1,6-enyne to a cyclopentenone through the incorporation of a carbonyl group. The reaction was carried out at 90° C and the products were obtained in high yield with high enantiomeric excess. Later on it was found that a decrease in the external CO pressure made the reaction feasible at room temperature [15, 17, 75]. Additionally, a kinetic study showed a rate dependence of the order of -2 in the CO concentration [125].

The system's ability to induce high enantiomeric excess at room temperature, makes it very interesting for synthetic applications. Our goal is to understand the mechanism of enantioselection in this system, and later on predict the enantiomeric excess in other similar systems. To achieve this goal, a detailed knowledge of the mechanism becomes indispensable.

7.1 A complex mechanistic landscape

A satisfactory mechanistic proposal should explain important experimental observations such as the rate dependence of the order of -2 in the CO concentration [125] as well as the decrease in reaction temperature upon a reduction of CO pressure.

Two CO dissociations from the metal complex occurring previous to the rate-determining TS of the reaction would explain the observed rate dependence. By also computing ΔG_{app} at different external CO pressures, we can check whether a reduced CO pressure leads to a faster reaction.

The catalyst precursor $[Rh(CO)_2(S\text{-}BINAP)]^+$ with the two carbonyls coordinated corresponds to a stable square planar d^8 complex and is likely to be unreactive. We thus assume that the first CO dissociation takes place from the catalyst precursor

UNIVERSITAT ROVIRA I VIRGILI
COMPUTACIONAL STUDIES ON THE MECHANISM OF THE PAUSON-KHAND REACTION
Torstein Fjermestad
ISBN:978-84-693-9441-0/DL:T.62-2011

previous to the coordination of the 1,6-enyne substrate.

The second CO dissociation must occur from some intermediate previous to the rate-determining TS. After the rate-determining TS, a carbonyl must coordinate to the metal complex in order to get incorporated in the final product.

The Magnus mechanism, proposed for the Co-catalysed Pauson-Khand reaction [38], has been used as a working hypothesis in several experimental work on the Rh-catalysed Pauson-Khand reaction [14, 125] (see figure 7.1). Recently, also a compu-

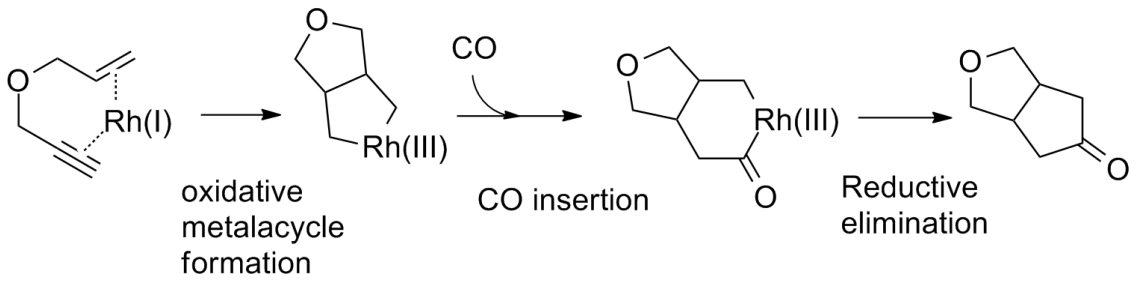

Figure 7.1: The Magnus mechanism for the Rh-Catalysed Pauson-Khand reaction.

tational work considering the Magnus mechanism for a Rh-catalysed Pauson-Khand reaction has appeared [126].

However, a rhodium monometallic complex is very different from a bimetallic cobalt complex, and we cannot exclude the possibility that other mechanisms might be operating in this and other Pauson-Khand systems catalysed by monometallic complexes. Indeed two recent publications on the Ru-catalysed PKR [104] and the Pd-catalysed PKR [127] showed that two alternative mechanisms to the Magnus mechanism were operating for these systems.

The potential relationship of the PKR mechanism to those of skeletal rearrangement processes is intriguing. In the presence of various transition metals, 1,6-enynes are known to follow the mechanism of skeletal rearrangement [128–134] (see figure 7.2). Importantly, the single and double cleavage products, **V** and **IV** respectively, of the

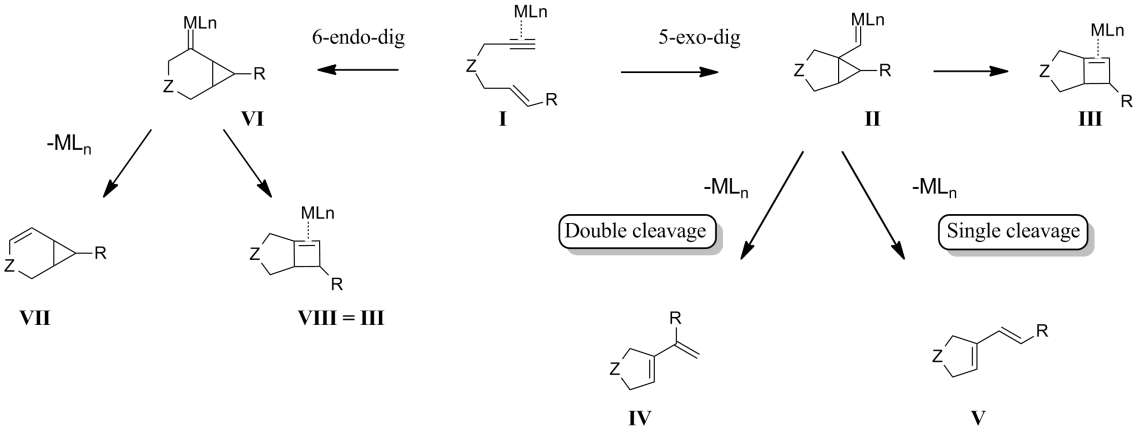

Figure 7.2: Possible skeletal rearrangements.

UNIVERSITAT ROVIRA I VIRGILI
COMPUTACIONAL STUDIES ON THE MECHANISM OF THE PAUSON-KHAND REACTION
Torstein Fjermestad
ISBN:978-84-693-9441-0/DL:T.62-2011

skeletal rearrangement are observed as side products of the Pauson-Khand reaction [15]. This indicates that the cyclopropyl carbene intermediate **II** is accessible under Pauson-Khand conditions. The accessibility of **II** should also imply accessibility of the intermediates **VI**, **I**, and **III**. Structures **VI**, **II** and **III** could be connected to the metallacycle and/or the carbonylated metallacycle intermediates of the Magnus mechanism, and thus to the final Pauson-Khand products. Mechanisms involving intermediates **VI**, **II** and **III** would thus be alternatives to the commonly accepted Magnus mechanism.

The complete mechanistic proposals involving intermediates **VI**, **II** and **III** are shown in figure 7.3. The cyclobutene intermediate **III** could be connected to the

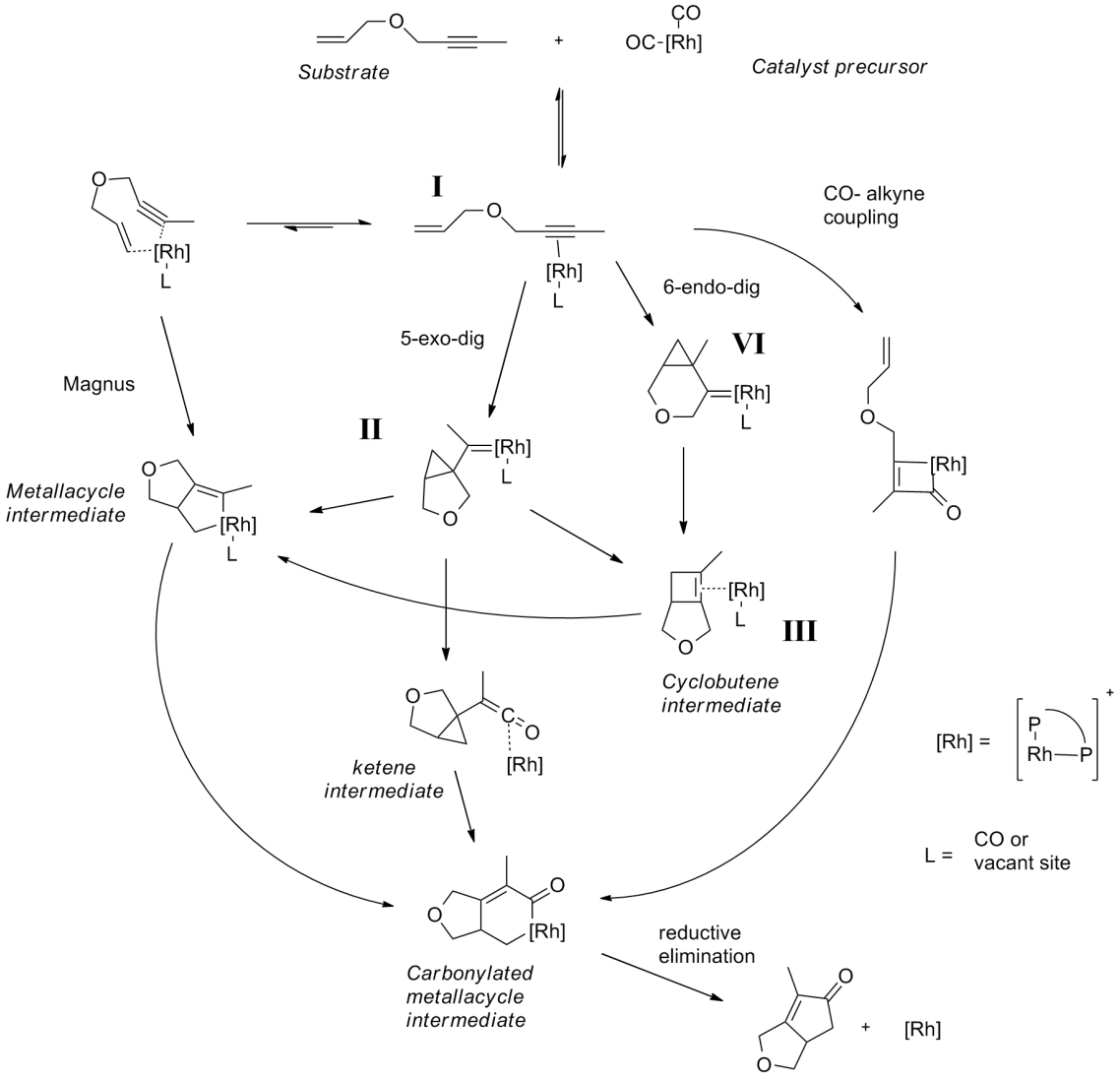

Figure 7.3: Proposed alternative mechanisms for the Rh-catalysed Pauson-Khand reaction.

metallacycle intermediate through an oxidative metallacycle formation. Intermediate **II** could be connected to the metallacycle intermediate through a simultaneous opening of the cyclopropyl ring and formation of a C-Rh bond. Alternatively **II**

UNIVERSITAT ROVIRA I VIRGILI
COMPUTACIONAL STUDIES ON THE MECHANISM OF THE PAUSON-KHAND REACTION
Torstein Fjermestad
ISBN:978-84-693-9441-0/DL:T.62-2011

can be connected to the carbonylated metallacycle through a formation of a ketene intermediate. Intermediate **VI** must first evolve to the cyclobutene intermediate **III** before going over to the metallacycle intermediate.

The ligand L of some intermediates in figure 7.3 symbolises a carbonyl ligand or a vacant site. Previous to the CO insertion, these intermediates can be with or without the carbonyl ligand. CO free intermediates will then represent points on the reaction path where two CO dissociations have taken place. We will test all proposed mechanisms in figure 7.3 computationally and check whether the lowest energy pathway involves two CO dissociations previous to the rate-determining TS.

For the mechanistic proposals described above, we introduce the following labelling system:

- We label the mechanism going through the 5-exo-dig intermediate **II** and the metallacycle as **5-exo-dig** (see figure 7.4). When L = vacant site, we add a * to the label: **5-exo-dig***
- We label the mechanism going through the 5-exo-dig intermediate **II** and the ketene intermediate as **5-exo-dig_ketene** (see figure 7.5).
- We label the mechanism going through intermediate **VI** as **6-endo-dig** (see figure 7.6). When L = vacant site, we add a * to the label: **6-endo-dig***
- We label the Magnus mechanism itself as **Magnus** if the oxidative metallacycle formation occurs with a CO coordinated and **Magnus*** if the oxidative metallacycle formation is CO free.

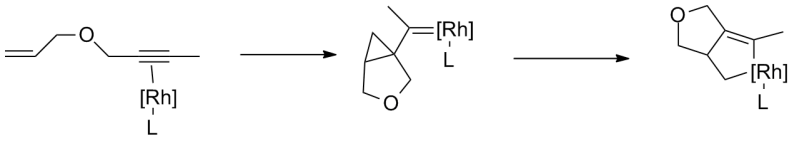

Figure 7.4: Schematic representation of the **5-exo-dig** (L=CO)/ **5-exo-dig*** (L=vacant site) mechanism.

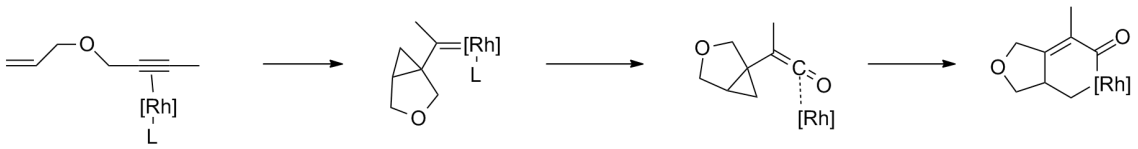

Figure 7.5: Schematic representation of the **5-exo-dig_ketene** mechanism. L=CO.

Figure 7.3 also shows an additional mechanistic alternative. In this mechanism, the carbonyl first reacts with the alkyne group. Thereafter the alkene coordinates to the metal and forms a carbonylated metallacycle through an oxidative C-C coupling. A computational study on this mechanism was published by Wu and co-workers [104] for the Ru-catalysed Pauson-Khand reaction. We label this mechanism **CO-alkyne** indicating that there is a coupling between the CO and the alkyne in the first step. Figure 7.7 shows a schematic representation.

UNIVERSITAT ROVIRA I VIRGILI
COMPUTACIONAL STUDIES ON THE MECHANISM OF THE PAUSON-KHAND REACTION
Torstein Fjermestad
ISBN:978-84-693-9441-0/DL:T.62-2011

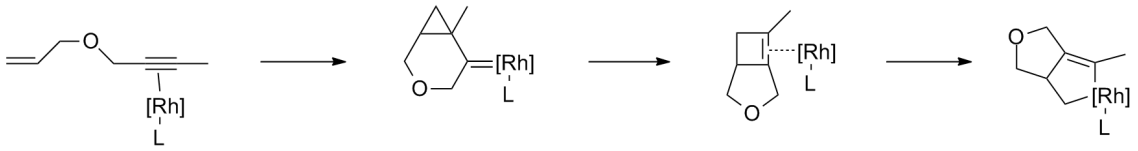

Figure 7.6: Schematic representation of the **6-endo-dig** (L=CO)/**6-endo-dig** (L=vacant site) mechanism.

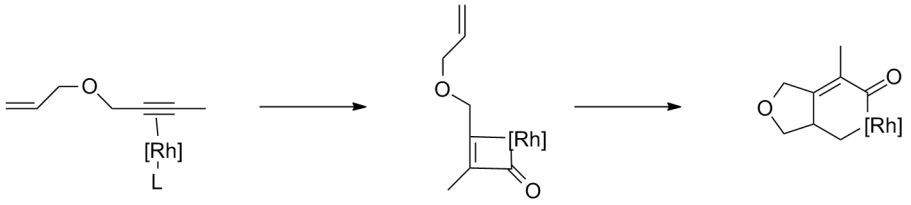

Figure 7.7: Schematic representation of the **CO-alkyne** mechanism. L=CO.

7.2 Computational details

The energy evaluations were done with the ONIOM(B3LYP:UFF) method. The basis set for the non-metal atoms was 6-31G(d) [106]. For the Rh atom the core electrons were substituted by the Los Alamos LANL2DZ effective core potential and the associated double zeta basis set was used for the valence electrons [107]. The partition of the molecule in QM and MM regions was chosen such that the binaphtyl and the phenyls of the BINAP were put in the MM region. The rest of the metal complex and all of the substrate were put in the QM region. See figure 7.8 for a schematic representation.

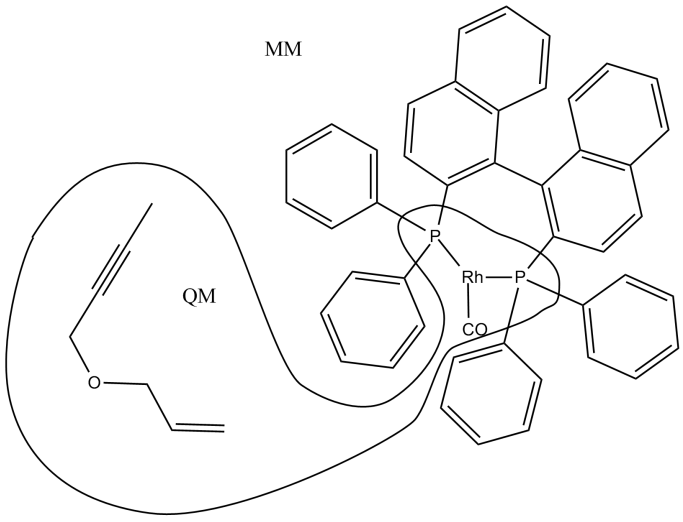

Figure 7.8: QM/MM partition of the Rh-catalyst and the substrate.

Figure 7.3 shows that there is competition between mechanisms with one CO coordinated and mechanisms with no CO coordinated. The CO concentration is held constant by the external CO pressure. Furthermore the solubility of CO in organic

UNIVERSITAT ROVIRA I VIRGILI
COMPUTACIONAL STUDIES ON THE MECHANISM OF THE PAUSON-KHAND REACTION
Torstein Fjermestad
ISBN:978-84-693-9441-0/DL:T.62-2011

unpolar solvents is generally low [135, 136]. The equilibrium between CO coordinated and CO dissociated should thus largely be shifted towards dissociated CO. To quantitatively compare the transition states with CO coordinated and CO dissociated, we use the apparent Gibbs free energy, ΔG_{app}, introduced in subsection 3.2.4. For the calculation of $\Delta G_{\mathrm{CO},corr}$ we used the SMD solvent model [108], THF was used as solvent. Apart from the CO concentration effect, solvent corrections were excluded from the calculations.

7.3 Free energy profiles

The free substrate and the catalyst precursor $[\mathrm{Rh(CO)_2(S\text{-}BINAP)}]^+$ are chosen as zero level of the energy scale. We present free energy profiles for the following mechanisms: **Magnus**, **Magnus***, **5-exo-dig**, **5-exo-dig***, **5-exo-dig_ketene**, **6-endo-dig**, **6-endo-dig*** and **CO-alkyne**.

Free energy values are reported in kJ/mol. The free energy profiles with all species at standard state concentrations, ΔG°, are reported first. Afterwards, the apparent Gibbs free energies, ΔG_{app}, at 1.0 atm. and 0.1 atm. of external CO pressure will be reported.

7.3.1 Free energy of solvation of CO in THF

To compute ΔG_{app}, we need $\Delta G_{\mathrm{CO},corr}$ as shown in equation (3.19). Equation (3.22) shows that $\Delta G_{\mathrm{CO},corr}$ has two contributions: $\Delta G^\circ_{\mathrm{CO},corr}$ of converting 1M of CO(g) to 1M of CO(solv), and the correction $RT\ln(24.5)$ for the conversion from a standard state of 1 atm. to a standard state of 1M. $\Delta G^\circ_{\mathrm{CO},corr}$ of CO in THF is 11 kJ/mol. The standard state correction is 8 kJ/mol. The standard Gibbs free energy, $\Delta G_{\mathrm{CO},corr}$, is thus 19 kJ/mol.

7.3.2 The Magnus Mechanism

According to the Magnus mechanism, an intermediate is formed where the alkyne and the alkene groups of the substrate both coordinate to the rhodium centre. From this intermediate an oxidative metallacycle formation takes place. Because the Magnus mechanism merges with **5-exo-dig** and **6-endo-dig** at the metallacycle intermediate, we present the free energy profile only for the oxidative metallacycle formation (see figure 7.9). The profiles of both **Magnus**, and **Magnus*** are discussed.

CO coordinated (L=CO), Magnus

We started off our search for possible transition state structures of the oxidative metallacycle formation by testing possible permutations of the alkene, the alkyne and the carbonyl in the coordination sphere of the rhodium atom. In the interest of time, we first screened these permutations in a simplified model system. In this

UNIVERSITAT ROVIRA I VIRGILI
COMPUTACIONAL STUDIES ON THE MECHANISM OF THE PAUSON-KHAND REACTION
Torstein Fjermestad
ISBN:978-84-693-9441-0/DL:T.62-2011

Figure 7.9: Schematic representation of the oxidative metallacycle formation of the Magnus mechanism. L=CO for the **Magnus** mechanism and L = vacant site for the **Magnus*** mechanism.

model system, the enyne substrate is modelled by an ethyne and an ethene, and the BINAP ligand is modelled by removing its binaphtyl backbone and its phenyl groups. By taking care not to overcount redundant permutations, we arrive at the total number of ten possible permutations of the ethyne, ethene and carbonyl in the coordination sphere of the rhodium atom. Figure 7.10 shows a schematic representation of the ten transition state geometries corresponding to the permutations, together with their potential energy. We have labelled each of them *mer* or *fac* indicating whether the phosphorus atoms and the carbonyl ligand are arranged in a *mer* or a *fac* configuration. Already at the level of this model, a trend can be seen: The TSs with the *fac* configuration are highly preferred over the TSs with the *mer* configuration. Because of this high preference for TSs with the *fac* configuration, TSs with the *mer* configuration were discarded as viable transition states of the oxidative metallacycle formation.

In the next step in our search for transition states, we expanded the model to include the full BINAP ligand. We then reoptimised the TS structures corresponding to the *fac* configuration. The two most stable of these had the ethyne and ethene in the same plane as the phosphorus atoms and the rhodium atom. The adoption of these geometries is presumably due to the avoidance of steric repulsion with the BINAP ligand. We expanded these two geometries to the real system by adding the linker between the ethyne and ethene as well as adding the methyl group of the ethyne. We managed to optimise one of these transition states and we labelled it TS_A. For the purpose of comparison, we also expanded the most stable *mer* transition state to the real system. This transition state we label TS_B. The free energies of TS_A and TS_B are 173 kJ/mol and 205 kJ/mol respectively.

TS_A was connected to the two adjacent minima, ADD3 of 138 kJ/mol and INT_A of 66 kJ/mol. The free energy profile of this step is shown in figure 7.11. A striking feature about the free energy profile, is the high instability of ADD3 relative to the common zero level. The barrier of the oxidative metallacycle formation, the difference between TS_A and ADD3, is only 35 kJ/mol. However, ADD3 is already 138 kJ/mol above the zero level. The high energy of ADD3 seems to be due to both steric crowding as well as the disfavoured presence of five ligands in the coordination sphere of the d^8 complex.

UNIVERSITAT ROVIRA I VIRGILI
COMPUTACIONAL STUDIES ON THE MECHANISM OF THE PAUSON-KHAND REACTION
Torstein Fjermestad
ISBN:978-84-693-9441-0/DL:T.62-2011

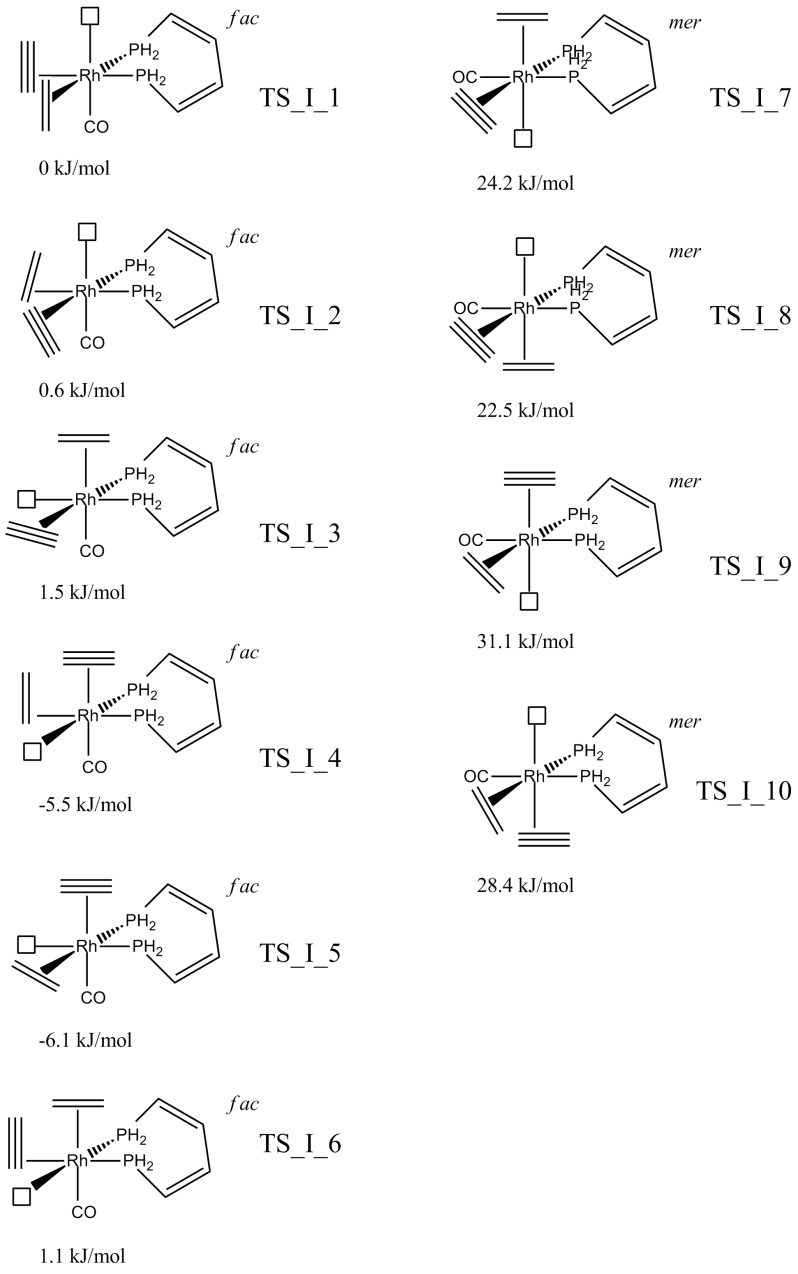

Figure 7.10: Schematic representation of the ten optimised TS structures of the oxidative metallacycle formation. Potential energies in kJ/mol.

UNIVERSITAT ROVIRA I VIRGILI
COMPUTACIONAL STUDIES ON THE MECHANISM OF THE PAUSON-KHAND REACTION
Torstein Fjermestad
ISBN:978-84-693-9441-0/DL:T.62-2011

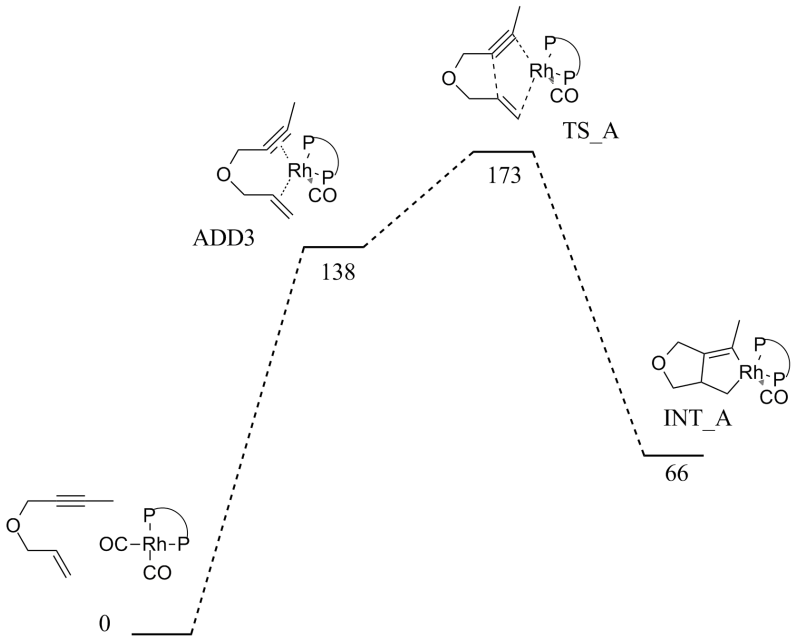

Figure 7.11: Free energy profile (ΔG°, kJ/mol) of the oxidative metallacycle formation step of the **Magnus** mechanism.

CO dissociated (L=vacant site), Magnus*

With the two carbonyls dissociated, the transition state of the oxidative metallacycle formation adopts a square planar geometry. This transition state, TS_A*, has a free energy, ΔG° of 171 kJ/mol. This is a decrease of 2 kJ/mol compared to TS_A. The increase in energy caused by the breaking of the metal-carbonyl bond is thus compensated by an adoption of a more stable configuration of the metal complex. TS_A* was then connected to the two adjacent intermediates, adduct ADD3* (84 kJ/mol) and INT_A* (108 kJ/mol) corresponding to ADD3 and INT_A respectively. The free energy profile of the oxidative metallacycle formation for the **Magnus*** mechanism (see figure 7.12) is qualitatively different from the corresponding step of the **Magnus** mechanism. ADD3* is 54 kJ/mol more stable than ADD3. Conversely, INT_A* is 42 kJ/mol less stable than INT_A. ADD3* is a 16e complex with the d^8 electron configuration, and it adopts the square planar geometry. This is associated with a low energy. INT_A* has an electron count of 14 which is associated with a high energy structure.

7.3.3 The 5-exo-dig mechanism

The next mechanisms we are going to discuss start with a reactant adduct where the 1,6-enyne coordinates only with its alkyne group to the metal complex. This coordination mode differs from that of the Magnus mechanism. In the 5-exo-dig mechanism, a 5-membered ring is formed through a nucleophilic attack of the alkyne by the alkene. The triple bond being broken is located outside the ring being formed. Figure 7.13 shows this mechanism schematically.

UNIVERSITAT ROVIRA I VIRGILI
COMPUTACIONAL STUDIES ON THE MECHANISM OF THE PAUSON-KHAND REACTION
Torstein Fjermestad
ISBN:978-84-693-9441-0/DL:T.62-2011

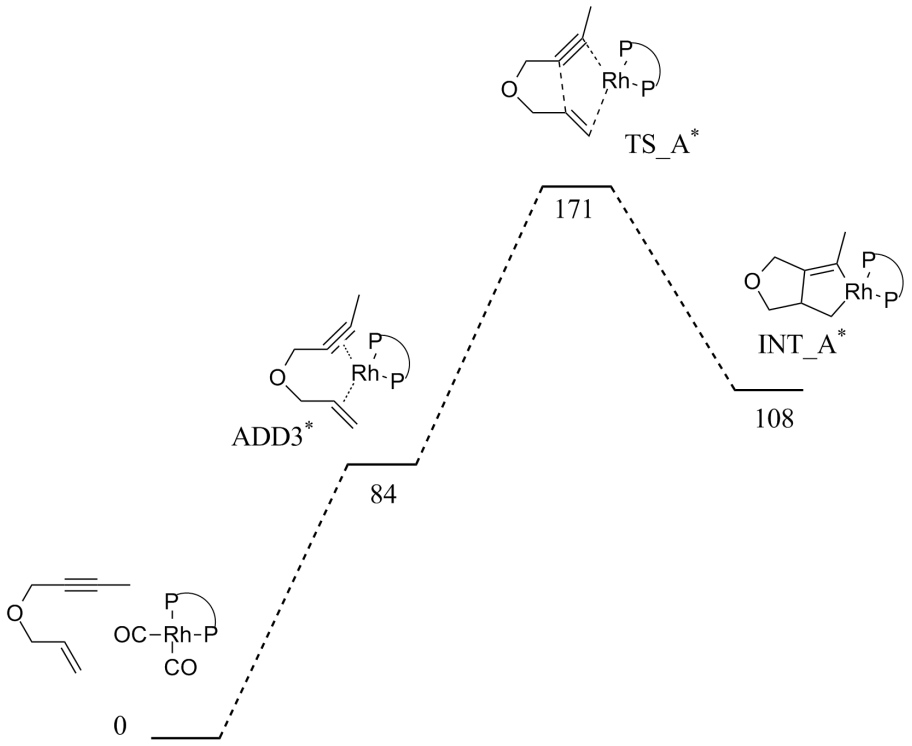

Figure 7.12: Free energy profile ($\Delta G°$, kJ/mol) of the oxidative metallacycle formation step of the **Magnus*** mechanism.

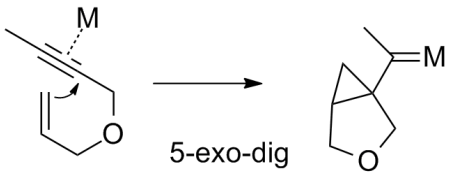

Figure 7.13: 5-exo-dig mechanism. Nucleophilic attack of the alkyne by the alkene. The triple bond being broken is located outside the 5-membered ring being formed.

UNIVERSITAT ROVIRA I VIRGILI
COMPUTACIONAL STUDIES ON THE MECHANISM OF THE PAUSON-KHAND REACTION
Torstein Fjermestad
ISBN:978-84-693-9441-0/DL:T.62-2011

CO coordinated, 5-exo-dig

With CO coordinated (L=CO in figure 7.4), the reactant adduct complex adopts a square planar geometry. The alkene group then attacks the alkyne group from the position *trans* to the rhodium atom. The reaction then goes over TS1 (104 kJ/mol) further to INT1 (4 kJ/mol), a cyclopropyl carbene intermediate. INT1 has the cyclopropyl group *trans* to the rhodium atom. In order for the metallacycle intermediate to form, INT1 must first isomerise over TS2 (52 kJ/mol) to INT2 (10 kJ/mol) with the cyclopropyl group being *cis* to the rhodium atom. From INT2 the reaction proceeds to the metallacycle (INT3 = 54 kJ/mol) over TS3 (127 kJ/mol).

Figure 7.14 shows the free energy profile of the 5-exo-dig mechanism from the reactant adduct to the metallacycle intermediate. From this profile we identify the transition state of the metallacycle formation, TS3, as the rate-determining transition state.

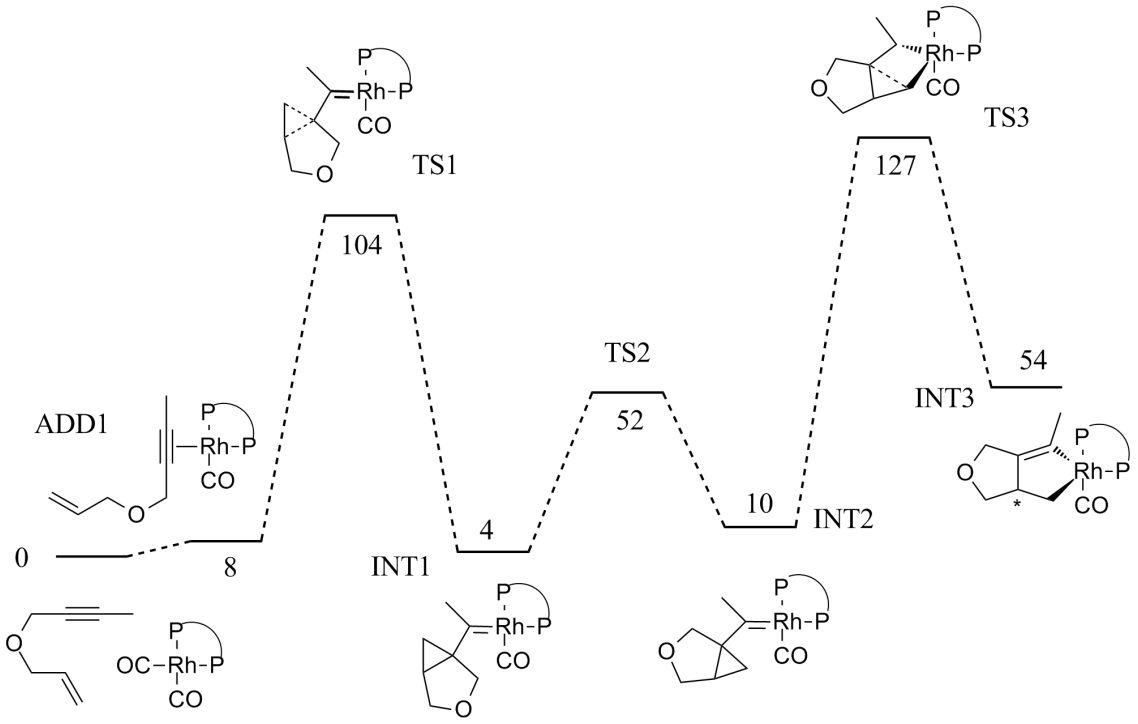

Figure 7.14: Free energy profile (ΔG°, kJ/mol) of the **5-exo-dig** mechanism.

CO dissociated, 5-exo-dig*

To investigate what effect the carbonyl ligand would have on the energy profile of the 5-exo-dig mechanism, we reoptimised the TSs and intermediates along the path with the carbonyl ligand removed (L = vacant site in figure 7.4). The removal of the carbonyl group leads to significant changes in the reaction profile (See figure 7.15). We now discuss how the energy of the intermediates and transition states is changed compared to the corresponding structures with CO coordinated. ADD2 is destabilised by 56 kJ/mol relative to ADD1, TS4 is destabilised by 95 kJ/mol relative

UNIVERSITAT ROVIRA I VIRGILI
COMPUTACIONAL STUDIES ON THE MECHANISM OF THE PAUSON-KHAND REACTION
Torstein Fjermestad
ISBN:978-84-693-9441-0/DL:T.62-2011

to TS1, INT4 is destabilised by 103 kJ/mol relative to INT1, TS4* is destabilised by 70 kJ/mol relative to TS2, INT5 is destabilised by 100 kJ/mol relative to INT2, TS5 is destabilised by 18 kJ/mol relative to TS3 and INT6 is destabilised by 73 kJ/mol relative to INT3.

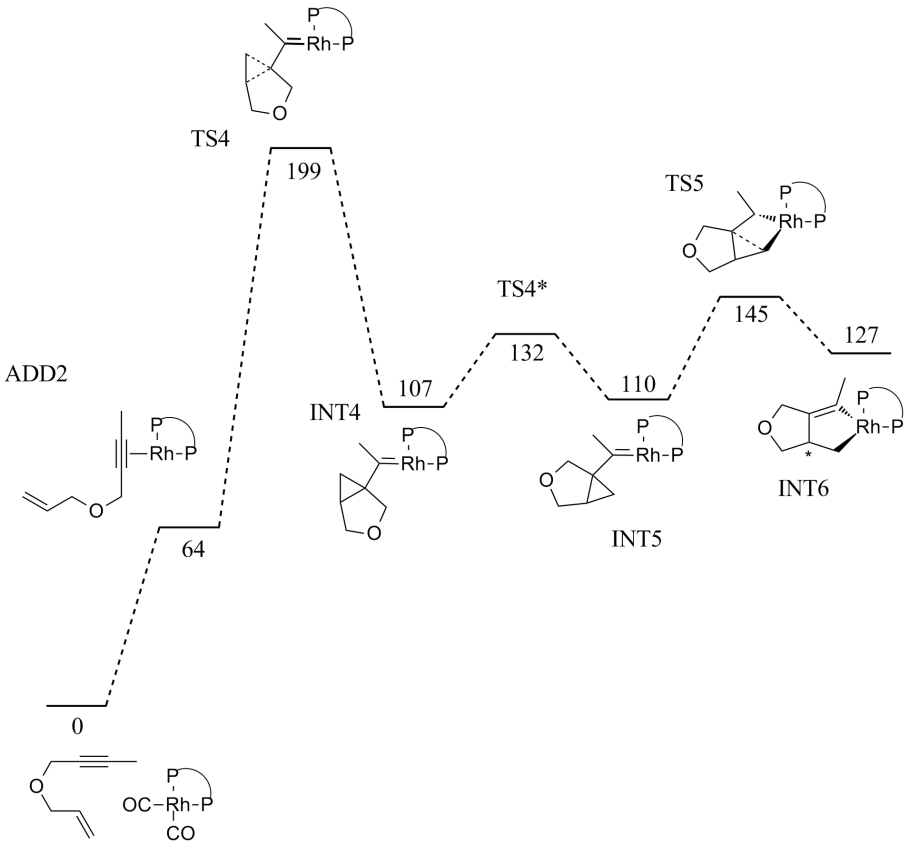

Figure 7.15: Free energy profile ($\Delta G°$, kJ/mol) of the **5-exo-dig*** mechanism.

As expected, the dissociation of the carbonyl leads to a destabilisation along the whole pathway. But, interestingly, the destabilisation varies significantly between the different intermediates and TSs of the profile. We observe the largest destabilisation for the two carbene intermediates INT4 (103 kJ/mol) and INT5 (100 kJ/mol) as well as for TS4 of the 5-exo-dig carbene formation (95 kJ/mol). This contrasts the small destabilisation for TS5 (18 kJ/mol). In the case of the carbene structures, the CO dissociation leads to an unstable 14e complex. Furthermore the carbene structures are not able to adjust their geometries by letting groups coordinate to the vacant site generated. In the case of TS5, on the other hand, the CO dissociation facilitates the metallacycle formation by generating a vacant site where the new C-Rh bond can be formed.

7.3.4 The 6-endo-dig mechanism

The 6-endo-dig mechanism is another example of a ring-closure mechanism. Likewise as for the 5-exo-dig mechanism, the alkyne is attacked nucleophilically by the alkene.

UNIVERSITAT ROVIRA I VIRGILI
COMPUTACIONAL STUDIES ON THE MECHANISM OF THE PAUSON-KHAND REACTION
Torstein Fjermestad
ISBN:978-84-693-9441-0/DL:T.62-2011

However, in this case a 6-membered ring is formed, and the triple bond being broken during the formation is located inside the ring (see figure 7.16).

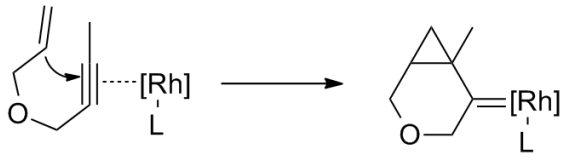

Figure 7.16: Ring formation of the 6-endo-dig mechanism. The triple bond being broken is located inside the ring. L = CO (**6-endo-dig**)/ L = vacant site (**6-endo-dig***).

CO coordinated, 6-endo-dig

With the carbonyl ligand coordinated (L=CO in figure 7.6), the metal complex adopts a square planar geometry. The alkene attacks the alkyne from the position *trans* to the rhodium atom. From ADD1 the reaction goes over TS6 (85 kJ/mol) towards INT7 (-4 kJ/mol), a cyclopropyl carbene intermediate. The reaction proceeds further over TS7 (89 kJ/mol) to INT8 (12 kJ/mol), a cyclobutene intermediate. From INT8 the reaction passes TS8 (135 kJ/mol) and goes on to form the metallacycle intermediate (INT9, 49 kJ/mol). Figure 7.17 shows the free energy profile of the 6-endo-dig mechanism from the reactant adduct to the metallacycle intermediate. We identify TS8 of the metallacycle formation as the rate-limiting transition state of this reaction.

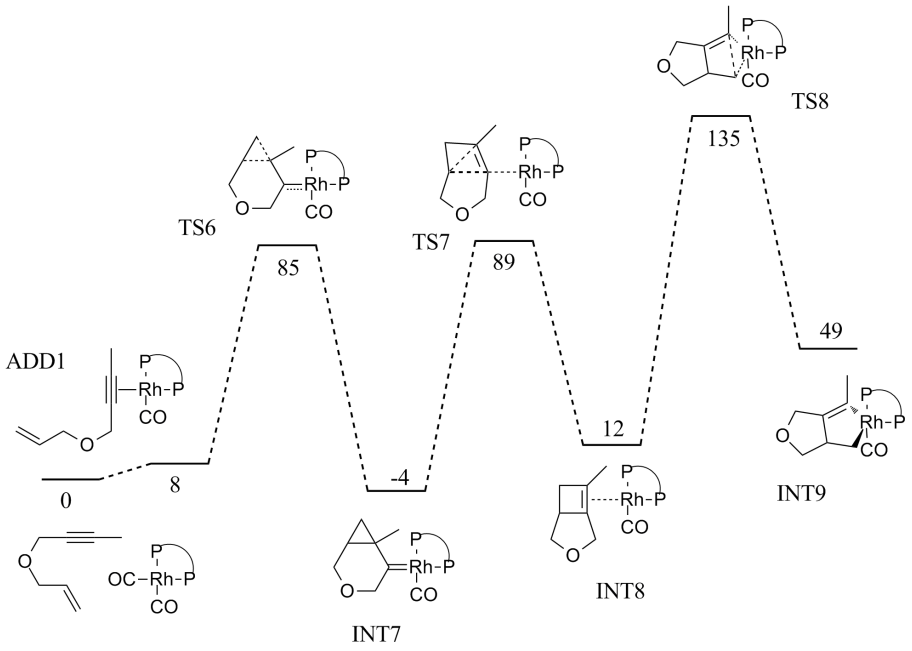

Figure 7.17: Free energy profile ($\Delta G°$, kJ/mol) of the **6-endo-dig** mechanism.

UNIVERSITAT ROVIRA I VIRGILI
COMPUTACIONAL STUDIES ON THE MECHANISM OF THE PAUSON-KHAND REACTION
Torstein Fjermestad
ISBN:978-84-693-9441-0/DL:T.62-2011

CO dissociated, 6-endo-dig*

To investigate the influence the carbonyl ligand has on the energy profile of the 6-endo-dig mechanism, we located transition state TS9 corresponding to TS8 of the **6-endo-dig** mechanism, but with the carbonyl dissociated. Subsequently we connected TS9 to the two adjacent intermediates. The resulting energy profile is presented in figure 7.18. The cyclobutene intermediate (INT10) has an energy of 69 kJ/mol, TS9 has an energy of 179 kJ/mol and the metallacycle intermediate (INT11) has an energy of 108 kJ/mol. Compared to the **6-endo-dig** mechanism, we see an approximately constant upward shift of the energies of this step. This increase in energies is due to the rhodium-carbonyl binding energy which must be overcome for the dissociation to take place. Because of the high energy of TS9, we did not compute the energy of the structures between INT10 and the reactant adduct.

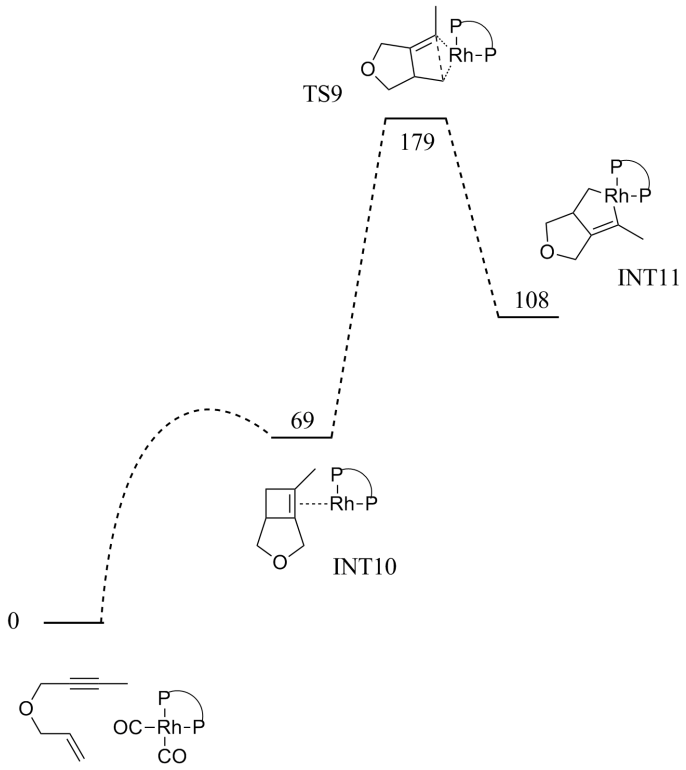

Figure 7.18: Free energy profile (ΔG°, kJ/mol) of the metallacycle formation step of the **6-endo-dig*** mechanism.

7.3.5 The 5-exo-dig_ketene mechanism

All of the mechanisms disscussed so far go through the metallacycle intermediate. The next two mechanisms by-pass this intermediate and go directly to the carbonylated metallacycle of the Magnus mechanism (see figure 7.3). The first two steps of the **5-exo-dig_ketene** mechanism are mechanistically similar to the corresponding steps of the **5-exo-dig** mechanism. The first step is a nucleophilic 5-exo-dig attack

UNIVERSITAT ROVIRA I VIRGILI
COMPUTACIONAL STUDIES ON THE MECHANISM OF THE PAUSON-KHAND REACTION
Torstein Fjermestad
ISBN:978-84-693-9441-0/DL:T.62-2011

from ADD1_B (23 kJ/mol) over TS1_B (101 kJ/mol) to INT1_B (5 kJ/mol). The second step is an isomerisation where the cyclopropyl goes from being *trans* to the rhodium to being *cis* to the rhodium. The isomerisation goes from INT1_B over TS2_B (73 kJ/mol) to INT2_B (13 kJ/mol). The difference between the two mechanisms, **5-exo-dig** and **5-exo-dig_ketene**, in the two first steps, is a 180° rotation of the substrate fragment around the Rh-carbene bond. This leads to slightly different energies of the intermediates and transition states of these two first steps.

After the *cis* carbene intermediate (INT2_B), the CO ligand inserts into the metal carbene bond and a ketene intermediate (INT12, 52 kJ/mol) is formed. From this ketene intermediate, the reaction evolves further to the carbonylated metallacycle. Figure 7.19 shows a schematic representation of the mechanism and figure 7.20 shows the free energy profile. From the free energy profile, we identify TS10 (133 kJ/mol) of the CO insertion into the metal carbene bond as the rate-determining transition state.

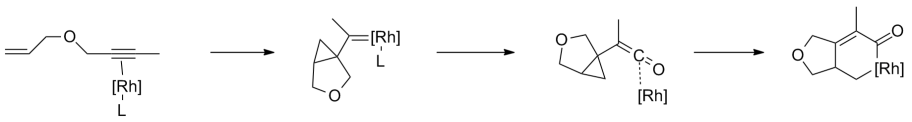

Figure 7.19: The **5-exo-dig_ketene** mechanism. L = CO.

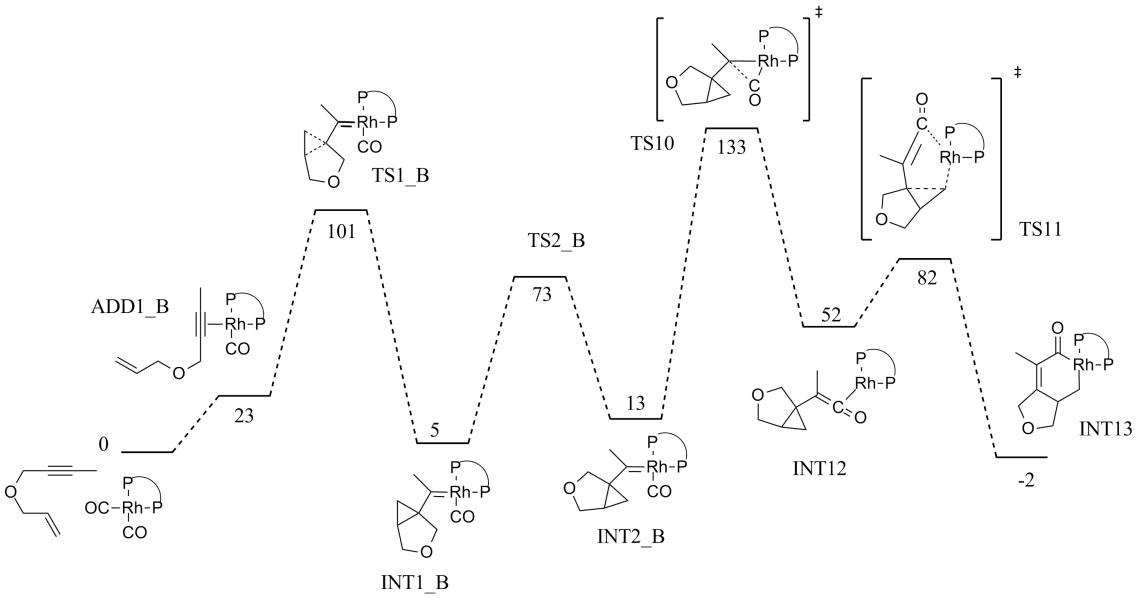

Figure 7.20: Free energy profile ($\Delta G°$, kJ/mol) of the **5-exo-dig_ketene** mechanism.

Because this mechanism involves a CO insertion in the step of the rate-determining transition state, a second CO dissociation previous to the rate-determing transition state becomes impossible.

UNIVERSITAT ROVIRA I VIRGILI
COMPUTACIONAL STUDIES ON THE MECHANISM OF THE PAUSON-KHAND REACTION
Torstein Fjermestad
ISBN:978-84-693-9441-0/DL:T.62-2011

7.3.6 The CO-alkyne mechanism

The last mechanism we discuss, is the coupling between CO and the alkyne group of the substrate [104]. Figure 7.21 shows a schematic representation.

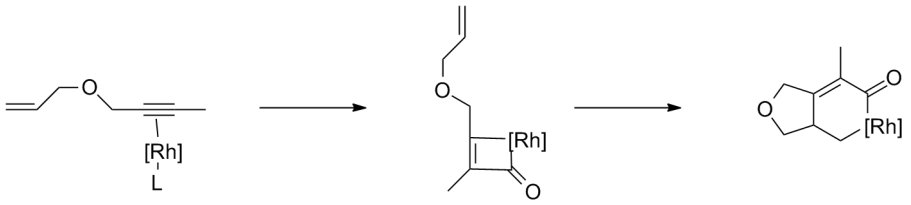

Figure 7.21: Schematic representation of the **CO-alkyne** mechanism. L = CO.

From the reactant adduct (ADD1 = 8 kJ/mol), there is a coupling between the carbonyl and the alkyne and a high-energetic 4-membered intermediate is formed (INT14 = 86 kJ/mol). Subsequently the alkene coordinates to the rhodium atom (INT15 = 92 kJ/mol), and a coupling between the alkene and alkyne leads to the formation of a carbonylated metallacycle (INT13 = -2 kJ/mol). The free energy profile is shown in figure 7.22. From the free energy profile, we identify TS12 (123 kJ/mol) of the CO coupling with the alkyne as the rate-determining transition state.

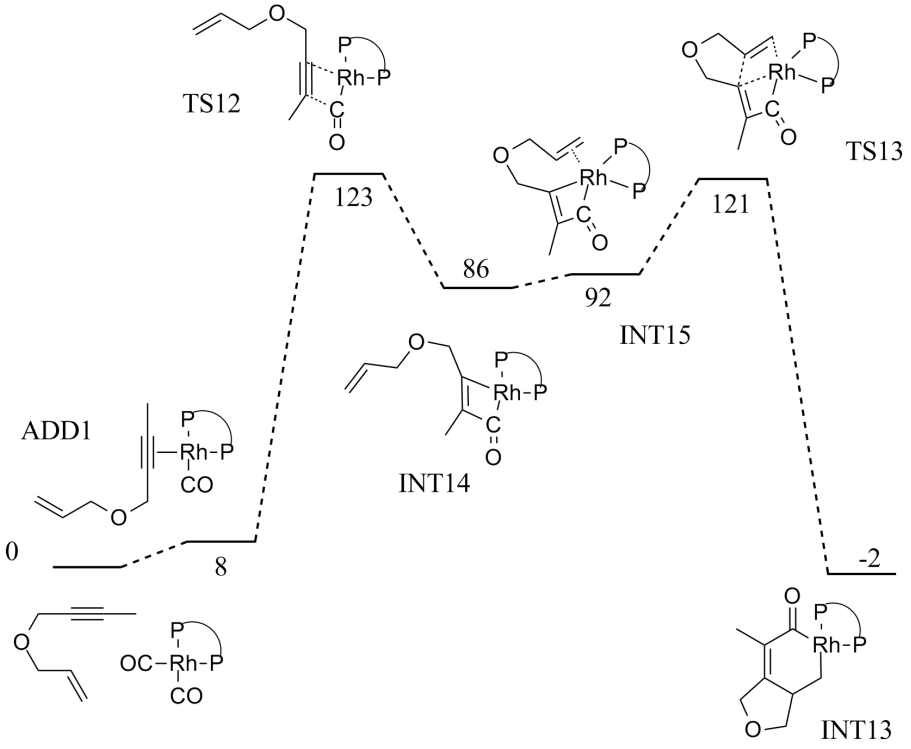

Figure 7.22: Free energy profile (ΔG°, kJ/mol) of the **CO-alkyne** mechanism.

UNIVERSITAT ROVIRA I VIRGILI
COMPUTACIONAL STUDIES ON THE MECHANISM OF THE PAUSON-KHAND REACTION
Torstein Fjermestad
ISBN:978-84-693-9441-0/DL:T.62-2011

7.4 ΔG_{app} at 1.0 atm. and 0.1 atm.

Based on the ΔG° profiles above, the pathways with the CO dissociated are disfavoured. This is mainly due to the rhodium-carbonyl binding energy that must be overcome for the dissociation to take place. However, taking into account the low concentration of CO in solution, the dissociation/association equilibrium of CO should be shifted towards carbonyl dissociation. Following the procedure described in subsection 3.2.4 we compute ΔG_{app} at an external CO pressure of 1.0 atm. and 0.1 atm., two of the pressures employed in the experiment by Jeong and co-workers [17].

As derived in subsection 3.2.4, ΔG_{app} is dependent on the external CO pressure, the solvation energy of CO, $\Delta G_{\mathrm{CO},corr}$, and the number of CO ligands being dissociated. In the following, we present ΔG_{app} at an external CO pressure of 1.0 atm. and 0.1 atm.

For the transition states and intermediates involving one CO dissociation relative to the catalyst precursor $[Rh(CO)_2BINAP]^+$, we employ equation (3.14). At 1.0 atm. this results in a ΔG_{app} 19 kJ/mol lower than ΔG°. At 0.1 atm. ΔG_{app} is 25 kJ/mol lower than ΔG°

For the transition states and intermediates involving two CO dissociations relative to catalyst precursor $[Rh(CO)_2BINAP]^+$, we employ equation (3.18). This results in a ΔG_{app} being 38 kJ/mol below ΔG° at 1.0 atm. and 50 kJ/mol below ΔG° at 0.1 atm.

Compared to ΔG° presented in the previous section, ΔG_{app} is lowered for structures with carbonyls dissociated. This lowering of ΔG_{app} may in some cases more than compensate for the increase in ΔG° due to the CO dissociation. In the next few sections we will analyse how the ΔG_{app} profiles differ from the ΔG° profiles for each of the mechanisms studied.

7.4.1 The Magnus mechanism

We have computed the Magnus mechanism with one and two carbonyls dissociated. We present the ΔG_{app} profile for the two cases separately.

One carbonyl dissociated

Figure 7.23 shows the profile of ΔG° as well as the ΔG_{app} profiles at an external CO pressure of 1.0 atm. and 0.1 atm. ΔG_{app} of TS_A is 154 kJ/mol at 1.0 atm and 148 kJ/mol at 0.1 atm.

Two carbonyls dissociated

With two carbonyls dissociated ΔG_{app} of the rate-determining TS of the **Magnus*** mechanism is 133 kJ/mol at 1 atm. of external CO pressure and 121 kJ/mol at an

UNIVERSITAT ROVIRA I VIRGILI
COMPUTACIONAL STUDIES ON THE MECHANISM OF THE PAUSON-KHAND REACTION
Torstein Fjermestad
ISBN:978-84-693-9441-0/DL:T.62-2011

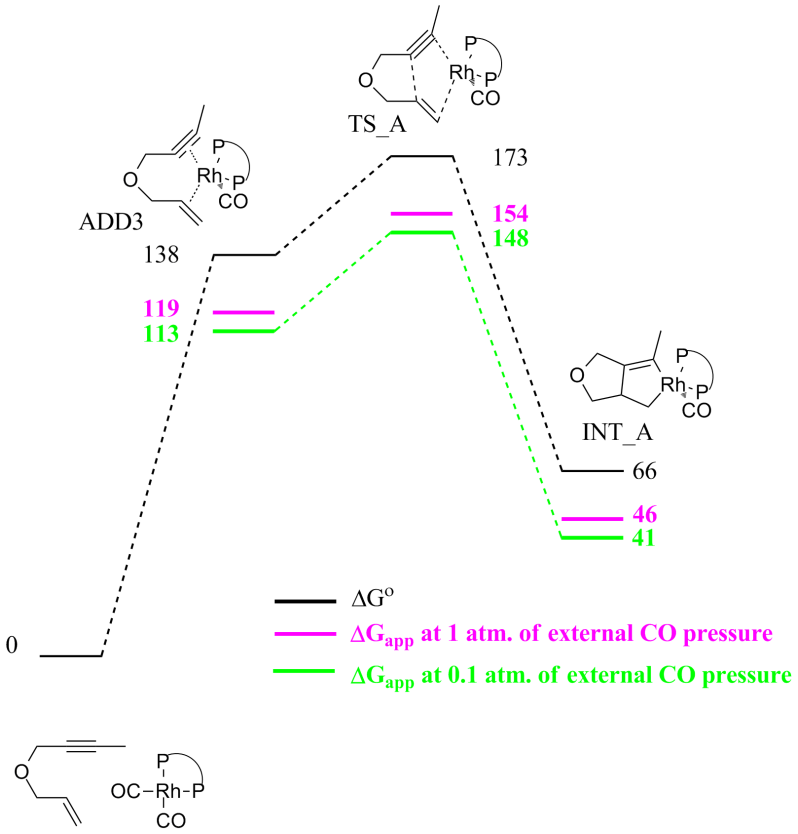

Figure 7.23: Free energy profiles (kJ/mol) of ΔG° and ΔG_{app} at CO pressures of 1.0 atm. and 0.1 atm. of the oxidative metallacycle formation step of the **Magnus** mechanism.

UNIVERSITAT ROVIRA I VIRGILI
COMPUTACIONAL STUDIES ON THE MECHANISM OF THE PAUSON-KHAND REACTION
Torstein Fjermestad
ISBN:978-84-693-9441-0/DL:T.62-2011

external CO pressure of 0.1 atm.

7.4.2 The 5-exo-dig mechanism

ΔG_{app} profiles for the 5-exo-dig mechanism with one (**5-exo-dig**) and two (**5-exo-dig***) carbonyls dissociated are presented below.

One carbonyl dissociated, 5-exo-dig

Figure 7.24 shows the energy profiles of the **5-exo-dig** mechanism. For the rate-

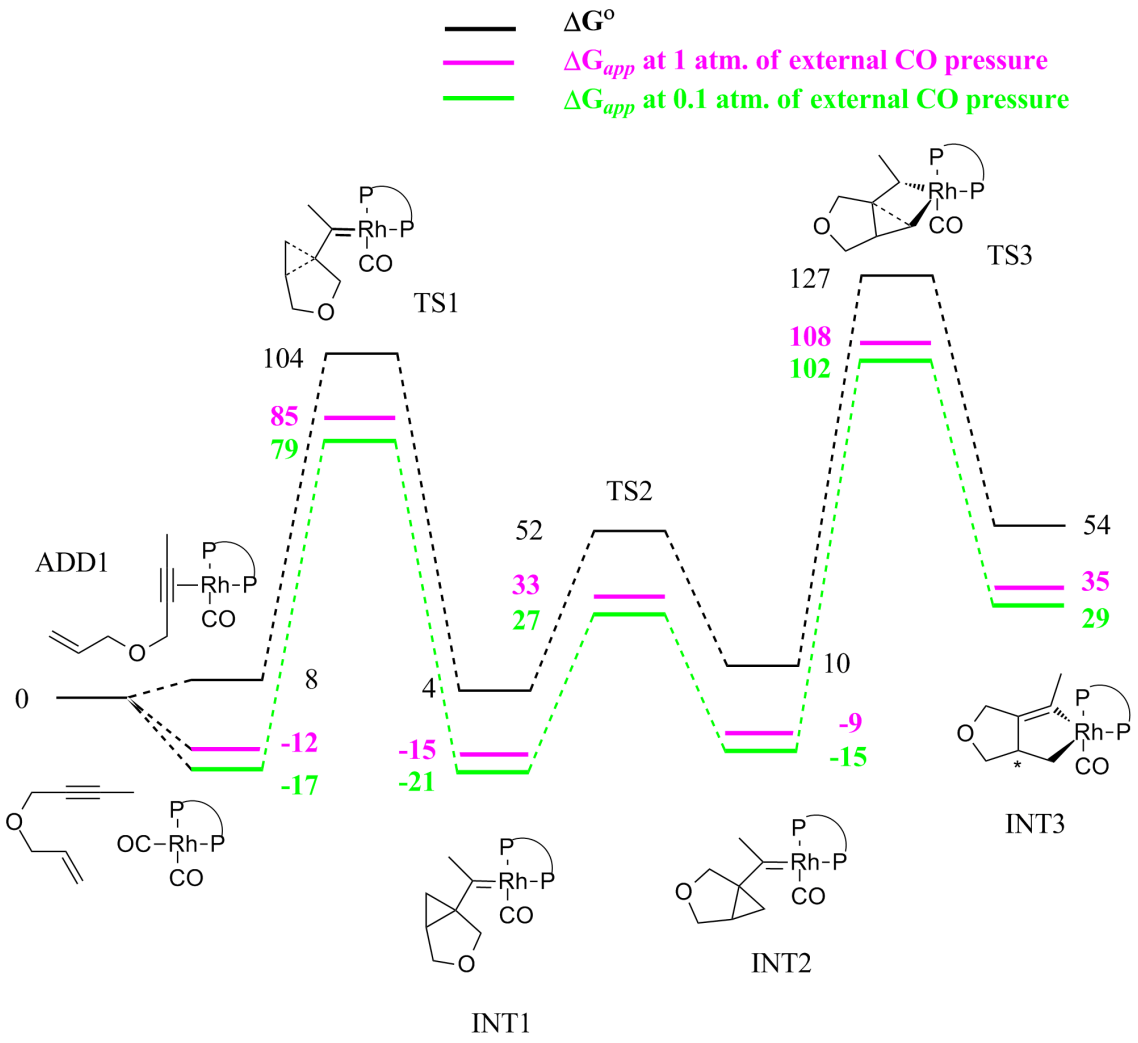

Figure 7.24: Free energy profiles (kJ/mol) of $\Delta G°$ and ΔG_{app} at CO pressures of 1.0 atm. and 0.1 atm. for the **5-exo-dig** mechanism.

determining transition state, TS3, $\Delta G°$ is 127 kJ/mol, ΔG_{app} is 108 kJ/mol at 1.0 atm. and 102 kJ/mol at 0.1 atm.

UNIVERSITAT ROVIRA I VIRGILI
COMPUTACIONAL STUDIES ON THE MECHANISM OF THE PAUSON-KHAND REACTION
Torstein Fjermestad
ISBN:978-84-693-9441-0/DL:T.62-2011

Two carbonyls dissociated, 5-exo-dig*

Figure 7.25 shows the free energy profiles of the **5-exo-dig*** mechanism. For the rate-determining transition state, TS4, ΔG° is 199 kJ/mol, ΔG_{app} is 161 kJ/mol at an external CO pressure of 1.0 atm. and 149 kJ/mol at an external CO pressure of 0.1 atm.

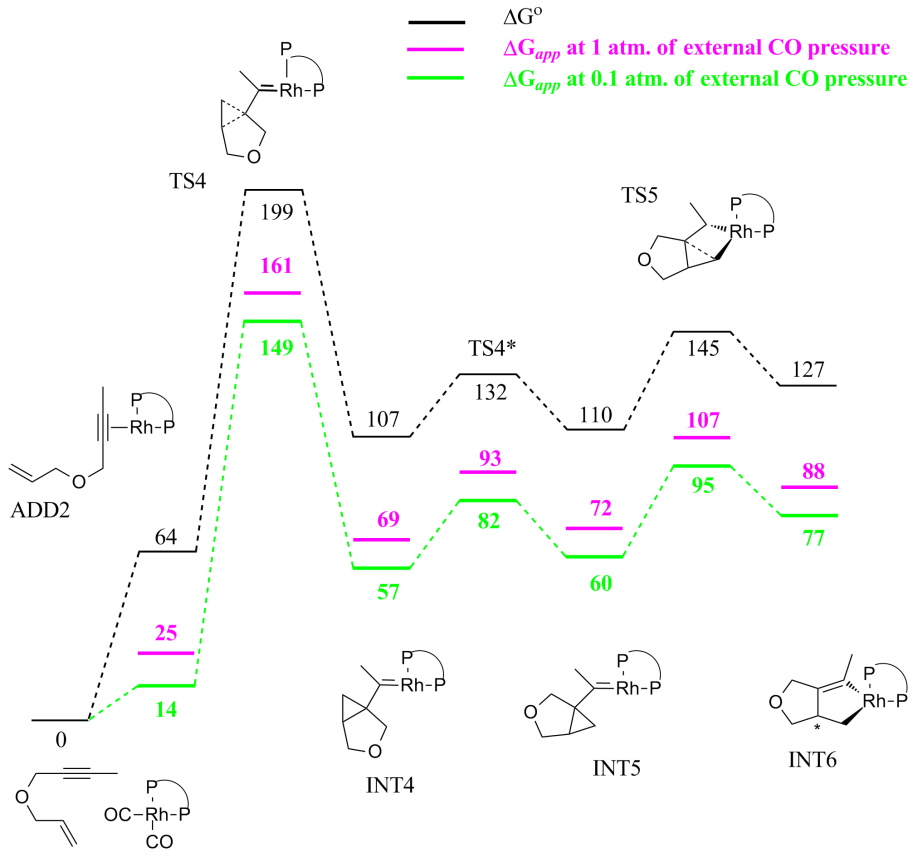

Figure 7.25: Free energy profiles (kJ/mol) of ΔG° and ΔG_{app} at CO pressures of 1.0 atm. and 0.1 atm. for the **5-exo-dig*** mechanism.

The energy profiles of **5-exo-dig** and the **5-exo-dig*** differ substantially. For **5-exo-dig** the transition state of the carbene intermediate formation (TS1) has an ΔG_{app} of 79 kJ/mol at an external CO pressure of 0.1 atm. Under the same conditions, the corresponding transition state of **5-exo-dig***, TS4, has an ΔG_{app} of 149 kJ/mol. For the transition states of the metallacycle formation, TS3 (**5-exo-dig**) and TS5 (**5-exo-dig***), the order is reversed, although in this case the energy difference is much less pronounced. At an external CO pressure of 0.1 atm., ΔG_{app} of TS3 is 102 kJ/mol. At the same external CO pressure ΔG_{app} of TS5 is 95 kJ/mol.

Importantly, the two profiles can be connected at any intermediate through a dissociation or coordination of a carbonyl group. In this way the high energy TS4 can be avoided and the lower energy TS5 is made available for the reaction. The lowest energy pathway from the separated substrate and catalyst to the metallacycle intermediate is thus to go over TS1 and TS2 of the **5-exo-dig** pathway to the carbene

UNIVERSITAT ROVIRA I VIRGILI
COMPUTACIONAL STUDIES ON THE MECHANISM OF THE PAUSON-KHAND REACTION
Torstein Fjermestad
ISBN:978-84-693-9441-0/DL:T.62-2011

intermediate INT2. From INT2 a CO dissociation takes the system to INT5 and the reaction continues along the **5-exo-dig*** pathway. At an external CO pressure of 0.1 atm., the apparent dissociation energy from INT2 to INT5 is 75 kJ/mol. The dissociation of the carbonyl generates a vacant site in the rhodium coordination sphere. This facilitates the formation of the metallacycle and the barrier for this step is only 35 kJ/mol. The metallacycle, INT6, has a ΔG_{app} of 77 kJ/mol at an external CO pressure of 0.1 atm. The complete free energy profiles (ΔG° and ΔG_{app} at a CO pressures of 1.0 atm. and 0.1 atm.) of the 5-exo-dig mechanism (**5-exo-dig** followed by **5-exo-dig***) up to metallacycle intermediate INT6 are shown in figure 7.26. To avoid confusion in the further discussion, we label this combination of the **5-exo-dig** and the **5-exo-dig*** mechanisms **5-exo-dig****.

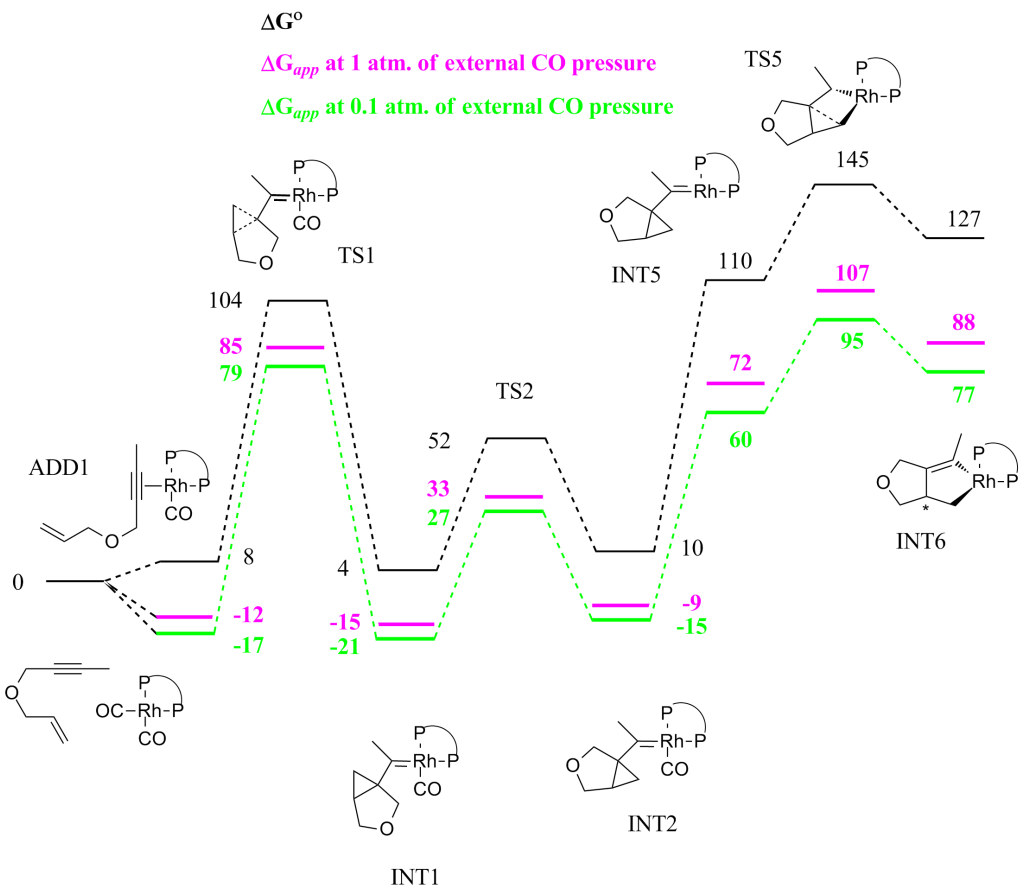

Figure 7.26: Free energy profiles (kJ/mol) of ΔG° and ΔG_{app} at CO pressures of 1.0 atm. and 0.1 atm. for the **5-exo-dig**** mechanism.

7.4.3 The 6-endo-dig mechanism

ΔG° of the rate-determining transition state of **6-endo-dig** (TS8) and **6-endo-dig*** (TS9) are presented in section 7.3 (Figures 7.17 and 7.18). Following the same procedure as described above, we find that ΔG_{app} of TS8 is 116 kJ/mol at an external CO pressure of 1.0 atm. and 110 kJ/mol at a CO pressure of 0.1 atm.

UNIVERSITAT ROVIRA I VIRGILI
COMPUTACIONAL STUDIES ON THE MECHANISM OF THE PAUSON-KHAND REACTION
Torstein Fjermestad
ISBN:978-84-693-9441-0/DL:T.62-2011

Likewise ΔG_{app} of TS9 is 140 kJ/mol at a CO pressure of 1.0 atm. and 129 kJ/mol at a CO pressure of 0.1 atm.

7.4.4 The mechanisms 5-exo-dig_ketene and CO-alkyne

In the **5-exo-dig_ketene** mechanism the rate-determining step is the CO insertion into the rhodium-carbene bond. A second CO dissociation occurring before the rate-determining transition state is thus impossible. The only CO dissociation that takes place is the dissociation from the catalyst precursor to generate the vacant site for the substrate. Compared to ΔG° of the **5-exo-dig_ketene** mechanism presented in subsection 7.3.5 (Figure 7.20), the ΔG_{app} is lowered by 19 kJ/mol at 1.0 atm. of CO pressure and by 25 kJ/mol at a CO pressure of 0.1 atm. ΔG_{app} of the rate-determining TS, TS10, is thus 114 kJ/mol at a CO pressure of 1.0 atm. and 108 kJ/mol at a CO pressure of 0.1 atm.

Also in the **CO-alkyne** mechanism, the carbonyl participates directly in the rate-determining TS. A second CO dissociation occurring before the rate-determining transition state, TS12, becomes thus impossible. Because only one CO dissociation takes place, ΔG_{app} of TS12 is 104 kJ/mol at 1.0 atm. of CO pressure and 98 kJ/mol at 0.1 atm. of CO pressure.

7.5 Discussion

7.5.1 The preferred mechanism

The selectivity-determining TS of a mechanism is the highest energy TS of the profile. In table 7.1 ΔG° and ΔG_{app} (CO pressure of 0.1 atm. and 1.0 atm.) are given for the selectivity-determining TS of each of the computed mechanisms. At a CO pressure of 0.1 atm., **5-exo-dig**** has the lowest selectivity-determining TS (95 kJ/mol). At low CO pressures, the **5-exo-dig**** mechanism is thus the preferred mechanism. Some other mechanisms (**CO-alkyne**, **5-exo-dig**) present barrier that are close in energy to that of the **5-exo-dig**** mechanism. However, these mechanisms are incompatible with the experimentally reported rate law [125].

Table 7.1 shows that the mechanisms with the two CO ligands dissociated in the selectivity-determining TS, **Magnus***, **5-exo-dig**** and **6-endo-dig***, are relatively more favoured at low CO pressures. When increasing the CO pressure from 0.1 atm. to 1.0 atm., the difference in ΔG_{app} between structures with two carbonyls dissociated and structures with one carbonyl dissociated decreases by 6 kJ/mol. In particular at a CO pressure of 0.1 atm., the difference between the selectivity-determining TS of **5-exo-dig**** and **CO-alkyne** is 3 kJ/mol. At a CO pressure of 1.0 atm., the order has changed and the selectivity-determining TS of **CO-alkyne** is 3 kJ/mol lower than **5-exo-dig****. The result that structures with carbonyls coordinated are favoured at higher CO pressures is in agreement with the the Le Chatelier principle.

UNIVERSITAT ROVIRA I VIRGILI
COMPUTACIONAL STUDIES ON THE MECHANISM OF THE PAUSON-KHAND REACTION
Torstein Fjermestad
ISBN:978-84-693-9441-0/DL:T.62-2011

Table 7.1: ΔG° and ΔG_{app} (CO pressure of 0.1 atm. and 1.0 atm.) of the selectivity-determining TSs of the different pathways. Energies in kJ/mol. The two most stable TSs in terms of each of the quantities are shown in boldface.

Mechanism	TS	ΔG_{app} at 0.1 atm.	ΔG_{app} at 1.0 atm.	ΔG°
Magnus*	TS_A*	121	133	171
Magnus	TS_A	148	154	173
5-exo-dig**	TS5	**95**	**107**	145
5-exo-dig*	TS4	149	161	199
5-exo-dig	TS3	102	108	**127**
6-endo-dig*	TS9	129	140	179
6-endo-dig	TS8	110	116	135
5-exo-dig_ketene	TS10	108	114	133
CO-alkyne	TS12	**98**	**104**	**123**

Interestingly, the commonly accepted Magnus mechanism is highly disfavoured for this system. ΔG_{app} of the selectivity-determining transition state of **Magnus*** is 121 kJ/mol at 0.1 atm. and 133 kJ/mol at 1.0 atm. ΔG_{app} of the selectivity-determining transition state of **Magnus** is 148 kJ/mol at 0.1 atm. and 154 kJ/mol at 1.0 atm.

7.5.2 From the metallacycle to the product

The **5-exo-dig**** mechanism is favoured at low CO pressures. In the following, when discussing how the metallacycle intermediate is connected to the final products, we use the values for ΔG_{app} at a CO pressure of 0.1 atm. The **5-exo-dig**** mechanism merges with the Magnus mechanism at intermediate INT6, this is an approximate square-planar complex with a free energy of 77 kJ/mol. INT6 isomerises to the more stable intermediate INT11 (59 kJ/mol). INT11 is of an approximate butterfly geometry with the alkyne moiety of the substrate in the plane of the rhodium and the two phosphorus atoms. A carbonyl group coordinates to INT11 and intermediate INT16 (33 kJ/mol) is formed. The carbonyl inserts into the metal-alkenyl bond and the carbonylated metallacycle INT17 (-27 kJ/mol) is formed after passing TS14 (43 kJ/mol). Form INT17 the reaction goes through a low-barrier reductive elimination (TS15 = 17 kJ/mol) towards product adduct ADD4 (-36 kJ/mol). Thereafter two successive carbonyl coordinations to the rhodium occur, and the catalyst precursor is regenerated. At 0.1 atm. of CO pressure, the reaction energy is -163 kJ/mol.

Figure 7.27 shows the free energy profile from metallacycle intermediate INT16 to the final reaction product. We see that this part of the reaction mechanism consists of low energy reaction barriers which confirms the selectivity-determining nature of the metallacycle formation step. An observation that can be made, is that the apparent reaction free energy, $\Delta G_{app,rxn}$, is decreasing with decreasing CO pressure.

UNIVERSITAT ROVIRA I VIRGILI
COMPUTACIONAL STUDIES ON THE MECHANISM OF THE PAUSON-KHAND REACTION
Torstein Fjermestad
ISBN:978-84-693-9441-0/DL:T.62-2011

At 1.0 atm. $\Delta G_{app,rxn}$ is -169 kJ/mol, and at 0.1 atm. $\Delta G_{app,rxn}$ is -163 kJ/mol. Decreasing the CO pressure has thus only a positive effect on the kinetics. From thermodynamic considerations, we see that the product formation is favoured at higher CO pressure. However, the reaction is highly exergonic at any CO pressure and the small reduction of the apparent reaction energy at low CO pressure is completely negligible.

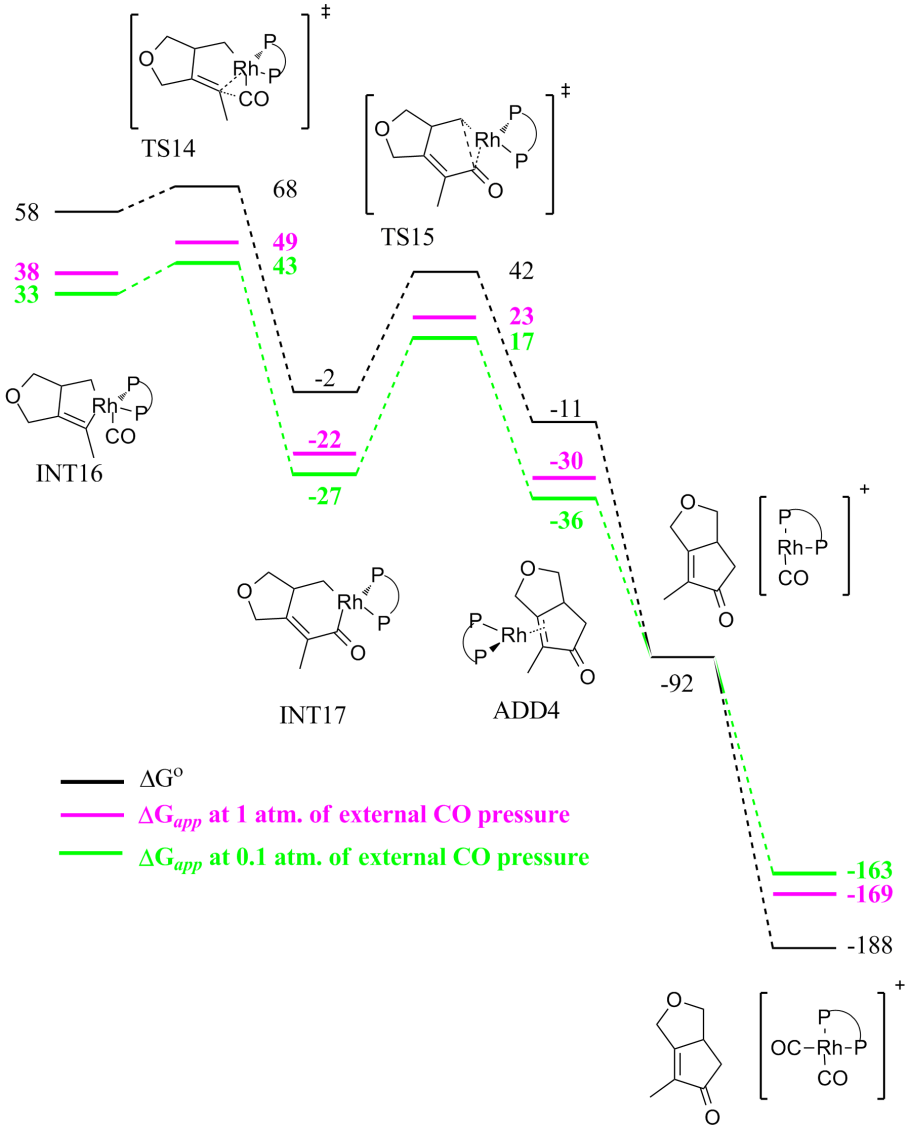

Figure 7.27: Free energy profiles (kJ/mol) of $\Delta G°$ and ΔG_{app} at CO pressures of 1.0 atm. and 0.1 atm. from the metallacycle to the product.

7.5.3 Kinetics

From the comparison of the selectivity-determining TSs in table 7.1, we have established the **5-exo-dig**** mechanism as the preferred mechanism at low CO pressures. From the energetic span model [99–102] we find that TS5 is the TOF-determining

UNIVERSITAT ROVIRA I VIRGILI
COMPUTACIONAL STUDIES ON THE MECHANISM OF THE PAUSON-KHAND REACTION
Torstein Fjermestad
ISBN:978-84-693-9441-0/DL:T.62-2011

TS (TDTS) and INT1 is the TOF-determining intermediate (TDI) of the **5-exo-dig**** mechanism. Previous to the TDTS, two carbonyl dissociations have taken place. By deriving the rate-equations for this reaction from the free energy profile of **5-exo-dig****, we arrive at a TOF dependence of the order of -2 in the CO concentration. This is in agreement with the kinetic study by Consiglio that shows a rate dependence of the order of -2 in the CO concentration [125].

The energetic span of the **5-exo-dig**** mechanism is the energy difference between TS5 and INT1. Calculations of ΔG_{app} show a decrease in the energetic span from 122 kJ/mol at 1.0 atm of CO pressure to 116 kJ/mol at 0.1 atm. of CO pressure. By lowering the CO pressure from 1.0 atm. to 0.1 atm. Jeong and coworkers observed that the reaction temperature could be lowered to room temperature (20°C) [17]. Our calculations are thus in agreement with the experimental results although this energy difference may be underestimated in our calculations. A lowering of the CO pressure lowers the energetic span of the reaction and consequently, allowing for a lower reaction temperature.

7.5.4 Mechanistic similarity with the skeletal rearrangement

Figure 7.28 shows a scheme of the favoured **5-exo-dig**** mechanism of this system. The first step from ADD1 to INT1 is the same as for the 5-exo-dig skeletal rear-

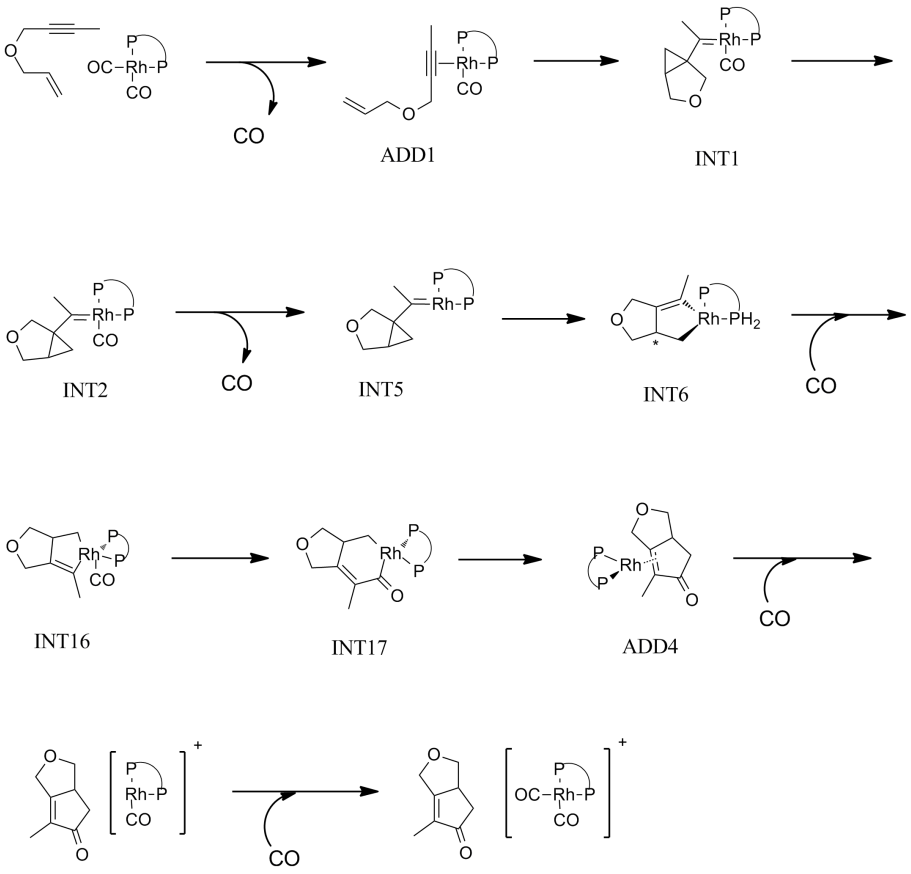

Figure 7.28: Schematic representation of the favoured **5-exo-dig**** mechanism.

UNIVERSITAT ROVIRA I VIRGILI
COMPUTACIONAL STUDIES ON THE MECHANISM OF THE PAUSON-KHAND REACTION
Torstein Fjermestad
ISBN:978-84-693-9441-0/DL:T.62-2011

rangement. It is interesting to see that the favoured mechanism of the Rh catalysed Pauson-Khand reaction shares a step with the important skeletal rearrangement mechanism. The skeletal rearrangement is well known to happen for enyne reactions catalysed by gold [131–134, 137, 138] and other transition metals [128, 139]. This study shows that there is a high degree of similarity between the Pauson-Khand reaction and reactions of enynes undergoing skeletal rearrangements.

7.5.5 Implications for studies on the enantioselectivity

The chiral centre of the product is being created in the first step from ADD1 to INT1. No change in the chiral centre takes place at any later stage of the **5-exo-dig**** mechanism. TS5 is the selectivity-determining transition state of the **5-exo-dig**** mechanism. It follows that TS5 is also enantiodetermining. Once the reaction has passed TS5, it can not go back to ADD1 to form the opposite chiral centre. TS5 will thus be the key transition state for studies of enantioselectivities. As shown in the previous chapters (Chapter 4 and 6), accurate calculations are required to obtain reliable results of the enantioselectivity. Full QM calculations and incorporation of solvent effects are likely necessary. Moreover, because the system is cationic, inclusion of the counterion may be critical for the computation of the enantiomeric excess.

7.6 Conclusions

In summary, we have found an alternative mechanism to be operative in the Rh catalysed Pauson-Khand reaction. The preferred mechanism shows mechanistic similarities with the 5-exo-dig skeletal rearrangement. Furthermore, the computationally proposed mechanism confirms the rate dependence of the order of -2 in the CO concentration observed by Consiglio [125]. Also the energetic span of the proposed mechanism decreases upon a reduction of the CO pressure. This agrees with the result reported by Jeong et al. [17] that the reaction temperature could be reduced at lower CO pressure.

UNIVERSITAT ROVIRA I VIRGILI
COMPUTACIONAL STUDIES ON THE MECHANISM OF THE PAUSON-KHAND REACTION
Torstein Fjermestad
ISBN:978-84-693-9441-0/DL:T.62-2011

Chapter 8

Conclusions

The asymmetric Pauson-Khand reaction catalysed by the $Co_2(CO)_6$(BINAP) complex follows the generally accepted Magnus mechanism previously proposed for $Co_2(CO)_8$ catalysts. The enantiodetermining transition state is that of the oxidative metallacycle addition. The enantiodiscrimination is caused by a difference in the steric interaction between a carbonyl and a phenyl located on the side of the catalyst opposite to where the chiral centre is created.

The activation barrier for the oxidation of metal carbonyl complexes by N-oxides can be correlated with the energy and shape of the unoccupied molecular orbital in the metal complex with the appropriate orientation. A similar correlation can be found for the activation of the Pauson-Khand precursor $Co_2(CO)_6(\mu^2$-prop-1-yne), but in this case there is also a steric factor preventing the attack to occur at the equatorial carbonyl ligands.

The interactions between the chiral brucine N-oxide and the pro-chiral dicobalt complex are responsible for the induction of chirality in the activated dicobalt complex R_{INT} in the brucine N-oxide assisted asymmetric Pauson-Khand reaction. The enantiomeric excess associated to the formation of the R_{INT} intermediate may be reduced in the product concentration through a racemisation to S_{INT} and to the small discrimination between the R TS and the S TS of the oxidative metallacycle addition. Thus, an improvement of the enantioselectivity of the brucine N-oxide activation step can at most give rise to an enantiomeric excess of 90% of the product.

The Magnus mechanism does not operate in the Pauson-Khand reaction catalysed by the $RhCO(BINAP)^+$. Instead, the reaction takes place through a 5-exo-dig mechanism, related to those proposed for gold-catalysed rearrangement of enynes. This mechanism explains the experimental results of a rate dependence of the order of -2 in the CO concentration and the fact that a lower CO pressure makes the reaction feasible at lower temperature. The enantioselectivity determining TS for this process is that of the metallacycle formation step.

UNIVERSITAT ROVIRA I VIRGILI
COMPUTACIONAL STUDIES ON THE MECHANISM OF THE PAUSON-KHAND REACTION
Torstein Fjermestad
ISBN:978-84-693-9441-0/DL:T.62-2011

UNIVERSITAT ROVIRA I VIRGILI
COMPUTACIONAL STUDIES ON THE MECHANISM OF THE PAUSON-KHAND REACTION
Torstein Fjermestad
ISBN:978-84-693-9441-0/DL:T.62-2011

Bibliography

[1] I. U. Khand, G. R. Knox, P. L. Pauson, W. E. Watts, A cobalt Induced Cleavage Reaction and a New Series of Arenecobalt Carbonyl Complexes, *J. Chem. Soc. Chem. Commun.* **1971**, 36a.

[2] I. U. Khand, G. R. Knox, P. L. Pauson, W. E. Watts, M. I. Foreman, Organocobalt complexes. Part II. Reaction of Acetylenehexacharbonyldicobalt dicobalt complexes, $(RC_2R)Co_2(CO)_6$, with norbornene and its derivatives, *J.C.S. Perkin I* **1973**, 977–981.

[3] K. M. Brummond, J. L. Kent, Recent Advances in the Pauson-Khand reaction and related [2+2+1] cycloaddition, *Tetrahedron* **2000**, *56*, 3263–3283.

[4] S. E. Gibson, A. Stevenazzi, The Pauson-Khand reaction: the catalytic age is here, *Angew.Chem.Int.Ed.* **2003**, *42*, 1800–1810.

[5] L. V. R. Boñaga, M. E. Krafft, When the Pauson-Khand and Pauson-Khand type reactions go awry: a plethora of unexpected results, *Tetrahedron* **2004**, *60*, 9795–9833.

[6] S. E. Gibson, N. Mainolfi, The intermolecular Pauson-Khand reaction, *Angew. Chem. Int. Ed.* **2005**, *44*, 3022–3037.

[7] T. Shibata, Recent advances in the catalytic Pauson-Khand-type reaction, *Adv. Synth. Catal.* **2006**, *348*, 2328–2336.

[8] J. H. Park, K.-M. Chang, Y. K. Chung, Catalytic Pauson-Khand-type reactions and related carbonylative cycloaddition reactions, *Coord. Chem. Rev.* **2009**, *253*, 2461–2480.

[9] H.-W. Lee, F.-Y. Kwong, A Decade of Advancements in Pauson-Khand-Type Reactions, *Eur. J. Org. Chem.* **2010**, 789–811.

[10] F. A. Hicks, N. M. Kablaoui, S. L. Buchwald, Titanocene-Catalyzed Cyclocarbonylation of Enynes to Cyclopentenones, *J. Am. Chem. Soc.* **1996**, *118*, 9450.

[11] F. A. Hicks, N. M. Kablaoui, S. L. Buchwald, Scope of the Intramolecular Titanocene-Catalyzed Pauson-Khand Type Reaction, *J. Am. Chem. Soc.* **1999**, *121*, 5881–5898.

UNIVERSITAT ROVIRA I VIRGILI
COMPUTACIONAL STUDIES ON THE MECHANISM OF THE PAUSON-KHAND REACTION
Torstein Fjermestad
ISBN:978-84-693-9441-0/DL:T.62-2011

[12] A. J. Pearson, R. A. Dubbert, Cyclocarbonylation of 1,6-Enynes Promoted by Iron Carbonyls, *Organometallics* **1994**, *13*, 1656–1661.

[13] N. Jeong, S. Lee, B. K. Sung, Rhodium(I)-Catalyzed Intramolecular Pauson-Khand Reaction, *Organometallics* **1998**, *17*, 3642–3644.

[14] N. Jeong, B. K. Sung, Y. K. Choi, Rhodium(I)-catalyzed asymmetric intramolecular Pauson-Khand-type reaction, *J. Am. Chem. Soc.* **2000**, *122*, 6771–6772.

[15] T. Kobayashi, Y. Koga, K. Narasaka, The rhodium-catalyzed Pauson-Khand reaction, *J. Organomet. Chem.* **2001**, *624*, 73–87.

[16] D. E. Kim, C. Choi, I. S. Kim, S. Jeulin, V. Ratovelomanana-Vidal, J.-P. Genêt, N. Jeong, Electronic and Steric Effects of atropisomeric Ligands SUNPHOS and DIFLUORPOHS vs. BINAPs in Rh(I)-catalyzed asymmetric Pauson-Khand reaction, *Adv. Synth. Catal.* **2007**, *349*, 1999–2006.

[17] D. E. Kim, I. S. Kim, V. Ratovelomanana-Vidal, J.-P. Genêt, N. Jeong, Asymmetirc Pauson-Khand-type Reaction Mediated by Rh(I) Catalyst at Ambient Temperature, *J. Org. Chem.* **2008**, *73*, 7985–7989.

[18] T. Kondo, N. Suzuki, T. Okada, T. aki Mitsudo, First Ruthenium-Catalyzed Intramolecular Pauson-Khand Reaction, *J. Am. Chem. Soc.* **1997**, *119*, 6187–6188.

[19] T. Morimoto, N. Chatani, Y. Fukumoto, S. Murai, $Ru_3(CO)_{12}$-Catalyzed Cyclocarbonylation of 1,6-Enynes to Bicyclo[3.3.0]octenes, *J. Org. Chem.* **1997**, *62*, 3762–3765.

[20] T. Kondo, M. Nomura, Y. Ura, K. Wada, T. aki Mitsudo, Ruthenium-catalyzed [2+2+1] Cocyclization of Isocyanates, Alkynes, and CO Enables the Rapid Synthesis of Polysubstituted Maleimides, *J. Am. Chem. Soc.* **2006**, *128*, 14816–14817.

[21] T. Shibata, K. Takagi, Iridium-Chiral Diphosphine Complex Catalyzed Highly Enantioselective Pauson-Khand-Type Reaction, *J. Am. Chem. Soc.* **2000**, *122*, 9852–9853.

[22] Z.-L. Lu, E. Neumann, A. Pfaltz, Asymmetirc catalytic intramolecular Pauson-Khand reactions with Ir(phox) catalysts, *Eur. J. Org. Chem.* **2007**, 4189–4192.

[23] M. Zhang, S. L. Buchwald, A Nickel(0)-Catalyzed Process for the Transformation of Enynes to Bicyclic Cyclopentenones, *J. Org. Chem.* **1996**, *61*, 4498–4499.

[24] E. ichi Negishi, S. J. Holmes, J. M. Tour, J. A. Miller, Zirconium-Promoted Bicyclization of Enynes, *J. Am. Chem. Soc.* **1985**, *107*, 2568–2569.

UNIVERSITAT ROVIRA I VIRGILI
COMPUTACIONAL STUDIES ON THE MECHANISM OF THE PAUSON-KHAND REACTION
Torstein Fjermestad
ISBN:978-84-693-9441-0/DL:T.62-2011

[25] K. M. Brummond, A. D. Kerekes, H. Wan, Chiral Nonracemic α-Alkylidene and α-Silylidene Cyclopentenones from Chiral Allenenes Using an Intramolecular Allenic Pauson-Khand-Type Cycloaddition., *J. Org. Chem.* **2002**, *67*, 5156–5163.

[26] H. Cao, J. Flippen-Anderson, J. M. Cook, The Synthesis of a Dicyclopenta[a,e]pentalene via a Molybdenum Hexacarbonyl-Mediated Tandem Allenic Pauson-Khand Reaction, *J. Am. Chem. Soc.* **2003**, *125*, 3230–3231.

[27] T. R. Hoye, J. A. Suriano, A [$W(CO)_5$·THF] Mediated Pauson-Khand Reaction: Cyclizations of 1,6-Enynes via a Batch-Catalytic Protocol, *J. Am. Chem. Soc.* **1993**, *115*, 1154–1156.

[28] Y. Tang, L. Deng, Y. Zhang, G. Dong, J. Chen, Z. Yang, Thioureas as Ligands in the Pd-Catalyzed Intramolecular Pauson-Khand Reaction, *Org. Lett.* **2005**, *7*, 1657.

[29] E. Fager-Jokela, E. Kaasalainen, K. Leppänen, J. Tois, J. Helaja, Development of intermolecular additive free Pauson-Khand reactions for estrone E-ring extension using microwaves, *Tetrahedron* **2008**, *64*, 10381–10387.

[30] K. D. Closser, M. M. Quintal, K. M. Shea, The Scope and Limitations of Intramolecular Nicholas and Pauson-Khand Reactions for the Synthesis of Tricyclic Oxyggen- and Nitrogen-Containing Heterocycles, *J. Org. Chem.* **2009**, *74*, 3680–3688.

[31] A. Vázquez-Romero, J. Rodríguez, A. Lledó, X. Verdaguer, A. Riera, Enantioselective Synthesis of Carbanucleosides from the Pauson-Khand Adduct of Trimethylsilylacetylene and Norbornadiene, *Org. Lett.* **2008**, *10*, 4509–4512.

[32] A. Vázquez-Romero, L. Cárdenas, E. Blasi, X. Verdaguer, A. Riera, Synthesis of Prostaglandin and Phytoprostane B_1 Via Regioselective Intermolecular Pauson-Khand Reactions, *Org. Lett.* **2009**, *11*, 3104–3107.

[33] S. Horn, M. O. Senge, The Intermolecular Pauson-Khand Reaction of *meso*-Substituted Porphyrins, *Eur. J. Org. Chem.* **2008**, 4881–4890.

[34] N. Martín, M. Altable, S. Filippone, A. Martín-Domenech, Highly efficient Pauson-Khand reaction with C_{60}: regioselective synthesis of unprecedented cis-1 biscycloadducts, *Chem. Commun.* **2004**, 1338–1339.

[35] N. E. Schore, M. C. Croudance, Preparation of Bicyclo[3.3.0]oct-1-en-3-one and Bicyclo[4.3.0]non-1(9)-en-8-one via Intramolecular Cyclization of α,ω-Enynes, *J. Org. Chem.* **1981**, *46*, 5436–5438.

[36] V. Rautenstrauch, P. Mégard, J. Conesa, W. Küster, 2-Pentylcyclopent-2-en-1-one by Catalytic Pauson-Khand Reaction, *Angew. Chem. Int. Ed. Engl.* **1990**, *29*, 1413.

UNIVERSITAT ROVIRA I VIRGILI
COMPUTACIONAL STUDIES ON THE MECHANISM OF THE PAUSON-KHAND REACTION
Torstein Fjermestad
ISBN:978-84-693-9441-0/DL:T.62-2011

[37] D. B. Belanger, D. J. R. O'Mahony, T. Livinghouse, Thermal Promotion of the Cobalt Catalyzed Intramolecular Pauson-Khand Reaction - An Alternative Experimental Protocol for Cyclopentenone Synthesis, *Tetrahedron Lett.* **1998**, *39*, 7637–7640.

[38] P. Magnus, L. M. Principe, Origins of 1,2- and 1,3-stereoselectivity in dicobaltoctacarbonyl alkene-alkyne cyclizations for the synthesis of substituted bicyclo[3.3.0]octenones., *Tetrahedron Lett.* **1985**, *26*, 4851–4854.

[39] B. E. La Belle, M. J. Knudsen, M. M. Olmstead, H. Hope, M. D. Yanuck, N. E. Schore, Synthesis of 11-Oxatricyclo[5.3.1.$0_{2,6}$] undecane Derivatives via Organometallic Cyclizations, *J. Org. Chem.* **1985**, *50*, 5215–5222.

[40] R. S. Dickson, P. J. Fraser, Compounds Derived from Alkynes and Carbonyl Complexes of Cobalt, *Adv. Organomet. Chem.* **1974**, *12*, 323.

[41] M. E. Krafft, I. L. Scott, R. H. Romero, S. Feibelmann, C. E. Van Pelt, Effect of Coordinating Ligands on the Pauson-Khand Cycloaddition: Trapping of an Intermediate, *J. Am. Chem. Soc.* **1993**, *115*, 7199–7207.

[42] E. Montenegro, M. Poch, A. Moyano, M. A. Pericàs, A. Riera, Highly Diastereoselective Pauson-Khand Reactions of a Stable, Internally Chelated, Dicobalt Pentacarbonyl Complex of a Chiral Acetylene Thioether, *Tetrahedron Lett.* **1998**, *39*, 335–338.

[43] X. Verdaguer, J. Vázquez, G. Fuster, V. Bernardes-Génisson, A. E. Greene, A. Moyano, M. A. Pericàs, A. Riera, Comphor-Derived, Chelated Auxiliaries for the Highly Diastereoselective Intermolecular Pauson-Khand Reaction: Experimental and Computational Studies, *J. Org. Chem.* **1998**, *63*, 7037–7052.

[44] I. Marchueta, E. Montenegro, D. Panov, M. Poch, X. Verdaguer, A. Moyano, M. A. Pericàs, A. Riera, Asymmetric Pauson-Khand Reactions Using Camphor-Derived Chelating Thiols as Chiral Controllers, *J. Org. Chem.* **2001**, *66*, 6400–6409.

[45] E. V. Banide, H. Müller-Bunz, A. R. Manning, P. Evans, M. J. McGlinchey, X-ray Crystal Structure of an Alkene-Pentacarbonyldicobalt-Alkyne Complex: Isolation of a Stable Magnus-Type Pauson-Khand Intermediate, *Angew. Chem. Int. Ed.* **2007**, *46*, 2907–2910.

[46] M. E. Krafft, A. M. Wilson, O. A. Dasse, B. Shao, Y. Y. Cheung, Z. Fu., B. naga. L. V. R., M. K. Mollman, The Interrupted Pauson-Khand Reaction, *J. Am. Chem. Soc.* **1996**, *118*, 6080.

[47] M. Yamanaka, E. Nakamura, Density functional studies on the Pauson-Khand reaction, *J. Am. Chem. Soc.* **2001**, *123*, 1703–1708.

[48] M. A. Pericàs, J. Balsells, J. Castro, I. Marchueta, A. Moyano, A. Riera, J. Vázquez, X. Verdaguer, Toward the understanding of the mechanism and enantioselectivity of the Pauson-Khand reaction. Theoretical and experimental studies, *Pure Appl. Chem.* **2002**, *74*, 167–174.

UNIVERSITAT ROVIRA I VIRGILI
COMPUTACIONAL STUDIES ON THE MECHANISM OF THE PAUSON-KHAND REACTION
Torstein Fjermestad
ISBN:978-84-693-9441-0/DL:T.62-2011

[49] A. C. Comely, S. E. Gibson, N. J. Hales, Polymer supported cobalt carbonyl complexes as novel traceless alkyne linkers for solid-phase synthesis, *Chem. Commun.* **1999**, 2075.

[50] A. C. Comely, S. E. Gibson, N. J. Hales, Polymer-supported cobalt carbonyl complexes as novel solid-phase catalysts of the Pauson–Khand reaction, *Chem. Commun.* **2000**, 305.

[51] S.-W. Kim, S. U. Son, S. I. Lee, T. Hyeon, Y. K. Chung, Cobalt on Mesoporous Silica The First Heterogeneous Pauson Khand Catalyst, *J. Am. Chem. Soc.* **2000**, *122*, 1550–1551.

[52] S. U. Son, S. I. Lee, Y. K. Chung, Cobalt on Charcoal: A Convenient and Inexpensive Heterogeneous Pauson-Khand Catalyst, *Angew. Chem. Int. Ed.* **2000**, *39*, 4158.

[53] S.-W. Kim, S. U. Son, S. S. Lee, T. Hyeon, Y. K. Chung, Colloidal cobalt nanoparticles a highly active and reusable Pauson Khand catalyst, *Chem. Commun.* **2001**, 2212.

[54] J.-L. Muller, A. Rickers, W. Leitner, Raney Cobalt: An Effective and Recyclable Catalyst for the Pauson-Khand Reaction, *Adv. Synth. Catal.* **2007**, *349*, 287–291.

[55] J. Castro, H. Sörensen, A. Riera, C. Morin, A. Moyano, M. A. Pericàs, A. E. Greene, Asymmetric Approach to Pauson-Khand Bicyclization. Enantioselective Formal Synthesis of Hirsutene, *J. Am. Chem. Soc.* **1990**, *112*, 9388–9389.

[56] J. Castro, A. Moyano, M. A. Pericàs, A. Riera, A. Alvarez-Larena, J. F. Piniella, Acetylene-Dicobaltcarbonyl Complexes with Chiral Phosphinooxazoline Ligands: Synthesis, structural Characterization, and Application to Enantioselective Intermolecular Pauson-Khand Reactions., *J. Am. Chem. Soc.* **2000**, *122*, 7944–7952.

[57] M. Poch, E. Valentí, A. Moyano, M. A. Pericàs, J. Castro, A. DeNicola, A. E. Greene, Asymmetric induction studies in the intramolecular Pauson-Khand cyclization of 7-alkoxy-1-hepten-6-ynes, *Tetrahedron Lett.* **1990**, *31*, 7505–7508.

[58] X. Verdaguer, A. Moyano, M. A. Pericàs, A. Riera, A. E. Greene, J. F. Piniella, A. Alvarez-Larena, Camphor-derived alcohols as chiral auxiliaries for asymmetric Pauson-Khand bicyclizations. Enantioselective synthesis of α-methoxyenones, *J. Organomet. Chem.* **1992**, *433*, 305–310.

[59] J. Castro, A. Moyano, M. A. Pericàs, A. Riera, A. E. Greene, Asymmetric synthesis of bicyclo[4.3.0]nonan-8-ones by intramolecular Pauson-Khand reaction, *Tetrahedron: Asymmetry* **1994**, *5*, 307–310.

[60] X. Verdaguer, A. Moyano, M. A. Pericàs, A. Riera, V. Bernardes, A. E. Greene, A. Alvarez-Larena, J. F. Piniella, A Dual-Function, Highly Efficient Chiral

UNIVERSITAT ROVIRA I VIRGILI
COMPUTACIONAL STUDIES ON THE MECHANISM OF THE PAUSON-KHAND REACTION
Torstein Fjermestad
ISBN:978-84-693-9441-0/DL:T.62-2011

Controller for Stereoselective Intermolecular Pauson-Khand Reactions, *J. Am. Chem. Soc.* **1994**, *116*, 2153–2154.

[61] V. Bernardes, N. Kann, A. Riera, A. Moyano, M. A. Pericàs, A. E. Greene, Asymmetric Pauson-Khand Cyclization: A Formal Total Synthesis of Natural Brefeldin A, *J. Org. Chem.* **1995**, *60*, 6670–6671.

[62] X. Verdaguer, A. Moyano, M. A. Pericàs, A. Riera, M. A. Maestro, J. Mahía, A New Chiral Bidentate (P,S) Ligand for the Asymmetric Intermolecular Pauson-Khand Reaction, *J. Am. Chem. Soc.* **2000**, *122*, 10242–10243.

[63] X. Verdaguer, M. A. Pericàs, A. Riera, M. A. Maestro, J. Mahía, Design of New Hemilabile (P,S) Ligands for the Highly Diastereoselective Coordination to Alkyne Dicobalt Complexes: Application to the Asymmetric Intermolecular Pauson-Khand Reaction, *Organometallics* **2003**, *22*, 1868–1877.

[64] S. J. Sturla, S. L. Buchwald, Cobalt-Phosphite-Catalyzed Asymmetric Pauson-Khand Reaction, *J. Org. Chem.* **2002**, *67*, 3398–3403.

[65] K. Hiroi, T. Watanabe, R. Kawagishi, I. Abe, Catalytic use of chiral phosphine ligands in asymmetric Pauson-Khand reactions, *Tetrahedron: Asymmetry* **2000**, *11*, 797–808.

[66] F. A. Hicks, S. L. Buchwald, An Intramolecular Titanium-Catalyzed Asymmetric Pauson-Khand Type Reaction, *J. Am. Chem. Soc.* **1999**, *121*, 7026–7033.

[67] K. Hiroi, T. Watanabe, R. Kawagishi, I. Abe, Asymmetric catalytic Pauson-Khand reactions with chiral phosphine ligands: Dramatic effects of substituents in 1,6-enyne systems, *Tetrahedron Lett.* **2000**, *41*, 891–895.

[68] N. Jeong, Y. K. Chung, B. Y. Lee, S. H. Lee, S.-E. Yoo, A dramatic acceleration of the Pauson-Khand reaction by timethylamine *N*-oxide, *Synlett* **1991**, 204–206.

[69] D. R. Carbery, W. J. Kerr, D. M. Lindsay, J. S. Scott, S. P. Watson, Preparation and reaction of desymmetrised cobalt alkyne complexes, *Tetrahedron Letters* **2000**, *41*, 3235–3239.

[70] W. J. Kerr, D. M. Lindsay, E. M. Rankin, J. S. Scott, S. P. Watson, The brucine *N*-oxide-promoted asymmetric Pauson-Khand reaction, *Tetrahedron Lett.* **2000**, *41*, 3229–3233.

[71] S. E. Gibson, S. E. Lewis, J. A. Loch, J. W. Steed, M. J. Tozer, Identification of an asymmetric Pauson-Khand precatalyst, *Organometallics* **2003**, *22*, 5382–5384.

[72] S. E. Gibson, K. A. C. Kaufmann, J. A. Loch, J. W. Steed, A. J. P. White, A study of $[Co_2(alkyne)(binap)(CO)_4]$ Complexes (BINAP=(1,1'-Binaphthalene)-2,2'-diylbis(diphenylphosphine)), *Chem. Eur. J.* **2005**, *11*, 2566–2576.

UNIVERSITAT ROVIRA I VIRGILI
COMPUTACIONAL STUDIES ON THE MECHANISM OF THE PAUSON-KHAND REACTION
Torstein Fjermestad
ISBN:978-84-693-9441-0/DL:T.62-2011

[73] F. Y. Kwong, H. W. Lee, L. Qiu, W. H. Lam, Y.-M. Li, H. L. Kwong, A. S. C. Chan, Rhodium-BisbenzodioxanPhos complex-catalyzed homogeneous enantioselective Pauson-Khand-type cyclization in alcoholic solvents, *Adv. Synth, Catal.* **2005**, *347*, 1750–1754.

[74] F. Y. Kwong, Y. M. Li, W. H. Lam, L. Qiu, H. W. Lee, C. H. Yeung, K. S. Chan, A. S. C. Chan, Rhodium-Catalyzed Asymmetric aqueous Pauson-Khand-Type reaction, *Chem, Eur. J.* **2005**, *11*, 3872–3880.

[75] Y. H. Choi, J. Kwak, N. Jeong, Solvent effects on the asymmetric Pauson-Khand-type reaction by rhodium, *Tetrahedron Lett.* **2009**, *50*, 6068–6071.

[76] P. Hohenberg, W. Kohn, Inhomogeneous Electron Gas, *Phys. Rev.* **1964**, *136*, B864–B871.

[77] W. Kohn, L. J. Sham, Self-Consistent Equations Including Exchange and Correlation Effects, *Phys. Rev.* **1965**, *140*, A1133–A1138.

[78] W. Koch, M. C. Holthausen, *A Chemist's Guide to Density Functional Theory* (Wiley-VCH, **2002**).

[79] R. G. Parr, W. Yang, *Density-Functional Theory of Atoms and Molecules* (Oxford University Press, **1989**).

[80] C. J. Cramer, D. G. Truhlar, Density functional theory for transition metals and transition metal chemistry, *Phys. Chem. Chem. Phys.* **2009**, *11*, 10757–10816.

[81] A. D. Becke, Density-functional exchange-energy approximation with correct asymptotic-behavior, *Phys. Rev. A* **1988**, *38*, 3098–3100.

[82] J. P. Perdew, Density-functional approximation for the correlation energy of the inhomogeneous electron gas, *Phys. Rev. B* **1986**, *33*, 8822–8824.

[83] C. Lee, W. Yang, R. G. Parr, Development of the Colle-Salvetti correlation-energy formula into a functional of the electron density, *Phys. Rev. B.* **1988**, *37*, 785–789.

[84] B. Miehlich, A. Savin, H. Stoll, H. Preuss, Results obtained with the correlation-energy density functionals of Becke and Lee, Yang and Parr, *Chem. Phys. Lett.* **1989**, *157*, 200–206.

[85] A. D. Becke, Densitiy-Functional Thermochemistry .3. The Role of Exact Exchange, *J.Chem.Phys* **1993**, *98*, 5648–5652.

[86] C. Lee, W. Yang, R. G. Parr, Development of the Colle-Salvetti correlation-energy formula into a functional of the electron density, *Phys. Rev. B.* **1988**, *37*, 785–789.

[87] Y. Zhao, D. G. Truhlar, A new local density functional for main-group thermochemistry, transition metal bonding, thermochemical kinetics, and noncovalent interactions, *J. Chem. Phys.* **2006**, *125*, 194101–194118.

UNIVERSITAT ROVIRA I VIRGILI
COMPUTACIONAL STUDIES ON THE MECHANISM OF THE PAUSON-KHAND REACTION
Torstein Fjermestad
ISBN:978-84-693-9441-0/DL:T.62-2011

[88] Y. Zhao, D. G. Truhlar, The M06 suite of density functionals for main group thermochemistry, thermochemical kinetics, noncovalent interactions, excited states, and transition elements: two new functionals and systematic testing of four M06-class functionals and 12 other functionals, *Theor. Chem. Acc.* **2008**, *120*, 215–241.

[89] A. K. Rappé, C. J. Casewit, K. S. Colwell, W. A. Goddard III, W. M. Skiff, UFF, a Full Periodic Table Force Field for Molecular Mechanics and Molecular Dynamics Simulations, *J. Am. Chem. Soc.* **1992**, *114*, 10024–10035.

[90] H. Lin, D. G. Truhlar, QM/MM: what have we learned, where are we, and where do we go from here?, *Theor. Chem. Acc.* **2007**, *117*, 185–199.

[91] H. M. Senn, W. Thiel, QM/MM Methods for Biomolecular Systems, *Angew. Chem. Int. Ed.* **2009**, *48*, 1198–1229.

[92] F. Maseras, K. Morokuma, IMOMM: A new integrated ab initio + molecular mechanics geometry optimization scheme of equilibrium structures and transition states, *J.Comput.Chem.* **1995**, *16*, 1170–1179.

[93] S. Humbel, S. Sieber, K. Morokuma, The IMOMO method: Integration of different levels of molecular orbital approximations for geometry optimization of large systems: Test for n-butane conformation and SN2 reactions: RCl+Cl-, *J. Chem. Phys.* **1996**, *105*, 1959–1967.

[94] T. Matsubara, S. Sieber, K. Morokuma, A Test of the New "Integrated MO+MM" (IMOMM) Method for the Conformational Energy of Ethand and n-Butane, *Int. J. Quantum Chem.* **1996**, *60*, 1101–1109.

[95] M. Svensson, S. Humbel, R. D. J. Froese, T. Matsubara, S. Sieber, K. Morokuma, ONIOM: A multi-layered integrated MO+MM method for geometry optimizations and single point energy predictions. A test for Diels-Alder reactions and Pt(P(t-Bu)3)2+H2 oxidative addition, *J. Phys. Chem.* **1996**, *100*, 19357–19363.

[96] M. Svensson, S. Humbel, K. Morokuma, Energetics using the single point IMOMO (integrated molecular orbital plus molecular orbital) calculations: Choices of computational levels and model system, *J. Chem. Phys.* **1996**, *105*, 3654–3661.

[97] T. Vreven, K. Morokuma, On the application of the IMOMO (Integrated Molecular Orbital + Molecular Orbital) method, *J. Comput. Chem.* **2000**, *21*, 1419–1432.

[98] T. Vreven, K. S. Byun, I. Komáromi, S. Dapprich, J. A. Montgomery Jr., K. Morokuma, M. J. Frisch, Combining quantum mechanics methods with molecular mechanics methods in ONIOM, *J. Chem. Theory and Comput.* **2006**, *2*, 815–826.

UNIVERSITAT ROVIRA I VIRGILI
COMPUTACIONAL STUDIES ON THE MECHANISM OF THE PAUSON-KHAND REACTION
Torstein Fjermestad
ISBN:978-84-693-9441-0/DL:T.62-2011

[99] S. Kozuch, S. Shaik, A Combined Kinetic-Quantum Mechanical Model for Assessment of Catalytic Cycles: Application to Cross-Coupling and Heck Reactions, *J. Am. Chem. Soc.* **2006**, *128*, 3355–3365.

[100] S. Kozuch, S. Shaik, Kinetic-Quantum Chemical Model for Catalytic Cycles: The Haber-Bosch Process and teh Effects of Reagent Concentration, *J. Phys. Chem. A* **2008**, *112*, 6032–6041.

[101] S. Kozuch, S. E. Lee, S. Shaik, Theoretical Analysis of the Catalytic Cycle of a Nickel Cross-Coupling Process: Application of the Energetic Span Model, *Organometallics* **2009**, *28*, 1303–1308.

[102] S. Kozuch, S. Shaik, Defining the optimal inductive and steric requirements for a cross-coupling catalyst using the energetic span model, *J. Mol. Catal. A* **2010**, *324*, 120–126.

[103] C. J. Cramer, *Essential of Computational Chemistry* (John Wiley & Sons, Ltd, **2004**).

[104] C. Wang, Y. D. Wu, Theoretical Studies on Ru-Catalyzed Pauson-Khand-Type [2+2+1] and Related [2+2+1+1] Cycloadditions, *Organometallics* **2008**, *27*, 6152–6162.

[105] M. J. Frisch, G. W. Trucks, H. B. Schlegel, G. E. Scuseria, M. A. Robb, J. R. Cheeseman, J. A. Montgomery, Jr., T. Vreven, K. N. Kudin, J. C. Burant, J. M. Millam, S. S. Iyengar, J. Tomasi, V. Barone, B. Mennucci, M. Cossi, G. Scalmani, N. Rega, G. A. Petersson, H. Nakatsuji, M. Hada, M. Ehara, K. Toyota, R. Fukuda, J. Hasegawa, M. Ishida, T. Nakajima, Y. Honda, O. Kitao, H. Nakai, M. Klene, X. Li, J. E. Knox, H. P. Hratchian, J. B. Cross, V. Bakken, C. Adamo, J. Jaramillo, R. Gomperts, R. E. Stratmann, O. Yazyev, A. J. Austin, R. Cammi, C. Pomelli, J. W. Ochterski, P. Y. Ayala, K. Morokuma, G. A. Voth, P. Salvador, J. J. Dannenberg, V. G. Zakrzewski, S. Dapprich, A. D. Daniels, M. C. Strain, O. Farkas, D. K. Malick, A. D. Rabuck, K. Raghavachari, J. B. Foresman, J. V. Ortiz, Q. Cui, A. G. Baboul, S. Clifford, J. Cioslowski, B. B. Stefanov, G. Liu, A. Liashenko, P. Piskorz, I. Komaromi, R. L. Martin, D. J. Fox, T. Keith, M. A. Al-Laham, C. Y. Peng, A. Nanayakkara, M. Challacombe, P. M. W. Gill, B. Johnson, W. Chen, M. W. Wong, C. Gonzalez, J. A. Pople, Gaussian 03, Revision C.02, Gaussian, Inc., Wallingford, CT, 2004.

[106] R. Ditchfield, W. Hehre, J. Pople, Self-Consistent Molecular-Orbital Methods. IX. An Extended Gaussian-Type Basis for Molecular-Orbital Studies of Organic Molecules, *J. Chem. Phys.* **1971**, *54*, 724–728.

[107] P. J. Hay, W. R. Wadt, "*Ab initio* effective core potentials for molecular calculations. Potentials for the transition metal atoms Sc to Hg, *J. Chem. Phys.* **1985**, *82*, 270–283.

UNIVERSITAT ROVIRA I VIRGILI
COMPUTACIONAL STUDIES ON THE MECHANISM OF THE PAUSON-KHAND REACTION
Torstein Fjermestad
ISBN:978-84-693-9441-0/DL:T.62-2011

[108] A. V. Marenich, C. J. Cramer, D. G. Truhlar, Universal solvation model based on solute electron density and a continuum model of the solvent defined by the bulk dielectric constant and atomic surface tensions, *J. Phys. Chem. B* **2009**, *113*, 6378–6396.

[109] D. R. Lide, *Handbook of Chemistry and Physics* (CRC Press LLC, **2003**), 84 edition.

[110] G. Chang, W. C. Guida, W. C. Still, An Internal Coordinate Monte Carlo Method for Searching Conformational Space, *J. Am. Chem. Soc.* **1989**, *111*, 4379–4386.

[111] M. Saunders, K. N. Houk, Y.-D. Wu, C. Still, M. Lipton, G. Chang, W. C. Guida, Conformations of Cycloheptadecane. A Comparison of Methods for Conformational Searching, *J. Am. Chem. Soc.* **1990**, *112*, 1419–1427.

[112] P. S. Shenkin, D. Q. McDonald, Cluster Analysis of Molecular Conformations, *J. Comput. Chem.* **1994**, *15*, 899–916.

[113] G. A. Kaminski, R. A. Friesner, Evaluation and Reparametrisation of the OPLS-AA Force Field for Proteins via Comparison with Accurate Quantum Chemical Calculations on Peptides, *J. Phys. Chem. B* **2001**, *105*, 6474–6487.

[114] *"Macromodel 8.5" Schrödinger, Inc. Portland, OR, 2003.*

[115] S. Shambayati, W. E. Crowe, S. L. Schreiber, N-oxide promoted Pauson-Khand cyclizations at room temperature, *Tetrahedron Lett.* **1990**, *31*, 5289–5292.

[116] N. Jeong, Y. K. Chung, B. Y. Lee, S. H. Lee, S. E. Yoo, A dramatic acceleration of the Pauson-Khand reaction by trimethyl N-oxide, *Synlett.* **1991**, 204–206.

[117] A. R. Kennedy, W. J. Kerr, D. M. Lindsay, J. S. Scott, S. P. Watson, Stereochemical and mechanistic features of asymmetric Pauson-Khand processes, *J. Chem. Soc., Perkin Trans.* **2000**, *1*, 4366–4372.

[118] Y.-L. Shi, Y.-C. Gao, Q.-Z. Shi, D. L. Kershner, B. Fred, Oxygen Atom Transfer Reaction to Metal Carbonyls. Kinetics and Mechanism of CO Substitution Reactions of $M(CO)_6$ (M=Cr, Mo, W) in the Presence of $(CH_3)_3NO$, *Organometallics* **1987**, *6*, 1528–1531.

[119] J.-K. Shen, Y.-C. Gao, Q.-Z. Shi, F. Basolo, Oxygen Atom Transfer Reaction to Metal Carbonyls. Kinetics and Mechanism of CO Substitution of $M(CO)_5$ (M=Fe, Ru, Os) in the Presence of $(CH_3)_3NO$, *Organometallics* **1989**, *8*, 2144–2147.

[120] J. Li, G. Schreckenbach, T. Ziegler, First Bond Dissociation Energy of M(CO)6 (M=Cr, Mo, W) Revisited: The Performance of Density Functional Theory and the Influence of Relativistic Effects, *J. Phys. Chem.* **1994**, *98*, 4838–4841.

[121] V. Derdau, S. Laschat, Alkaloid *N*-oxide promoted asymmetric cobalt-mediated Pauson-Khand reaction, *J. Organomet. Chem.* **2002**, *642*, 131–136.

UNIVERSITAT ROVIRA I VIRGILI
COMPUTACIONAL STUDIES ON THE MECHANISM OF THE PAUSON-KHAND REACTION
Torstein Fjermestad
ISBN:978-84-693-9441-0/DL:T.62-2011

[122] E. Santos Garcia, *Computational studies on supramolecular hydrogen-bonded structures: from nanocapsules to proteins*, Ph.D. thesis, Universitat Rovira i Virgili, **2008**.

[123] G. R. Desiraju, The C-H$\cdots$O Hydrogen Bond: Structural Implications and Supramolecular Design, *Acc. Chem. Res.* **1996**, *29*, 441–449.

[124] S. C. Berk, R. B. Brossman, S. L. Buchwald, Titanocene-Catalyzed Conversion of Enynes to Bicyclic Cyclopentenones, *J. Am. Chem. Soc.* **1993**, *115*, 4912–4913.

[125] T. M. Schmid, G. Consiglio, Mechanistic and stereochemical aspects of the aymmectic cyclocarbonylation of 1,6-enynes with rhodium catalysts, *Chem. Commun.* **2004**, 2318–2319.

[126] H. Wang, J. R. Sawyer, P. A. Evans, M.-H. Baik, Mechanistic Insight into the Diastereoselective Rhodium-Catalyzed Pauson-Khand Reaction: Role of Coordination Number in Stereocontrol, *Angew. Chem. Int. Ed.* **2008**, *47*, 342–345.

[127] Y. Lan, L. Deng, J. Liu, C. Wang, O. Wiest, Z. Yang, Y.-D. Wu, On the Mechanism of the Palladium Catalyzed Intramolecular Pauson-Khand-Type Reaction, *J. Org. Chem.* **2009**, *74*, 5049–5058.

[128] V. Michelet, P. Y. Toullec, J. P. Genet, Cycloisomerization of 1,n-enynes: Challenging metal-catalyzed rearrangements and mechanistic insights, *Angew. Chem., Int. Ed.* **2008**, *47*, 4268–4315.

[129] S. I. Lee, N. Chatani, Catalytic skeletal reorganization of enynes through electrophilic activation of alkynes: double cleavage of C-C double and triple bonds, *Chem. Commun.* **2009**, 371–384.

[130] C. Ferrer, M. Raducan, C. Nevado, C. K. Claverie, A. M. Echavarren, Missing cyclization pathways and new rearrangements unveiled in the gold(I) and platinum(II)-catalyzed cyclization of 1,6-enynes, *Tetrahedron* **2007**, *63*, 6306–6316.

[131] E. Jimenez-Nunez, C. K. Claverie, C. Bour, D. J. Cardenas, A. M. Echavarren, cis-selective single-cleavage skeletal rearrangement of 1,6-enynes reveals the multifaceted character catalyzed cycloisomerizations, *Angew. Chem., Int. Ed.* **2008**, *47*, 7892–7895.

[132] C. Nieto-Oberhuber, M. P. Munoz, S. Lopez, E. Jimenez-Nuner, C. Nevado, E. Herrero-Gomez, M. Raducan, A. M. Echavarren, Gold(I)-catalyzed cyclizations of 1,6-enynes: Alkoxycyclizations and exo/endo skeletal rearrangements, *Chem. Eur. J* **2006**, *12*, 1677–1693.

[133] C. Nieto-Oberhuber, S. Lopez, E. Jimenez-Nunez, A. M. Echavarren, The mechanistic puzzle of transition-metal-catalyzed skeletal rearrangements of enynes, *Chem. Eur. J* **2006**, *12*, 5916–5923.

UNIVERSITAT ROVIRA I VIRGILI
COMPUTACIONAL STUDIES ON THE MECHANISM OF THE PAUSON-KHAND REACTION
Torstein Fjermestad
ISBN:978-84-693-9441-0/DL:T.62-2011

[134] C. Nieto-Oberhuber, S. Lopez, M. P. Munoz, D. J. Cardenas, E. Bunuel, C. Nevado, A. M. Echavarren, Divergent mechanisms for the skeletal rearrangement and [2+2] cycloaddition of enynes catalyzed by gold, *Angew. Chem., Int. Ed.* **2005**, *44*, 6146–6148.

[135] V. S. Nair, S. P. Mathew, R. V. Chaudhari, Kinetics of hydroformylation of styrene using homogeneous rhodium complex catalyst, *J. Mol. Catal. A* **1999**, *143*, 99–110.

[136] U. J. Jáuregui-Haza, E. J. Pardillo-Fontevila, A. M. Wilhelm, H. Delmas, Solubility of hydrogen and carbon monoxide in water and some organic solvents, *Lat. Am. appl. res* **2004**, *34*, 71.74.

[137] C. Nieto-Oberhuber, M. P. Muñoz, E. Buñuel, C. Nevado, D. J. Cardenas, A. M. Echavarren, Cationic Gold(I) Complexes: Highly Alkynophilic Catalysts for the exo- and endo-Cyclization of Enynes, *Angew. Chem. Int. Ed.* **2004**, *43*, 2402–2406.

[138] A. Escribano-Cuesta, V. Lopez-Carrillo, D. Janssen, A. M. Echavarren, Gold-Catalyzed Reactions of 1,5-and 1,6-Enynes with Carbonyl Compounds: Cycloaddition vs. Metathesis, *Chem. Eur. J* **2009**, *15*, 5646–5650.

[139] S. I. L. Lee, N. Chatani, Catalytic skeletal reorganization of enynes through electrophilic activation of alkynes: double cleavage of C-C double and triple bonds, *Chem. Commun.* **2009**, 371–384.